University College London
Gower Street, London WC1E 6BT

A PRELIMINARY DETERMINATION OF A GRAVIMETRIC GEOID IN PENINSULAR MALAYSIA

by

Wan Abdul Aziz Wan Mohd Akib

May, 1995

DEPARTMENT OF PHOTOGRAMMETRY & SURVEYING
UNIVERSITY COLLEGE LONDON
GOWER STREET
LONDON WC1E 6BT

Thesis submitted for Doctor of Philosophy Degree
of the University of London

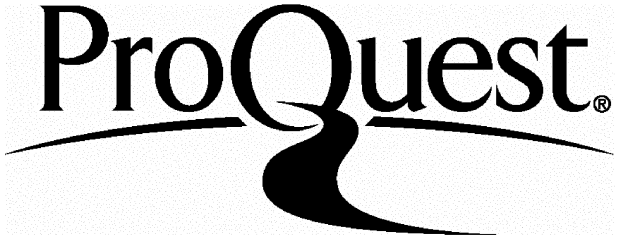

ABSTRACT

It is considered that precise gravimetric geoid determination is one of the main geodetic problems in Peninsular Malaysia for the near future, since the Global Positioning System (GPS) defined ellipsoidal coordinates require geoidal heights in practice. Geoidal heights can be determined by either a geopotential model alone, or in combination with local gravity and height data.

The reference gravity field contributed by the geopotential model can be improved by a tailoring method. This is the main objective of the study; a tailored model called *OSU89B-MM (Malaysian Model)* complete to degree and order 360 was developed by fitting the pre-existing geopotential model OSU89B to the updated mean free-air anomalies of half degree blocks in the peninsular region. Numerical analyses indicate that the tailoring technique has improved the reference gravity field by about 50% for point anomalies (from 23 mgals to 11 mgals). Tests on absolute geoid heights in selected areas where GPS and levelling data were available have demonstrated about 10% improvement (1 cm to 2 cm) of the tailored model over OSU89B, whereby the long wavelength errors have been partly diminished.

The gravimetric geoid height has been computed in three test areas (which were characterised by different types of topography, gravity density and coverage) by Least Squares Collocation (LSC) and Fast Fourier Transforms (FFT). The local height data were also utilised in a remove-restore procedure in order to study the gravitational influence of the topography, especially in test areas of rough terrain. Results show that the standard deviation of the absolute differences between the control GPS/levelling derived geoid heights and predicted gravimetric geoid heights have improved by 5 cm (from 11 cm to 6 cm) compared to the corresponding differences implied by OSU89B-MM. Work carried out in areas of high topographic relief (for which no GPS data were available) has nevertheless shown the terrain contribution to the geoid height to be as much as 0.5 m to 1.5 m .

" IF YOU'VE EVERYTHING BUT HAVE NO FAITH IN GOD,
YOU'LL HAVE NOTHING;
IF YOU'VE NOTHING BUT HAVE FAITH IN GOD,
YOU'LL HAVE EVERYTHING "

ACKNOWLEDGEMENT

I wish to thank my supervisor Dr. Jonathan Charles Iliffe for excellent supervision given throughout this study. His constant encouragement and advice is very much appreciated.

Special thanks are due to Associate Professor Dr. Majid Kadir, Department of Survey, University Technology Malaysia for providing the gravity data and relevant information which were vital for this study. Many thanks are also due to Mr. Samad Abu, the Director of the Division of Geodesy & Topography, Directorate of Surveying & Mapping, Malaysia for supplying some new gravity data, topographical maps, GPS data, relevant documents and information, and to Dr. Wan Zawawi, the Principal of the Geophysical Section, Geological Survey of Malaysia, who also supplied the gravity data and relevant information.

Many thanks are extended to Professor Dr. Denker, University of Hannover (Germany) for providing tailored model software. His distant advice and comment during the implementation of the tailoring procedure is highly appreciated. Similar thanks are also addressed to Dr. Forsberg, National Survey and Cadastre (Denmark) and Professor Dr. Tscherning, Institute of Geophysics, University of Copenhagen (Denmark) for providing the GRAVSOFT program modules which have been used throughout this study. Their distant suggestions and comments are very much appreciated.

Thanks also has to be given to Mr. James Pearson for his assistance in the computer programming and facilities. Many thanks are also due to post-graduate colleagues for their support and assistance throughout my stay in the department, in particular, Mr. Patrick Nyamangunda for sharing his knowledge in a very fruitful exposure of discussions and comments.

Thanks also has to be given to my sponsor, the Public Service Department of Malaysia and my employer, the University of Technology Malaysia for granting financial assistance and study leave throughout the course of this study.

Finally, I am greatly indebted to my wife, Esah and my two lovely children, Norhayatul Husnee and Mohd Rasyid for their understanding and sacrifices throughout the years of study. The support and encouragement given by my parents and also from my late brother and my late sister have given me the strength to carry out this study.

TABLE OF CONTENTS

CHAPTER 3

REVIEW OF DATA TYPES AND GEOID DETERMINATION METHODS

CHAPTER 4

THE DATA USED

CHAPTER 5

THE FORMULATION AND APPLICATION OF A TAILORED MODEL FOR THE MALAYSIAN PENINSULAR REGION

CHAPTER 6

PRACTICAL GEOID COMPUTATION

CHAPTER 7

PRESENTATION AND ANALYSIS OF RESULTS

CHAPTER 8

SUMMARY, CONCLUSION AND FUTURE WORK

LIST OF FIGURES

LIST OF TABLES

LIST OF ABBREVIATIONS AND NOTATIONS

2D	:	Two Dimensional Coordinates
3D	:	Three Dimensional Coordinates
BIH	:	Bureau International de l'Heure
BVP	:	Boundary Value Problem
CCD	:	Charge Couple Device
C.I	:	Contour Interval
COVFIT	:	COVariance FITting
CTP	:	Conventional Terrestrial Pole
CTS	:	Conventional Terrestrial System
DEM	:	Digital Elevation Model
DMA	:	Defence Mapping Agency
DSMM	:	Directorate of Surveying & Mapping, Malaysia
EMPCOV	:	EMPirical COVariance Function
FFT	:	Fast Fourier Transforms
GEOCOL	:	GEOdetic COLlocation
GEOFOUR	:	GEOid FOURier
GPS	:	Global Positioning System
GRAVSOFT	:	GRAVimetric SOFTware
GRS67	:	Geodetic Reference System 1967
GRS80	:	Geodetic Reference System 1980
GSM	:	Geological Survey of Malaysia
IAG	:	International Association of Geodesy
IGS	:	International Geoid Service
IGSN71	:	International Gravity Standardisation Net 1971
IUGG	:	International Union of Geodesy and Geophysics
LSC	:	Least Squares Collocation
LSD1912	:	Land Survey Datum 1912
MEE	:	Modified Everest Ellipsoid
MRT48	:	Malayan Revised Triangulation 1948
NNSS	:	Navy Navigation Satellite System
OSU89B-MM	:	OSU89B-Malaysian Model
ppm	:	Part Per Million, 10^{-6}
RA	:	Right Ascension
rms	:	Root Mean Squares
RTM	:	Residual Terrain Model
SST	:	Sea Surface Topography
USM	:	University Sciences Malaysia

UTM	:	University Technology Malaysia
WGS84	:	World Geodetic System 1984
a	:	Semi-major Axis of the Reference Ellipsoid
b	:	Semi-minor Axis of the Reference Ellipsoid
b_k	:	The Coefficients of Function in Collocation
C	:	Geopotential Numbers
C_o	:	Variance
c_n	:	Anomaly Degree Variance
C_{nm}, S_{nm}	:	The Coefficients of the Geopotential Model
$C_{\varepsilon\varepsilon}$	:	Error Covariance Matrix
C_{ss}	:	The Variance of Predicted Signal
$C_{\Delta g,\Delta g}$	:	Auto-Covariance of Gravity Anomalies
$C_{\Delta g,N}$	:	Cross-Covariance of Gravity Anomalies and Geoid Heights
e	:	Eccentricity of the Ellipsoid
f	:	Ellipsoidal Flattening
F^{-1}	:	Inverse Fourier Transform
g	:	Gravity
h (Δh)	:	Ellipsoidal Height (Differences)
H(ΔH)	:	Orthometric Height (Differences)
n	:	Noise of Observations
N	:	Legendre Degree Expansions (Model Covariance)
N(ΔN)	:	Geoid Height (Differences)
N_{GM}	:	Geoid Height from Geopotential Model
N_{max}	:	Maximum Degree and Order of Geopotential Models
$N_{\Delta g}$	:	Geoid Height from Reduced Anomalies
N_{TC}	:	Geoid Height from Terrain Contribution (Indirect Effect)
P_{nm}	:	Polynomial Coefficients
R	:	Mean Radius of the Earth (6371 km)
R_B	:	Bjerhammer Sphere
R_x, R_y, R_z	:	Rotation Parameters of Coordinate Transformation
s	:	Signal of Observations
S(ψ)	:	Stoke's Kernel Function
T	:	The Anomalous Gravity Field
U	:	The Gravity Potential on the Ellipsoid
V	:	The Gravitational Potential
W	:	The Gravity Potential on the Geoid
X, Y, Z	:	Geocentric Cartesian Coordinates
α	:	Azimuth
β_n	:	Damping Factor for Mean Anomalies

χ	:	Curvature Parameter
ε	:	Deflection of the Vertical
Δg	:	Gravity Anomaly (Free-air Anomalies)
Δg_{Fil}	:	'Filled-in' Anomalies
Δg_{GM}	:	Gravity Anomalies from Geopotential Model
Δg_r	:	Reduced Anomalies
Δg_{TC}	:	Gravity Anomalies from Terrain Contribution
$\Delta X, \Delta Y, \Delta Z$	:	Cartesian Coordinate Differences
$\Delta\phi, \Delta\lambda, \Delta h$	:	Ellipsoidal Coordinate Differences
ϕ, λ	:	Geodetic Latitude and Longitude
Φ, Λ	:	Astronomical Latitude and Longitude
γ	:	Normal Gravity
φ	:	Wavelength Signal
ε	:	Deflection of the Vertical
ξ	:	Prime Vertical Component of the Deflection of the Vertical
η	:	Meridian Component of the Deflection of the Vertical
ρ	:	Density of the Topographic Masses
ω	:	Velocity of the Earth's Rotation
ξ	:	Correlation Length (Covariance Fucntion)
ψ	:	Spherical Distance
ψ_o	:	First Zero Variance
ζ	:	Sea Surface Topography

CHAPTER 1

INTRODUCTION

1.1 Background

Geodesy can be considered as that branch of geoscience which is concerned with the determination of the size and figure of the earth, as well as its gravity field; this can be described in various ways, for example, providing the form and position of *equipotential surfaces*. Among the infinite number of these surfaces, the *geoid* is distinct insofar as it is loosely defined as an equipotential surface at mean sea level. It is the reference surface for the system of *geopotential numbers*, from which most existing height systems can be derived, see Heiskanen and Moritz, (1967-Chapter 4) and Bomford, (1980-Chapter 6). The height of the geoid is a geometrical representation of variations in the earth's gravity field and has important applications in geophysics, oceanography and geodesy.

With the rapid expansion of applications of the *Global Positioning System* (GPS) and the improvement of positioning accuracy, the determination of an accurate geoid has been one of the main interests of geodesists in recent years. The position of points derived from GPS measurements are usually computed in a three-dimensional (3D) *Cartesian coordinate system*, and the resulting X, Y, Z coordinates are easily convertible into *ellipsoidal coordinates*, namely latitude (ϕ), longitude (λ) and height (h) above the *reference ellipsoid*. However, the conversion of an *ellipsoidal height* into a meaningful physical quantity, namely *orthometric height* (H) or height above the geoid requires a correspondingly accurate knowledge of the *geoid-ellipsoid separation* (N), or so-called *geoid height*. The only feasible method of determining geoid heights over the area of interest, to the required accuracy and density is the *gravimetric method*. In mountainous and remote areas like the central part of Peninsular Malaysia and many parts of the world, it would be practically too expensive and time consuming to cover all parts of the country by conventional levelling. Thus, the GPS surveys and the computation of gravimetric geoids are of importance as an alternative method for levelling operations.

Several theories and gravimetric methods such as *Stokes' integral*, *Least Squares Collocation* (LSC) and *Fast Fourier Transforms* (FFT) have been developed to provide geoid models, each having their inherent strengths and weaknesses. In principle, the geoid model solution is determined using various data types that include information belonging to separate wavelengths of the total gravity spectrum. For example, *geopotential models* are basically sensitive to long wavelength signals

whereas gravity anomalies and topographic heights have principally medium and short wavelength sensitivities, respectively. The gravimetric geoid solutions are usually carried out with respect to the *Geodetic Reference System 1980* (GRS80).

In practice, global geoid solutions are obtained directly from geopotential models which are given as a set of coefficients. The coefficients are those of a series of spherical harmonic expansion, i.e. the numerical version of an infinite spectrum that allows analysis per degree of the series. High degree geopotential models are a major source of gravity field information and are invaluable in local studies leading to a solution of the *boundary value problem* (BVP). They define the global behaviour of the gravitational potential and provide an absolute datum on which to build the *anomalous gravity field.* Thus, in local geoid solutions, the high degree geopotential models are commonly used as reference fields where effects of long wavelength signals are removed from a set of terrestrially-observed anomalies prior to computations. This procedure will improve the homogeneity of the anomalous gravity field and has been successfully proven by Tziavos, (1987), Arabelos and Tziavos, (1992), Sevilla, (1993) and Tsui, et.al., (1994). In the case that the available global geopotential models do not approximate the regionally existing gravity field data very well, there are alternate procedures to create the high degree models. One such procedure leads to a *'tailored'* potential coefficient model, see Weber and Zommorodian, (1988). The tailoring means fitting to the surface gravity data in a specific region, thus locally improving the reference field and removing long wavelength residuals. The tailored method could be of great benefit in areas where gravity data, not included in the analysis for the coefficients for the global models, becomes available.

When topographic height data are available, for example, in the form of a *Digital Elevation Model (DEM),* it is possible to smooth the irregularities of the gravity field on a local scale by removing the gravitational effects calculated from models of the topographic masses. In this way, significant improvements of the geoid determination can be obtained, especially in mountainous areas, see Forsberg and Tscherning, (1981), Kearsley, et.al., (1985), Sideris and Forsberg, (1990) and Smith, (1992).

An optimal combination of the gravity anomalies and height data with existing geopotential models is a complicated process, considering the quantities and qualities of each data type used in the areas of interest. The accuracy achieved is dependent upon factors such as error estimates, densities and distribution of data used and the adopted solution models. For example, errors of the long wavelength coefficients in the geopotential models and sparsely distributed surface gravity data may produce biased

geoid solutions. The precision limitations, data requirements and their error sources which affect the accuracy of the gravimetric geoid determination can be found in Kearsley, (1984) and Tziavos, et.al., (1992).

It is very important to compare the gravimetric solutions with independent external results. It has become standard practice in recent years to compare computed gravimetric geoid heights with those derived independently from a combination of GPS observations and orthometric levelling. Since the ellipsoidal heights can be obtained with high accuracy from GPS observations, the question arises of whether geoid heights can be gravimetrically determined with comparable accuracy. Some practical evaluations are fully presented in Engelis, et.al., (1985), Denker and Wenzel, (1987), Forsberg and Madsen, (1990), Veroneau, (1992), Li and Sideris, (1994) and Sideris and She, (1995).

1.2 Significance of the Study

The advent of the GPS has created a revolution in spatial positioning methods in most parts of the world, including the Malaysian Peninsula region. Since the GPS defined coordinates require geoid heights in practice, i.e. conversion from ellipsoidal heights to orthometric heights, it is considered that precise gravimetric geoid determination is one of the main geodetic problems for Peninsular Malaysia in the near future. In addition to the orthometric height determination, transformation of the GPS-derived coordinates from the World Geodetic System 1984 (WGS84) into a local datum, the baseline reduction and the vertical datum determination require high accurate geoids. Consequently, the attempt for high accurate geoid determination is self-evident.

So far, no serious attempts have been made to compute the gravimetric geoid for Peninsular Malaysia. Because of the unavailability of uniform gravity data, especially in the remote and mountainous areas, and also the lack of local DEM data, it is almost impossible at the present stage to produce a precise geoid for the whole country. The significance of this preliminary study can therefore be outlined as follows:

(i) To study the quality of gravity field estimation for geoid height computation in three test areas in Peninsular Malaysia with respect to the density of available terrestrial gravity data, area coverage, 'pre-existing' or 'tailored' reference models and topographic data.

(ii) To provide a 'preliminary platform' of geoid height for the test areas which can be significantly improved in the near future when the 'on-going gravity

survey project' in the unsurveyed areas, and the digitisation of a local DEM is completed.

(iii) To fully capitalise upon the capacity of GPS technology in providing height values for the Malaysian region so that the GPS users can easily and accurately convert the existing GPS-based heights, which have limited practical use, to a height which can be used in engineering, surveying and other scientific applications. Thus, the preliminary local geoid is an essential element and testing platform to perform this height transformation.

1.3 Scope of Research

As mentioned previously, various strategies can be followed for precise determination of the geoid heights where the combination of a global model or equivalent model with local data has become a standard procedure. This study is primarily concerned with the investigation of tailored models to provide a reference field for the anomalous gravity field used for geoid determination in Peninsular Malaysia. The computation of tailored models has proven to be an efficient method which yields very good results in areas where some new terrestrial gravity data (updated data) not included in the development of existing global models, have become available. The tailoring means fitting the surface gravity data into a global model, in a specific region. The tailoring procedure of global models was first published by Weber and Zommorodian, (1988) and refined by Basic, (1989).

The experiments include testing the resulting tailored models against the point gravity data, to see if there has been any improvement over the existing geopotential model. Apart from the anomalies comparison, the geoid heights generated from the existing model and the tailored model are also tested against control values of N, to discover if the tailored model has improved the geoid determination. The control data N is provided by values found from available GPS-derived ellipsoidal heights and orthometric height from heighting operations, e.g. levelling or trigonometric heighting. The main tasks of this study, therefore, can be summarised as follows:

(i) To review the current availability of the related data to be used in the region.

(ii) To develop a 'tailored model' which is based on a fitting of the pre-existing geopotential model OSU89B to match the regional structure implied by updated gravity data in the region.

(iii) To investigate the superiority, reliability and capability of the tailored models as reference fields for geoid height determination in Peninsular Malaysia compared to the original OSU89B model. These tests will be carried out by comparing the results with corresponding point gravity observations and geoid height values derived from available GPS/levelling points.

(iv) To model covariance functions for the gravity data which represent sufficiently the features of the gravity field in the test areas. Here, a proper choice of covariance function is of considerably importance in geoid height determination using the LSC method.

(v) To apply the LSC method for geoidal height computations in the three test areas, each having different characteristics of data density, data coverage, and terrain features.

(vi) The very fast and flexible FFT method is also to be used for geoid computations in the same test areas, mainly for comparison reasons.

(vii) To evaluate and to analyse the computed geoid height values (using the LSC and the FFT methods) at the GPS points with corresponding geoid height values derived from GPS/levelling operations.

(viii) To propose future work for a precise geoid determination in Peninsular Malaysia.

1.4 Thesis Overview and Structure

A brief description of some basic properties and detailed formulation of the earth's gravity field is given in Chapter 2. A general review of reference surfaces, harmonic functions, the formulation of the BVP and its solution is also presented in this chapter. Finally, this chapter also briefly focuses on the gravity reduction necessary for the gravimetric computations.

Chapter 3 presents a review of the relationship between the orthometric height, ellipsoidal height and geoid height. This is followed by a description of data types and their characteristics, e.g. spectral resolution, density, and coverage that can be used to determine the geoid height. The gravimetric methods that are commonly used in geoid determination are also discussed in this chapter. This includes a local gravimetric geoid which can be evaluated using a combination of a geopotential model and local terrestrial data via computational procedures such as Stokes' integral, LSC method and FFT technique. The terrain reduction as part of the contribution to gravimetric

geoid solutions is also discussed in this chapter. The methods of improving geoid height estimation are briefly discussed in the last section of this chapter.

An extensive review of the existing gravity data used for this study is given in Chapter 4. This chapter also includes a description of the GPS survey campaign in the Malaysian Peninsula. The available topographic data is also described in detail in this chapter. There then follows a brief description of the OSU89B model used for the development of the tailored model. Finally, the analysis of these data is briefly presented, to look at any limitations imposed by them which will give an insight into the estimated accuracy of the geoid height computations in the test areas.

Chapter 5, which is the main contribution of this study, mainly deals with the description of the theory and model development of a tailored model for improving the reference field for anomalous gravity used for the geoid determination in Peninsular Malaysia. In this chapter, the results of tailored models are evaluated and analysed against the corresponding values derived from point gravity observations and the available derived GPS/levelling operations.

The detailed discussion of the gravimetric computational methods used in this study is given in Chapter 6. This includes the fundamental mathematical properties for the definition of the LSC method and the FFT technique. The various assumptions used in each method, their practical evaluations and the computer software used in this study are also discussed in this chapter.

Chapter 7 presents and analyses the results obtained from the various tests performed on the LSC and FFT methods described in chapter 6 using three test areas.

All practical geoid computations are summarised and concluded in Chapter 8. Suggestions for possible future research work that can be carried out are also given in this chapter.

Appendices contain relevant information not shown in the main sections.

References and Bibliography contain lists of sources which were consulted in the course of the research. They are listed under the authors' names arranged in alphabetical order, chronologically for each author.

CHAPTER 2

FUNDAMENTALS OF PHYSICAL GEODESY

2.1 Introduction

Geodetic measurements, from which coordinates defining points must be derived, are carried out on the earth's physical surface using instrumentation, that relies greatly on the earth's gravity field. These measurements must be transferred from this irregular surface into the reference surface with respect to equipotential surfaces (surface of constant gravity potential) whose study thereby becomes a concern of geodesy. The physical aspect of the problem of geodesy follows from the consideration of the earth's physical surface and the geoid as bounding surfaces in the earth's gravity field.

The gravity field of the earth is used for estimation of geoid heights and deflections of the vertical, definition of height systems, estimation of gravity field information in unsurveyed areas and satellite orbit determinations. In Physical Geodesy, there are fundamental problems which must be overcome before the nature of the gravity field of the earth is fully understood. This is the Boundary Value Problem (BVP), where the boundary is a chosen surface dividing the internal and external gravity fields.

The BVP incorporates a geometrical (the physical and mathematical surface of the earth) and a physical (gravity field) formulation of problem; both are closely related. The boundary values are gravimetric quantities on this surface which provide constraints in the determination of the equipotential surface. This chapter will start therefore with some basic properties of the earth's gravity field. The reference surfaces and the anomalous gravity field are discussed in the following sections. To discuss the solution to the BVP, it is necessary to understand the concept of harmonic functions as the BVP solutions rely on the boundary values being *harmonic*. Therefore, this chapter will also overview spherical harmonics and their adaptation to the BVP solutions. The determination of the geoid height through Stokes' solution to the BVP are also discussed. It closely follows Heiskanen and Moritz, (1967 - Chapters 1 and 2) and Bomford, (1980 - Chapter 6) which could be consulted for further details. Finally, the *gravity reductions* and *atmospheric correction* which are also needed for the anomalous gravity field assumption discussed at the beginning of this chapter is described and the necessary formulae for these reductions and correction will be derived.

2.2 The Gravity Field of the Earth

From the time when Isaac Newton developed his *Universal Law of Gravitation*, it has been accepted that the weight of a body is caused by the gravitational attraction of the earth's mass. Similarly, a body rotating with the earth experiences the *gravitational forces* of the earth and of other celestial bodies, as well as the *centrifugal force* due to the earth's rotation. The resultant force is the *force of gravity*. It is a function of position, but also undergoes temporal variations of secular and periodic nature which can occur globally, regionally and locally. In principle, measured gravity has three main uses:

- it provides information on the internal structure of the earth;
- it is applied in geodesy in the determination of the figure (the size and the shape) of the earth; and
- it is applied in celestial dynamics in the calculation of the effect of the earth's attraction on celestial bodies such as moon, artificial satellites and space vehicles.

2.2.1 The Gravitational Potential

The derivation of the gravitational force F is based on *Newton's Law of Gravitation (1687)* which applies only to particles or point masses and states that, see Figure: 2.1:

> *"Every particle in the universe attracts every other particle with a force which is directly proportional to the product of the two masses and inversely proportional to the square of the distance between them; the direction of the force being in the line joining the two particles ".*

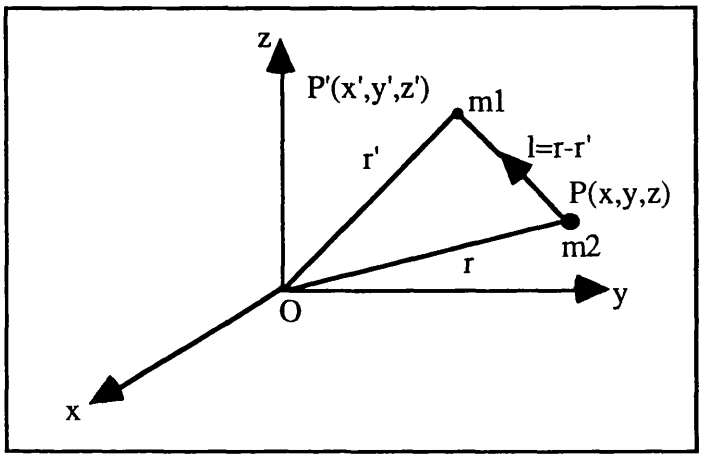

Figure : 2.1 - Gravitational attraction of point masses

This can be written mathematically as:

$$F = \frac{Gm_1m_2}{l^2} \qquad .....(2.1)$$

where G is the *Newtonian Gravitational Constant* and l is a distance between point masses.

If a unit mass m_2 is situated at point P is attracted by another point P' of unit m_1, then the force of attraction would be exerted on m_2 by m_1. Consequently, m_2 would be caused to accelerate towards m_1. For a mass external to and orbiting the earth, the acceleration would be *gravity* g, and from *Newton's Second Law of Motion,* we have:

$$F = m_2g \qquad .....(2.2)$$

Thus, from equation (2.1), we have

$$g = \frac{Gm_1}{l^2} \qquad .....(2.3)$$

It is more convenient to obtain the gravitational force by introducing and differentiating a scalar function V, termed the *Newtonian Potential Function,* that is:

$$F = \left(\underset{-}{i}\frac{\partial}{\partial x} + \underset{-}{j}\frac{\partial}{\partial y} + \underset{-}{k}\frac{\partial}{\partial z}\right)V = \text{grad}(V) \qquad .....(2.4)$$

where

$$V = \frac{Gm}{l} \qquad .....(2.5)$$

The value of the potential at point P in the gravitational field indicates the work that must be done by the gravitation in order to move the unit mass from infinity (V=0) to P. When celestial bodies are considered as solid particles rather than point masses, their masses (dm) depend on volume and density:

$$dm = \rho dv \qquad .....(2.6)$$

where ρ is the density and dv is an element of volume.

A finite dimensional body such as the earth, composed of an infinite number of particles induces a gravitation on the unit mass at P which is computed by summing the individual accelerations vectorially. Once more, this is simplified by changing from the

vector to scalar field. Consequently, the potentials dV of all the particles in the body are summed to give V. Thus, the potential V_P at point P is computed from:

$$V_P = G\iiint_{earth} \frac{dm}{l} = G\iiint_{earth} \frac{\rho dv}{l} \qquad .....(2.7)$$

or

$$V_P = V(x,y,z) = G\iiint \frac{\rho(x',y',z')dx'\,dy'\,dz'}{l} \qquad .....(2.7a)$$

The potential V in equation (2.7) is continuous throughout the whole space and actually vanishes at infinity where for very large distances l, the mass bodies act like point masses.

2.2.2 Centrifugal Potential

The centrifugal acceleration or force arises as a result of the rotation of the attracting body, as exemplified by the earth, about its axis. If a unit mass, on or detached from a rotating physical body, rotates with an angular velocity ω, then the centrifugal force, F', caused at point P (see Figure: 2.2) is given by:

$$F' = \omega^2 r \qquad .....(2.8)$$

where r is the distance from the centre of the mass and ϕ is the latitude of the point.

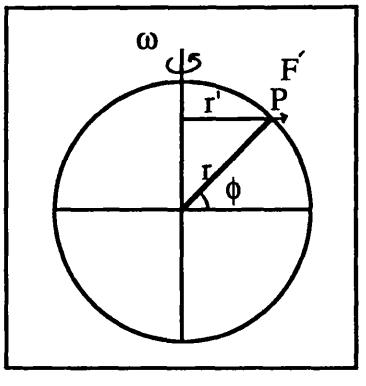

Figure: 2.2 - The rotational potential

If the z-axis of an earth-fixed x, y, z system coincides with the axis of rotation, then

$$r = \begin{pmatrix} x \\ y \\ 0 \end{pmatrix}, \qquad r = |r| = \sqrt{x^2 + y^2} \qquad .....(2.9)$$

with

$$F' = \text{grad } F \qquad .....(2.10)$$

we introduce the *centrifugal potential*

$$\Phi = \Phi(r) = \frac{1}{2}\omega^2 r^2 \qquad .....(2.11)$$

or $$\Phi = \frac{1}{2}\omega^2(x^2 + y^2) \qquad .....(2.11a)$$

2.2.3 Gravity and Equipotential Surfaces

The potential of gravity W is the sum of the gravitational (equation 2.7) and centrifugal potentials (equation 2.11a):

$$W = W(x,y,z) = G\iiint_{earth} \frac{\rho}{1} dv + \frac{1}{2}\omega^2(x^2 + y^2) \qquad .....(2.12)$$

Surfaces for which the gravity potential W is a constant are designated *equipotential, level* or *geopotential surfaces* of gravity. These surfaces can be determined by evaluating equation (2.12) if the density distribution and angular velocity are known. Of course, the density distribution of the earth is not precisely known. Geodetic theories are available to determine the equipotential surface without explicit knowledge of the density distribution. Thus, the geoid is defined to be a specific equipotential surface having gravity potential:

$$W(x,y,z) = \text{Constant} \qquad .....(2.13)$$

The gravity vector $\vec{g}$ is the gradient of W and can be written as:

$$\vec{g} = \text{grad}W = \begin{pmatrix} W_x \\ W_y \\ W_z \end{pmatrix} \qquad .....(2.14)$$

where the components W_x, W_y, W_z are the partial derivatives of W with respect to a rectangular coordinate system (x, y, z). Of particular interest is the magnitude of this vector because it is a measurable quantity. It is usually denoted by:

$$g = \left|\vec{g}\right| \qquad .....(2.15)$$

and it is called gravity. Gravity is the resultant of the gravitational force and the centrifugal force of the earth's rotation which is traditionally measured in unit of *gals* where 1 gal = 1 cm/sec^2. Gravity g is in the first approximation, a function of position;

consequently it is a vector field (the gravity field) and is defined at every point of the region where it exists:

$$g_i = g(x_i, y_i, z_i) \qquad .....(2.16)$$

The equipotential surfaces are intersected perpendicularly by the plumb lines. Figure: 2.3 depicts a direction of gravity (g) at a point which is the direction of the plumb line or direction of the vertical. The distance along a plumb line from the geoid to a point is called orthometric height (H).

There is an important relationship between the direction of the gravity force and equipotential surfaces, demonstrated by Figure: 2.3. It provides the link between the potential difference (a physical quantity) and the difference in height (a geometrical quantity) of neighbouring equipotential surfaces.

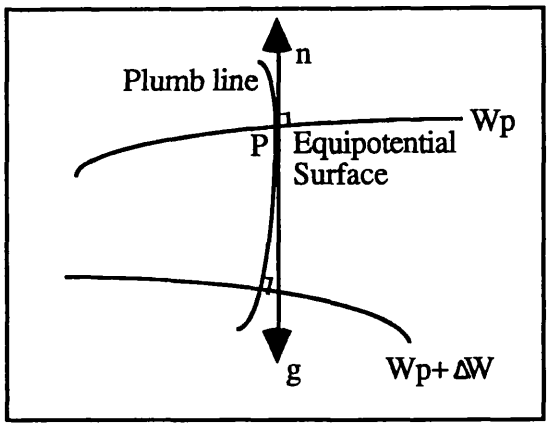

Figure: 2.3 - Equipotential surface, plumb line and the gravity vector

The total differential of the gravity potential at a point is given:

$$\Delta W = - g\, dn \qquad .....(2.17)$$

where dn is the differential of the outer surface normal.

The above equation can also be rewritten as:

$$g = -\frac{\Delta W}{dn} \qquad .....(2.18)$$

It can be seen from Figure: 2.3 that if g varies on an equipotential surface, then the distance dn to a neighbouring equipotential surface must also vary. Therefore, it is obvious that the gravity g cannot be constant on the same equipotential surface because the equipotential surfaces are neither regular nor concentric with respect to the centre of

mass of the earth. Consequently, because the equipotential surfaces are not parallel, points of equal orthometric height are not situated on the same equipotential surface.

A surface point P can be determined in the system of equipotential by its potential difference to the geoid. Alternatively, one can describe the orthometric height in terms of potential, using geopotential numbers (C). The geopotential number is simply the algebraic difference between the potential at the geoid and at point P.

From equation (2.18), it can be shown that:

$$C = W_o - W_P = -\int_{P_o}^{P} \Delta W = \int_{P_o}^{P} g\,dn \qquad .....(2.19)$$

For geodetic and plane surveying, the geopotential number C is less suitable than the orthometric height, which is the linear distance reckoned along the 'curved' plumb line from the geoid to the surface point. Alternatively, from equation (2.19), we may get:

$$H = -\int_{W_o}^{W} \frac{\Delta W}{g} = \int_{0}^{C} \frac{dC}{g} \qquad .....(2.20)$$

Finally, according to equation (2.20), it can be seen that gravity observations and levelling height differences yield potential differences.

2.3 The Reference Surface

From observed quantities and through subsequent geodetic computations, one attempts to determine the parameters of the physical earth's surface and the external gravity field. To this end, *reference surfaces* and hence *reference systems* have to be introduced. They consist of a *coordinate system* with defined metric and curvature (2D or 3D), and its realisation through a set of coordinates of reference points.

Throughout human history, the earth has been attributed many shapes, from a convex disc to rectangle. But, with Aristotle (350 BC), came the idea that the earth was spherical, a perfect shape. However, the physical theories of Isaac Newton led to the idea that the earth was not exactly spherical, but in the form of *an ellipsoid of rotation.* However, it has been shown in Section 2.2.1, that variations in potential are caused by the variations in internal density and so the actual surface of the earth must also vary if it is to remain equipotential. The fundamental reference surface in the context of geodesy is the geoid and the rotational ellipsoid whereby their formulation problems are used to define a *vertical datum* and a *horizontal datum*, respectively.

2.3.1 The Geoid

Let us consider the waters of the ocean as a freely moving homogeneous matter, which is subject only to the force of the gravity of the earth. Upon attaining a state of equilibrium, the surface of such an idealised ocean assumes an equipotential surface of the gravity field. As mentioned previously, this equipotential surface is called the *geoid*. Here, the geoid can be loosely defined as mean sea level which would be the equipotential surface and it is this surface that is considered to be closest to the figure of the earth. However, the earth does have land masses, so the oceans are confined, and they are also susceptible to other forces. The position of a hydrostatic sea level is therefore obscured and the visible sea surface does not coincide with geoid.

The shape of the geoid is considered as time invariant, due to daily earth tides, contraction of oceanic lithosphere, land uplift and glacial rebound. Its shape is quite well known nowadays, particularly over oceans due to satellite coverage and increased knowledge of the sea surface topography. The geoid is smooth and continuous, although its shape reflects the distribution of mass inside the earth, i.e. geophysical phenomena. The curvature of the geoid displays discontinuities at abrupt density variations. Consequently, the geoid is not an analytic surface, and it is thereby eliminated as a reference surface for position determinations. However, it is well suited as a reference surface for heights defined in the gravity field.

2.3.2 The Reference Ellipsoid

The problem in determining the geoid has led to the introduction of a similar shape which can defined mathematically and hence 'located' for use as a horizontal datum. If we recognise that the geoid has no simple mathematical expression, we will find it convenient to define a relatively simple mathematical surface that closely approximates the actual geoid. Here, a simple mathematical surface is very important because the position of points on the earth's surface must be expressed by coordinates on an arbitrary defined geometrical surface (or figure). The approximation of such geometrical reference surfaces can be made for a local area or on a global scale.

Because it rotates, the earth assumes the shape of a sphere that is flattened at the poles and bulging at the equator, see Figure: 2.4. In other words, an assumption is made that the normal figure of the earth is represented well by an *ellipsoid of revolution*. The reference ellipsoids, therefore, will have certain characteristics that can geometrically represent the actual figure of the earth in several ways. As a result, geometrically defined ellipsoidal system is very useful as mathematical device in formulating the 2D and 3D mathematical models of surveying and geodesy.

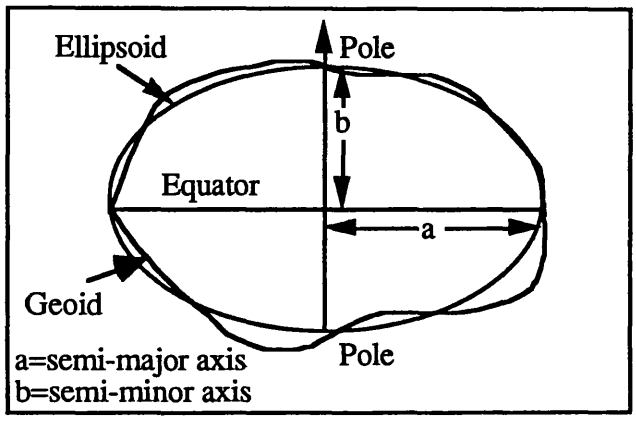

Figure: 2.4 - The Geometry of the ellipsoid as an approximation to the geoid

As illustrated in Figure: 2.4, the rotational ellipsoid is created by rotating the meridian ellipse about its minor axis. It represents the nearest mathematical shape of the geoid and is defined by the specification of two parameters:

- size, a, the semi-major axis, and
- shape, f, the flattening which is equal to $(1-\frac{b}{a})$ where b is the semi-minor axis.

The parameter f is sometimes replaced by the dynamic form factor J_2, which also describes the shape of ellipsoid. In addition, for a global fit, the ellipsoid must be positioned with its centre at the geocentre and its semi-minor axis parallel to the axis of rotation. The coordinates of a point on the ellipsoid are defined in the same way as natural coordinates, except that the normal is perpendicular to the surface of the ellipsoid rather than the geoid.

The parallel is drawn between the ellipsoid and the geoid where the ellipsoid is to be the normal form of the geoid. Thus, a global reference ellipsoid can also be assigned values for potential and gravity. It is postulated that the surface of the ellipsoid is of equal potential, $U = U_o$, and this should be equal to the gravity potential of the geoid, W_o. U is known as the theoretical or *normal gravity potential* which is the gravity field generated by an ellipsoid adopted to approximate the earth's figure and size. Consequently, *normal gravity* (γ) serves to approximate the actual gravity field at any point on the geoid. As gravity is the gradient of W, normal gravity is the gradient of U along the normal given by:

$$\gamma = \frac{\partial U}{\partial n} \qquad .....(2.21)$$

The equipotential ellipsoid provides a useful reference system for geodetic purposes and it is also a theoretical gravity field which can be considered as a first approximation to the actual. The difference between the theoretical and actual gravity fields of the earth is called the anomalous gravity field. This quantity is reviewed in Section 2.4.

2.3.2.1 Global and Local Reference Ellipsoid

Several ellipsoids have been derived although not all of these are geocentric or equipotential and so do not have an associated gravity field. Global reference ellipsoids are those used for general positioning anywhere on the earth's surface and are employed by all the major satellite positioning systems (e.g. Doppler System and GPS) as well as a number of world-wide terrestrial based systems (e.g. Very Long Baseline Interferometry -VLBI). In general, such systems are defined such that the centre of the system is as close as possible to the centre of mass of the earth. The global 'best fit' ellipsoids such as *Geodetic Reference System 1980* (GRS80) and *World Geodetic System 1984* (WGS84) were produced for purposes of global geodetic applications and suitable for gravity field studies. These two global reference ellipsoids are reviewed in the next section.

The local ellipsoids can also be determined as local *'best fits* ' to the geoid and as such are used in one particular area as reference surfaces for horizontal datum. Thus, in contrast to the global reference system, many countries adopt their own reference ellipsoid. For convenience, an ellipsoid is usually adopted which minimises the geoid-ellipsoid separation in the area of interest. The Malaysian Peninsula has adopted the *Modified Everest Ellipsoid* (MEE) as a national geodetic datum with the semi-major axis (a) and the flattening (f) as 6377276.345 metres and 0.0033244, respectively.

The origin of the MEE datum was located at *Kertau Station.* As is the case common for many local datums, the present *Kertau datum* is basically a horizontal datum rather than a three dimensional datum. This means that the position of the ellipsoid relative to the surface of the earth is well defined in the sense that specific geodetic (ellipsoidal) coordinates (ϕ, λ) are assigned to the points in the *Malayan Revised Triangulation 1948* (MRT48). Unfortunately, in the three dimensional space the position of the ellipsoid is not well defined. The reason for this is the lack of geoidal heights, errors in the astronomical observations and deficiencies in the height system. The *United States Defence Mapping Agency* (DMA), however, has established a better

relationship between WGS84 and the Kertau datum through a GPS survey project. Details of the GPS surveys in Peninsular Malaysia and the datum transformation between WGS84 and MRT48 will be discussed in Section 4.5.

2.3.2.2 Geodetic Reference System 1980

This reference system, denoted as GRS80 has been developed as a replacement of GRS67 because GRS67 no longer represents the size, shape and gravity field of the earth to an accuracy adequate for many scientific applications (Moritz, 1980). Thus, the GRS80 was adopted by the *International Union of Geodesy and Geophysics* (IUGG) as an update to the GRS67 due to more accurate values for the ellipsoidal parameters being available to suit the increasing demand from scientific areas. As such GRS80 is the official reference system for geodetic work and in its recommendations, the *International Association of Geodesy* (IAG) "encourages computations of the gravity field both on the earth's surface, and in outer space based on this system", (ibid). Therefore, any geophysical and global geodetic applications should make use of this system. Table: 2.1 shows the parameters used to define GRS80, as chosen by the IUGG.

Parameter	Value
a	6378137 m
GM	3986 005 x 10^8 m^3s^{-2}
J_2	108 263 x 10^{-8}
ω	7292 115 x 10^{-11} rad s^{-1}

Table: 2.1 - Parameters defining the Geodetic Reference System 1980

In general, the closed formulae for geometrical and physical constants of the GRS80 are derived in the same way as those for GRS67. Details of all geometrical and physical constants of GRS80 used in this study is shown in Appendix A.

2.3.2.3 World Geodetic System 1984

This global datum, which is simply denoted as WGS84 has been developed as replacement for WGS72 and represents the DMA modelling of the earth from a geometric, geodetic and gravitational standpoint using updated data, techniques and technology available throughout 1984. It is an improvement over WGS72 in several

applications. WGS84 is a *Conventional Terrestrial System* (CTS), realised by modifying the *Navy Navigation Satellite System* (NNSS) or *Transit Doppler Reference System* in origin, scale and rotating it to bring its reference meridian into coincidence with the *Bureau International de l'Heure* (BIH) - defined zero meridian.

Analogous to the BIH - defined CTS, the origin of the WGS84 coordinate system is the centre of mass of the earth. Figure: 2.5 depicts the 3D-Cartesian coordinate system of the WGS84 which consists of:

- the Z-axis is in the direction of the *Conventional Terrestrial Pole* (CTP);
- the X-axis is the direction of the WGS reference meridian plane and the plane of the CTP's equator; and
- the Y-axis is completed by a right-handed earth-fixed orthogonal coordinate system measured in the plane of the above equator, 90° east of the X-axis.

The coordinate system of WGS84 is used as a basis for global geodetic work, particularly that using the Global Positioning System. The GPS satellites are positioned according to WGS84 and this positional information is broadcast on the satellites' signal (describing their orbits in terms of this reference system).

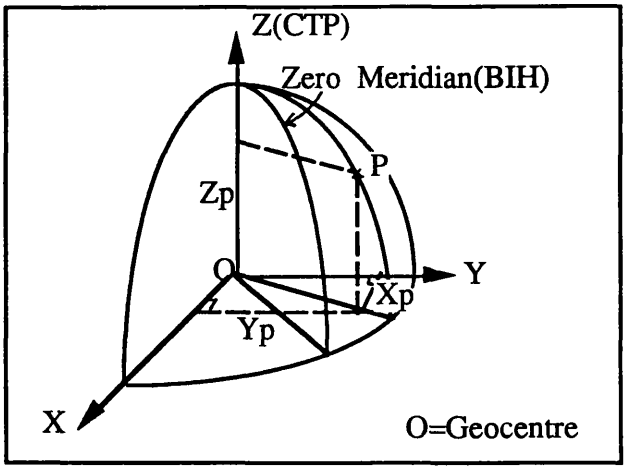

Figure: 2.5 - The World Geodetic System 1984
(Cartesian coordinate system)

The WGS84 is very similar to GRS80 in its description (see Table: 2.2) as its development was greatly influenced by the recommendations of the IAG in establishing GRS80. The parameters defining the WGS84 are the same as for GRS80 apart from the shape factor C_{20} although this is directly related to J_2 (DMA, 1987). C_{20} is the

normalised second degree zonal gravitational constant from a harmonic expansion of the WGS84 gravity model. Translating the two shape factor into a third common one, flattening, it is seen how close the two ellipsoids are:

$$f_{WGS84} = 298.257223563$$

$$f_{GRS80} = 298.257222101$$

Parameter	Value
a	6378 137 m
GM	3986 005 x 10^{8} m^3s^{-2}
C_{20}	-484.16685 x 10^{-6}
ω	7292 115 x 10^{-11} rad s^{-1}

Table: 2.2 - Parameters defining the World Geodetic System 1984

Many parameters associated with the WGS84 ellipsoid other than the four defining parameters are needed for geodetic and gravimetric applications. Using four defining parameters, it is possible to derive these associated constants. Details of these constants can be found in (DMA, 1987).

Due to the similarities of the two reference ellipsoids, differing slightly in just one parameter, they are considered identical for the purpose of the work described in this thesis.

2.4 The Anomalous Gravity Field

The normal gravity field is a natural approximation of the actual gravity field, and its derivation is based on the assumption that the actual gravity potential $W=W_0$ on the geoid is equal to the normal gravity potential on the ellipsoid $U=U_0$. In practice, however, the reference ellipsoid does not necessarily coincide with the geoid, and the actual gravity is not equal to the normal gravity.

The equipotential ellipsoid provides a useful reference system for geodetic purposes and it is also a theoretical gravity field which can be considered a first approximation to the actual. The deviation between the actual gravity potential W and the normal potential U is small. Since U can be expressed by closed formulae, it is often used as a convenient first approximation of W. The difference between the actual and the theoretical gravity fields is known as the anomalous gravity potential for which

there are similar parameters. Table: 2.3 shows each gravity field with its corresponding anomalous gravity field parameters.

Actual	Normal	Anomalous	Parameter
W	U	T	Potential
g_o	γ_o	Δg	Gravity
g_p	γ_p	δg	Gravity
Φ	ϕ	ξ	Latitude
Λ	λ	η	Longitude
h	H	N	Height

Table : 2.3 - Parameters of the gravity fields

The basic, and perhaps the most important quantity in the anomalous gravity field is T, the *anomalous potential* or *disturbing potential.* At a point P, the disturbing potential is defined as the difference:

$$T_P = W_P - U_P \qquad .....(2.22)$$

All the anomalous gravimetric quantities can be expressed in terms of T by simple relationships. If T is determined, the related values can be derived; however, this is not possible in an exact sense. The determination of T has become a major challenge in Physical Geodesy, through which enable the computation of the other quantities for practical applications. The problem is termed as a Boundary Value Problem (BVP). Details of the BVP are described in Section 2.6.

It should be noted that the values of the anomalous gravity field are very small quantities, for example, the separation between the geoid and a best-fitting ellipsoid is not more than 100 metres anywhere in the world, (Schwarz, et.al., 1990). The anomalous quantities therefore can be considered in spherical approximation, which simplifies their relationships and eases their use as data in the Physical Geodesy problems.

2.5 Harmonic Functions

As was mentioned in Section 2.2.1, the potential V is continuous throughout the whole space and actually vanishes at infinity. The first derivatives of V, which are the force components are also continuous in space, however the second derivatives

have a discontinuity at points of abrupt density changes. This is shown by the fact that the second derivative of the gravitational potential inside the earth satisfies *Poisson's Equation*, see Heiskanen and Moritz, (1967, p. 5):

$$\nabla^2 V = -4\pi G\rho \qquad .....(2.23)$$

Outside the surface of the earth where there are no masses, $\rho = 0$ and so equation (2.23) reduces to:

$$\nabla^2 V = 0 \qquad .....(2.24)$$

This is *Laplace's Equation*, and in full:

$$\nabla^2 V = \frac{\partial^2 V}{\partial x^2} + \frac{\partial^2 V}{\partial y^2} + \frac{\partial^2 V}{\partial z^2} = 0 \qquad .....(2.25)$$

is valid outside the gravitating masses of the earth. Continuous functions having continuous first and second derivatives and which fulfil equation (2.25) are called *harmonic functions* or *potential functions*, and any value, e.g. disturbing potential T which satisfies it is also harmonic.

It is often more convenient to consider Laplace's Equation in terms of spherical coordinates, as much geodetic work is based on a spheroid. Equation (2.25) becomes:

$$\nabla^2 V = r^2 \frac{\partial^2 V}{\partial r^2} + 2r\frac{\partial V}{\partial r} + \frac{\partial^2 V}{\partial \varphi^2} + \frac{1}{\sin^2 \varphi}\frac{\partial^2 V}{\partial \lambda^2} = 0 \qquad .....(2.26)$$

As was stated in Section 2.4, the disturbing potential T, as a harmonic function, replaces W in gravity field studies. Harmonic functions provide simple and logical solutions to geodetic problems, a property which should be exploited. It can be shown mathematically that every harmonic function is analytic in the space where it satisfies Laplace's equation. The simplest harmonic function is the reciprocal distance 1/l.

The harmonic functions have three basic properties which are of importance in their application to Physical Geodesy.

- Every function and its derivatives is continuous over a surface;
- Every function can be expanded as a series in terms of spherical harmonics;
- If the function satisfies Laplace's Equation in the region outside a closed surface, then it must be regular and vanish at infinity.

The BVP has a solution based on the product of these harmonic functions each depending on one spherical coordinate:

$$\nabla V = f(r)\, g(\phi)\, h(\lambda) \qquad .....(2.27)$$

Each part is a differential equation which can be solved and the solution will be linear. Combination of these linear solutions provides an answer for T. For external field, the solutions take the form:

$$\begin{aligned} f(r) &= \frac{1}{r^{n+1}} \\ g(\phi) &= P_{nm} \cos\varphi \\ h(\lambda) &= \cos m\lambda \\ h(\lambda) &= \sin m\lambda \end{aligned} \qquad .....(2.28)$$

where n, m are integers and φ is the co-latitude.

It is seen that the functions in r and λ are quite simple. For ϕ however, it is not so straightforward and the solution is expressed in terms of the *Legendre Polynomials*, P_{nm}.

Stated in a somewhat loose fashion, gravity field approximation is the estimation of the disturbing potential T in the space Ω outside the earth's surface S from discrete and noisy data given on S and in Ω. In spherical approximation, the disturbing potential may be expanded in a series of spherical harmonic functions written as:

$$T(P) = \sum_{n=2}^{\infty}\left(\frac{a}{r}\right)^{n} \sum_{m=0}^{n}[\delta C_{nm} \cos(m\lambda) + \delta S_{nm} \sin(m\lambda)]P_{nm}(\cos\theta) \qquad .....(2.29)$$

where P_{nm} are the associated Legendre functions; δC_{nm} and δS_{nm} are the differences of the spherical harmonic coefficients for W and U; a is the semi-major axis of the reference ellipsoid; and r, θ, λ are the spherical coordinates of point P.

In principle, the approximation problem can be solved by determination of the unknown coefficients C_{nm}, S_{nm} in some suitable manner. An important application is the use of spherical harmonic models as a reference for local gravity approximations using gravimetric methods. A series of spherical harmonic expansions of equation (2.29) is termed as *geopotential solutions* (models). Details of the gravimetric method and geopotential solutions will be discussed in the next chapter.

2.6 Boundary Value Problems and Their Solutions

In general, the harmonic functions can be generated by many different mass distributions. For example, a function V, harmonic outside a surface S is uniquely determined by its values on S, but there are infinitely many mass distributions which have the harmonic function V as exterior potential. These constitute the direct and inverse problems of potential theory. The inverse problem has no unique solution. This leads to Stokes' theorem which states that there is only one harmonic function V that assumes given boundary values on a surface S, provided that such a harmonic exists. The assertion that for arbitrarily prescribed boundary value is called *Dirichlet's principle*. The problem of computing the harmonic function (inside or outside S) from its boundary values on S is called *Dirichlet's problem*, or *the first BVP of potential theory*. In second BVP called *Neumann's problem*, the normal derivative of the function V, i.e. dV/dn is given on the surface S, instead of V itself. The normal derivative dn is the derivative along the outward directed surface normal n towards S. In third BVP called *Stoke's problem*, a linear combination of V and its normal derivative is given on the surface S and this problem is of great interest to Physical Geodesy. The determination of the geoid from gravity anomalies is in fact a third BVP, with the gravity anomalies as a boundary values.

The BVP comprises the determination of the physical surface of the earth or the geoid, as well as the external gravity field from the gravity potential W and gravity acceleration g = grad W on the earth's surface. The problem arises from the first BVP of potential theory in a harmonic function which must be fitted to surface values of the potential. The gravity potential, however, is not a harmonic value on and outside the surface of the earth. Hence, W does not satisfy Laplace's Equation (equation 2.25). Solutions to the BVP all rely on the boundary value being harmonic and so W must be replaced by a harmonic parameter, T. Since normal gravity field parameters all include a rotational potential equivalent to that of the actual earth, it follows that all anomalous values are, by derivation, harmonic and satisfy Laplace's Equation.

By having the anomalous gravity vector $\Delta\vec{g}$:

$$\Delta\vec{g}(P) = \vec{g}(P) - \vec{\gamma}(Q) \qquad .....(2.30)$$

we will have the following components, (see Table: 2.3):

$$\vec{\Delta g} = \begin{pmatrix} \gamma\eta \\ \gamma\xi \\ \Delta g \end{pmatrix} = \begin{pmatrix} \gamma(\Lambda - \lambda)\cos\phi \\ \gamma(\Phi - \phi) \\ |\vec{g}| - |\vec{\gamma}| \end{pmatrix} \qquad .....(2.31)$$

where

P(Φ, Λ) is a point on the geoid and

Q(ϕ, λ) is the corresponding point on the ellipsoid.

The projection from point P on the geoid to the corresponding point Q on the ellipsoid, along the ellipsoid normal is shown in Figure: 2.6.

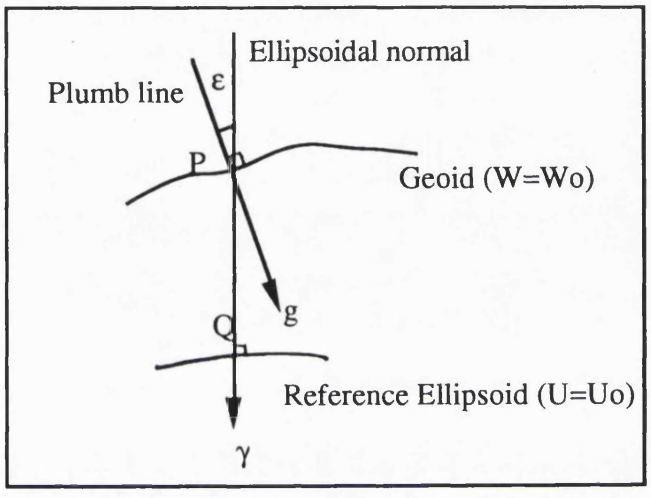

Figure: 2.6 - The relationship between the actual and the normal gravity fields

From the above figure, the difference between the two height parameters pertaining to each gravity field is the geoid-ellipsoid separation (N) or the geoid height. It is well known that this parameter can be related to disturbing potential T (Section 2.4) and normal gravity γ by *Brun's Formula* :

$$N = \frac{T}{\gamma} \qquad .....(2.32)$$

The difference between the actual gravity g at point P and the normal gravity γ at point Q is called the *gravity anomaly vector*. Its magnitude Δg is called the *gravity anomaly*. It is thus equal to the difference between the two gravity vectors.

$$\Delta g_P = g_P - \gamma_Q \qquad .....(2.33)$$

The parameter γ can be expressed by a closed formula as derived by Somigliana in 1929 which was accepted by the IUGG as the *International Gravity Formula* in 1930:

$$\gamma = \frac{a\gamma_e \cos^2\phi + b\gamma_p \sin^2\phi}{\sqrt{(a^2\cos^2\phi + b^2\sin^2\phi}} \qquad .....(2.34)$$

where γ_e and γ_p is the normal gravity at the equator and at the poles, respectively.

In fitting the ellipsoid, it was specified that U_o should equal W_o so $W_P=W_Q$ as the points are on the respective surfaces. Thus

$$\gamma_P = \gamma_Q + \frac{\partial \gamma}{\partial n} N \qquad .....(2.35)$$

Substituting, equation (2.35) into (2.33), we have

$$\Delta g_P = g_P - (\gamma_P + \frac{\partial \gamma}{\partial n} N) \qquad .....(2.36)$$

and using Brun's formula, equation (2.36) becomes

$$-\frac{\partial T}{\partial n} = \Delta g - \frac{\partial \gamma}{\partial n} N \qquad .....(2.37)$$

Rearrange equation (2.37):

$$\frac{\partial T}{\partial n} + \Delta g - \frac{\partial \gamma}{\partial n} N = 0 \qquad .....(2.38)$$

or

$$\frac{\partial T}{\partial n} + \Delta g - \frac{1}{\gamma}\frac{\partial \gamma}{\partial n} T = 0 \qquad .....(2.39)$$

This is a *Fundamental Equation in Physical Geodesy*, showing the relationship between the gravity anomaly and the anomalous potential.

If the reference ellipsoid is approximated to a sphere of radius R, then n = R with the volume equal to that of the ellipsoid. Without going into derivations, it has been shown by Heiskanen and Moritz, (1967, p. 87):

$$\frac{1}{\gamma}\frac{\partial \gamma}{\partial n} = -\frac{2}{R} \qquad .....(2.40)$$

Altogether, equation (2.39) becomes:

$$\frac{\partial T}{\partial n} + \frac{2}{R} T + \Delta g = 0 \qquad .....(2.41)$$

This is the *Fundamental Boundary Theorem*, in spherical approximation, which is used in the determination of the disturbing potential from gravity anomalies.

The difference in the directions of the two gravity vectors caused by relative slope of the geoid and the reference ellipsoid (see Figure: 2.6) are called *deflections of the vertical* (ε) . This gravimetric quantity is resolved into two components; a meridian or north-south component (ξ) and a prime vertical or east-west component (η). As elements of the anomalous gravity field, the deflection of the vertical can also be expressed in terms of T by simple relationships:

$$\xi = -\frac{1}{\gamma}\frac{\partial T}{\partial \phi} \qquad .....(2.42)$$

$$\eta = -\frac{1}{\gamma}\frac{\partial T}{\partial \lambda} \qquad .....(2.43)$$

The solution of the BVP by integral equation leads, for a known spherical boundary, to Stokes' integral and, for an unknown boundary surface, to *Molodensky's problem* and the resulting integral series. In its simplest form, the solution is:

$$T(P) = \frac{R}{4\pi}\iint_{\sigma} \Delta g S(\psi) d\sigma \qquad .....(2.44)$$

where R is the mean radius of the earth; Δg is the gravity anomaly function on the sphere σ with radius R; $S(\psi)$ is Stokes' kernel function; ψ is the spherical distance between P and the data points Q; σ is a surface of unit sphere with the element $d\sigma = \text{Sin}\,\psi d\psi d\alpha$ and α is azimuth of the point in question. It should be noted that T is determined from one data type only, the gravity anomaly Δg. Upon invoking Brun's theorem, equation (2.44) becomes the basic formula for gravimetric determination of the geoid:

$$N = \frac{R}{4\pi\gamma}\iint_{\sigma} S(\psi)\Delta g d\sigma \qquad .....(2.45)$$

where

$$S(\psi) = \frac{1}{\sin\frac{\psi}{2}} - 6\sin\frac{\psi}{2} + 1 - 5\cos\psi - 3\cos\psi \ln(\sin\frac{\psi}{2} + \sin^2\frac{\psi}{2}) \qquad .....(2.46)$$

The BVPs are important in Physical Geodesy because they define the minimum information needed to construct an approximation of T outside S. However, in terms of data availability, these formulations are not realistic. A more general approach was proposed by Krarup in 1969 who sought an approximation of T using *collocation* solution. The advantage of the collocation solution is that it allows all functional T to be treated as observables and thus makes it possible to handle the actual data more

easily. It also is not restricted to data on the boundary surface but allows the consistent treatment of data on S and in Ω outside S. If the data are available in gridded form, the BVP could be solved in a frequency domain using the FFT method. These two methods of the BVP solutions will be briefly reviewed in the next chapter while details of their mathematical properties and computational procedures used in this study is fully discussed in Chapter 6.

2.7 Gravity Reduction and External Masses

Stokes' problem in equation (2.44) deals with the determination of a potential, harmonic outside the masses, from gravity anomalies given everywhere on the geoid surface. In other words, gravity anomalies as boundary values on the geoid are required for gravimetric determination of the geoid. Since we observe the gravity on the earth's surface, however, this condition is violated by the presence of the topographical masses of the earth. Consequently, in order to implement Stokes' integral, the topography of the earth must be eliminated mathematically. In such a case, the topography is condensed to form a surface mass layer on the geoid. This process is called gravity reduction, (Heiskanen and Moritz, 1967, p. 126). The purpose of gravity reduction is therefore to reduce the observed gravity values to the geoid and to displace the topographic masses exterior to the geoid in such a way that the geoid becomes a bounding surface. In the process of gravity reductions, certain assumptions must be made as to the distribution of mass density; the gravimetrically determined geoid is subject to the errors of the density hypothesis.

The various methods differ mainly by the way in which they allow for the earth masses to be removed. The most common reductions are the *Free-air*, the *Bouguer* and the *Isostatic* reductions which will be briefly explained in the following sections. Each method provides a value for gravity on the geoid. However, with the displacement of the topographic masses, the gravity potential changes and this is termed an *indirect effect* of the gravity reduction which can be accounted for. The equipotential surface possessing the potential W_0 of the geoid after the masses have been displaced is known as *co-geoid* (compensated geoid).

The Free-air, the Bouguer and the Isostatic reductions are the main practically useful methods available. The requirements that make a gravity anomaly useful in geoid determination are:

- the anomaly should be small and smooth, allowing easier interpolation and giving a good representation of the surrounding area;
- the reduction should be geophysically meaningful; and

- the indirect effect should not be too large.

2.7.1 Free-air Reduction

The most pertinent reduction in terms of its practical importance, is the free-air reduction. With the assumption that no masses exist between the geoid and the surface of the earth, and gravity g changes linearly over the orthometric height H, the free-air gravity anomaly can be obtained as follows:

$$g_P = g - \frac{\partial g}{\partial H} H \qquad .....(2.47)$$

where g_P is the reduced gravity value on the geoid.

Since $\frac{\partial g}{\partial H}$ is unknown, it is estimated by $\frac{\partial \gamma}{\partial h}$, so that:

$$g_P = g - \frac{\partial \gamma}{\partial h} H \qquad .....(2.48)$$

The value $- \frac{\partial \gamma}{\partial h} H$ is known as the free-air reduction (F), and has the value:

$$F = - (0.3086)\, H \qquad .....(2.49)$$

Thus,

$$g_P \approx g + F = g_P - (0.3086)H \qquad .....(2.50)$$

The free-air gravity anomaly is then:

$$\Delta g_P = g_P - 0.3086H - \gamma_P \qquad .....(2.51)$$

Equation (2.51) is used to compute free-air anomalies in Peninsular Malaysia. Details of the free-air anomalies in the Peninsular Malaysia region will be discussed in Section 4.2.

Point free-air anomalies are known to oscillate around a zero average with oscillation frequencies depending strongly on the topographical features. They comprise regional and local gravity field information. This anomaly is, in general, not representative for a large area because of its local character and its strong dependence on topography, see Section 4.2.2. It can only be less accurately predicted if the gravity data is sparsely distributed and if topography is ignored, especially for mountainous areas, see (Sunkel, 1981). The free-air anomaly will be small and the indirect effect is practically negligible. However, they are not smooth and are difficult to interpolate,

especially in rugged terrain. The fact that free-air anomalies are simple to produce lends a lot of weight to their choice.

2.7.2 Bouguer Reduction

The objective of Bouguer reduction is the complete removal of the topographic masses between the earth and the geoid to infinity and then reducing the point to the geoid by free-air correction The topographic correction is derived mathematically from the attraction of a plate of infinite extent that exists between the measured point and the geoid. This plate is called *Bouguer plate.* The Bouguer plate is considered as a uniform plate of constant density, ρ, and thickness, H. The attraction of this plate is computed as an additional correction to the free-air reduction.

The attraction of an infinite Bouguer plate is given by:

$$\delta_B = 2\pi G\rho H \qquad .....(2.52)$$

where G is the gravitational constant.

With standard density of $\rho = 2.67 gcm^{-3}$ and $G = 6.672 \times 10^{-11} m^{-3} kg^{-1} s^{-2}$, equation (2.52) can be written as:

$$\delta_B = 0.1119H \qquad .....(2.53)$$

The Bouguer reduction uses the Bouguer gradient, given by:

$$g_B = g - \delta_B + F = g + 0.1967H \qquad .....(2.54)$$

where $F = 0.3086H$ is the free-air correction and H is the orthometric height of the gravity station. The Bouguer gravity anomaly is given by:

$$\Delta g_B = g_B - \gamma_Q \qquad .....(2.55)$$

Bouguer anomalies tend to be smooth, although large, and so are good for interpolation. The indirect effect, however, is also large.

2.7.3 Isostatic Reduction

There are several theories concerning the isostatic compensation of large masses at depth which lead to the Isostatic reduction. This is a further term added to the Bouguer anomaly that involves shifting some masses into the geoid to account for deficiencies existing under the continents. The evaluation of the isostatic terms depend on the compensation theory followed and is more complex, involving a zone

summation, see Heiskanen and Moritz, (1967, p.137-141). The isostatic anomaly is given as:

$$\Delta g_I = g_P - \text{Free-air} - \text{Bouguer} + \text{Isostatic} - \gamma_P \qquad .....(2.56)$$

The isostatic anomalies combine the respective benefits of each reduction, as they combine the actual corrections. These anomalies therefore fulfil all the requirements, but they are difficult to compute.

2.7.4 The Atmospheric Effect Correction

This effect is caused by the attraction of the atmosphere outside the earth's surface. Since the boundary condition requires that there be no masses external to the geoid, the atmosphere outside the geoid has to be removed. This causes a correction to the gravity anomaly Δg termed the atmospheric correction. The magnitude of this effect is very small, (Moritz, 1980). Usually a very simple model is sufficient for this purpose, (ibid). By assuming the atmosphere has a spherically symmetric layer distribution, the atmospheric corrections can be computed by Wichiencharoen, (1982):

$$\delta g_A = (0.8658 - 9.727 \times 10^{-5} H + 3.482 \cdot \times 10^{-9} H^2) \text{ mgals} \qquad .....(2.57)$$

where H is the orthometric height in metres.

CHAPTER 3

REVIEW OF DATA TYPES AND GEOID DETERMINATION METHODS

3.1 Introduction

As previously mentioned in Section 2.3.1, the geoid, loosely defined as an equipotential surface at mean sea level, is of considerable importance for the definition of a consistent height system. An accurate determination of geoid heights is one of the principal aims of geodesy nowadays because it forms a 'bridge' between the orthometric heights of levelling operations and the ellipsoid heights of GPS measurements. More specifically, the geoid height needs to be evaluated so that ellipsoidal height from GPS can be transformed to the orthometric height used in surveying and mapping applications.

This chapter touches first on the relationship between these height systems and is followed by a description of data sources that are commonly used in geoid height computations. A review of various gravimetric methods is also presented. In addition, various terrain effects on gravity field modelling are discussed, as well as techniques which can be exploited to improve geoid height estimation.

3.2 The Relationship Between GPS, Levelling and Geoid Height

In remote unsurveyed and mountainous areas, it would be too expensive and time-consuming to establish orthometric heights by conventional spirit levelling. The advent of high precision relative positioning by use of the GPS technology has opened up an alternative to the classical method of height determination in the near future. As mentioned before, the GPS surveys determines the position of points in terms of the WGS84-Cartesian coordinate system (X, Y, Z), at a very high accuracy. In an absolute sense, these Cartesian coordinate components can be converted into ellipsoidal components, i.e. ϕ, λ, and h. Similarly, we can also transform the ΔX, ΔY and ΔZ into $\Delta\phi$, $\Delta\lambda$, Δh components as we are often dealing with relative positioning measurements.

The ellipsoidal height (h) of a point is the distance from the reference ellipsoid to the point, measured along the line normal to the ellipsoid. The orthometric height (H) of a point on the earth's surface is the distance from the reference surface to the point, measured along the plumb line normal to the geoid. The difference between the ellipsoidal height and the orthometric height is defined as the geoid-ellipsoid separation or geoid height (N). Figure: 3.1 illustrates the relationship between ellipsoidal height, orthometric height and geoid height.

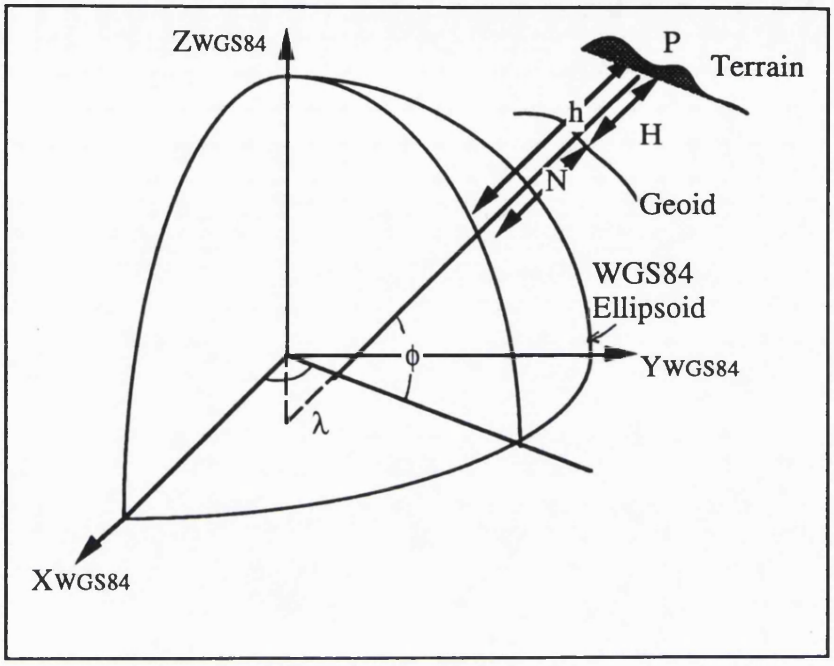

Figure: 3.1- Relationship between ellipsoidal, orthometric and geoid heights for single point

Thus, the conversion of ellipsoidal height into a meaningful physical quantity, orthometric heights can be employed through the following expression:

$$h = H + N \qquad .....(3.1)$$

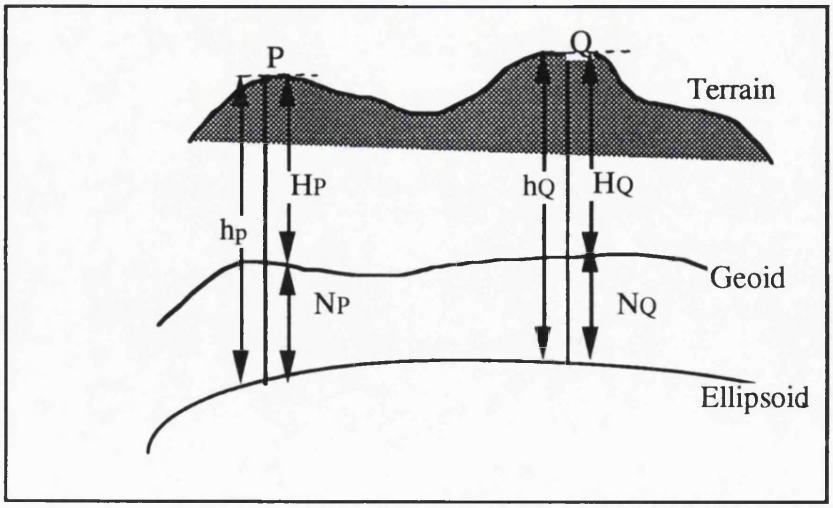

Figure: 3.2 - Relationship between ellipsoidal, orthometric and geoid heights for two points (relative positioning)

The orthometric height differences between two points P and Q in Figure: 3.2, is given by:

$$H_p - H_q = (h_p - h_q) - (N_p - N_q) \qquad .....(3.2)$$

or

$$\Delta H_{pq} = \Delta h_{pq} - \Delta N_{pq} \qquad .....(3.2a)$$

In a simplified approach, one can propagate orthometric heights from a datum point (say, H_p) through a network using the differential elements Δh and ΔN, where the former are determined from GPS, and the latter from gravimetry. Several error sources that affect the accuracy of orthometric, ellipsoidal, and geoid height values are generally common to nearby points. Because these error sources are common, the uncertainty of height differences between nearby points is significantly smaller than the absolute heights at a point. Thus, equation (3.2a) implies that the accuracy of relative geoid height will be greater than that for absolute values and so less error will be introduced into the derived orthometric height. This fact is the reason why GPS can be considered as an alternative method to levelling. However, there remains the problem of obtaining sufficiently accurate ΔN for converting Δh to accurate ΔH. Can the accuracies achieved for these orthometric height differences provide a viable alternative to classical levelling techniques with the growing interest in recovering ΔH from GPS?. This interest has generated the need for models capable of recovering geoidal features to finer detail.

3.3 Data Sources Used In Geoid Computation

There are many different kinds of data types which can be used to compute geoid height. In principle, the gravity field information of data types can be evaluated and represented in the form of a series of spherical harmonic expansions (Section 2.5) with respect to various groups of wavelengths (or spectral resolution) namely: *long wavelength* (low frequency), *medium wavelength* (medium frequency) and *short/very short wavelength* (high/very high frequency). Contributions per degree can be expressed in terms of wavelength, since the degree of expansion is related to the angular half-wavelength of the information, φ° :

$$n = \frac{180^\circ}{\varphi^\circ} \qquad .....(3.3)$$

The extent of features defined by each degree is the corresponding wavelength, and it is shown in Table: 3.1. Thus, in a spherical harmonic expansion of the earth's potential, each degree adds increasing information to the gravity field. Details of this expansion are fully described in Section 3.3.5 .

Degree	Wavelength		
	°	km	Category
20	9	900	Long
180	1	100	Medium
360	0.5	50	Medium
≥ 3600	≤ 0.05	≤ 5	Short / very short

Table: 3.1 - Degree of expansion corresponding to wavelength signals

The current data types shown in Table: 3.2 can be characterised according to spectral resolution, data density, area coverage and data distribution. The spectral properties of each data type have different error characteristics in geoid computation. Thus, it can be seen from this table that the quality of geoid height estimation depends on several factors such as the density of the available data, area coverage (global or local), measurement accuracy and the spectral sensitivity of the gravimetric functionals to a given data set.

Theoretically, each data type contains the total spectrum; however, in practice the measuring process acts as a bandpass filter limiting the range of the spectrum. Therefore, a single data type cannot resolve the complete spectrum and it is necessary to combine different types of measurements to obtain a homogenous spectral resolution. The combination of data types most frequently used for accurate determination of geoid heights are a global geopotential model, point or mean gravity anomalies and height data. This type of data combination will be discussed in Section 3.5.

It can be seen from Table: 3.2 that low frequency information comes from satellite observations and no other source is in sight for this frequency range. The medium range is currently determined from 30'x30' mean gravity anomalies on land combined with satellite altimeter data over the oceans. The above data types are regular in distribution and global in coverage, and therefore, are used in series of spherical harmonic expansion of geopotential models, for example OSU89B and OSU91A. The high frequency spectrum currently is resolved by mean anomalies of 5'x5', or deflection of the vertical, and some of the very high frequency range is resolved by point gravity anomalies. The very high frequency range currently is very little known, and thus the height data may improved the situation in the future. Some of the very

Data Type	Terrestrial Gravity Anomalies			Deflec	Satellite	Satellite	GPS	Height	Satellite
Character -istics	Mean Anomalies 30'x 30'	Mean Anomalies 5' x 5'	Point Anomalies	-tion of Vertical	Alti -metry	Pertur -bation	Level	Data	Gradio -metry
Spectral Resolution									
Low						*			
Medium	*				*		*		*
High		*		*					
Very High			*					*	
Data Density									
Low						*			
Medium	*			*	*		*		*
High		*	*					*	
Data Coverage									
Global	*				*	*			*
Regional		*	*				*		
Local				*				*	
Data Distri -bution									
Regular	*	*			*	*		*	*
Irregular			*	*			*		

Table : 3.2 - Characteristics of various data types (partly taken from Szabo, 1986)

high frequency range is removed from gravity anomalies by terrain corrections computed from height data on a grid, e.g. 1km x 1km. This removes the frequencies dependence on the topography. The GPS level is resolved in medium frequency range, and this type is irregular in distribution and regional in coverage. Details of the gravity data, geopotential model and height data used for geoid determination in Peninsular Malaysia, and also the GPS data will be discussed in Chapter 4.

3.3.1 Terrestrial Gravity Data

On land, the contemporary techniques of measuring gravity entail the determination of either the acceleration of mass moving under the influence of gravity alone or the force required to balance the mass of a body against gravity attraction. *Absolute gravity measurements* are largely done by determining acceleration of test bodies using *free-fall devices* or *pendulums*. These methods are quite laborious. The stations where absolute gravity measurements are observed provide the anchoring points of the network, while ties between points are provided by the *relative gravity measurements*. The principle for relative gravity observations involve recording of relative forces required to balance a test mass against gravity attraction, using *gravimeters*. With these devices, the measurements are much more simplified and the instruments are easily transportable for rapid gravity surveys.

All regional gravity networks should be tied to a global gravity reference system so that they referred to a uniform world gravimetric system. The gravity reference system is defined by values of gravity at a number of accurately surveyed gravity control points. Since 1971, the *International Gravity Standardisation Net 1971* (IGSN71) was used as the international gravity reference system to replace the *Potsdam Gravity System,* see Torge, (1989). One of the IGSN71 stations was located at the Kuala Lumpur International Airport, Malaysia - (IGSN71 station no. 02631A).

In order to reduce the terrestrially-observed gravity value (g) to the geoid (g_0), we have to use an appropriate gravity gradient to correct the surface gravity for the effect of height (H_0) of the observing station, see Section 2.7. Gravity error estimates are normally found in the gravity files associated with the data. For modern land gravity, the error estimate is between 0.1 mgals to 0.3 mgals. However, it is important to know how the heights of observing stations were obtained, either by levelling or barometric observations. Details of gravity measurement in Peninsular Malaysia will be described in Section 4.2.

3.3.2 Astronomical Latitude and Astronomical Longitude

The geoid height differences between two points on the surface of the earth can be derived by integrating the deflection of the vertical along the path between two points. The deflection of the vertical is defined as the angle between the ellipsoidal normal and the normal to the geoid, i.e. plumb line as depicted in Figure: 3.3. In other words, the deflection of the vertical is also equivalent to the angle between the geoid and the ellipsoid surface. It can be split into a meridian component and prime vertical component which are horizontal derivatives of the geoid height. They can be evaluated as the 'differences' between *astronomical* and *geodetic coordinates.*

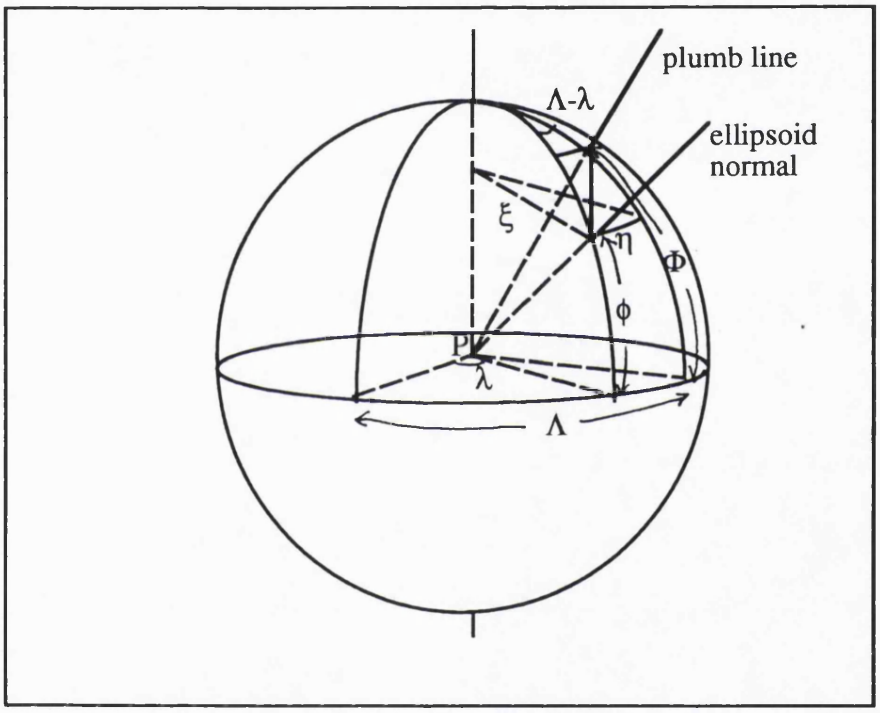

Figure: 3.3 - The deflection of the vertical

At any point the relationship between the geodetic coordinates (ϕ, λ) and astronomical coordinates (Φ, Λ) can be expressed as:

$$\xi = \Phi - \phi \qquad .....(3.4)$$

and

$$\eta = (\Lambda - \lambda)\cos\phi \qquad .....(3.5)$$

where ξ and η are the components of the deflection of the vertical in the meridian and prime vertical, respectively.

The components of the deflection of the vertical can be related to geoid height by:

$$\xi = \frac{1}{r}\frac{\partial N}{\partial \phi} \qquad .....(3.6)$$

$$\eta = \frac{1}{r \sin\phi}\frac{\partial N}{\partial \lambda} \qquad .....(3.7)$$

Since these quantities represent the slope of the geoid, they give ΔN between end-points of a baseline. Figure: 3.4 shows the intersection with a vertical plane of arbitrary azimuth.

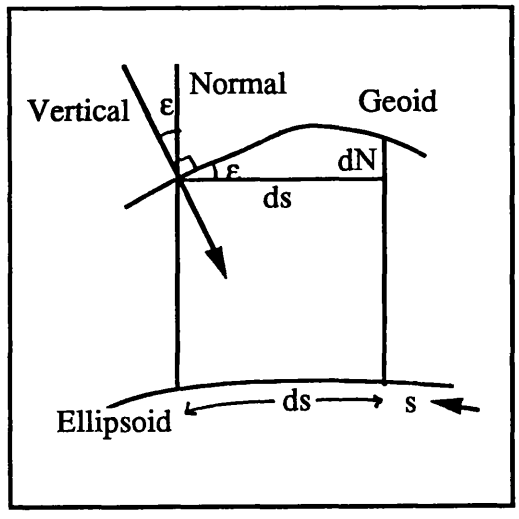

Figure: 3.4 - The relation between geoid height and the deflection of the vertical

If ε is the component of the vertical deflection in this plane, then

$$dN = -\varepsilon ds \qquad .....(3.8)$$

Integrating two vertical deflection points, say between point P and point Q, we get:

$$N_P - N_Q = \int_P^Q \varepsilon ds = -\int_P^Q (\xi \cos\alpha + \eta \sin\alpha) ds \qquad .....(3.9)$$

where α is the azimuth; ds is the distance between point P and point Q.

The above method is known as *astro-geodetic levelling*. The astro-geodetic method has several shortcomings such as a limited accuracy of astronomical observations and atmospheric refraction corrections. Astronomical observations require highly trained personnel and are very much weather dependent.

It has been shown that the astronomic latitude and astronomic longitude can also be determined by the transformation of image coordinates of stars. These image coordinates of the stars are observed by using the *Charge Couple Device* (CCD) - photo electronic imaging device. Details of this approach can be found in Fosu, (1994). In general, the whole process involves the following observational and computational procedures:

(i) The star observations using CCD integrated telescope; the CCD serves as recording device while the telescope gathers the light.
(ii) Automated data reduction and measurement and image processing of the images on the CCD.
(iii) Star identification.
(iv) Reduction of star places.
(v) Computation of Right Ascension (RA) and declination (∂) of the zenith.
(vi) Conversion of RA and ∂ of the zenith to astronomic latitude and astronomic longitude.
(vii) The astronomic coordinates are then compared with geodetic coordinate to obtain ΔN.

This method is less accurate compared to gravimetric procedures because it is believed that although the CCD integrated telescope has a high geometric precision and stability, it does not have a high spatial resolution required in geodetic astronomy, (ibid). In terms of observational and computational procedures, the CCD-astronomical method, however, is more efficient since the whole process is highly automated and fully computerised, ensuring rapidity and reliability of taking measurements as compared to collecting gravity anomaly data which at present still involves manual bisection and recording.

3.3.3 Combined Satellite-Based Data and Levelling

Satellite positioning methods such as the Transit Doppler System or GPS determines positions in a terrestrial 3D-Cartesian frame and the resulting X, Y and Z coordinates are easily convertible (or transform) into horizontal (ϕ, λ) and vertical (h) components, with respect to an arbitrary reference ellipsoid. Details of the coordinate transformations can be found in Bowring, (1976).

The (X, Y, Z) coordinates can be transformed into the (ϕ, λ, h) coordinates by using the following expressions:

(i) The longitude (λ) can be computed directly from:

$$\lambda_P = \arctan\left(\frac{X_P}{Y_P}\right) \qquad .....(3.10)$$

(ii) Computing the latitude, however, is not a straight forward procedure and can be accomplished by using:

$$\phi_P = \arctan\left[\frac{Z_P + e^2 V_P \sin\phi_P}{(X_P^2 + Y_P^2)^{\frac{1}{2}}}\right] \qquad ....(3.11)$$

Here, a problem arises as the right hand terms of equation (3.11) contains ϕ_P, the value sought after. The usual approach is to solve using an iterative method where the initial approximation of ϕ_P is calculated from:

$$\phi_P = \arctan\left[\frac{Z_P}{(X_P^2 + Y_P^2)^{\frac{1}{2}}}\right] \qquad .....(3.12)$$

Using this initial approximation, computation is iteratively carried out until the value of ϕ_P converges.

(iii) Finally, the geodetic height h_P can be computed using:

$$\begin{aligned} h_P &= (X_P^2 + Y_P^2)^{\frac{1}{2}} \sec\phi - V_P \\ &= Z_P \operatorname{cosec}\phi_P - (1 - e^2)V_P \end{aligned} \qquad .....(3.13)$$

where $\nu = \dfrac{a}{(1 - e^2 \mathrm{Sin}^2\phi)^{\frac{1}{2}}}$ is the radius of the prime vertical.

The X, Y, Z coordinates of points in a global geodetic coordinate system observed using satellite techniques (e.g. GPS in WGS84 - Section 2.3.2.3) can be transformed to a local coordinate system (e.g. MEE - see Section 2.3.2.1) through:

$$\begin{bmatrix} X \\ Y \\ Z \end{bmatrix}_{\text{LOCAL}} = \begin{bmatrix} X \\ Y \\ Z \end{bmatrix}_{\text{GEOCENTRIC}} + \begin{bmatrix} \Delta X \\ \Delta Y \\ \Delta Z \end{bmatrix} \qquad .....(3.14)$$

where ΔX, ΔY, ΔZ are the datum shifts that are needed to transform the geocentric coordinate to the local coordinate system.

If additional information on the transformation parameters i.e., rotations (R_x, R_y, R_z) and scale (s), is needed, then the seven parameter transformation methods can be implemented using either *Bursa-Wolf* or *Molodensky* models. Details of datum transformation between the WGS84 and the MRT48 will be briefly described in Section 4.5.2.

The GPS surveys determine ellipsoidal height which will not correspond to geoid height. This parameter, however, is related to the orthometric height and the geoid height using equation (3.1). The orthometric height is derived using the conventional levelling technique referring to a vertical datum which is typically defined by one or more reference tide gauges. If a fairly large number of well distributed points with known ellipsoid and orthometric heights are available for an area, then the parameter N can be determined, which then can be represented as a geoid chart, see Section 4.5.1 and Section 4.5.3.

3.3.4 Satellite Altimetry

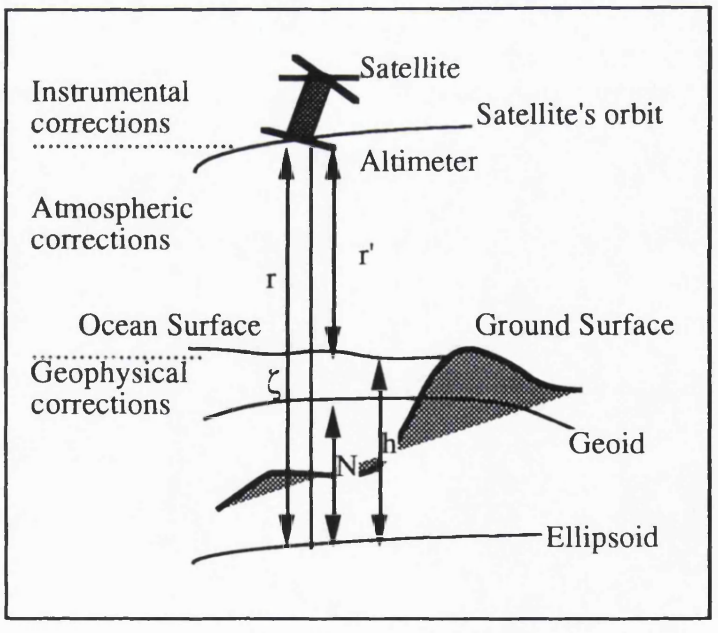

Figure: 3.5 - The geometry of geoidal and sea surface height determination by the Satellite Altimetry

As illustrated in Figure: 3.5, a satellite carrying a vertically orientated radar altimeter can measure continuously the distances to the sea surface below the satellite. Such altimeters have been flown on board the *SKYLAB* in 1974, *GEOS-3* in 1975,

SEASAT in 1978, *GEOSAT* in 1985, *ERS-1* in 1991 and *TOPEX* in 1992. Satellite altimetry is a technique whereby a satellite orbiting above the earth both emits shorts bursts of electromagnetic waves downward and records the time of arrival of pulses reflected from a footprint on the surface of the ocean. From these timings, the vertical distance between the satellite and sea surface can be derived. The satellite is constantly tracked by a number of ground tracking stations of known position in order to determine the orbit.

From Figure: 3.5, knowing the orbital altitude of the spacecraft above the reference ellipsoid, the geoid height can be obtained as:

$$N = h - \zeta = (r - r') - \zeta \qquad .....(3.15)$$

where:

- N is the geoid height;
- r is the geodetic height of the spacecraft;
- r' is the measured altitude of space craft above the ocean surface corrected for the instrumental, atmospheric and geophysical effects;
- h is the height of sea surface above the reference ellipsoid; and
- ζ is the sea surface topography.

The *sea surface topography* (SST) is the departure of the mean sea level from the geoid. The causes of SST include ocean currents, water density variation , as well as air pressure and wind stress. The effect of unremoved SST from the altimeter observations can cause long wavelength error in the recovered gravity anomalies.

In an ideal case, a satellite altimeter measurement is equal to the instantaneous distance between the satellite geocentre and the sea surface. However, an altimeter measurement is subject to many disturbances which have to be accounted for. The measured quantities in the satellite altimetry are therefore usually given as a set of geophysical data records that include altimeter measurement information as well as corrections that should be applied to the data. The corrections include: corrections due to position offset of the altimeter instrument from the satellite's geocentre; geophysical corrections for the atmosphere's effect on radar range measurement, i.e. atmospheric and ionospheric correction; and corrections for the effect of earth tides and ocean tides.

3.3.5 Satellite Perturbation Data Analysis and Combined Data Sources

On a global scale, the geoid height of a point can be derived from sets of coefficients consisting of a series of spherical harmonic expansions. The coefficients of the various terms in the series are determined using satellite perturbations data

analysis which are known as *satellite-only solutions.* These models (for the long wavelength geoid features) involve only low order spherical harmonics and thus contain relatively few coefficients. Some examples of this type of model are shown in Table: 3.3.

Model	Degree (Harmonic)	Number of Coefficients
GEM-9 (Lerch et.al., 1979)	30	594
GEM-L2 (Lerch et.al., 1982)	30	594
GEM-T1 (Marsh et.al., 1988)	36	1406
GEM-T2 (Marsh et.al., 1989a)	50	2028

Table: 3.3 - Satellite-only solution

Satellite-only geopotential models have varied applications. Their use in local gravity field studies, however, is restricted as they lack the detailed information of higher degrees. Terrestrial data accounts for this extra detail but lacks the global coverage needed to determine lower frequencies well. A combination of the two data sources allows the definition of the spectrum over a greater range of frequencies which are more appropriate to local and detailed studies. Therefore, in the past several years, a number of advances have taken place that enable a more accurate high-degree to be computed. These developments include improved theoretical modelling, more accurate and complete satellite models, improved and expanded terrestrial data, more accurate processing of satellite altimeter data, and advancement of computer technologies that enabled large-scale computational problems to be solved.

A series of geopotential models of increasing harmonic coefficients is developed by adding surface gravimetry and satellite altimeter data over the ocean (both having medium to short wavelength features, respectively - see Table: 3.2) to the satellite-only solutions. This combination is then adjusted in a least squares sense. Generally, the more coefficients there are in a model, the more precise the model usually is since it contains shorter wavelength information of the earth's gravity field. Such models have now been published up to a maximum degree and order (n_{max}=360°) which, theoretically at least, can model features in the geoid with half wavelength of 0.5 degrees, or about 55 km spatial resolution, to an accuracy of ± 0.2 m as described by Rapp, et.al, (1991). All higher degree geopotential models have contributed to the more accurate approximation of the gravity field in local and

regional evaluations. The enormous impact of high degree geopotential models on local geoid determination is due to the need to reduce the size of computation areas without inducing errors through neglecting long wavelengths and remote effects. Table: 3.4 shows examples of these type of geopotential models.

The difference in degree of expansion is due to the amount of terrestrial data involved: as a general rule, the degree of expansion is determined by equation (3.3) where φ is the size of the block in which gravity anomaly is given. Therefore, for example, GPM2 uses 1° x 1° mean gravity anomalies and OSU89B is based on 30' x 30' data.

Model	Degree (Harmonic)	Number of Coefficients
GEM10B - (Lerch et.al., 1981)	36	1406
RAPP78 - (Rapp, 1978)	180	32942
RAPP81 - (Rapp, 1981)	180	32942
GPM2 - (Wenzel, 1985)	200	40602
OSU86E and OSU86F - (Rapp and Cruz, 1986)	360	130682
OSU89A and OSU89B - (Rapp and Pavlis, 1990)	360	130682
OSU91A - (Rapp et.al., 1991)	360	130682

Table: 3.4 - Higher degree geopotential models

The development of the GEM10B and RAPP81 models are based on GEM-9 satellite-only solution. GPM2 and OSU86E/F are based on the GEM-L2 model, and OSU89A/B and OSU91A on the GEM-T2 model. The geopotential models are normally checked and tested in several ways so that they represent a substantial improvement over previous high-degree expansions. These tests include satellite orbit residual analysis, Geosat geoid height comparisons and GPS/levelling geoid height differences. Details can be found in Rapp and Pavlis, (1990) and Rapp, et.al., (1991).

The geoid height N_{GM} of a point is computed from a set of normalised geopotential coefficients C_{nm} and S_{nm} using the following formula relating to the spherical harmonic expansions of the geopotential (Heiskanen and Moritz, 1967):

$$N_{GM} = \frac{GM}{r\gamma}\sum_{n=2}^{n_{max}}\left(\frac{a}{r}\right)^n \sum_{m=0}^{n}[\bar{C}^{*}_{nm}\cos m\lambda + \bar{S}_{nm}\sin m\lambda]\bar{P}_{nm}(\sin\phi) \qquad .....(3.16)$$

where:

n_{max} is the maximum degree at which the coefficients are known, e.g. 360;
$\bar{C}^{*}_{nm}$ is C_{nm} less the zonal coefficients of the normal potential of the selected reference ellipsoid;
GM is the earth's gravitational constant;
a is the earth's equatorial radius;
r is the distance from the earth's centre of mass;
ϕ, λ is the geocentric latitude and longitude;
$P_{nm}(\sin\phi)$ is the normalised associated Legendre function;
γ is the normal gravity; and
n, m are the degree and order, respectively.

In practice, the ability of geopotential models to provide a reference field for local geoid determination varies according to the model used, and its maximum degree and order which also depends on a number of factors including the data type used and the extent and density of the data coverage. Some areas will be better modelled than others, and tests have shown significant differences in the ability of geopotential models to recover geoidal height differences, see Kearsley, (1987) and Rapp and Wang, (1993). In terms of computing time, it can be expected that the higher the degree and order of the harmonic adopted, the more computer time is needed is solving the above equation. A comprehensive discussion and comparison of methods for computing equation (3.16) is given by Tscherning et.al., (1983). In this study, the available OSU89B geopotential model is to be tested for modelling the gravity field over the region of Peninsular Malaysia. The exercise will be presented and discussed in Section 5.3.

3.3.6 Satellite Gradiometry

The Satellite gradiometry technique makes use of *gravity gradiometers* to measure values of the spatial second derivatives of gravitational potential in situ in satellite orbits, see Torge, (1989 - Chapter 8). The primary objective of satellite gradiometry missions is the determination of a detailed structure of the earth's gravity field with a precision of approximately ±5 to ± 10 cm, when expressed in terms of geoid heights, or ±3 to ±5 mgal in terms of gravity anomalies and with a resolution of 50 to 100 km over land as well as over oceans. In order to meet this objective, several mission requirements must be considered, for example, using a gradiometer with a

precision around 10^{-2} to 10^{-4} Eötvös (E) and selecting a low altitude orbit less than 200 km.

Because of physical inaccessibility problems, e.g. mountainous areas, it is almost impossible to collect gravity data covering the whole peninsula region. Therefore, satellite gradiometer technique is one of the gravimetric tool to determine the gravity field precisely. In the near future, the analysis of satellite gradiometer data is expected to be effective in increasing our knowledge of the fine structure of the earth's gravity field over the land and ocean of this region and elsewhere.

There are two gradiometer missions proposed for the 1990's that promise high-resolution gravity data. They are the *Aristoteles Mission* and the *Superconducting Gravity Gradiometer Mission.* The gradiometer measurements are represented by the tensor component Γzz, Γzy, Γyy where the subscripts z and y denote components in the satellite radial and cross-track directions, respectively. The outputs of the gradiometer will be the differences of the gravity field measured at each accelerometer centre. Consequently, gravity gradients can be derived from these outputs. In an earth-fixed orientation, the gravity gradient is along the Γzz component.

There are two types of error that effect the measurements of the accelerometers namely: the system errors and the measurement errors. The system errors are introduced by the non-gravitational perturbations, satellite angular motion, change of satellite geometry and mass distribution. These errors in turn will induce measurement errors that include bias, scale error and orientation error for each accelerometer.

3.4 Geoid Users and Their Requirements

The general approach which will be emphasised in this section is that which uses gravimetry to find N. In its strict sense, the term gravimetric method refers to solutions of the BVP described in Section 2.6, whereby N is determined from gravity anomalies Δg on the boundary surface.

Table 3.5 summarises the uses for which geoid heights are required, the precisions to which they are required by the user, and possible ways of obtaining N. Obviously, the choice will be dependent on the availability of geopotential models, terrestrial gravity data and topographic models. In general, if the area is adequately sampled with these types of data, there should be no barriers to gaining ΔN to the highest possible precision.

N used for	Order of N	Possible means of evaluating N
1.Geophysical exploration, Reconnaissance surveys	Low: $\sigma_N \sim \pm 5$-10m	Low order ($n_{max} = 36°$) geopotential models
2.Transforming between geodetic datums	3rd. order: $\sigma_N \sim \pm 1$-2m	High order ($n_{max}=180°$) geopotential models
3.Control surveys for large scale mapp., engineering projects	2nd. order: $\sigma_{\Delta N} \sim \pm 10$-20cm over 20 km (5-10ppm)	a) Surface fitting N, as measured by GPS and levelling b) Detailed gravimetric evaluation
Height control: (between 2nd.to 3rd. order) from GPS: Special projects	1st. order: $\sigma_{\Delta N} \sim \pm 20$-30cm over 100 km (2-3ppm)	Detailed gravimetric evaluations

Table: 3.5-Geoid requirements and methods of evaluation (taken from Kearsley, 1988)

3.5 Overview of Gravimetric Methods

Using a geopotential model with local gravity data and digital elevation data in geoid computation has become a very commonly used methodology. The geopotential model information contains long and medium wavelength features. The contribution of local gravity is mainly of medium and short wavelength nature whereas the local height data is short wavelength in nature. The optimum combination of these data types leads to solutions that currently give the best resolution of those wavelengths important for a good representation of the geoid. Formally, this solution can be written as:

$$N = N_{GM} + N_{\Delta g} + N_{TC} \qquad .....(3.17)$$

where N_{GM}, $N_{\Delta g}$ and N_{TC} are the contributions of the geopotential model, the gravity anomalies, and the height data, respectively. Figure: 3.6 shows the different contributions for a typical geoid profile in mountainous terrain.

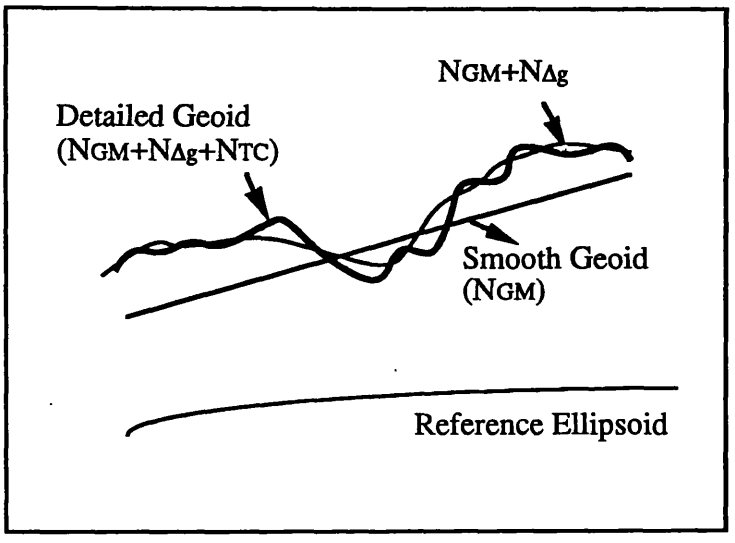

Figure: 3.6 - Contribution of different data to local geoid determination

The contribution of $N_{\Delta g}$ in equation (3.17) is computed using *reduced gravity anomalies* (Δg_r) or *residual anomalies* . These values are obtained by subtracting the observed gravity anomalies (Δg_o) from the effect of long wavelength component, Δg_{GM} (from a chosen geopotential model), and the effect of short wavelength component, Δg_{TC} (from height data). Thus we have:

$$\Delta g_r = \Delta g_o - \Delta g_{GM} - \Delta g_{TC} \qquad .....(3.18)$$

where Δg_{GM} is computed from:

$$\Delta g_{GM} = \frac{GM}{r^2}\sum_{n=2}^{n_{max}}(n-1)\left(\frac{a}{r}\right)^n \sum_{m=0}^{n}(\bar{C}_{nm}\cos m\lambda + \bar{S}_{nm}\sin m\lambda)\bar{P}_{nm}(\cos\phi) \qquad .....(3.19)$$

where the terms are similar to the terms described in equation (3.16). The computation of Δg_{TC} is necessary to account for two effects. First, for the smooth interpolation of gravity anomalies via some type of gravity reductions as discussed in Section 2.7; and second, for the approximate determination of the high frequency part of the geoid heights via *terrain effect*. The terrain effect can be computed using conventional prism integration. The evaluation of the terrain effect is discussed in Section 3.6.

Eliminating these contributions considerably 'smooths' the gravity field causing a much lower variation and more homogeneity. If the global geopotential models perfectly represent the local gravity field, the mean value of the Δg_r should be close to zero. The procedure described for the reduction of the signal to only the medium wavelength component and the later addition of these effects given by (equation 3.17) is known as the 'remove-restore ' technique, and is used nowadays

for most local gravity field studies (especially in mountainous areas) by any gravimetric method. If the geoid height is to be estimated without terrain-reduced anomalies, the free-air anomalies are to be reduced according to:

$$\Delta g_r = \Delta g_o - \Delta g_{GM} \qquad .....(3.20)$$

and no terrain effect is accounted for in the final geoid heights, i.e.

$$N = N_{GM} + N_{\Delta g} \qquad .....(3.21)$$

The remove-restore technique described by equations (3.17), (3.18), (3.20) and (3.21) will be implemented in this study, see Sections 6.6.1, 6.6.3.2, 6.7.1 and 6.7.3.

As mentioned previously, the determination of a detailed gravimetric geoid has been one of the main interests of geodesists because it is needed to convert the high precision ellipsoidal heights obtained from modern GPS technology to orthometric heights. There are several techniques being used in computing the local geoid, such as Stokes' formula, and the LSC method using a combination of heterogeneous data. For faster computation speed, Stokes' formula can also be implemented in the frequency domain using the FFT algorithm. Although all of these three methods have been successfully used in gravimetric solutions, very few direct comparisons between solutions have been made however, see Barzaghi, et.al., (1988) and Arabelos and Tziavos, (1994).

3.5.1 Stoke's Integral

A solution to the BVP was first developed in 1849 by Stokes, a Cambridge mathematician. Stokes formulated a unique solution to Laplace's equation (equation 2.25), as a function, $S(\psi)$, of spherical distance through which the disturbing potential could be determined. In this classical approach the geoid height at any point on the surface of the earth is analytically expressed as an integral of the gravity anomalies, weighted by the Stoke's function over an entire sphere. Thus, the integral that Stokes proposed must be evaluated across the earth and the gravity anomalies must be continuous across the surface. This is clearly not the situation that exists and so problems are introduced. The integration must be limited to a small area around the prediction point, commonly referred to as a spherical cap, where the data will be more consistent with requirements. However, continuous data is still an impossibility; gravity measurements are made at discrete points at some separation. An approximation to the integral is acceptable due to the data situation, in the form of a summation over a set of blocks into which the cap is divided:

$$N = \frac{R}{4\pi\gamma}\sum_{k} S(\psi)\bar{\Delta g}\sin\psi\partial\psi\partial\alpha \qquad .....(3.22)$$

where $\bar{\Delta g}$ is the mean anomaly of the block; and

k is the number of blocks.

For each block, ψ and hence $S(\psi)$ can be evaluated; it is often tabulated for values $0 \leq \psi \leq \pi$ to ease computation. The most information will be contained in a region close to the prediction point.

As stated before, Stokes' function is a solution to Laplace's equation. It is therefore harmonic and can be expanded in a series of harmonic expansion:

$$S(\psi) = \sum_{n=2}^{\infty}\frac{(2n+1)}{(n-1)}P_n(\cos\psi) \qquad .....(3.23)$$

Because the integral is only extended over a local area, the distant, global effects can be eliminated from equation (3.22) leaving the *Modified Stokes' Function.* Lower degrees of expansion in the series may be evaluated by satellite observations as a reference field on which to build the long wavelength geoidal features. The integral kernel becomes:

$$S(\psi)_{N_{max}} = \sum_{n=N_{max}+1}^{\infty}\frac{(2n+1)}{(n-1)}P_n(\cos\psi) \qquad .....(3.24)$$

where n_{max} is the maximum degree covered by the reference fields. The modified Stokes' integral is given by:

$$N = N_{GM} + \frac{R}{4\pi\gamma}\iint_{\sigma}[S(\psi) - S(\psi)_N](\Delta g - \Delta g_{GM})\partial\sigma \qquad .....(3.25)$$

where:

N_{GRAV} is the total geoid height;

N_{GM} is computed using equation (3.16);

R is the mean earth radius;

Δg are the gravimetric observations given as free-air gravity anomalies;

$s(\psi)$ is Stokes' Kernel function (Heiskanen and Moritz, 1967. p. 94); and

Δg_{GM} are free-air gravity anomalies computed in spherical approximation from the geopotential model by the equation (3.19).

The selection of the optimum cap size can be quite tricky. If the geopotential model used were perfect, then the cap size corresponding to the resolution of the global model should in principle be sufficient. However, as the global models may have quite large errors in the coefficients of higher degrees, larger cap sizes are required in many cases, (Sideris and Schwarz, 1986).

Stokes' function is often modified in search of an optimum solution that would minimise the truncation error in equation (3.25), e.g. Molodenskii's Truncation Method and Miessl's Modified Function. Details of this classical method used in determining the geoid height can be found in Wichiencharoen, (1984), Despotakis, (1987), Chang, et.al., (1989), Featherstone, (1992) and Featherstone and Olliver, (1994).

3.5.2 Least Squares Collocation (LSC)

Collocation is a least squares approach to modern estimation theory utilising statistical information based on covariances to describe the function being estimated. Mathematically, the technique is the determination of a function through the approximation of a set of linear functionals, (Moritz, 1980). More simply, the LSC is a generalisation of Least Squares Interpolation such that any arbitrary value can be predicted from any other value. The methods allows an approximation to the anomalous potential T, and subsequently other elements of the anomalous gravity field, (see equations 2.41, 2.42 and 2.43). The data used can be any gravimetric or geodetic measurement, the only requirement being that it can be related to T by a simple linear (or linearised) function. As such, LSC is an optimal estimation technique which statistically combines gravity field information to predict other quantities. This method involves estimation, filtering and prediction processes.

The *covariance function*, as the essential basis of LSC, is a function that allows quantities to be estimated with a minimum variance, and therefore implicitly contains the characteristics of the gravity field of which these quantities are a direct consequence. The vector of signals involved in the collocation formulae can include several different types of signal and the covariance matrices for these are the key to handling such heterogeneous data, e.g. gravity anomalies, deflections of the vertical, and satellite altimeter data. This method has been used extensively in the computation of geoid heights by Forsberg and Tscherning, (1981), Kearsley, et.al, (1985), Dodson and Gerrard, (1989), and Ayhan, (1993) amongst others.

When used specifically to derive N, the relationship can be expressed as:

$$N_{GRAV} = N_{GM} + (A^T C^{-1} A)^{-1} A^T C \Delta g \qquad .....(3.26)$$

where N_{GRAV}, Δg are the vectors of the geoid height and gravity anomalies, respectively; A is the design matrix; C is the covariance matrix, derived from the covariance function; and N_{GM} is the geoidal height computed in spherical approximation using equation (3.16). Details of the LSC method used for this study is fully discussed in Sections 6.2 and 6.6.

3.5.3 Fast Fourier Transforms (FFT)

From a practical point of view, the two categories as described above require either very time consuming numerical integration or large matrix inversion. The need for large amounts of computation time for these methods is particularly significant when dealing with large scale computations in which large volumes of data are involved. This drawback could be overcome by using the FFT method. The FFT method of gravity field approximation is a frequency domain method in planar approximation.

In the FFT method, Stoke's integral is planarised and integrated over a Cartesian rectangular zone of gravity anomalies defined on a grid. However, many approximations are involved that decrease the amount of true information from the gravity field. A full account of FFT and their application to gravity field approximation can be found in Schwarz, et.al., (1990). This approach has been successfully implemented by Zhao, (1989), Mainville et.al., (1990), Tscherning and Forsberg, (1992) and Li and Sideris, (1994). Another similar approach has been carried out by Steward and Hipkin, (1989) who computed the geoid for the British Isles by integrating separately the Bouguer anomaly and the attraction of a terrain model and applying the FFT algorithm.

In general, the computed geoid using the FFT technique is as:

$$N = N_{gm} + \frac{1}{2\pi\lambda} F^{-1} \{ \frac{1}{(k - \frac{2}{R})} F(\Delta g - \Delta g_{gm}) \} \qquad .....(3.26)$$

where F and F^{-1} denote the two-dimensional discrete Fourier transforms and its inverse, respectively and k is the radial frequency.

The FFT method requires gridded gravity data. Thus in this approach, a grid of gravity data is derived from observed gravity over the area of interest and gravity anomalies are transformed to the geoid separation at the same grid point by using the spectrum of the gravity field. The value of N at the points of computation

are then obtained by interpolation from the grid. Details of the FFT technique used in this study is also discussed in Sections 6.3 and 6.7.

3.6 The Terrain Effect Evaluation

As previously mentioned in Section 3.3 (Table: 3.2), the short (or very short) wavelength variations of the gravity field come mainly from the topographic masses, i.e. rugged terrain. The influence of these masses will not be great on the geoid height, but will be considerable in the case of gravity anomalies and deflection of vertical which are much more terrain dependent. A terrain correction causes the gravity field to be much smoother and more homogeneous, as particular detail is removed prior to computations. Thus, in mountainous areas, the terrain effects completely dominate the local variation of the gravity field, and some kind of terrain reduction is indispensable when attempting gravity field modelling in such areas. The application of a good terrain reduction in mountainous areas decreases the gravity field variation to levels comparable with lowland areas, (Forsberg, 1984).

When a topographic model or height data is available, usually in the form of a Digital Elevation Model (DEM), the potential due to the terrain may be developed as a harmonic function to be subtracted from the original function. Again, the signal retains its harmonicity. The various terrain effects in use are illustrated in Figure: 3.7. To use terrain reduced data in a remove-restore technique for gravity field modelling, the utilisation of known or assumed density models is very essential covering a given geographical area.

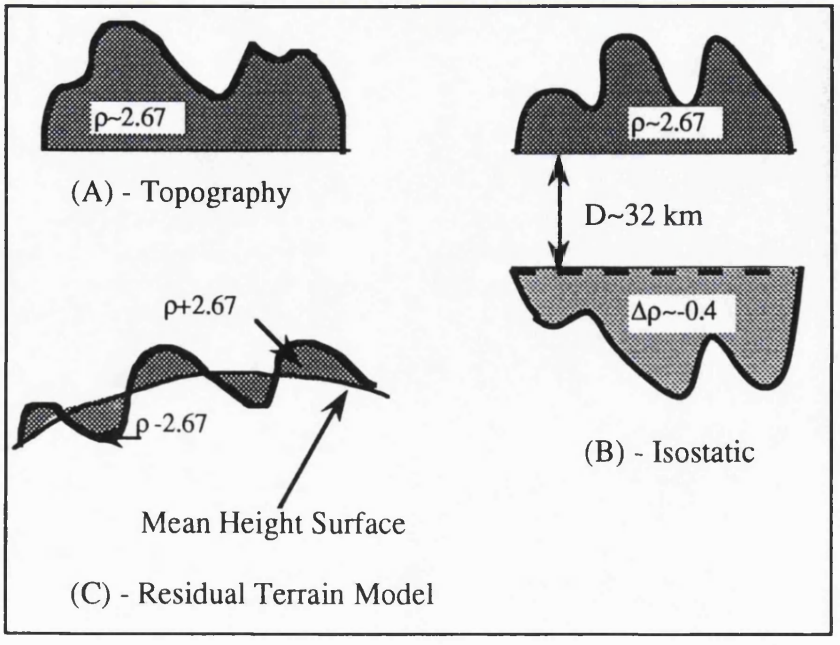

Figure: 3.7 - Density anomalies associated with various terrain effects

The most well known terrain reduction is the topographic reduction or '*a complete Bouguer reduction* ', consisting of the effects of a Bouguer plate minus the terrain correction. The topographic effect is well suited for geophysical work and the prediction of mean free-air anomalies, but is not applicable for reduction of geoid heights. Conventional isostatic reduction (see Section 2.7.3) formalises the prevailing tendency of the earth's topography to be compensated at depth. This type of terrain effect evaluation provide the smoothest residual fields and is easily applicable to all the various types of gravity field data available. A drawback of the isostatic reduction is that it primarily should be global, that is, it requires height or depth data to be integrated over large regions.

An alternative to the use of the isostatic reduction is only to take the short periodic variations of the topography into account. This is done by only considering the deviations of the topography from some mean elevation surface using a *Residual Terrain Model* (RTM) method, see Figure: 3.7 (C). The RTM method has the advantage over the topographic and isostatic reduction methods that a fixed area is unnecessary in the calculations. Another advantage of the RTM method is that, because there is no need for any sort of isostatic compensation masses, the calculation is also quicker as fewer prisms are involved in the '*building* ' of the terrain masses. Moreover, as the RTM have oscillating in positive and negative densities corresponding to the '*removal* ' of mountains and '*filling* ' of valleys, the effect of these will, in general, cancel out at certain distance from the calculation point. Thus, the total mass removed by using a reference surface will on average equal zero, but the major requisite is that the mass removed be a harmonic function. In this way, the recovery of only short wavelength information from the topography has the advantage that elevation data is only needed for a limited area. The application of the terrain reduction used in this study is presented in Section 6.5.

In general, the terrain effect can be quantified for the disturbing potential by:

$$T_{TC} = G\rho \int_{x_1}^{x_2}\int_{y_1}^{y_2}\int_{z_1}^{z_2} \frac{1}{r}\partial z\partial y\partial z \qquad .....(3.28)$$

where $r = \sqrt{(x-x_p)^2+(y-y_p)^2+(z-z_p)^2}$

and ρ is the density for the element.

This computation is most naturally done using the simplest form of finite element representation of the density distribution by assuming that the density anomaly $\Delta\rho$ is constant in each finite element or sub-block with each sub-block being a

rectangular prism, see Figure: 3.8. For terrain reductions using digital models, these prisms, for example, naturally correspond to the subdivision defined by the height data grid. For computational efficiency, the size of these sectors is increased at a distance whereby the majority of the effect is due to very near topography. The integral described in the above equation gives a global estimation. Thus, in practice, the integral need only extend to a given distance from computation point, as the effect of distant topography is negligible. For contributions at a distance r, a condensed formula is used through which equation (3.28) is modified to:

$$T_{TC} = G\kappa \int_{x_1}^{x_2}\int_{y_1}^{y_2} \frac{1}{r}\partial y \partial x \qquad .....(3.29)$$

where κ is the surface mass density $\rho(z_2 - z_1)$.

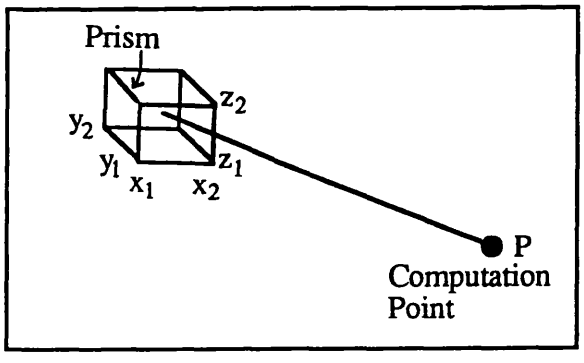

Figure: 3.8 - Terrain effect of distant prism

Terrain contributions to the gravity anomaly and geoid height are given by:

$$\Delta g_h = \frac{\partial T_{TC}}{\partial z} - \frac{2}{r} T_{TC} \qquad .....(3.30)$$

and

$$N_{TC} = \frac{T_{TC}}{\gamma} \qquad .....(3.31)$$

where γ is the normal gravity.

3.7 Techniques of Improving the Geoid Height Estimates

The geoid height computed using the three methods described in Sections (3.5.1), (3.5.2) and (3.5.3) may contain biases due to several factors, such as the problem arising from the differences in the GPS and geoid model datums. This is especially apparent in the case of using a regional or local geoid computed by combining a global solution with terrestrial gravity data. Here, the biases may consist of long wavelength errors contributed by geopotential model errors, poor gravity

coverage and a bad elevation datum for the gravity observations, since barometric levelling is commonly used. These biases can be reduced or absorbed by implementing some kind of transformation procedure as that used by Forsberg and Madsen (1990). The geoid change ($N'-N_{Model}$) due to these biases can be expressed in geodetic coordinates in the form of a *regression formula*, (ibid):

$$N'-N_{Model} = a_1 + a_2\cos\phi\cos\lambda + a_3\cos\phi\sin\lambda + a_4\sin\phi \qquad .....(3.32)$$

By using at least four known geoid heights, N', in the above equation, the four coefficients in the regression model can be computed. These coefficients are then used in computing the correction that will be applied to N_{Model} in deriving the geoid height and orthometric heights at the other points.

The geoid height estimation can also be improved by a technique of 'tailoring' the existing geopotential model with updated gravity anomalies in a specific region. These data should be representative of the block means used to derive the '*corrections* ' to the potential coefficients, see Weber and Zomorrodian, (1988) and Basic, (1989). An analysis of 'tailored' model approach to potential coefficients determination has been carried out by Kearsley and Forsberg, (1990). This paper, however, points out some of the problems in the creation and use of tailored models, for example, poorly distributed and inaccurately observed data (updated data) will seriously degraded the model. As previously mentioned in Section 1.3, the tailoring technique of the geopotential model to fit the regional gravity field will be tested for Peninsular Malaysia. Details of this technique, results and analyses will be fully presented in Chapter 5.

The estimation of the gravimetric geoidal heights can also be improved by optimising the potential coefficient model and by replacing Stokes' kernel function with weighting function, and then reduced the total error in a least squares sense, see Wang, (1993). Thus, by using this technique, the geoid error due to the truncation error, the coefficient error and the error of the terrestrial gravity data is minimised. Finally, the tailoring technique together with the use of *a spatial filter* that considers the statistical information of the geopotential coefficients has also been applied to improve the geoid height estimation, see Li and Sideris, (1994).

CHAPTER 4

THE DATA USED

4.1 Introduction

As previously mentioned in Section 3.3.5, high degree geopotential models are a major source of gravity field information and are invaluable in local studies leading to a solution of the BVP. The combination of the geopotential model with local gravity data and height data currently lead to the optimum resolution of the gravity field which is important for obtaining a good representation of the geoid. This chapter therefore describes and analyses these data types that are most commonly used for this gravimetric geoid height solution, for the Malaysian Peninsular region. These include the available surface gravity data, the existing geopotential model OSU89B and the height data. In addition, some GPS data used as a test for geoid height comparisons is also described as well as the limitations imposed by the data used which offers insight into the accuracy of geoid height estimation.

4.2 Gravity Data

Since 1983, more than 4500 gravity points have been observed independently in Peninsular Malaysia at the international, regional, road traverse and local scales by different organisations for various purposes. All gravity data were tied to the IGSN71 stations (Section 3.3.1) and these observations can be divided into four categories:

(i) Occupation of 180 gravity base stations carried out by the Department of Surveying, University of Technology Malaysia (UTM) and Directorate of Surveying and Mapping, Malaysia (DSMM) to form the Gravity Base Network throughout the country, started from 1983 to late 1991. The first net comprising 31 stations covering the most strategic areas, was established by UTM from 1983 to 1985 to meet the requirements of geophysics, geology and geodesy. These were the first order gravity measurements which were carried out along the coastal areas and levelling lines to produce the first comprehensive gravity base network for the country. Two *La Coste and Romberg gravimeters* (G540 and G542) were used in the measurements of the base net. The gravity base stations were tied and adjusted within the framework of the three IGSN71 stations, namely at Kuala Lumpur (02631A) and Singapore (02613A) and Songkla, Thailand (G9). The final adjustment showed a point standard error of better than ± 0.05 mgals, (Majid, 1987). The number of regional gravity base stations has been increased to 180 points covering the entire country.

These gravity surveys were also conducted independently by UTM (1987-1989) and DSMM (1990-1991).

(ii) A total of about 1200 gravity data points covering the upper part of the west coast area have been collected by the Department of Physics, University of Sciences, Malaysia (USM). The gravity surveys were carried out from 1983 to 1988, (Loke and Lee, 1989). The observed accuracy is estimated as ± 0.2 mgals. The regional gravity surveys covering the southern part of the Peninsular Malaysia have been carried out by UTM since 1989. Up to 1991, a total of about 700 gravity data distributed over the accessible area had been gathered with an observed accuracy of ± 0.1 mgals, (Majid, et.al., 1989). The example of gravity data format supplied by UTM is shown in the Appendix B.

(iii) The regional gravity surveys irregularly distributed over the peninsula had also been carried out by the DSMM from 1990 to 1993. These surveys were conducted for the purpose of applying orthometric corrections to the levelled heights throughout the peninsula and the gravity survey was designed to follow the gravity base network route and the proposed levelling route. Out of a total of about 1200 gravity observations, only 601 'validated' gravity values were made available in March, 1994 to be used in this study, (Samad - Private Communication). Appendix C shows the format of the gravity data files from the DSMM.

(iv) The GSM is in the process of establishing gridded gravity survey with a density of one station at every 25 km^2 for this region. These include a total of 1775 stations in the northern region (covering an area of 40,000 km^2) and 520 stations in the southern region (covering an area of 13,000 km^2). The accuracy of this gravity is of the order of ± 0.2 mgals. These gravity data were made available in June, 1994 to be used in this study, (Zawawi, Private Communication). The format of the gravity data files from the GSM is shown in Appendix D.

4.2.1 Formatting the Gravity Data

It has to be mentioned here that, since the gravity data were supplied by the DSMM and the GSM at a very late stage of this study, only the gravity data collected by the USM and the UTM were used in the tailoring procedure, see Section 5.5. However, all gravity data collected by these two universities, the DSMM and the GSM were used in the geoid determination for the three test areas. The analysis of these test areas will be presented in Section 6.4.

Since three separate files were obtained with different formats, these files therefore have to be individually edited to yield files with the same format structure, and

which could be eventually concatenated. Consequently, a number of *FORTRAN77* programs had to be written for this editing exercise. The program *FILORG.FOR* was written to read and to format the gravity data files provided by the DSMM and the GSM, so that they will have the same format as with the UTM gravity data file. The written *SORDAT.FOR* program was employed in sorting the data in the UTM, DSMM and GSM files in order of increasing latitude. Three original files contained common points, and in some cases each file contained one or more duplicates of some of the gravity points. These had to be eliminated, and the program *DELDAT.FOR* was designed for this purpose. For this purpose, it was decided that two stations were deemed to be the same, if they are within 0.° 0005 (approximately 50 m) of each other. A total of 23 common points were eliminated from the original 4891 data points, leaving 4868 data points which were then stored in file *GRAV.MSIA*. This gravity data file listed the identification number of each point; its position in latitude and longitude; elevation; the free-air anomaly and the Bouguer anomaly. The Bouguer anomaly in this case is the simple Bouguer anomaly, since the terrain reduction methods described in section 3.6 have not been applied.

4.2.2 Distribution and Characteristic of Gravity Data

In general, much attention has been paid to and enormous effort put into gravity measurement with a dense and sufficiently uniform distribution along the coastal and fairly flat areas, while in remote land areas and mountainous regions, gravity data is very sparsely distributed or simply not available because of physical inaccessibility problems or lack of levelled heights. Thus, the observed gravity data are seen to be very unevenly distributed and in some areas there is no observed gravity at all. The area containing the terrestrial observed gravity points is basically plateau, lying between 5 metres to 1000 metres altitude. The heights of the stations were obtained mainly by two means: some 20% of the total stations were located on the levelling benchmarks and the heights of the remaining stations were obtained by altimeter readings with resulting accuracy of ± 1.5 meters, implying the accuracy in the gravity anomaly of ±0.5 mgals. The estimated errors for the regional gravity surveys is of the order ± 0.2 mgals. The distribution of the gravity points extracted from *GRAV.MSIA* file is shown in Figure: 4.1.

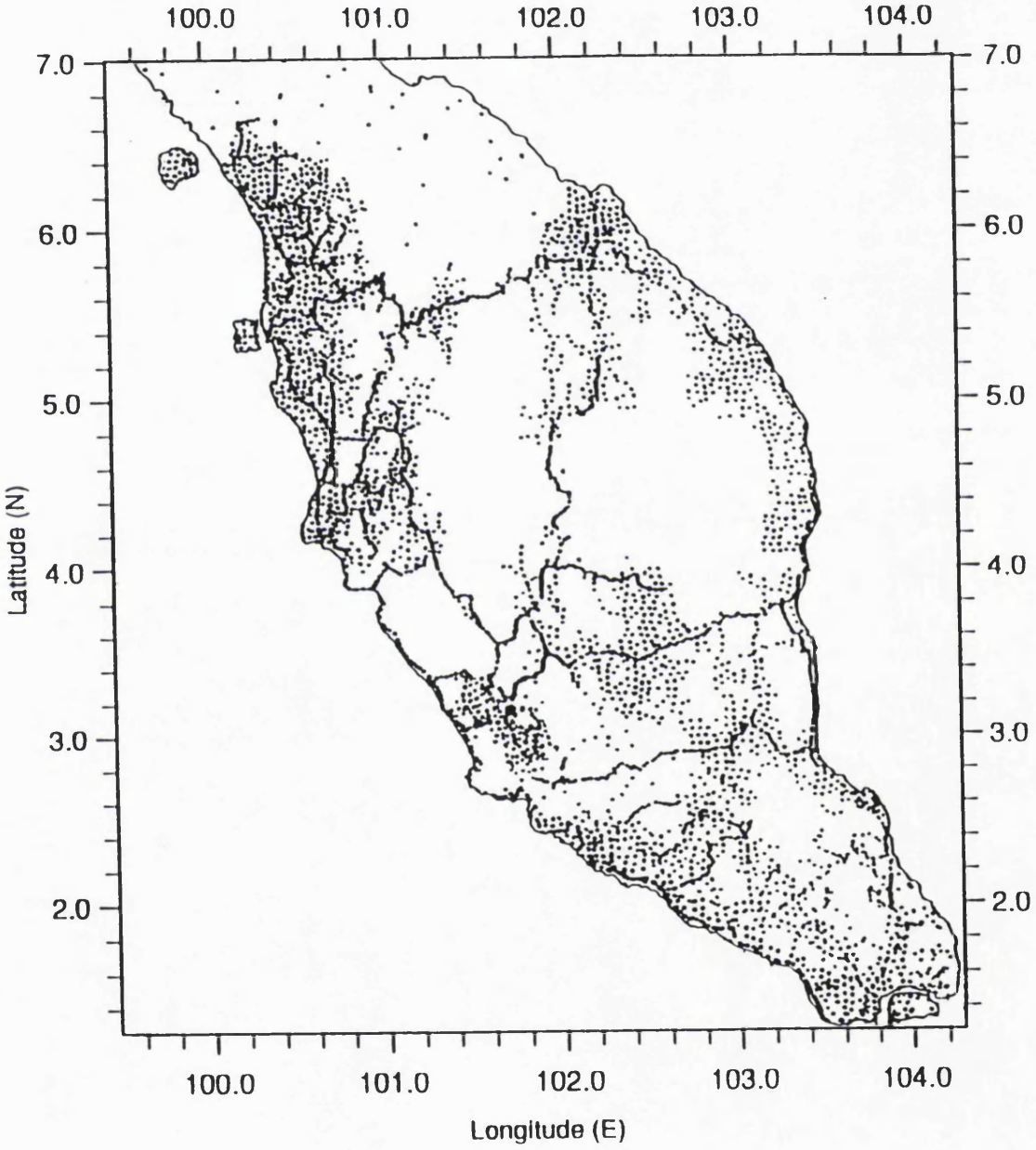

Figure: 4.1 - The Distribution of gravity points in Peninsular Malaysia

It can be seen from Figure: 4.1 that the density of gravity data for the northern region is quite low and irregular, for example on average one gravity station per 40 km^2, compared to, on average one gravity station per 30 km^2 for the southern region. A reasonably good gravity coverage is found on smooth to medium terrain in the south-west region of the peninsula which is, on average about one gravity station per 20 km^2. The rest of the region is considered to be medium to poor gravity coverage regardless of whether they are located in the smooth or medium topography. Due to very rough topography and the remoteness of the area, most parts of the north-east, the south-east and the central-north of the peninsula have less than ten gravity points or have no observed gravity at all.

The first compilation and adjustment of the measured gravity data in the Malaysian Peninsula can be found in (UTM, 1989). The gravity data obtained from UTM consisted of 1900 stations, parts of which was the gravity data from USM. Data reduction was done using the GRS80 formula and the Bouguer correction was made with an assumed density of 2.67 g/cm^3. In the creation of the gravity data base, the main problem was the detection of gross errors in gravity anomalies. The procedure applied to validate the gravity data, in principle, depends on the predicted value for each point using weighted means and the data collected inside a radius of 50 km, (Majid, 1992 - Private Communication). In this prediction method, the differences between the predicted and the observed values larger than 2.5 times the standard error of the differences, then the gravity data have been detected as doubtful gross errors. Consequently, about 5% of the points in the gravity data base were excluded after being indicated as gross errors. Thus, in total 1815 validated gravity data points extracted from the UTM gravity database are specifically used for the formation of mean free-air anomalies in the tailoring procedure, see Section 5.4.

The free-air anomaly values vary between -30 to 83 mgals. Figure: 4.2 shows the contour map of these anomalies with a contour interval of 5 mgals. It can be seen from this figure that the free-air anomaly associated with points of height less than 200 metres varies from -30 to 30 mgals in the northern part of the peninsula and from 0 to 30 mgals in the south. Due to the fact that the free-air anomaly at low altitude approximates the Bouguer anomaly, the variation of the anomalies is believed to be influenced mainly by the variation in the bedrock density of those particular areas.

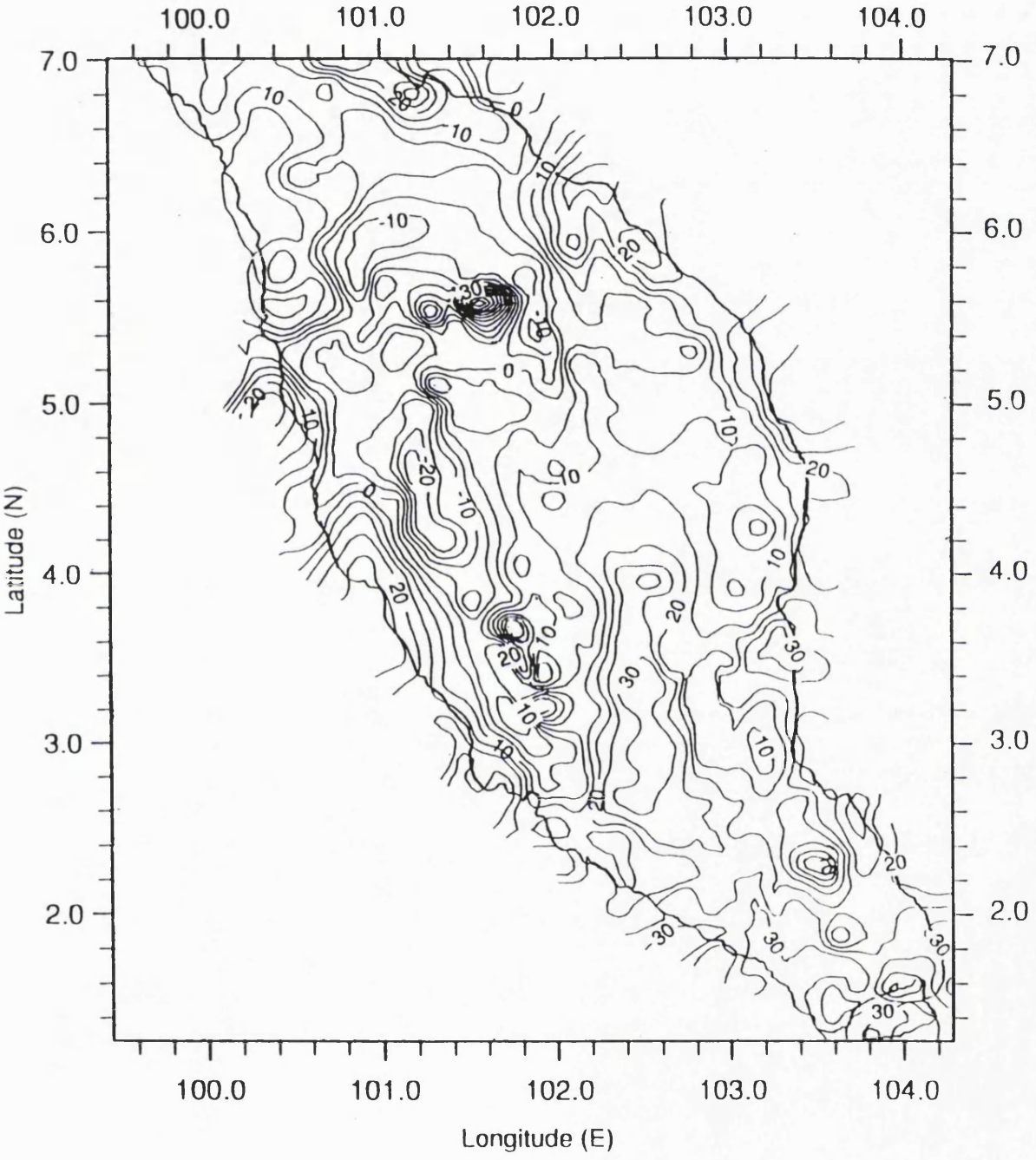

Figure: 4.2 - Free-air anomaly map for Peninsular Malaysia - (C.I = 5 mgals)

Free-air anomalies are usually found to be correlated with the point height due to the effect of topographic masses in the short-wave range. The correlation is approximately expressed by:

$$\Delta g_F = a + bH \qquad .....(4.1)$$

where 'a' is a variable which approximates the simple Bouguer anomaly Δg_B; and 'b' is also a variable which usually regarded as an approximation of the constant in the Bouguer reduction, see equation (2.52). The a value changes from area to area but its variability is much less than the free-air anomaly, and b is almost constant, (Sunkel and Kraiger, 1983).

The variation of the free-air anomalies with respect to heights in the peninsular region is shown in Figure: 4.3. In this figure, it can be seen that, at points higher than 100 metres, the free-air anomaly increases proportionately with the increment of height, i.e. between -30 to 80 mgals.

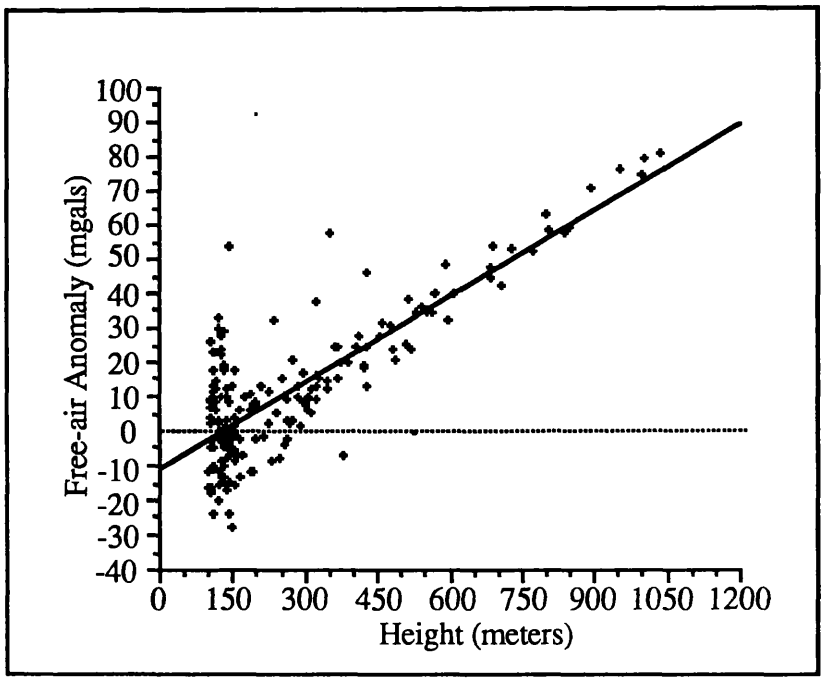

Figure: 4.3 - Correlation between free-air anomaly and height for Peninsular Malaysia

4.3 Height Data

As previously mentioned in Section 3.5, precise gravity field modelling requires the combination of all the available data especially in areas showing strong variations in the gravity field, e.g. mountainous areas. Among other data types, the information concerning the visual topography and its isostatic compensation is very important for smoothing the gravity field. Such information relates to the effect of the topography on

the earth's gravity field, i.e. the high frequencies of the gravimetric signals (see tables 3.1 and 3.2). For the computation of various kinds of topographic corrections discussed in Section 3.6, a DEM is needed comprising the appropriate coverage and resolution. For regional or global scale computations there are global DEMs available with different resolutions. Such a DEM is the *ETOPO5U* 5' x 5' mean heights and depths. In local scale computations, precise and high resolution local DEMs are usually available in the framework of national geodetic banks.

4.3.1 ETOPO5U Global Digital Elevation Model

The original DEM supplied by the *International Geoid Service* (IGS), Milano-Italy was the ETOPO5U 5' x 5' mean heights, covering the peninsula region in the geographical window ($0° \leq \phi \leq 7°$, $99° \leq \lambda \leq 105°$), see Figure: 4.4. The resolution of this global scale terrain database is, however, known to be very poor in many regions, especially in the Asian regions, (Sanso, 1993 - Private Communication). On land, the 5' x 5' height data have been interpolated from a 10' x 10' mean height data set, originally estimated by visual inspection of small scale maps. It has been shown that, the use of this global DEM may produce errors in the gravity field modelling process, as any systematic errors in the DEM will show up as corresponding errors in the estimation of mean free-air data. For example, this was found in a preliminary determination of the geoid in the Philippines where the poor gravimetric results are mainly due to low resolution (inaccurate) of the ETOPO5U model and also sparse local gravity data, see Forsberg, (1990).

4.3.2 Local Height Data

An improved DEM of, e.g. 5' x 5' mean height from ETOPO5U would have made the resolution of the geoid prediction a lot better. Ideally, of course, a fine height grid, say 1 km to 5 km, depending on the roughness of the topography should be used because a strong gravity signal is due to the gravitational attraction of the topographic masses itself, i.e. a signal which dominates at shorter wavelengths, see Forsberg, (1984). However, no such data were available for the whole peninsula.

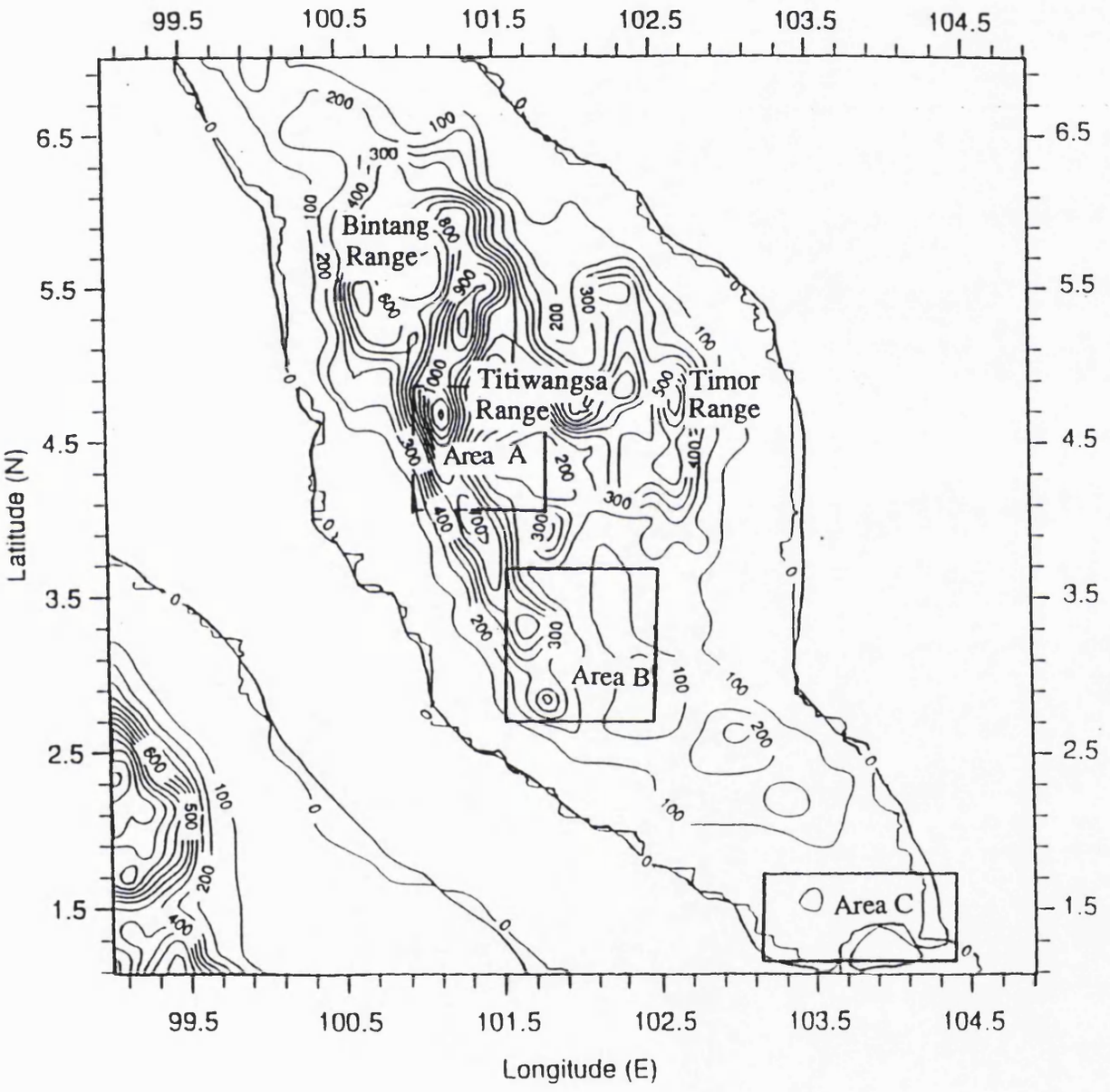

Figure: 4.4 - The 5'x5' mean heights and depths of Peninsular Malaysia (C.I.=100 m)

Since the principal use of terrain data in local gravity field modelling is to provide a smoother residual field making interpolation easier (see Section 3.6), some form of local DEM should be used. Due to the non-availability of suitable DEM which can be used in this study, the height data were visually estimated by the author from 25 topographical maps (supplied by the DSMM in May, 1994) for three test areas; Area A, Area B and Area C - (see Figure: 4.4). These three test areas were chosen with respect to terrain types, gravity density and coverage viewpoint. Details relating to these three test areas are given in Table: 4.1 and also depicted in Figure: 4.5, Figure: 4.6 and Figure: 4.7, respectively. The height data were gridded in west to east rows sequentially from north to south, according to the format specifications as required by the 'terrain evaluation program *TC1* '- see Section 6.5. Each latitude row comprising one record of elevation values in metres. First record in file is a label record (ϕ_1, ϕ_2, λ_1, λ_2, $\Delta\phi$, $\Delta\lambda$) defining boundary of grid. Obviously, this procedure is very tedious and time-consuming.

Test Area	Block Size (Approx.)	Relief Type (Average Height)	Gravity Coverage	Scale Map/ Contour Interval	Gridded Mean Height
Area A	90km x 90km	Medium - Rough with 15% smooth ~ 600 m	Poor (at lowland area only)	1:50000/ 20 m	1km x 1km
Area B	100km x 90km	Smooth - Medium ~300 m	Average	1:63360/ 30 m	2km x 2km
Area C	60km x 100km	Smooth ~ 30 m	Good	1:63360/ 30 m	5km x 5km

Table: 4.1 - Details of the gravity coverage and heights characteristics in test areas

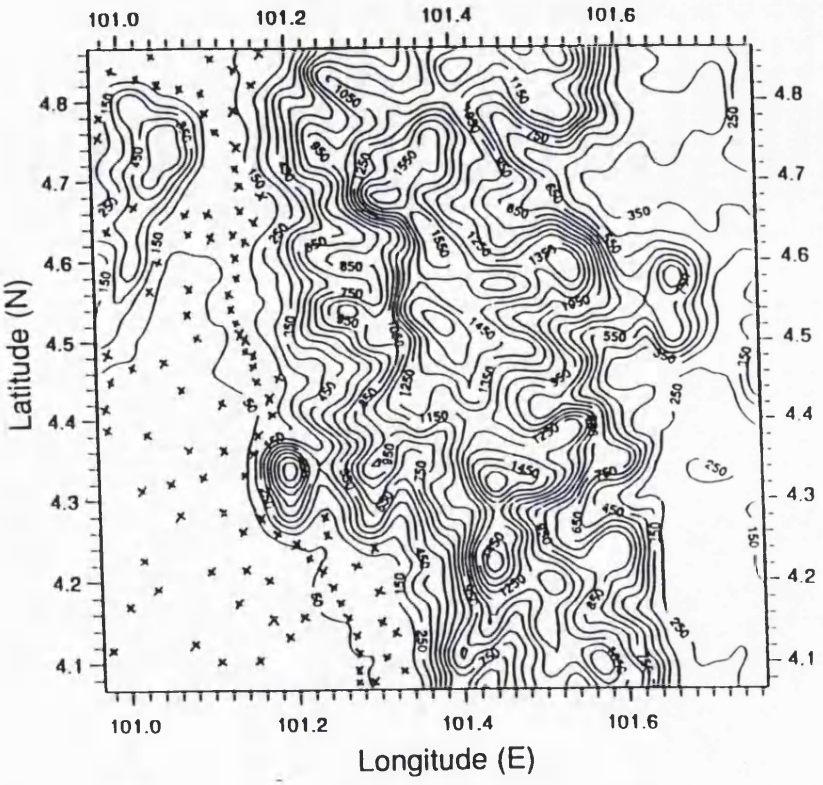

Figure : 4.5 - The Contour Heights and Gravity Coverage of Area A - (C.I.= 100 m)

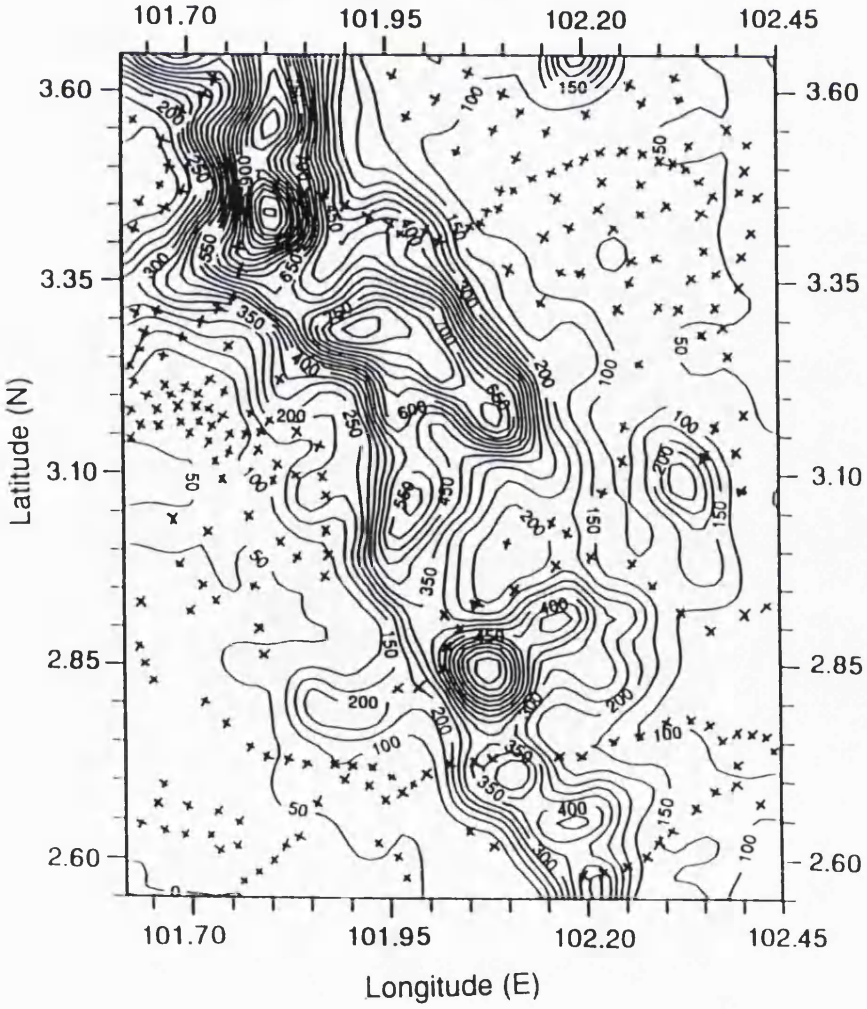

Figure: 4.6 - The contour heights and gravity coverage of Area B - (C.I.= 50 m)

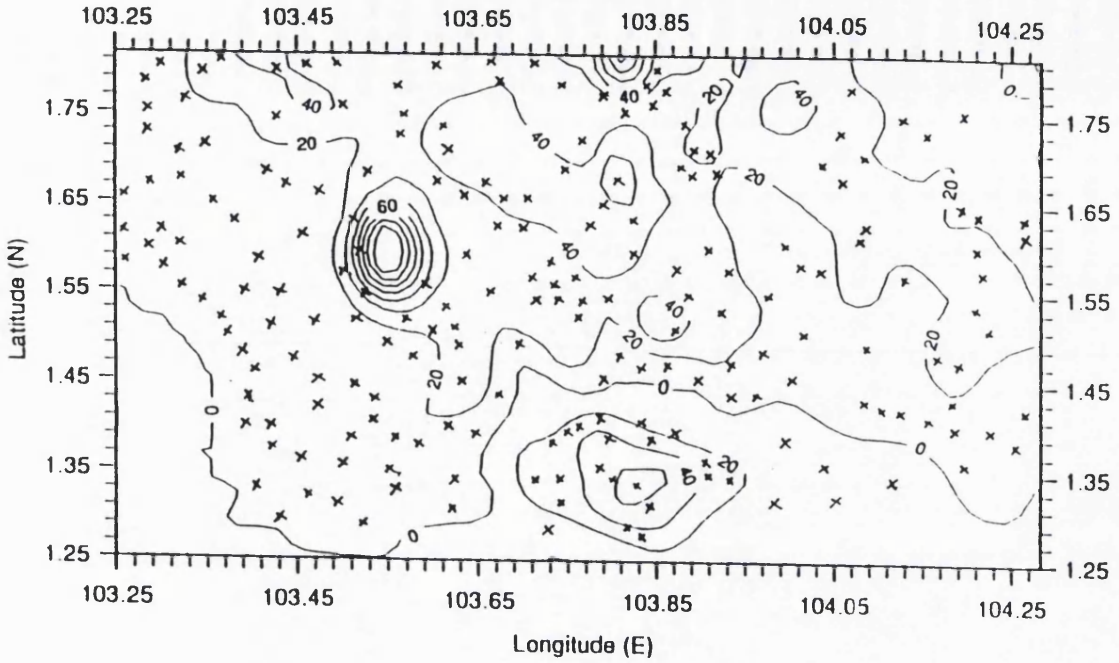

Figure: 4.7 - The contour heights and gravity coverage of Area C - (C.I.= 20 m)

From Table: 4.1, it can be expected that the precision of estimation of heights for the 1: 50000 and 1: 63360 topographical maps, varies from about ±1m for spot heights and points through which contours pass, to about ±10m and ±15m, in between contours where heights are interpolated, respectively. The accuracy of DEM may be assessed by comparison of height values derived from the DEM surface with heights of the corresponding points obtained by measurement of the terrain surface to a known (higher) order of accuracy. The data obtained from such a comparison will consist of height differences at the test points, i.e. gravity points. These values may be positive or negative in sign, depending on the relative heights of the two surfaces at successive points. The computations of the RTM contribution using the height data for all test areas will be presented in Section 6.5.

4.4 Geopotential Model OSU89B

The OSU89B is a high degree spherical harmonic expansion model that has been developed from the combination of satellite perturbation analysis with both surface gravity and satellite altimetry data. The development of the OSU89B geopotential model is briefly described below. Details of the development and analysis of this geopotential model can be found in Rapp and Pavlis, (1990).

The OSU89B global model has been developed through a combination of the GEM-T2 satellite-only solution model ($n \leq 36$), in a least squares sense, with 30'

mean free-air anomalies, to obtain an adjusted set of coefficients and gravity anomalies. The adjusted anomalies were then harmonically analysed to yield a set of potential coefficients to degree 360. The 30' mean anomalies were estimated from updated terrestrial gravity data, from altimeter-derived anomalies, and from 1° x 1° terrestrial anomalies where such data were available. For areas devoid of gravity information, e.g. most part of Asia, Arctic and Antarctic regions, the anomalies were computed in two ways: (i) from the GEM-T2 coefficients only; and (ii) from the GEM-T2 coefficients to degree 36 plus coefficients implied by a topographic-isostatic model. These values will not provide the resolution of the 30'x30' mean anomalies but they will provide valuable gravity field information beyond what is available from satellite orbit perturbations. These 'filled in' anomalies led to two potential coefficient models; OSU89A for method (i) and OSU89B for method (ii). The general development leading to OSU89B potential coefficient model is illustrated in Figure: 4.8. Figure: 4.9 portrays different types of 30' mean anomalies used in a combination solution for this global geopotential model.

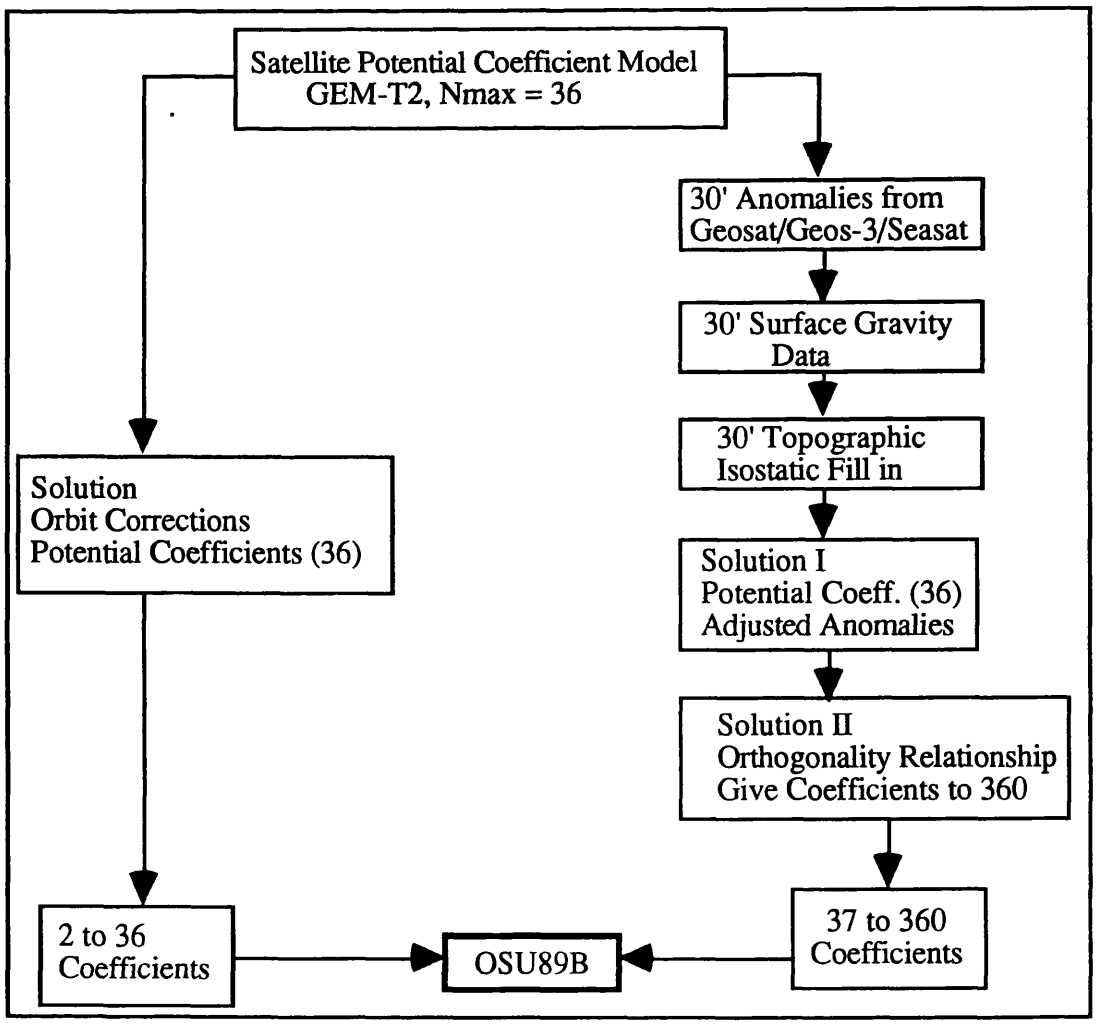

Figure: 4.8 - General development leading to OSU89B potential coefficient model

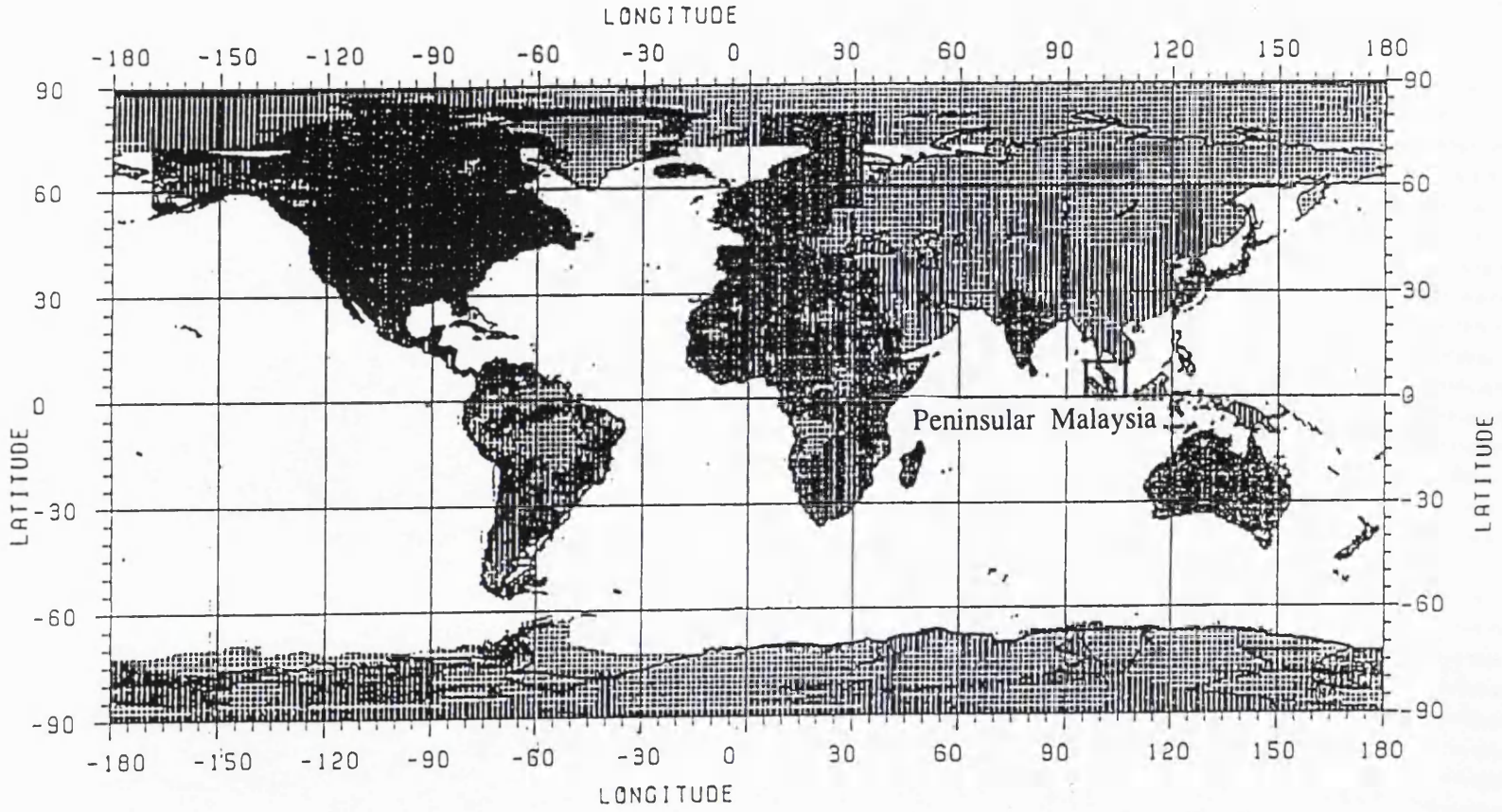

Figure: 4.9 - The distribution of of 30'x30' mean anomalies used in the development of the geopotential model OSU89B.
(The darkest stripping represents the original 30' terrestrial anomalies obtained from the split up of 1° x 1° terrestrial anomalies. The lightest stripping represents the 'filled in' 30' anomalies from a modified topographic/isostatic expansion. Blank areas designate locations where satellite altimeter derived anomalies were used).
(taken from Rapp, 1994)

The OSU89B geopotential model were checked in several ways including satellite orbit residual analysis, GEOSAT geoid height comparisons and GPS/levelling geoid height differences. After correction for sea surface topography, orbit error, and permanent tidal effects, the geoid heights from the OSU89B model had an rms discrepancy with GEOSAT-implied geoid height of ± 59 cm over a complete 17-day exact repeat cycle. The comparisons with GPS information in Canada, Scandinavia, and Australia indicated the accuracy of computation of a relative geoid height is of the order of 3 - 4 ppm of the distance between stations. The OSU89B geopotential model represents a substantial improvement over previous high-degree expansions such as OSU81, OSU86E and OSU86F.

The OSU89B geopotential model has been extensively used to provide reference fields for the anomalous gravity field used for local and regional geoid determination. For example, Sevilla, (1993) and Sevilla, et.al., (1993) used this geopotential model together with the latest geopotential model, OSU91A, and the tailored model IFE88E2 for the gravimetric geoid for the Mediterranean Sea and Portugal, respectively. The tailored model IFE88E2 was proved to be the best reference gravity field for this region when compared to the OSU89B and OSU91A models. It also revealed that there was no significance improvement of the OSU91A model over the OSU89B model, (ibid). It was decided that the OSU91A model will not to be used in this study, due to the following reasons:

(i) This model was not available at the Department of Photogrammetry and Surveying, University College London; and

(ii) No new terrestrial gravity data from this region has been incorporated into world gravity database for the solutions of this latest geopotential model.

Therefore, it is important to discover if the available OSU89B model (although some new gravity data from the peninsular region have not been released to be included in this model) can be used as a reference field for geoid determination in Peninsular Malaysia. This experiment is fully exercised in the next chapter.

4.5 GPS Data

The existing geodetic networks which are currently used are mainly based on field observations and computations made in the first decade of this century. Studies carried out by the DSMM indicated that the network does not meet the requirements of geodetic standard for surveying and mapping purposes. The definition of the Kertau Datum discussed in 2.3.2.1 is incomplete since the geoid height and deflection of the

vertical is not taken into account in the data reduction. Therefore, in Peninsular Malaysia, with many difficult and inaccessible areas, coupled with unpredictable climatic conditions, the use of GPS offers significant advantages both from cost-effectiveness and accuracy in setting-up of a highly precise geodetic network. Details of the GPS satellite surveying method, e.g. satellite configuration, characteristics of satellite and receiver frequency modes, field observations, computation and adjustment procedures can be found in Leick, (1990).

The following section will give a brief description of the work and the results obtained in a GPS campaign in Peninsular Malaysia carried out by the DSMM and the *Overseas Agency of Land Survey of Sweden* (Swedsurvey). Details of the GPS surveys in the peninsula region are fully documented in Thomas and Bo-Gunner, (1991) and DSMM, (1994).

4.5.1 The Malaysian GPS Campaign

The first Malaysian GPS campaign was started in late 1990 when the DSMM and Swedsurvey made a joint project to use GPS technology in positioning of control points. The main objectives of the project are as follows:

(i) To establish a new Geodetic Network for Peninsular Malaysia;
(ii) To analyse the existing geodetic network, i.e. the MRT48;
(iii) To densify points for the production of topographical maps.

The first phase of the project was started in December, 1990 and completed in March, 1991. During this period, 108 points in the southern part of Peninsular Malaysia which consist of existing Doppler, geodetic, primary, secondary and new GPS points were observed with *L1 frequency Ashtech LXII GPS receivers*, see Thomas and Bo-Gunner, (1991). A closer analyses revealed that there were weak spots in the mountainous areas and the eastern part of the new network and in late 1991, a campaign of complementary measurements started in order to strengthen the network by using receivers with both *L1 and L2 frequencies* (*Dual Frequency Ashtech GPS Recievers*). In early 1993, the National GPS Network was also extended to include the northern network by using the same dual frequency Ashtech GPS receivers. In total, 238 GPS stations have been observed that include:

- 5 existing Doppler Stations,
- 13 existing geodetic,
- 8 existing primary,
- 8 existing secondary,

- 8 existing benchmarks, and
- 196 new GPS stations.

However, only 35 GPS stations which partly constitute the Southern GPS Network was made available by the DSMM, (Samad, 1993 - Private Communication). These GPS stations have their orthometric height values either because they were tide gauge stations or partly connected by the trigonometric heighting. Figure: 4.10 shows the contour map of the geoid height that was derived from 35 GPS/levelling points for the 'Southwest GPS network'. Details of the Southwest GPS Network is listed in Appendix E.

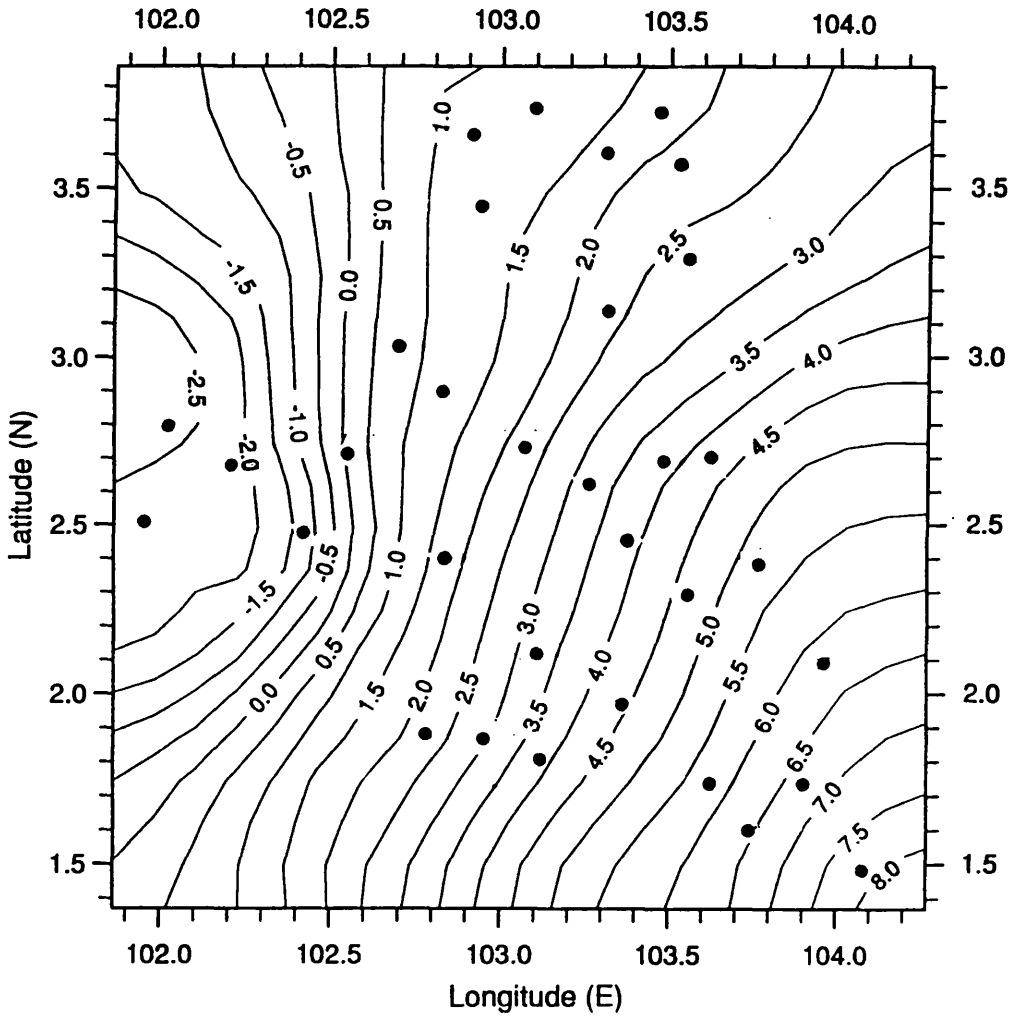

Figure: 4.10 - The contour map of geoid heights derived from 35 GPS/Levelling points for the Southwest Network - (C.I = 0.5 m)

4.5.2 The Analysis of the GPS Campaign

The new GPS network has been computed on an approximate WGS84 datum. For the network adjustment, the *GEOLAB* software was used to perform a simultaneous adjustment in 3D-Cartesian coordinates, (DSMM, 1994). The baseline components or the coordinates sets must be adjusted to a unified network for the whole project. A minimally constrained adjustment was made with Kertau as the fixed point. This datum was constructed by transforming the MRT48 for Kertau Station with the DMA-formula, and then using it as the starting point for the GPS campaign. The DMA-transformation formula was in the form of a three parameter transformation of Cartesian coordinates, (ibid):

$$\begin{bmatrix} X \\ Y \\ Z \end{bmatrix}_{WGS84} = \begin{bmatrix} X \\ Y \\ Z \end{bmatrix}_{MRT48} + \begin{bmatrix} -11m \\ 851m \\ 5m \end{bmatrix} \qquad .....(4.2)$$

Before the computation of the Çartesian coordinates is done, the levelled heights must be corrected for geoid heights according to the formula, (ibid):

$$N_{MRT48} = -3.833 - 2.701U + 17.861V + 0.386U^2 + 0.980V^2 - 0.793V^3 - 2.390UV^3 - 1.455\,U^2V^3 \qquad .....(4.3)$$

where:

$U = K(\phi - 3°)$

$V = K(\lambda - 102°)$

$K = 0.41887902$

There is no description of how the calculation of the formulas was done. The only information is that five Doppler points were used for the three parameter formula and that the accuracy was ± 3m/coordinate, (ibid). The Ashtech's transformation software called *DATUM* used these parameters for the transformation from WGS84 to MRT48.

With this new network, a better relationship can be made between the WGS84 and the MRT48. The *Bursa-Wolf transformation model* was used for the coordinate transformations. In the GPS observations, 32 existing MRT48 points had been observed and then were used for getting the six transformation parameters. These six parameters are as follows, (ibid):

(a) 3 translations:

$\Delta x = 378.57465 \pm 18.32329s$
$\Delta y = -774.53796 \pm 4.68657s$
$\Delta z = 86.17115 \pm 13.30894s$

(b) 3 rotations:

$R_x = 2".59801 \pm 0".43118$
$R_y = 2".10423 \pm 0".23204$
$R_z = -12".11313 \pm 0".60995$

In the case of the MRT48, it was agreed to use the above six parameters instead of seven since a scale factor is not introduced because this parameter is probably more homogeneous in the GPS network, (Thomas and Bo-Gunner, 1991). Another reason is that it gives a better fit in the plane to the existing MRT48 than the solution with the three translations, (ibid). Furthermore, the rotations are fairly small, giving rise to errors in the azimuth of less than one second of arc.

The results of the transformation revealed that the planimetric and height differences between the existing coordinates and the GPS derived coordinates are within ± 1-3 m level. Thus, they are good enough to qualify for use in all mapping works. Furthermore, the distances derived from GPS for the five Doppler points were compared with the original distances and found to come within 1- 6 ppm. By using a three dimensional, six parameter similarity transformation the maximum difference between transformed geodetic heights and the *Land Survey Datum 1912* (LSD1912)[1] mean sea level heights is about one metre for the southern part of the MRT. This difference is principally the result of inaccuracies in the heights of the triangulation points and geoid heights. Thus, in the author's opinion, the results show that GPS cannot be used for height determination (as an alternative to levelling operations) for the entire country until the entire GPS network has been connected to the first-order levelling network.

The on-going scientific work with the advent of the GPS network now includes an analysis of a new MRT to replace the old MRT, for surveying and mapping purposes. To improve the accuracy of heights derived from GPS measurements, the measurement and computation of the precise levelling network should be completed. The new MRT system (from GPS surveys) also should be connected to the precise

---

[1] The LSD1912 had been established by the British Admiralty who carried out tidal observations at Port Kelang (known as Port Swettenham before independence) in order to determine the mean sea level (MSL). This 'uncorrected' value for the MSL was then adopted as the origin for the levelling network.

levelling network, so that in the near future, the precise geoid heights implied by gravimetric methods can be evaluated against the external geoid height estimates, i.e. the geoid heights derived from GPS/levelling network.

Currently, a revision of the first-order levelling network is being executed by the DSMM with the aim of carrying out a simultaneous adjustment of this levelling network. The input data consists of both old data from conventional levelling and new data from the *Motorised Levelling* programme. Up to now, the only results revealed in connection with vertical datum realisation is that the difference between the LSD1912 and the mean sea level values obtained for consecutive years, 1983-1987, at Port Klang tide gauge station is 59mm. Moreover, it has been estimated that the accuracy of the revised heights of the triangulation points is of the order of about half a metre, (DSMM, 1994).

4.5.3 The Federal Territory GPS Project

Since it is impossible at the present stage to produce a precise local geoid for the whole Peninsular Malaysia (mainly because of the unavailability of uniform gravity data -Section 4.2, and lacks of local DEM -Section 4.3), the Federal Territory area has been chosen by the DSMM as the test area for a pilot project in establishing the optimum height values in a fully observed heighting system. The aim of this project is to fully capitalise upon the impact of GPS to provide meaningful height values for the Federal Territory area which can be used for surveying and scientific purposes. Therefore, in early 1994, about 50 GPS stations, spacing between 2 km to 30 km in length were established in the Federal Territory area using four Ashtech dual frequency receivers. One receiver was always operated on a fixed reference station, whereas the other three receivers were used on the traverse simultaneously. The field work as well as the coordinate adjustment computations of these control points were done by the DSMM, which made this data set available in April 1994, (Samad - Private Communication).

In conjunction with this GPS campaign, orthometric heights were also established at these control points from the second order and tertiary levelling lines, for which no homogeneous adjustment has been performed. Details of the Federal Territory GPS Network project is listed in Appendix F. Figure: 4.11 depicts the location of GPS stations and the contour of GPS-derived geoid heights.

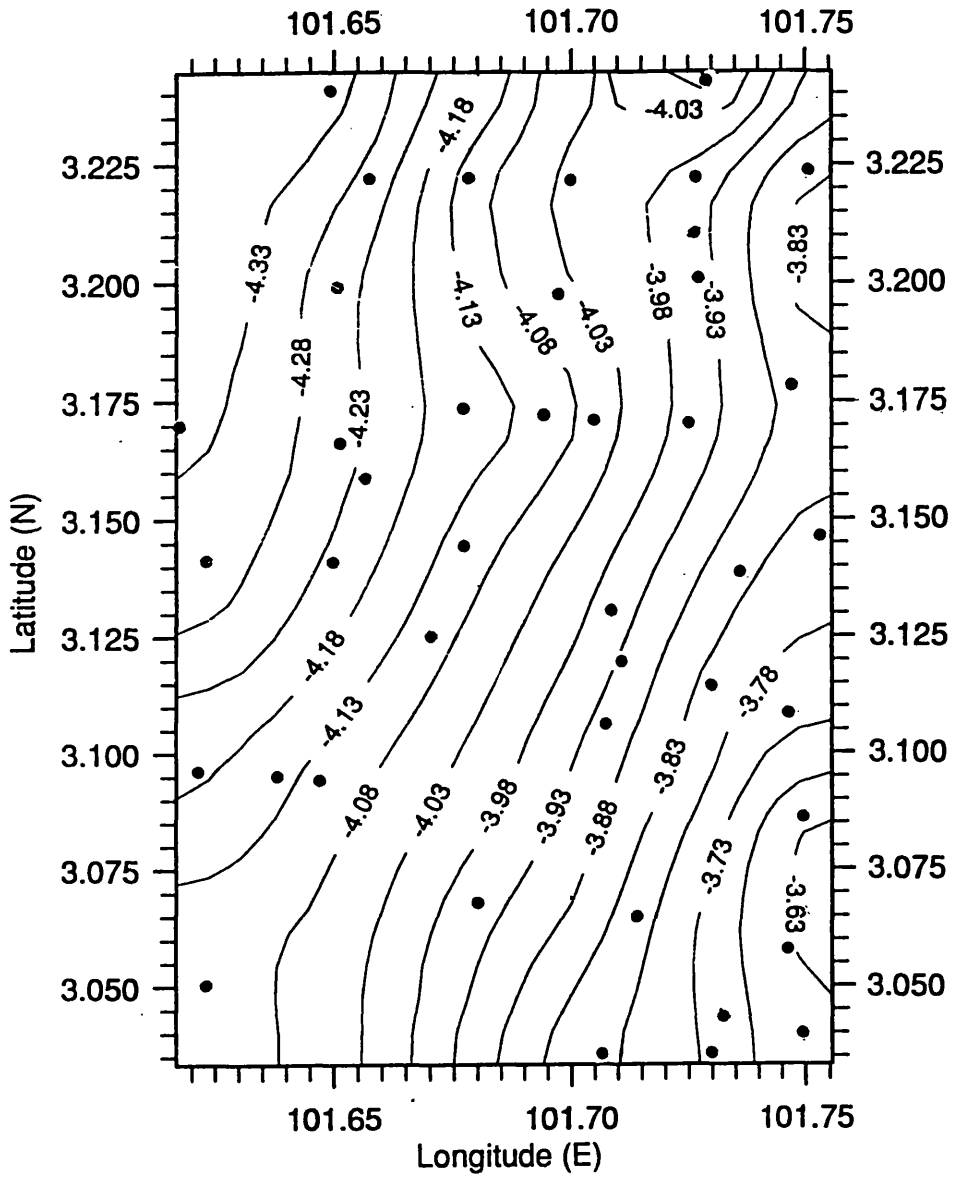

Figure: 4.11 - The Federal Territory GPS stations and geoid height contour (C.I.= 0.05m)

4.6 Analysis of the Data Used for Geoid Height Estimation

The gravimetric geoid estimation has an important role to play in the propagation of orthometric heights from GPS heighting (equation 3.2). The question may arise how well N will need to match h in higher precision so that the precision of H will not be seriously eroded. However, the precision required for H will depend upon the purpose for which heights are being used. For example, some tasks will only require H to a few metres, in which case the constraints on the determination of h and N can be relaxed (see Table: 3.5). For the highest order requirement, the precision to which h (or Δh) can be found limits the precision of H (or ΔH), and dictates the precision requirements for N (or ΔN). The following sections therefore, will analyse

the limitations imposed by the data used in this study which will give an insight into the accuracy of geoid height estimation and its evaluation against the available GPS/levelling-derived geoid in some of the test areas.

4.6.1 Analysis of Elements Δg and N

In general, the quality of the estimation of N or ΔN depends on several factors such as the choice of the reference field, density of the data set, data coverage and measurement accuracy. These factors show interrelated phenomena. A number of different estimates of geoid height accuracies have been quoted by many geodesists, and it is informative to review some of these. The aim of this section is to look at some limitations which may be imposed by the data used in evaluation of accuracy estimates for geoid determination in Peninsular Malaysia.

As previously mentioned in Section 3.5, apart from a geopotential model, the main contribution to the regional or local geoid height computation comes from terrestrial gravity data and height data. In practice, the measurements (signals) are always given in some regular grid or randomly distributed in a finite area. According to the sampling theorem (Bracewell, 1978), it is in fact possible to recover the intervening signal from sample data if the signal is band limited. In reality, however, there is always an error in the spectrum of the gravity quantity due to insufficient sampling which is termed an '*aliasing effect*', see Figure: 4.12.

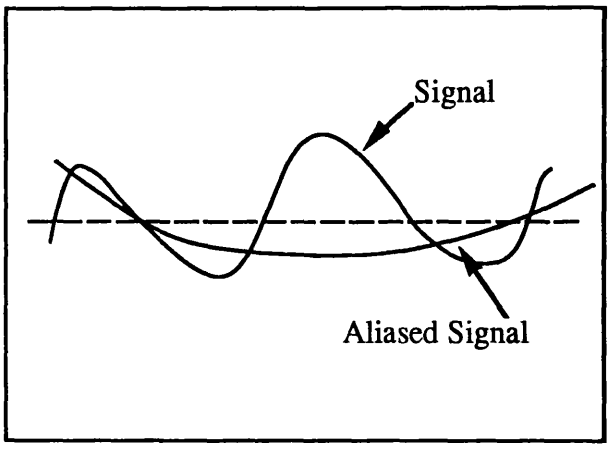

Figure: 4.12 - Aliasing effect due to insufficient sampling rate

Since the gravity data in most parts of the peninsula region are not well covered, it is rather difficult to reduce the aliasing error of a given data set. However, this error could be minimised in a very dense data set, for example in the southern area of the peninsular. According to Tscherning and Forsberg, (1986), the short wavelength part of the gravity field is mainly contained in the topographic information, especially in the

mountainous areas. If we, e.g. have gravity anomalies predominantly from the valleys, the gravity field will generally be too low, resulting in a biased geoid. Thus, using the terrain correction, discussed in Section 3.6, can also in some sense reduce the aliasing error for the test areas which have accurate (high resolution) gridded elevation data.

The question also arises as to how well the geopotential model OSU89B can represent the medium to long wavelength characteristics of the gravity field, e.g. Δg and N (or ΔN) for the peninsula region. The accuracy of the geopotential model is dependent on that of the observational data, i.e., gravity field information from which it is derived. The medium to long wavelength errors in the geopotential model may originate in insufficient satellite tracking data, lack of terrestrial gravity data and systematic errors in satellite altimetry, (Forsberg and Madsen, (1990).

As previously mentioned in Section 3.5, the main effect of reducing the data from the geopotential is to get a more homogeneous gravity field, i.e. the mean value of the reduced anomalies should decrease to a small value (preferably close to zero). Since the gravity anomalies for areas hampered by lack of surface gravity data, e.g. in most Asian regions including Peninsular Malaysia, were 'filled in' by low resolution of gravity field information for the OSU89B model solutions (see Section 4.4), the model therefore, is not expected to give accurate representation of the Δg field in this region. However, before any definite conclusion can be drawn, the geopotential model OSU89B needs to be analysed against available point gravity anomalies in the peninsula, and this exercise will be presented in the next chapter.

Various tests have been carried out to evaluate the ability of geopotential models for recovering the medium to long wavelength features of geoid heights. For example, the analyses of four data sets (in Ontario, Manitoba, Western Australia and South Australia) has shown that the ability of the geopotential model, for example, OSU81(n_{max}=180) model to fit ΔN varies greatly with location; being 4 to 5 ppm in the Ontario and South Australia areas, and about 10 ppm in the Manitoba and Western Australia areas, see Kearsley, (1986). The report by Schwarz and Sideris, (1985) suggested that, in Canadian areas, high order geopotential models can recover ΔN at the 5 to 7 ppm level in flat terrain and 6 to 9 ppm in mountainous terrain. Another test has also been carried out by Rapp and Wang, (1993) which showed that the relative geoid height comparisons between the N_{OSU91A} and the $N_{GPS/levelling}$ was about 4 ppm, 5 ppm and 7 ppm for the areas of Europe, Australia and Canada, respectively. Tests in the Irian Jaya (Indonesia) region have shown that the OSU89A model can recover the relative geoid at about 10 ppm, see Kasenda and Kearsley, (1992). These large differences probably reflect the comparative weakness in the gravity field information from this region used in the solution of the OSU89A (and OSU89B) and

the poor quality of the height information used (ETOPO5U global DEM) in the gravimetric solution. Therefore, as was the case for the Indonesian region, it can be expected that the contribution of the medium to long wavelength components (N_{GM}) of the OSU89B model to ΔN could be as much as 10 ppm for the Peninsular Malaysia region.

In the case where the available geopotential models do not approximate the regional gravity field data very well, a tailored model could be used. The tailoring means fitting to the surface gravity data in a specific region. This method has proved useful in some areas. For example, the comparisons of the OSU86F model and the tailored model IFE88E2 with GPS/levelling data from the Scandinavian GPS traverse has shown an improved accuracy of the IFE88E2 model, see Basic et.al., (1989). Since the tailoring method has proved to yield very good results for local computations, the available geopotential model OSU89B is therefore, to be tailored to updated gravity anomalies in this region. As previously mentioned in Section 1.1, it has become standard practice in recent years to compare computed geoid heights with those derived independently from a combination of GPS observations and orthometric levelling, i.e. $N_{GPS/levelling}$. Thus, the results of '$N_{Tailored\ model}$' will be compared against $N_{GPS/levelling}$ and also N_{OSU89B}, see Section 5.7.3.

The accuracy of the short wavelength component ($N_{\Delta g}$) can be estimated by analysing the density of the gravity data coverage within the area where the control point is positioned. The short wavelength component (N_{TC}) can be analysed using the topographic features of the site. It is expected that for the smooth areas with plentiful gravity, e.g. Area C (see Figure: 4.4), and Federal Territory (located in Southwest of Area B- see Figure 4.5), the accuracy of the gravimetric geoid will be better. In the eastern part of Area A (see Figure: 4.6) and the central part of Area B with very sparse gravity coverage and rugged terrain, the accuracy of the gravimetric geoid will be considerably worse.

4.6.2 Analysis of Element h

Apart from problems in the coverage and roughness of the gravity field, the possible error in the element h and H of the control data, i.e. GPS data also has to be considered in the estimation of N and ΔN. In general, there is little significant variation in the error estimation of h at all the control points after the adjustment, reflecting reasonably homogeneous and well-conditioned data. This parameter is, therefore, not a critical, or sensitive gauge of the veracity of the h values used in the analysis. Probably the only errors occurring in element h are the relative error of ellipsoidal heights ($\partial\Delta h$), which were directly observed in the GPS surveys. These errors are subjected to satellite

orbit error and the tropospheric and ionospheric effects, and therefore they might have degraded the integrity of the GPS heights in the vicinity of these baselines. Otherwise, the h element is expected to be the most trustworthy element as compared to H. In the author's opinion, the element h therefore, is the one which is probably the best determined of all elements. This is because the relative accuracy of the element h for baselines between 10 to 50 km is about 2-3 ppm, (DSMM, 1994). However, it should be emphasised that not all levelled lines were directly measured by GPS, and that the Δh over these lines were determined indirectly, (ibid).

4.6.3 Analysis of Element H

Spirit levelling is a highly precise procedure for relative height determination (ΔH), but as with all observational techniques relying on mechanical instruments, it is subject to errors. For example, there are sources of error within a levelling loop, due to such factors as the length of line, number of stations (and topography) and even the amount of time spent in observing. Errors are classified as *systematic* and *random* (Bomford, 1980). The accuracy of levelling is conventionally described as a function of line length, even though the accumulation of error may be due to other factors. In 1948, the IAG defined first-order levelling, i.e. geodetic levelling to have a probable total error (systematic and random effects) of less than 2 millimetres per $\sqrt{km}$ of length (2 mm $\sqrt{km}$) along a line. The error in second and third-order levelling derived height is difficult to ascertain, but an estimate for peninsular Malaysia is adopted from the tolerance of ± 6 and ± 12 millimetres per $\sqrt{km}$, respectively, (Khairul, 1994-Private Communication). The specifications translate into relative accuracy of 0.6 to 1.9 ppm in the first case and 1.2 to 3.8 ppm in the second case for distances between 10 to 100 km. It has been shown by Featherstone, (1992) that the assumed errors in orthometric height (σ_H) and ellipsoid height (σ_h) can be combined to give the geoid height uncertainty (σ_N) using simple error propagation theory; ($\sigma_N = \sqrt{\sigma_H^2 + \sigma_h^2}$). This gives the following estimates of GPS derived geoids to be: ± 4 cm for geodetic levelling, ± 6 cm for secondary levelling, ± 9 cm for tertiary levelling, ± 50 cm for trigonometric heighting over a distance of 50 km, (ibid). Figure: 4.13 depicts the allowable errors in levelling operations.

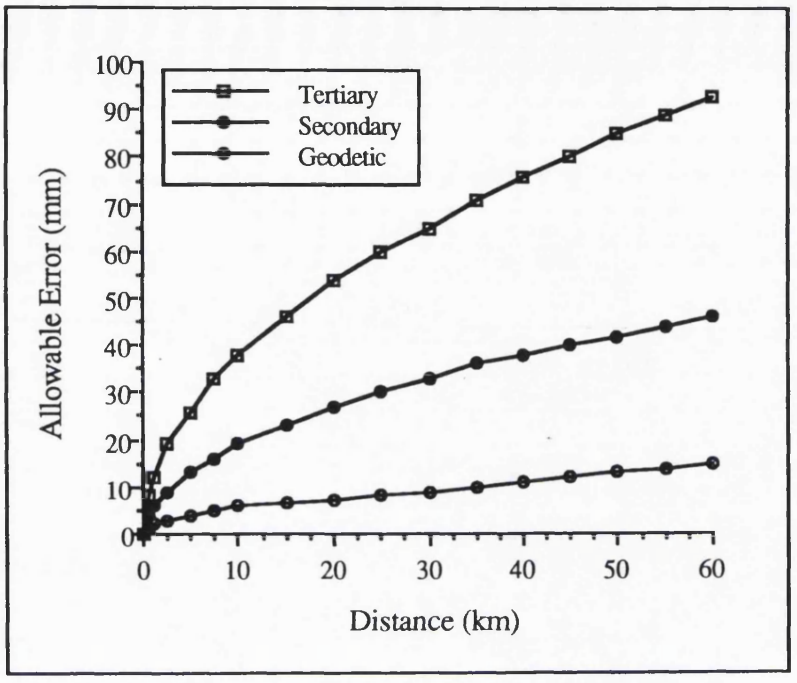

Figure: 4.13 - Allowable error in levelling

By looking at the above estimated accuracies of various levelling procedures and element N(and Δg) and h, the H value is the most likely to be in error and, as such, is most likely to be suspect. Since most of the orthometric heights at GPS points have been taken from the second order and tertiary levelling lines, for which no homogeneous adjustment has been performed, the accuracy for the Federal Territory GPS-derived geoid height can be estimated not better than $\pm$ 10 cm. The accuracy for the Southwest GPS-derived geoid height can also be estimated, but as low as half a metre because most of the orthometric heights of these GPS points have been determined using trigonometric heighting. Thus, it is obvious that orthometric heights at each GPS station have been determined with varying degrees of accuracy making comparisons between gravimetric and geometrical geoids inhomogeneous and unreliable. At the time that this study takes place, it therefore cannot be used to ultimately control the gravimetric geoid in the test areas but does provide a valuable comparison.

CHAPTER 5

THE FORMULATION AND APPLICATION OF A TAILORED MODEL FOR THE MALAYSIAN PENINSULAR REGION

5.1 Introduction

As previously mentioned in Section 3.5, the role of existing geopotential models in geoid studies is mainly to determine the medium to long wavelength geoidal features and to provide a reference field for terrestrially-derived gravity anomalies used in for example, Stokes' Integral, to find the short wavelength component of the geoid signal. 'Tailored' geopotential models fitted to the regional anomalous gravity field have also been developed to provide a similar reference field although they are restricted to certain conditions. The need for these geopotential models is further augmented by the increasing use of GPS data. This is because of the need to recover geoid features to a higher precision in order to obtain compatible precise orthometric heights from the GPS. This chapter therefore will present the information on the work done for the application of the existing geopotential model and the development of the tailored model as reference field for the anomalous gravity field used for this study. The analysis of the test results with respect to point gravity anomalies and GPS control data are also presented and discussed in this chapter.

The significance of the application of the available geopotential models and tailored models as reference gravity fields for geoidal studies is first discussed in this chapter. Next, the pre-analysis of the existing OSU89B model that was used to smooth the available local gravity anomalies is briefly presented. The following sections then will describe the theoretical background of the tailored method and its development. The numerical results for both, the existing OSU89B model and tailored model for residual gravity anomalies and geoid model (medium to long wavelength features) compared to GPS-derived geoid heights is fully presented and analysed in the last section of this chapter .

5.2 Review of Existing Geopotential and Tailored Models Used as Reference Gravity Fields

The representation of the earth's gravitational potential by a set of spherical harmonic potential coefficients (C_{nm}, S_{nm}) has evolved considerably in the past 25 years. Initial representations were of low degree and hampered by lack of surface gravity information (see Table: 3.3). The improvements in data availability, mathematical developments, and computer hardware and software facilities have led to

solutions that are complete to degree and order 360, (see Table 3.4). These high degree geopotential models have proven to be very useful to provide medium and long wavelength reference fields for anomalous gravity, enabling geoid determination to be carried out using local gravity data, as demonstrated by many geodesists, e.g. see Kearsley and Holloway, (1989), Mainville, et.al, (1992) and Gil, et.al., (1993). Depending on the maximum degree of the geopotential model applied and on the regional extent of the computation area, the medium part of the gravity spectrum is contributed from the overlapping portion of the geopotential model and the observed gravity data. Here, the main effect of reducing the data by the geopotential model is a decrease in variation of the gravity field, i.e. the mean value is close to zero and the gravity field becomes more homogeneous. However, it has been recognised that the modelled part of the gravity may contain long wavelength errors, which adversely affect the geoid heights derived therefrom (Forsberg and Kearsley, 1989).

The development of accurate geopotential models is dependent on accurate satellite observations from a variety of satellites at different inclinations, from the use of satellite altimeter data in some form, and the use of updated surface gravity data. However, as progress in the collection and compilation of new gravity field data is slow, improved geopotential models are released only at time intervals of two to five years, e.g. OSU81, OSU86E&F, OSU89A&B and the latest OSU91A model. Thus, it is not guaranteed that both sources of information represent the same structures because regional studies of the geoid, carried out by local authorities, are often based on detailed gravity information some or all of which did not enter into the computation of the existing geopotential models. Consequently, the models do not approximate the regionally existing gravity field data very well in some parts of the world.

Various strategies can be followed for optimum combination of geopotential model and local data for determination of medium and short wavelength signals of the geoidal height. One way of resolving the contributions of these wavelength signals is the truncation of harmonic expansions to a certain low degree and extending the size of the area within which the data is evaluated by the LSC method, see Sideris and Schwarz, (1986). Unfortunately, the advantages of having a high degree harmonic expansions are lost.

One development in this area is the tailoring of the available geopotential model to fit the gravity field over the area under consideration. This approach was originally developed by Weber and Zommorodian, (1988) and further refined by Basic, (1989). The resultant tailored models, for example, IFE87E2 (Basic, 1989), IFE88E2 (Basic, et.al., 1989), GPM2-T1 (Ayhan, 1993) and OSU91AT (Li and

Sideris, 1994) have been proven to yield very good reference fields for local geoid solutions. An analysis of tailored model approach to potential coefficient determination has been carried out by Kearsley and Forsberg, (1990). This paper points out that tailored models can only provide a good reference field for local or regional geoid solutions, if the gravity data used in the tailoring procedure has improved, in density and quality, since the original geopotential models were developed. Furthermore, these 'updated' data should be distributed evenly over the areas of the fit. In areas where no new gravity data were available, no geoid model improvements were found, (ibid).

It should be emphasised that there is no improvement of the fitted models with respect to global applications as they are derived specifically to improve local geoid solutions. Nevertheless, their solution is fairly straightforward, and significantly less demanding than a full global solution, i.e. no global database is used. This method also has the advantage over the other methods in that the application of high degree harmonic expansions are preserved since no truncation is necessary. The tailored method could be of great benefit for Peninsular Malaysia since most of the updated gravity data in the region were not released for the available geopotential model computations, (Majid, 1992 - Private Communication).

5.3 Pre-analysis of the OSU89B Geopotential Model for the Malaysian Peninsular Region

The use of a higher degree and order geopotential model like OSU89B to smooth the terrestrially-derived gravity anomalies is a well known procedure before a local or regional gravimetric geoid computation takes place. The choice of the global model must be done by subtracting the contribution of such models from the local gravity data and then analysing the residuals that must have: (i) an empirical mean value as near to zero as possible. If OSU89B were a perfect representation of the field then these residuals would be very close to zero; (ii) A small standard deviation as evidence of the internal consistency of the gravimetric values, and (iii) a small signal variance. The results can also be tested using the root mean square (rms) which gives some measure of the fluctuation of the residual gravity field from the geopotential model.

To visualise the effect of the gravity reductions achieved by the OSU89B geopotential model, the medium to long wavelengths contribution of this model to gravity anomalies are computed at 1815 points, using the written program *GEOMOD.FOR* . The residual anomalies (Δg_r) are then derived as a difference between

the corresponding observed anomalies (Δg_0) and the model derived-anomalies, i.e. Δg_{GM} at n_{max} =360° using equation (3.19):

$$\Delta g_r = \Delta g_0 - \Delta g_{GM} \qquad .....(5.1)$$

The techniques utilised for testing the OSU89B geopotential model are standard statistical tests. The *STAT.FOR* program was written to calculate these statistical tests which include the mean, the standard deviation, the rms and the variance values for the residuals (differences) between the observed Δg value and the corresponding global gravity model.

The mean value takes account of the sign of the residual gravity anomalies, and will tend to zero if there are similar magnitudes of positive and negative values. The mean value of the residual gravity anomalies is given by:

$$\bar{\Delta g} = \frac{\sum_{i=1}^{n} \Delta g_i}{n} \qquad .....(5.2)$$

A standard deviation of residual gravity anomalies is evidence of the internal consistency of these gravimetric value, and is given as:

$$\text{Std.Dev}(\Delta g) = \sqrt{\frac{\sum_{i=1}^{n} \Delta g_i^2 - \frac{\left(\sum_{i=1}^{n} \Delta g_i\right)^2}{n}}{n-1}} \qquad .....(5.3)$$

The rms value is derived from equation (5.4) below, which indicates how well the model picks up the high frequency signal in the gravity field.

$$\text{rms}(\Delta g) = \sqrt{\frac{\sum_{i=1}^{n} \Delta g_i^2}{n}} \qquad .....(5.4)$$

Variance is a measure of variation that is the averaged the squared deviation of the n sample observation from the sample mean. Thus, the variance of the residual gravity anomalies is given by:

$$\text{Var}(\Delta g) = \frac{\sum_{i=1}^{n} \Delta g_i^2 - \frac{\left(\sum_{i=1}^{n} \Delta g_i\right)^2}{n}}{n-1} \qquad .....(5.5)$$

The statistical characteristics of observed gravity anomalies and the corresponding anomalies reduced to the OSU89B model are given in Table: 5.1.

Statistical Test (in mgals)	Observed Anomaly	Residual Anomaly
Mean	12.85	-16.09
Rms	19.92	27.85
Standard Deviation	15.22	22.74
Variance	231.6	517.1

Table: 5.1 - Statistical results of anomalies using OSU89B as a reference model

From the results of Table: 5.1, it is apparent that the mean of the residual anomalies was not close to zero value and in fact was bigger than the counterpart mean value of the observed anomalies. Similarly, the rms, the standard deviation and the variance values of the residual anomalies have shown that the use of OSU89B does not perfectly represent the gravity field over this region. It is of more importance to discover if the tailored model has a similar effect when comparing against point values of geoid height (N) because such factor is not so critical as when comparing to gravity anomalies (point or mean anomalies), see Kearsley and Forsberg, (1990). However, this test on N and more comprehensive statistical tests of the residual anomalies using this OSU89B with the tailored model will be analysed later. To this end, it can be recognised that the available OSU89B model does not approximate the regionally existing gravity field data very well. Thus, the modelled part of the gravity signals in the OSU89B coefficients, may contain long wavelength errors, which may also affect the geoid heights derived therefrom.

5.4 A Tailored Method

This section describes a method for geopotential model improvements based on a fitting of the model to match the regional structure implied by the terrestrial gravity data. The mathematical derivation is based on the method published by Weber and Zomorrodian, (1988). The method leads to a harmonic expansion of non-global distributed differences between model and regional terrestrial data up to a certain degree and order. The resultant potential difference coefficients consequently have to be added to the original coefficients, giving an improved geopotential model fitted to the regional gravity field, which is suited for further consistent combination solutions.

In spherical approximation the expansion for gravity anomalies is given by:

$$\Delta g' = \frac{GM}{r^2}\{\sum_{n=2}^{n_{max}} \left(\frac{a}{r}\right)^n (n-1)\beta_n \sum_{m=0}^{n} (\Delta \bar{C}_{nm} \cos m\lambda + \Delta \bar{S}_{nm} \sin m\lambda)\bar{P}_{nm}(\cos\theta)\} \quad .....(5.6)$$

where GM is the product of the gravitational constant and the mass of the earth; r is the geocentric radius; a is the semi-major axis of the reference ellipsoid; P_{nm} is a fully normalised associated Legendre function; n_{max} is the maximum degree of expansion; β_n is a damping function which can be evaluated from a recurrence relation; θ is the spherical polar distance and λ is the longitude.

As we are primarily interested in finding the potential coefficients from gravity anomalies, the orthogonality relationship can be applied on (5.6) yielding:

$$\begin{Bmatrix} \Delta \bar{C}_{nm} \\ \Delta \bar{S}_{nm} \end{Bmatrix} = \frac{1}{4\pi} \iint_{\sigma} \frac{r^2}{GM}\left(\frac{r}{a}\right)^n \frac{1}{n-1} \Delta g \begin{pmatrix} \cos m\lambda \\ \sin m\lambda \end{pmatrix} \bar{P}_{nm}(\cos\theta) d\sigma \quad .....(5.7)$$

where $d\sigma$ is the element of unit sphere.

The actual evaluation of (5.7) is carried out using a set of mean gravity anomalies. Thus a mean anomaly can be computed from (5.6) as follows:

$$\bar{\Delta g}' = \frac{GM}{r^2 \Delta\sigma} \sum_{n=2}^{\infty} (n-1)\left(\frac{a}{r}\right)^n \sum_{m=0}^{n} \int_{\lambda_W}^{\lambda_E} (\Delta \bar{C}_{nm} \cos m\lambda + \Delta \bar{S}_{nm} \sin m\lambda) d\lambda \int_{\theta_N}^{\theta_S} \bar{P}_{nm}(\cos\theta) \sin\theta d\theta$$

.....(5.8)

where $\Delta\sigma$ is the surface element of the unit sphere, and θ_N, θ_S, λ_W, λ_E are the boundaries of the integration area.

The mean anomalies $\bar{\Delta g}'$, computed from the potential coefficients of the start model $\Delta \bar{C}_{nm}$, $\Delta \bar{S}_{nm}$ using (5.8), are subtracted from the terrestrial mean anomalies $\bar{\Delta g}$ yielding residual anomalies:

$$\delta \bar{\Delta g}' = \bar{\Delta g} - \bar{\Delta g}' \quad .....(5.9)$$

These residual anomalies can be expanded in spherical harmonics to yield corrections to the higher order potential coefficients:

$$\begin{Bmatrix} \partial\Delta\bar{C}'_{nm} \\ \partial\Delta\bar{S}'_{nm} \end{Bmatrix} = \frac{1}{4\pi}\sum_{i=1}^{l}\frac{r_i^2}{GM}\left(\frac{r_i}{a}\right)^n \frac{1}{(n-1)\beta_{ni}}\partial\Delta\bar{g}'\iint_{\Delta\sigma i}\begin{Bmatrix}\cos m\lambda \\ \sin m\lambda\end{Bmatrix}\bar{P}_{nm}(\cos\theta)d\sigma \qquad .....(5.10)$$

where l is the number of differences occurring between model and terrestrial anomalies, $\Delta\sigma$ is the area of integration, and β_n is the Pellinen damping function which can be viewed as a de-smoothing operator that tries to take into account that frequencies are damped out in taking the average to obtain the mean anomaly. The β_n function can be computed using the following expression:

$$\beta_n = \frac{1}{1-\cos\psi_0}\frac{1}{\sqrt{2n+1}}(P_{n-1}(\cos\psi_0)) - P_{n+1}(\cos\psi_0)) \qquad .....(5.11)$$

where ψ_0 is the radius of a spherical cap with the same size as the area of integration $\Delta\sigma$. A computation of the β_n can be performed using the recurrence procedure, see Sjöberg, (1980).

Finally, the coefficients of the fitted potential model are obtained by adding the potential difference coefficients obtained from (5.10) to the start coefficients, that is:

$$\begin{Bmatrix} \Delta\bar{C}''_{nm} \\ \Delta\bar{S}''_{nm} \end{Bmatrix} = \begin{Bmatrix} \Delta\bar{C}'_{nm} \\ \Delta\bar{S}'_{nm} \end{Bmatrix} + \begin{Bmatrix} \partial\Delta\bar{C}_{nm} \\ \partial\Delta\bar{S}_{nm} \end{Bmatrix} \qquad .....(5.12)$$

Mean anomalies from this improved set of potential coefficients can be obtained by analogy to equation (5.8):

$$\Delta\bar{g}'' = \frac{GM}{r^2\Delta\sigma}\sum_{n=2}^{n_{max}}(n-1)\left(\frac{a}{r}\right)^n\sum_{m=0}^{n}\int_{\lambda_W}^{\lambda_E}(\Delta\bar{C}''_{nm}\cos m\lambda + \Delta\bar{S}''_{nm}\sin m\lambda)d\lambda\int_{\theta_N}^{\theta_S}\bar{P}_{nm}(\cos\theta)\sin\theta d\theta$$

.....(5.13)

where n_{max} is the maximum degree of expansion. Then the differences $\partial\Delta g''$ will give the residual misfit to the new model where:

$$\partial\Delta g'' = \Delta\bar{g} - \Delta\bar{g}'' \qquad .....(5.14)$$

is defined in analogy to equation (5.9).

From the new tailored model the differences $\partial\Delta g''$ may once again be formed iteratively. Thus, the iteration procedure will give the following residual misfit as:

$$(\partial\bar{\Delta g})_i = \bar{\Delta g} - (\bar{\Delta g'})_i \qquad .....(5.15)$$

where the index i signals the ith tailoring step. The differences $(\partial\bar{\Delta g})_i$ will not vanish completely, i.e. will not be zero due to aliasing and leakage effect, and the various approximations in the method. Equations (5.10), (5.11), (5.12), (5.13) and (5.15) can be used iteratively until $(\partial\bar{\Delta g})_i$ no longer shows a significant decrease in the rms variation. In practice, two to four iterations are required before sufficiently small $\partial\Delta g$ values are obtained. When the integration of equation (5.10) is carried out over a local area only, it is thus implicitly assumed that the $(\partial\bar{\Delta g})$ is equal to zero outside σ.

5.5 The Data

A set of 0.5° x 0.5° mean anomalies was constructed for the test area using 1815 gravity data points. As described in Section 4.2(ii), these data were observed by the Department of Physics, USM and the Department of Surveying, UTM, and their values are referred to the IGSN71. For the construction of the mean anomaly set for the peninsula, the area of ($1° \leq \phi \leq 7°$, $99° \leq \lambda \leq 105°$) was divided into small grid cells of 5' x 5'. For each of these cells the gravity mean anomalies were estimated using weighted means prediction method from the available gravity points in the area under consideration. Due to poor resolution of ETOPO5U global DEM and the absence of detailed local DEM for the whole peninsula, the mean anomalies are directly predicted from point free-air anomalies without anticipation of topographic effect. The prediction of point or mean gravity anomalies based on point gravity anomalies can be processed directly without associated with terrain reductions, as long as the terrain is reasonably flat within the area of consideration, (Sunkel, 1981). In fact, more than 95% of the gravity points are located in the area of considerably smooth terrain, i.e. less than 200 metres in altitude, and therefore, no data reduction seems to be necessary. The correction for atmospheric effects according to equation (2.57) was also applied for the observed gravity anomalies. In the computation, a constant term $\delta g_A = 0.87$ mgals, which is the atmospheric correction at sea level, was used. Doing this will not cause any accuracy loss in this correction considering the smooth terrain in most areas, and the small effect of the atmospheric effect itself.

The weighted means method predicts the gravity anomaly at a prediction point by taking the weighted mean of the nearest observations surrounding the point. Weights are assigned to the observations inversely proportional to the distance d, raised to some power v, of the observations from the prediction point. The observed anomalies which are closest to the prediction point contribute most to the prediction value. However, the method performs very well in areas where data is comparatively

dense, and may yield unacceptable results where data coverage is sparse. The weighted mean prediction method is simple, and requires minimal programming effort.

The program *WEGT.FOR* was written to perform these computations. The mathematical model of the weighted means prediction method is given by:

$$\Delta g_P = \frac{\sum_{i=1}^{n} \frac{\Delta g_i}{d_{iP}^v}}{\sum_{i=1}^{n} \frac{1}{d_{iP}^v}} \qquad .....(5.16)$$

where Δg_P is the predicted gravity anomaly at point P; Δg_i is the value of anomaly at ith. data point; d_{iP} is the separation between ith. data point and P; n is the number of observations; v is the exponent of d for the weights, and in practice, it is usually taken as 2, see Kostainien and Kakkuri, (1980).

The accuracy of the prediction is obtained by error propagation:

$$\sigma^2_{\Delta g_P} = \left[\frac{\partial \Delta g_P}{\partial \Delta g_i}\right]^2 \sigma^2_{\Delta g_i} \qquad .....(5.17)$$

where $\sigma^2_{\Delta g_i}$ is the variance of the i'th observed gravity anomaly, so that

$$\sigma^2_{\Delta g_P} = \frac{\sum_{i=1}^{n}\left[\left(\frac{1}{d^2_{P_i}}\right)^2 \sigma^2_{\Delta g_i}\right]}{\left[\sum_{i=1}^{n}\left(\frac{1}{d^2_{P_i}}\right)^2\right]^2} \qquad .....(5.18)$$

where $\sigma^2_{\Delta g_P}$ is the variance of the predicted anomaly at point P.

The mean anomalies of 10' x 10' blocks were obtained by taking a simple average of the 5' x 5' grid cells anomalies. The mean 0.5° x 0.5° mean free air anomalies were then obtained by averaging the values of 10' x 10' sub-blocks. For the final product, mean anomalies were deleted where no observation or sparsely distributed data was located inside corresponding 0.5° x 0.5° blocks. This editing resulted in a set of 38 mean free-air anomalies for the peninsula that were used for the computation of the tailored model. A full set of mean gravity anomaly values are

given in Appendix G and Figure: 5.1 shows the location of their corresponding 0.5° x 0.5° blocks that were used in the tailoring procedure.

The stepwise averaging, taking 10' x 10' block means as intermediate results used for this computation of 0.5° x 0.5° mean anomalies, supports the need for higher resolution gravity data and avoids the generation of block means from insufficiently distributed sub-blocks. The stepwise averaging procedures have been implemented in Weber and Zommorodian, (1988) and Basic, (1989).

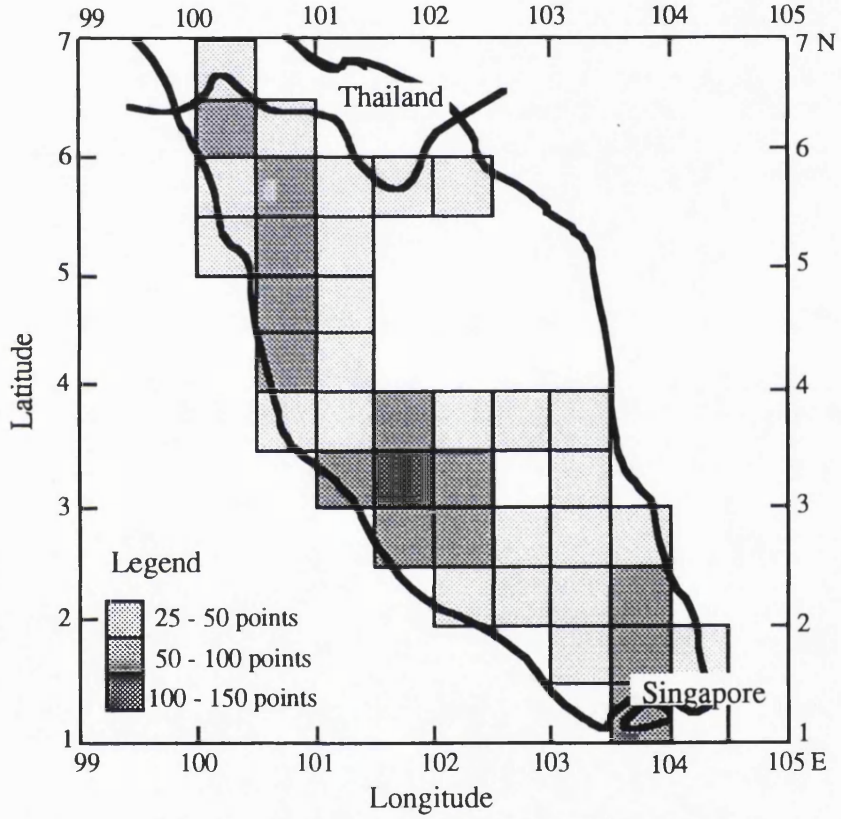

Figure: 5.1 - The 0.5° x 0.5° mean anomaly blocks used in the computation of the tailored model OSU89B-MM

5.6 The Tailored Model Development

The 0.5° x 0.5° mean anomaly data set was used to compute a tailored model, called *OSU89B-MM* (*MM* stands for *Malaysian-Model*). The available geopotential model OSU89B complete to degree and order 360, was chosen as a start model in the program *GEOIGP*, (Denker,1993-Private Communication). The program was modified to perform this task. As previously mentioned, the very low degree harmonics should not be modified based on local data, both because of the limited data collection area and systematic effects, and because these coefficients are well determined from satellite

solutions, see Basic, (1989). In this experiment, the coefficient changes for the low degree harmonics, i.e. $n \leq 20$ were then tapered off to reduce leakage effects since they have relatively little influence on the results. This was achieved by multiplying the potential difference coefficients $\partial\Delta\bar{C}'_{nm}$, $\partial\Delta\bar{S}'_{nm}$ obtained from equation (5.10) by a weight function W_n depending on the harmonic degree n. Here, a weight function was put equal to zero up to degree 20, and equal to 1.0 above degree 20.

$$W_n = 0; \quad \text{for } 2° \leq n \leq 20° \text{ and } W_n = 1; \text{ for } 21° \leq n \leq 360° \qquad .....(5.19)$$

The differences $\partial\Delta g'$ between the corresponding 0.5° x 0.5° mean anomalies from the observed data and the start model OSU89B were calculated, and then expanded into a series of spherical harmonics up to degree and order 360. A consequence, however, of using such a procedure is a reduced rate of convergence of the whole process and the necessity to carry out the computations iteratively until $\partial\Delta g$ no longer shows a significant decrease in the rms variation. In total, 3 iterations were performed for the computation of the tailored model, OSU89B-MM.

Results from the comparison of the 0.5° x 0.5° mean gravity anomalies between the start model OSU89B and the tailored model OSU89B-MM is summarised in Table: 5.2. The improvement of the results is graphically reflected in Figure: 5.2.

Iteration	0	1	2	3
Geopotential Model	Start Model OSU89B	Tailored	Model	OSU89B-MM
Mean	-13.80	-1.37	-0.12	-0.02
Std. Dev.	21.45	3.85	1.74	1.15
Rms	25.26	4.04	1.72	1.14
Min.	-83.23	-12.96	-2.88	-2.48
Max.	7.15	4.58	2.42	2.00

Table: 5.2 - Comparison of 0.5° x 0.5° mean gravity anomalies with the start model OSU89B and the tailored model OSU89B-MM

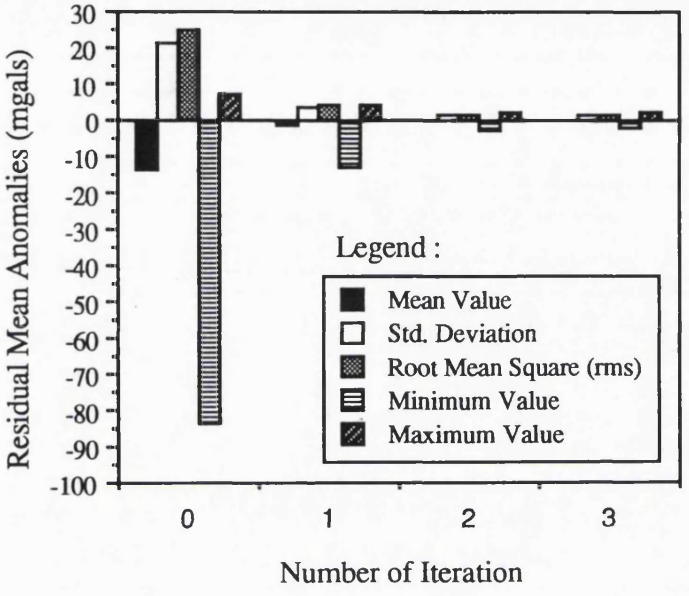

Figure: 5.2 - Decrease of differences between mean gravity anomalies from OSU89B and OSU89B-MM with respect to iteration number

As can be seen from Table: 5.2 and Figure: 5.2 the tailored model OSU89B-MM improves the mean value significantly over the start model OSU89B, decreasing from -13.80 mgals to 1.37 mgals after only the first iteration. More improvement occurs with successive iterations. The rms fit of OSU89B-MM shows a very significant improvement, changing from 25.26 mgals to 4.04 mgals in the first iteration and 1.14 mgals in the last iteration. Similarly, the standard deviation, minimum and maximum values also show a very dramatic improvement in the first iteration, with lesser improvements in the subsequent iterations. Thus, to this end, it could be concluded that OSU89B-MM fits the mean gravity anomalies ($\bar{\Delta g}$) in the Peninsular Malaysia region significantly better than OSU89B.

As previously mentioned in Section 5.2, the analysis carried out by Kearsley and Forsberg, (1990) has pointed out that a tailored model will only provide a good reference gravity field to the area for which new gravity data (updated data) was added, and these data must also be accurate and distributed sufficiently over the area of the fit. In other words, in areas where no updated gravity data was included in the analysis for the coefficients of the available geopotential model, no model improvements can be obtained. Thus, in order to substantiate the above statements, the computation of another tailored model, called *OSU89B-MM1* was then carried out.

The tailored model OSU89B-MM1 was developed using the same gravity data as with OSU89B-MM tailored model development, *with the exception* that the gravity points (about 300 points), located in the selected test area, Area X ($2.5° \leq \phi \leq 3.5°$, $101.5° \leq \lambda \leq 102.5°$ - see Figure: 5.3) were not used for this tailoring computation. It was revealed that most of the updated gravity data in this area have not been released to be included in the geopotential model OSU89B, (Majid, 1993-Private Communication). The same tailoring procedures described in Sections 5.4, 5.5 and 5.6 was applied to develop OSU89B-MM1 model. Figure: 5.3 also shows the location of the mean free-air anomalies of 0.5° x 0.5° blocks that were used to develop tailored model OSU89B-MM1.

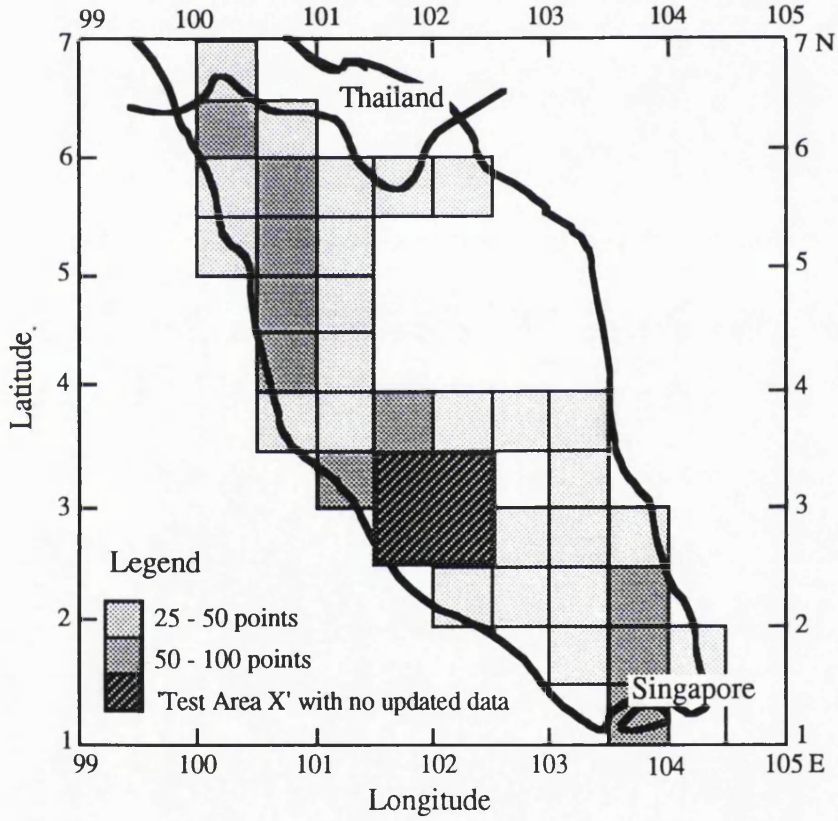

Figure: 5.3 - The 0.5° x 0.5° mean anomaly blocks used in the computation of the tailored model OSU89B-MM1

5.7 Evaluation of the Pre-existing Geopotential Model OSU89B and Tailored Models OSU89B-MM and OSU89B-MM1

The following sections deal with various tests between the pre-existing geopotential model OSU89B and the two developed tailored models OSU89B-MM and OSU89B-MM1 against point gravity anomalies and mean anomalies in the area of

interest. These higher degree and order models will also be tested against the available GPS-derived geoid heights.

5.7.1 Evaluation of Point and Mean Gravity Anomalies

A number of tests have been carried out to evaluate the ability of the pre-existing geopotential model OSU89B and the tailored models, OSU89B-MM and OSU89B-MM1 against point gravity observations. These models were used to estimate values of the gravity signal at points where they have been observed. A subtraction of the estimation values from the observations leave the residual values which will describe the local behaviour of the gravity signals only. As previously mentioned in Section 5.3, the signals are required to have a small mean value (preferably zero mean value) and to describe a homogeneous (smooth) gravity field. To assess how far each model behaves, the Δg_{GM} (equation 3.19) at each data point was generated from each model's potential coefficients using the program GEOMOD. The test can be divided into four parts:

(i) Test I - Test of OSU89B and OSU89B-MM against 1815 point gravity anomalies (supplied by UTM in July 1992) for the whole peninsula. The aim is to evaluate which one of these reference models can describe adequately the local behaviour of the gravity field and also can provide the most homogeneous gravity field information for Peninsular Malaysia.

(ii) Test II - Test of OSU89B and the two tailored models against point gravity anomalies in the test area X (Figure: 5.2). The aim is to see whether the tailored model is degraded or not, when the updated gravity data (accurate and good coverage) from this test area is excluded in the tailoring procedures. This test will also highlight the conditions under which such fitted models are an improvement over the pre-exising geopotential model, i.e. reflects the strengths and weaknesses of the data used in the tailored model developments.

(iii) Test III - Test against new point gravity observations, supplied by the DSMM in March, 1994. These new gravity values were not used in the development of the tailored model OSU89B-MM. The aim is to see whether tailored model OSU89B-MM can approximate the 'recent updated' regional gravity field very well compare to geopotential model OSU89B. Also, from this test results, one may verify the improvement of OSU89B-MM over OSU89B because this verification is of considerably importance before combining the reference model (either pre-existing or tailored models) with local gravity data for preliminary gravimetric geoid determination in Peninsular Malaysia, see Chapter 6.

(iv) Test IV - Test between the mean residual anomalies of OSU89B and OSU89B-MM. The mean residual anomalies were derived using equation (5.2). The aim this test is to evaluate the closeness of fit to mean anomalies (mean residual anomalies on 0.5° x 0.5° block basis) for each model with respect to gravity density and coverage, and the terrain types over Peninsular Malaysia. Again, the analysis will suggest how good the coverage of the long wavelengths is, per model, in this region.

5.7.1.1 Test I

In this test, the statistical data of the residuals (differences) between the generated gravity model from OSU89B and OSU89B-MM, and the corresponding 1815 observed Δg values were analysed for the whole peninsula. The differences between the observed and predicted values suggest how good the coverage of the long wavelengths is, per model, in the peninsula region. The results of these comparisons are summarised in Table: 5.3.

Unit in mgals	Observed Gravity Δg_o	$\Delta g_o - \Delta g_{OSU89B}$	$\Delta g_o - \Delta g_{OSU89B\text{-}MM}$
Mean	12.85	-16.09	-0.60
Standard Dev.	15.22	22.74	11.22
Rms	19.92	27.85	11.23
Min.	-31.45	-96.10	-65.55
Max.	82.09	37.25	65.69

Table: 5.3 - Statistical comparisons between OSU89B and OSU89B-MM for point gravity anomalies over the Peninsular Malaysia

From Table: 5.3, it is clear that the tailored model OSU89B-MM gives better results for the gravity reference fields over the peninsula region with the mean of residuals of only -0.60 mgals, compared to -16.09 mgals for the original model OSU89B. The standard deviation and the rms value is reduced by more than 50% with the OSU89B-MM, i.e. 11.22 mgals and 11.23 mgals compared to 22.74 mgals, 27.85 mgals for the OSU89B, respectively. From the above statistical results, it is obvious that the tailored model OSU89B-MM describes more homogeneous gravity field of Δg compared to the pre-existing model OSU89B, implying better long

wavelength signals in this region. This condition is very important in local studies leading to a solution of the BVP.

5.7.1.2 Test II

It is quite interesting to discover if OSU89B-MM can approximate the available gravity field data very well for the test Area X, compare to OSU89B-MM1 and OSU89B. This test will lead to the conclusion that a tailored model can provide a superior reference gravity field, even for a small area if the gravity data used in the tailoring procedure has improved, in both density and quality, and is also well distributed, since the original model coefficients were evaluated. On the other hand, poorly distributed and inaccurate updated gravity data may not improve the existing model, see Kearsley and Forsberg, (1990). As a result of these tests, it can also be suggested that geopotential models, properly fitted to the local gravity field, may have significant applications in local or regional geoid solutions. The results of these comparisons are summarised in Table: 5.4.

Unit in mgals	Observed Free-air Anomalies (Δg_o)	$\Delta g_o - \Delta g_{OSU89B}$	$\Delta g_o - \Delta g_{OSU89B\text{-}MM}$	$\Delta g_o - \Delta g_{OSU89B\text{-}MM1}$
No. of points	295	295	295	295
Mean	10.31	-22.38	-1.27	-17.75
Std. Dev.	14.39	20.91	11.10	15.20
Rms	17.68	30.60	11.31	22.60
Min.	-19.35	-60.91	-23.40	-53.01
Max.	57.89	23.27	57.35	29.28

Table: 5.4 - Comparison against gravity points in the test Area X

From Table: 5.4, it is clear that OSU89B-MM offers the best results for Area X with the mean of residual anomalies only -1.27 mgals. The improvement in the gravity signal is also reflected with OSU89B-MM whereby its standard deviation and rms value in the differences are smaller compared to OSU89B and OSU89B-MM1. From the same table, one may seen that OSU89B-MM1 was, in this instance, unable to recover significant improvement over OSU89B. For example, the mean value of the OSU89B-MM1 solution is slightly better than that from OSU89B (-17.75 mgals cf.

-22.38 mgals). One of the possible reasons for its slight improvement over the OSU89B might be the contribution from other updated gravity anomalies (30'x30' mean anomalies) surrounding the test Area X during the development of the tailored model OSU89B-MM1, see Figure: 5.2. In general, it is apparent that the tailored model OSU89B-MM1 does not provide smooth gravity field for the test area, compared to the tailored model OSU89B-MM. Because of the inhomogeneity of the gravity field information occurring in the tailored model OSU89B-MM1, this model therefore, will not produce suitable reference boundary values, i.e. reference anomalies for the BVP solutions.

From this test, it is apparent that the fit of the models depends on the variation in the gravity field information in the area of interest. Thus, one may recognise that the reference models which were developed from insufficient data density and coverage will have poor long wavelength gravity signals, and this may adversely affect the geoid heights derived therefrom. As new gravity data becomes available (with good quality, density and coverage) then incorporation of these data to a new tailored model will result in improved gravity field modelling. Finally, it can be expected that the tailored model OSU89B-MM will provide better estimate of the reference gravity field for the large unsurveyed areas and areas of sparse gravity coverage, e.g. Titiwangsa, Timor and Bintang Ranges (Figure: 4.4), than OSU89B and OSU89B-MM1 do. Obviously, such estimates will not be as accurate as those based on the actual measurements.

5.7.1.3 Test III

The existing model OSU89B and the tailored model OSU89B-MM were also tested against new point gravity observations. As previously mentioned in Section 4.2(iii), these new gravity values were supplied by the DSMM at a very late stage, i.e. in March 1994, and therefore were not used in the development of OSU89B-MM. A comparison of 601 observations with OSU89B and OSU89B-MM resulted in the same statistical tests as listed in Table : 5.5.

Unit in mgals	Observed Free-air Anomalies	$\Delta g_o - \Delta g_{OSU89B}$	$\Delta g_o - \Delta g_{OSU89B\text{-}MM}$
Mean	14.16	-16.00	-1.09
Rms	19.45	26.28	12.76
Std. Dev.	13.34	20.86	12.73
Variance	178.0	435.1	162.1

Table: 5.5 - Comparisons of OSU89B and OSU89B-MM against new gravity points in Peninsular Malaysia

From Table: 5.5, it is apparent that the mean value of the residual anomalies relative to OSU89B-MM is smaller, i.e. -1.09 mgals whereas the counterpart mean value of the residual anomalies relative to OSU89B is far from zero, i.e. -16.00 mgals. Similarly, the rms, the standard deviation and the variance values of the residual anomalies have shown that the use of OSU89B-MM has a better fit on the regional gravity field over the OSU89B, implying good long wavelength coverage. Again, this condition is of considerably importance in local studies leading to a solution of the BVP. Thus, it could be concluded that the tailored model OSU89B-MM offers a better reference model for Peninsular Malaysia compared to the pre-existing model OSU89B. It could be also pointed out that the computation of tailored model OSU89B-MM was carried out in a correct procedure.

Since OSU89B-MM fits the gravity field over the Peninsular Malaysia better than OSU89B-MM1, the following further comparisons and analyses are therefore carried out to this tailored model only and also to the existing geopotential model OSU89B.

5.7.1.4 Test IV

In order to further verify the fitness of OSU89B and OSU89B-MM over the peninsula, the mean of residual anomalies with respect to both models were analysed on 0.5° x 0.5° block basis for 1815 gravity points, i.e. extracted from the UTM gravity database. This gravity database has a maximum of 145 and minimum of 2 points in any of the 0.5° x 0.5° blocks. The aim of this test is to analyse the variations in the gravity field produced by OSU89B and OSU89B-MM, in more detail with respect to the topographic point of view in this region. The program *RESDAT.FOR* was written to perform the statistical tests on the reduced gravity anomalies in a user-defined area by analysing the mean, minimum and maximum values as well as the sample size. The

chosen category bins of the mean fit differences are summarised in Table: 5.6 and are reflected in the form of a histogram in Figure: 5.4. The distributions of their corresponding mean residual anomalies analysed on the 59 blocks for the whole peninsula is also illustrated in Figure: 5.5 and Figure: 5.6, respectively. Details of these results for both OSU89B and OSU89B-MM are given in Appendix H.

Bin No.	Geopotential Model	Original Model OSU89B		Tailored Model OSU89B-MM	
	Bin Category (In mgals)	Frequency Distribution	Percentage (%)	Frequency Distribution	Percentage (%)
1	5 to 15	7	11.9	4	6.8
2	0 to 5	10	16.9	18	30.5
3	0 to -5	11	18.6	22	37.3
4	-5 to -10	9	15.3	10	16.9
5	-10 to -20	6	10.2	3	5.1
6	- 20 to -30	2	3.4	2	3.4
7	< - 30	14	23.7	0	0.0

Table: 5.6 - Chosen bin limit and results of mean distribution of gravity points

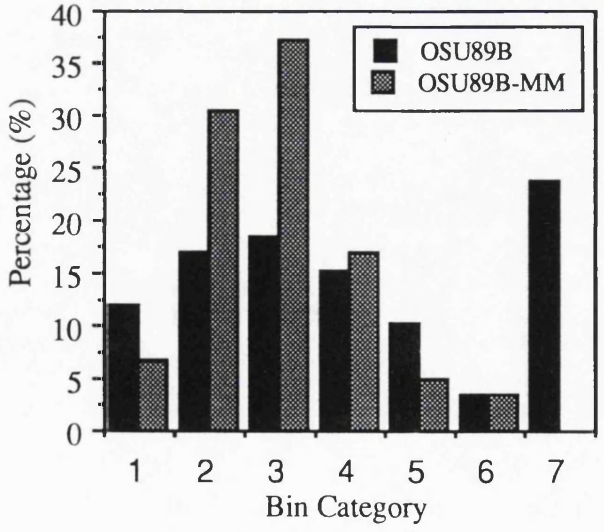

Figure: 5.4 - The histogram of mean residual anomalies analysed on a 0.5°x0.5° block basis

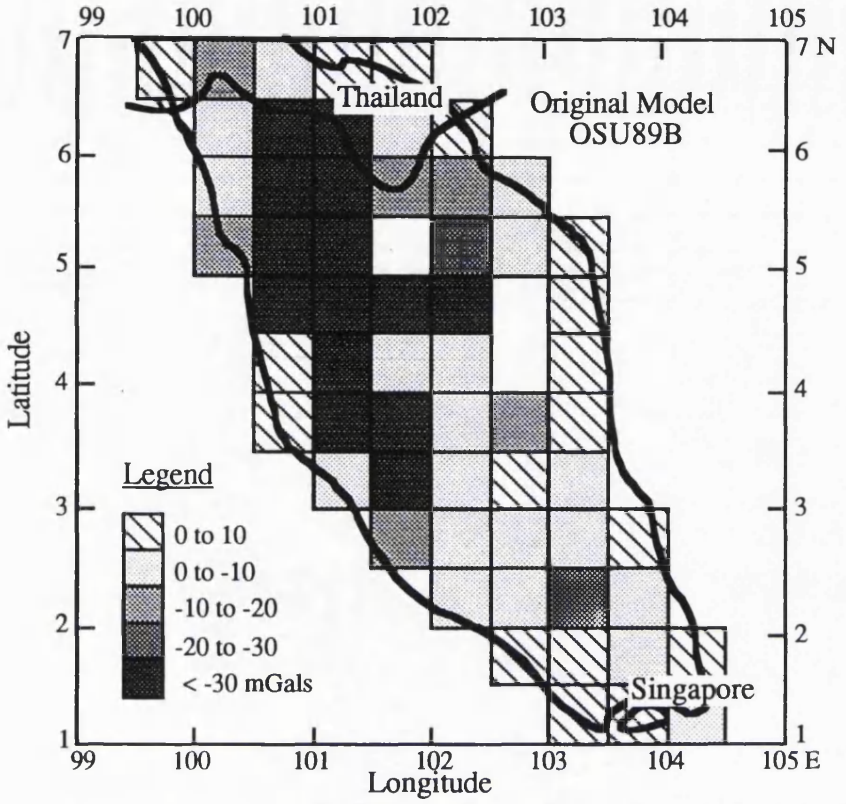

Figure: 5.5 - Distribution of mean residuals analysed on a 0.5 x0.5 basis-OSU89B

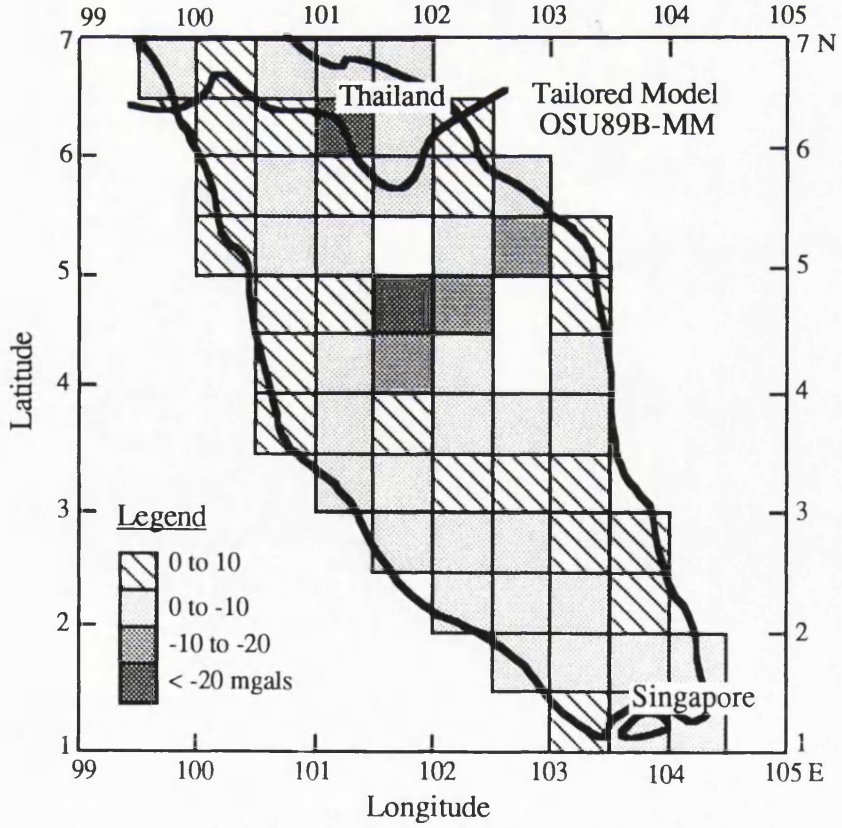

Figure: 5.6 - Distribution of mean residuals analysed on a 0.5 x0.5 basis - OSU89B-MM

The histogram of the residual anomalies in Figure: 5.4 shows that only 35.5% of the 0.5° x 0.5° blocks have a mean residual of between 0 to ± 5 mgal (Bin 2 and Bin 3) for OSU89B, compared to 67.8% for OSU89B-MM. The fit of OSU89B-MM is much better than that of OSU89B where 23.7% of the blocks have the mean residuals between ±5 mgals to ± 10 mgals (Bin 1 and Bin 4) compared to 27.2% generated by OSU89B for the same bin categories. The mean residuals greater than -30 mgals (Bin 7) visible in OSU89B have almost disappeared when using the Δg field generated by OSU89B-MM.

A noticeable feature in the distribution of mean fit is the dominance of negative biases with OSU89B having about 71.2% and OSU89B-MM, 62.7% of negative blocks. The histogram has shown that OSU89B-MM does approximate the regionally existing gravity field data quite well, compared to OSU89B, suggesting that the former model is suitable as a reference field for the Malaysian Peninsular region.

From Figure: 5.5, it can be seen that the areas of poorest mean residual representation with respect to terrestrial gravity implied by OSU89B are in the central north Peninsula Malaysia. The main reason for these biases over the mainland is that no terrestrially observed gravity data were supplied over the area that covers the mountainous areas, i.e. Titiwangsa Range, Bintang Range and Timor Range. This reason is supported by the fact that in the development of the pre-existing geopotential model OSU89B, for areas devoid of gravity information (especially in Asia, Arctic and Antarctic regions), the mean anomalies were estimated from coefficients implied by a topographic-isostatic model, see Figure: 4.9. These 'filled in' mean anomalies do not provide the resolution of the 30' x 30' data but rather provide valuable gravity field information beyond what is available from satellite orbit perturbations (low degree harmonic), and therefore, will not be as accurate as those based on actual measurements, see Rapp and Pavlis, (1990).

On the contrary, the poorest fits occurring in OSU89B almost disappear in OSU89B-MM. This phenomenon is clearly shown in Figure: 5.6. These areas do have a reasonable number of sample points for each half degree block although most of these were not well distributed and are concentrated mainly along accessible roads, with very few points on the highlands (less than 1000 m elevation). The larger biases of the mean residual anomalies for OSU89B-MM however are still concentrated in the central parts of the peninsula. This is the region of rough terrain, and thus probably indicates problems in the mean free-air anomalies in the existing values of the global data sets for these regions. This is not a suprising result because essentially the same gravity field information from these regions was used for the development of OSU89B-MM, i.e.

low resolution gravity field information which was estimated from coefficients implied by a topographic-isostatic model for the development of OSU89B. Thus, it is evident that the high order geopotential models do not model the medium to high frequency components well, particularly in the mountainous areas. However, when a complete terrestrially-observed gravity data set is available in the unsurveyed area (especially in the Titiwangsa, Bintang and Timor Ranges), it is expected that the mean residual anomalies for these mountainous areas will substantially be reduced, i.e. the variation of the gravity field in these areas will be smooth and homogeneous.

In general, the results show that the OSU89B and OSU89B-MM models fit the Δg field quite well along the eastern coastal areas and in most of the southern region (smooth terrain). These areas have a good number of sample points, evenly distributed. It is obvious from this analysis that the tailored model OSU89B-MM shows good long wavelength quality and clearly behaves better than the pre-existing geopotential model OSU89B, especially over the lowland and coastal areas. Thus, to this end, it could be concluded that the tailored model OSU89B-MM represents the reference gravity field information in the area under investigation better than does the OSU89B. However, it is more important to discover if this improvement is repeated when using this tailored model to generate the geoid heights and compare with those independently from a combination of GPS observations and orthometric levelling in the test region. The comparison between the $N_{OSU89B\text{-}MM}$ (and also N_{OSU89B}) with the corresponding $N_{GPS/levelling}$ will be presented in Section 5.7.3.

5.7.2 Geoid Height Difference Between OSU89B and OSU89B-MM

Absolute geoid heights across the peninsula region from both OSU89B and OSU89B-MM have been generated on a 15' x 15' gridded format, using equation (3.16) in the program GEOMOD. The geoid height map from OSU89B-MM as shown in Figure 5.7, ranges between -20 m to 13.5 m from North to South. From the differences in height between these two models, the geoid heights from OSU89B-MM have a wider range compared to OSU89B (see Figure: 5.8), consisting of negative geoid height values (-19.5 m) in the central part of Peninsular Malaysia but having about the same positive geoid height values (13.5 m) in the South.

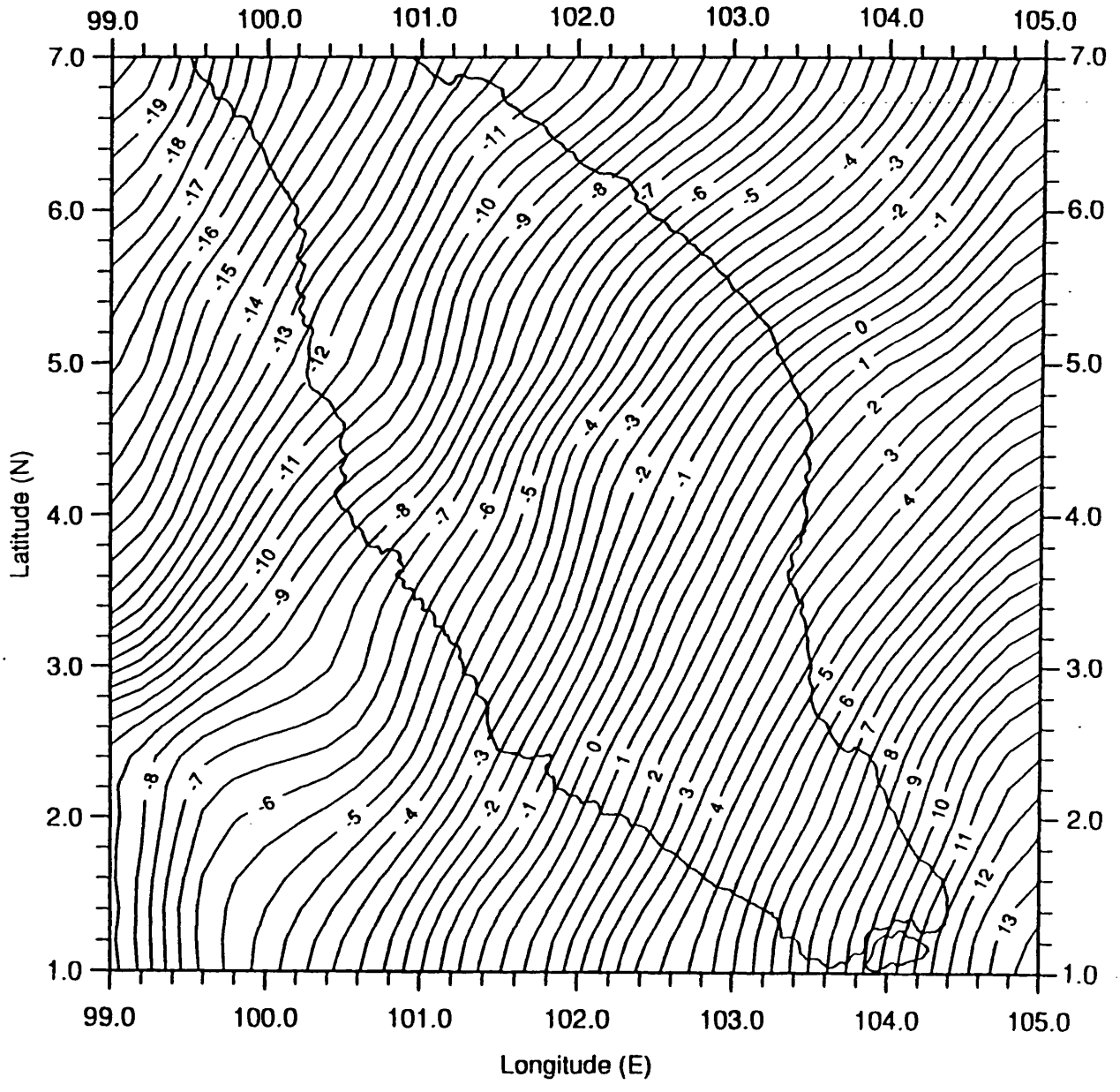

Figure: 5.7 - The geoid height map of OSU89B-MM for Peninsular Malaysia
(C.I = 0.5 metres)

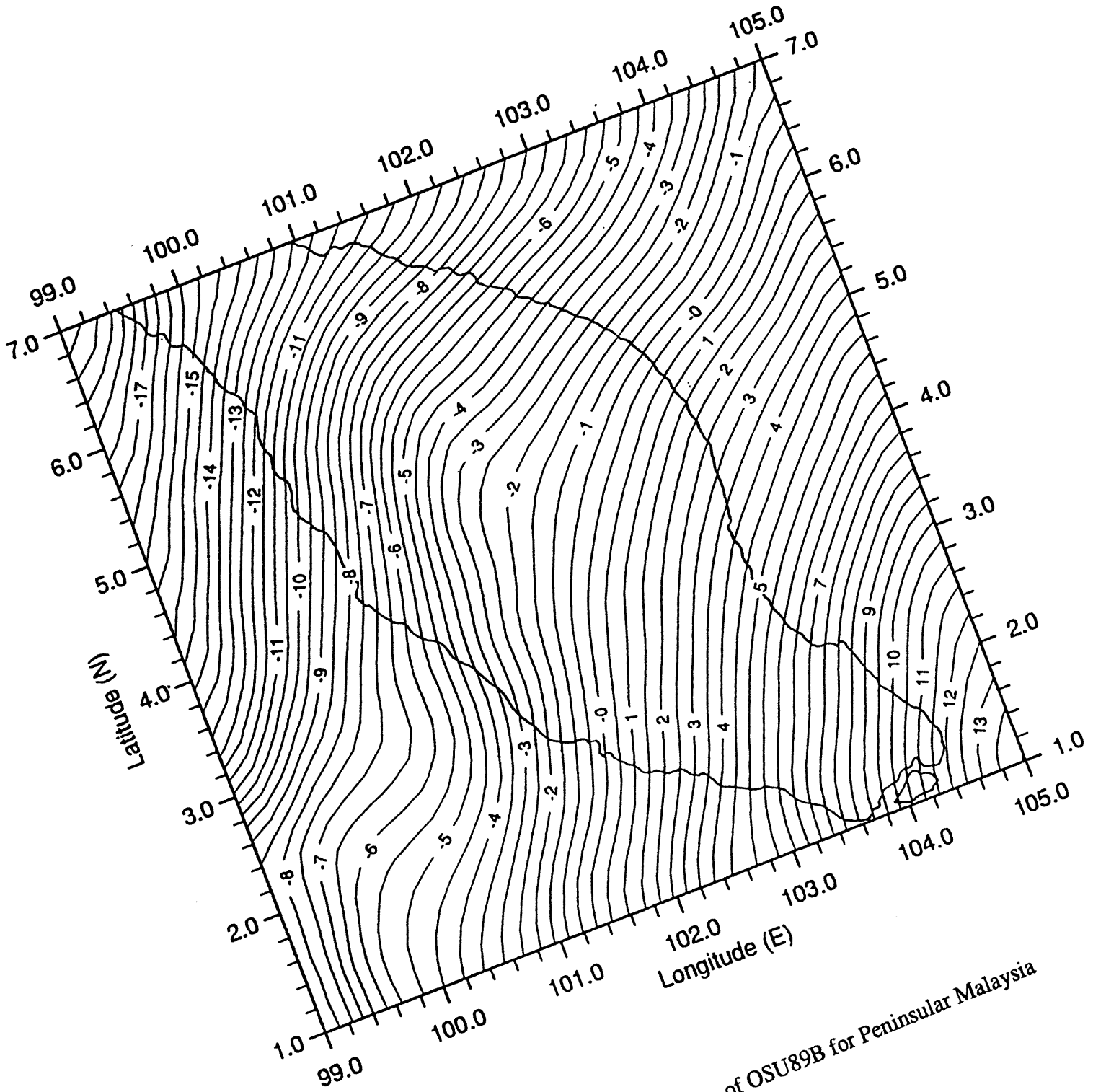

Figure: 5.8 - The geoid height map of OSU89B for Peninsular Malaysia
(C.I = 0.5 metres)

The differences in geoid heights between OSU89B and OSU89B-MM over the Peninsular Malaysia region have also been generated and are shown in Figure: 5.9. This figure which is the map of ($N_{OSU89B-MM}$ - N_{OSU89B}) indicates the difference of geoid heights with a range between -4 m to 0 m throughout the peninsula.

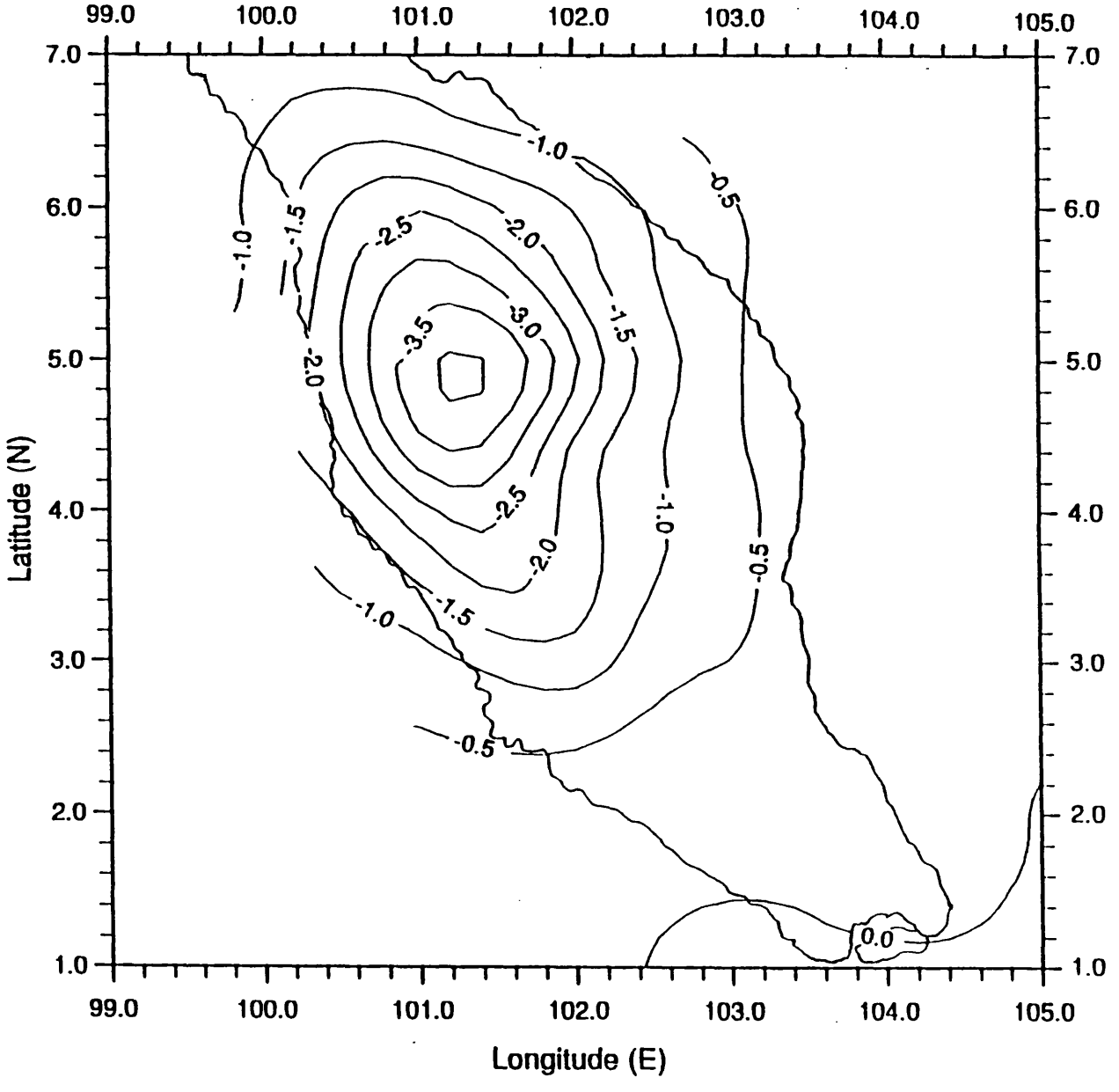

Figure: 5.9 - The map of $N_{OSU89B-MM}$ - N_{OSU89B} for Peninsular Malaysia
(C.I = 0.5 metres)

From Figure: 5.9, it is apparent that the effect of the tailoring is fairly benign in the coastal areas and most parts of the southern regions where the differences between this tailored model and the OSU89B geoid is about 0 m to -1 m. This phenomenon may reflect the fact that the resolution of OSU89B-MM has little influence for these smooth-terrain areas. From the same figure, it is also apparent that the central regions attract rather large geoidal height differences between these two models. For example, $N_{OSU89B\text{-}MM}$ - N_{OSU89B} have values between -2 m to -3 m in most parts of the moderate topography areas, that is the north-east, north-west and the central south-west areas. These differences are thought to be due to a low resolution gravity field from pre-existing gravity field information (OSU89B) in these regions that have been used in combination with new (updated) data to develop tailored model OSU89B-MM.

From the same figure, it can be seen that very large differences occur in the region of the central north area of the peninsula where changes of over 3 m occur. This is the region of highest mountains (see Figure 4.4), and thus probably indicates the problems in the mean anomalies in the existing values in the global data sets for these regions. Again, as mentioned previously, these mean anomalies are of considerably low resolution gravity field because they were estimated from coefficients implied by a topographic-isostatic model in the OSU89B model. The similar disturbing phenomenon is also observed in Kearsley and Forsberg, (1990) where the geoid height differences between the existing geopotential GPM2 and the tailored model GPM2F has shown more than 3 m level in the rough terrain and less dense gravity coverage of the western coast of Norway, north-west coast of Western Australia and Papua New Guinea regions.

5.7.3 Evaluation Against GPS/Levelling Derived Geoid Height

As previously mentioned in Section 4.5, the GPS surveys were carried out to provide the geodetic control network for the DSMM surveying and mapping purposes. The orthometric heights at each GPS point have been determined with varying degrees of accuracy, either from the trigonometric heighting or from second order and tertiary levelling network. These gave geometric evaluations of the geoid height, i.e. $N_{GPS/levelling}$ and provided valuable comparison with the corresponding N_{model}. The analysis of the GPS/levelling data has been discussed in Sections 4.6.2 and 4.6.3.

5.7.3.1 Comparison of Geoid Heights in the Southwest GPS Network

The GPS network in the Southwest region of the peninsula (Figure: 4.10) was used for the comparison with the corresponding N_{model}. For this test, the geoid heights were computed from both OSU89B and OSU89B-MM models at the 35 GPS points, and compared against the geoid heights found from GPS-derived ellipsoidal heights

and orthometric heights from levelling data. The results of these comparisons are summarised in Table: 5.7. Figures 5.10 and 5.11 illustrate the ∂N values from OSU89B and OSU89B-MM along latitude and longitude profiles, respectively. Details of comparisons are given in Appendix I.

Unit in Metre	$N_{GPS/Lev}$ (N1)	N_{OSU89B} (N2)	$N_{OSU89B-MM}$ (N3)	∂N1=N1-N2	∂N2=N1-N3
Mean	2.98	4.88	4.57	-1.90(0.00)	-1.59(0.00)
Std. Dev.	2.68	2.82	2.80	0.34(0.33)	0.32(0.31)
Min	-2.76	-0.24	-0.02	-2.80(-0.90)	-2.02(-0.43)
Max	8.82	10.69	10.50	-1.32(0.58)	-0.82(0.77)
Range	11.58	10.73	10.52	1.48(1.48)	1.20(1.20)

Table: 5.7 - Results of comparisons of absolute geoidal heights for the Southwest GPS Network. Numbers in parentheses represent values after removing the systematic biases.

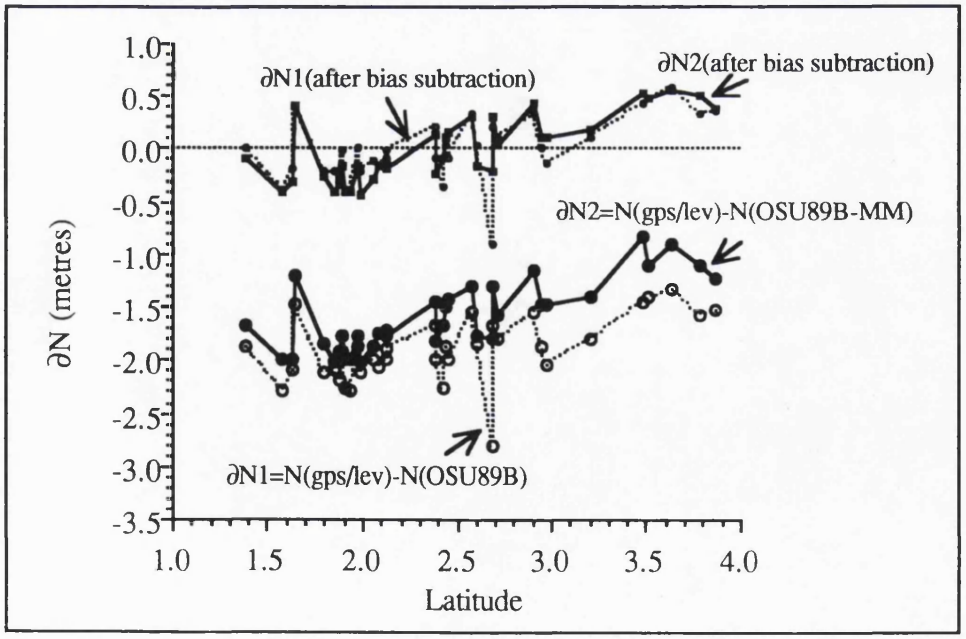

Figure: 5.10 - Tilts of geoid heights along the latitude profile

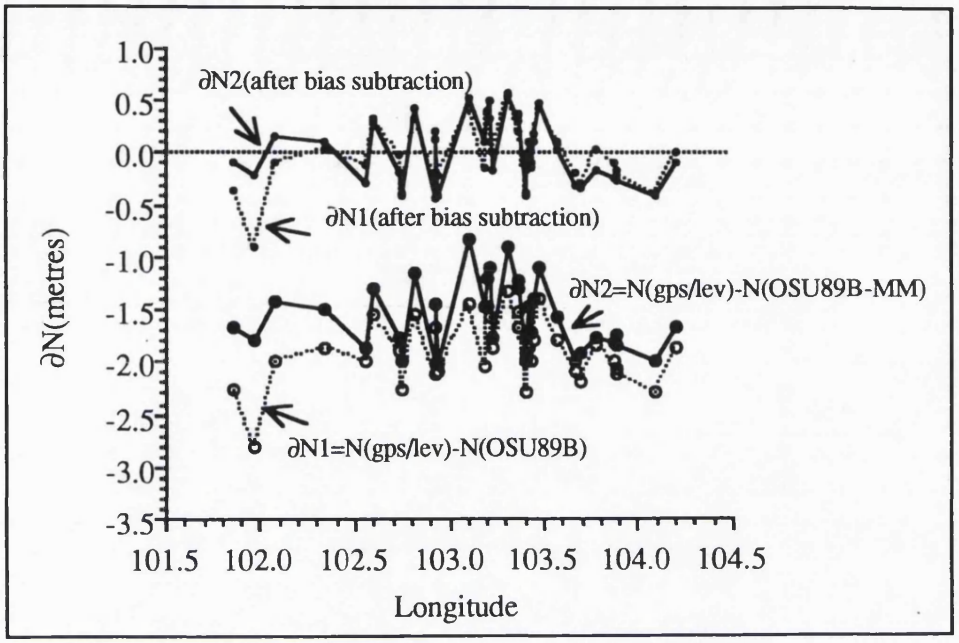

Figure: 5.11 - Tilts of geoid heights along the longitude profile

Table: 5.7 indicates that the overall agreement between the models and the GPS/levelling-derived geoid is around 30 cm in terms of standard deviation, and there exist systematic biases between two kinds of geoid representations with a mean value of less than 2 m, i.e. -1.59 m cf.-1.90 m. These systematic biases may be due to a systematic difference between the medium to long wavelength errors in N_{GM}, errors in orthometric heights from levelling (H) and errors in GPS-derived ellipsoidal heights (h), see Section 4.6. It is also apparent from this table that the range of the differences is significantly improved with OSU89B-MM, i.e. decreased by about 30 cm. This implies that the absolute geoid height differences are found more accurately by using the tailored model.

After removing the systematic biases, it can be seen that there is a 1 cm improvement for the standard deviation of the differences for both models. The results in Figure: 5.10 and Figure: 5.11 (before and after removing the systematic biases) show that the most striking geoid height difference occurring at point ϕ= 2.°68N, λ=101°.97 E, is reduced significantly to a smaller difference using the tailored model OSU89B-MM compared to OSU89B model, although the overall absolute differences (∂N) or *tilts* are almost the same for both models.

To look at this interesting phenomenon in more detail, a comparison based on geoid differences over the individual GPS baselines, which range in length from 10 km

to 260 km were carried out. The calculation is done between two stations along the line according to the following:

$$\Delta N = \Delta N_{GPS/Lev.} - \Delta N_{Model} \qquad .....(5.20)$$

where:

$\Delta N_{GPS/Lev}$ is the control geoid difference between the two points; and
ΔN_{Model} is the model geoid difference between the two points.

The relative geoid height (ΔN) is divided by the length of the line and expressed in parts per million (ppm, 10^{-6}). This is then averaged for all lines to get the mean value ($\bar{m}$):

$$\bar{m} = \frac{\sum_{i=1}^{n} \left| \frac{\Delta N_i}{s} \right|}{n} x10^6 \qquad .....(5.21)$$

where s is the length of i^{th} line and n is the number of baselines.

Figure: 5.12 depicts the relative differences of the model and the GPS/levelling-derived geoid heights in ppm. Appendix J summarises details of these relative geoid height differences.

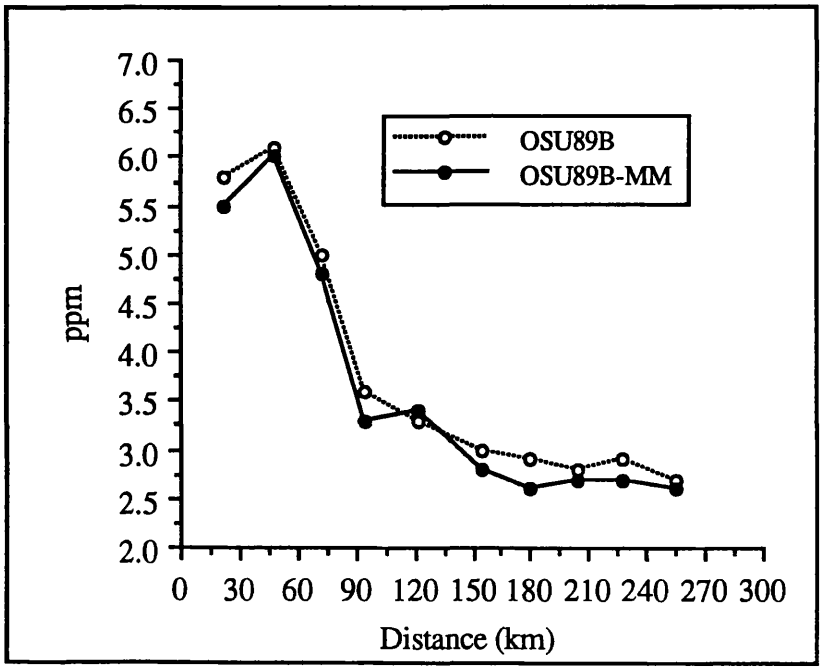

Figure: 5.12 - Relative differences between the N_{model} and the $N_{GPS/Levelling}$ for the Southwest GPS Network

From Figure: 5.12, it is apparent that the tailored model OSU89B-MM has a slight improvement over the original model OSU89B. In general, the relative agreement between the geoid height derived from these two models against NGPS/levelling is of the same order of accuracy, i.e. is about 6 to 2.5 ppm for distances between 50 to 250 km. The use of tailored model OSU89B-MM provides a relative differences about 6 to 5.5 ppm for distance less than 50 km when compared to the existing model OSU89B (cf. 6.1 to 5.8 ppm). One of the possible reasons for this slight improvement of the relative geoid height differences might be caused by the difference in data density and data distribution (coverage) within the area of the Southwest GPS network which are used to form the mean anomalies in the tailoring procedure. The southern areas ($1° \leq \phi \leq 2.5°$ N, $103.5° \leq \lambda \leq 104°$ E) and the central areas ($2.5° \leq \phi \leq 3.5°$ N, $101.5° \leq \lambda \leq 102.5°$ E) are characterised by good sample gravity points and reasonably good coverage, see Figure: 5.1. In contrast, less dense point gravity data in the areas of ($2° \leq \phi \leq 3°$ N, $102.5° \leq \lambda \leq 103.5°$ E) is biasing the 30' mean gravity anomalies derived from the terrestrial gravity which may partly distort the corrections to the potential coefficients in the development of the tailored model OSU89B-MM. In other words, the combination of these two kinds of gravity field resolutions may have little effect on reducing the long wavelength errors from the existing model OSU89B. Of course, it is obvious that this phenomenon is not so critical when comparing the point gravity values (Section 5.7.1) since the tailoring procedure is carried out by fitting the surface gravity data (medium to short wavelength signals) to the existing geopotential model in this region. A similar phenomenon was observed by Kearsley and Forsberg, (1990) when they tested the tailored model GPM2F against the original model GPM2 for 37 GPS baselines in the south eastern coast of Australia. In general, however, it appears that OSU89B-MM would be slightly more suited to N or ΔN evaluation for this region compared to OSU89B, implying that the critical long wavelength errors have been partly diminished by means of tailoring procedure.

5.7.3.2 Comparison of Geoid Height in the Federal Territory GPS Network

A similar test on the ability of OSU89B-MM to represent the medium to long wavelength geoid features has been extended to include the 51 GPS/levelling control points in the Federal Territory area (Figure: 4.11). Apart from having a reasonably good gravity coverage and smooth topography, this area was chosen because of the expected homogeneity in its height datum (close to Port Klang tide gauge station - the LSD1912).

The geoid height values were computed from OSU89B and OSU89B-MM at the 51 control points, and compared against the geoid height values derived from differences between GPS-ellipsoidal heights and orthometric heights from levelling. In this case, the absolute geoid height differences (∂N) at control points are compared, as in Section 5.7.3.1, but in a fairly small GPS network or across relatively short baselines, i.e. between 2 km to 30 km in length. The aim is to limit the analysis to points of similar characteristics, such as terrain type and height datum. The results of these comparisons are summarised in Table: 5.8. Details of these outputs is listed in Appendix K.

Unit in Metres	$N_{GPS/Lev}$ (N1)	N_{OSU89B} (N2)	$N_{OSU89B\text{-}MM}$ (N3)	∂N1=N1-N2	∂N2=N1-N3
Mean	-4.02	-1.43	-3.30	-2.59(0.00)	-0.72(0.00)
Std. Dev.	0.21	2.76	2.60	0.11(0.10)	0.09(0.08)
Min	-4.37	-1.78	-3.70	-2.86(-0.27)	-0.86(-0.14)
Max	-3.61	-1.09	-2.81	-2.38(0.21)	-0.49(0.22)
Range	0.76	0.69	0.89	0.48(0.48)	0.37(0.36)

Table: 5.8 - Comparison between N_{model} and $N_{GPS/Levelling}$ in the Federal Territory GPS Network. Number in parentheses represent values after removing the systematic biases.

It is interesting to see from the above table (before removing the systematic biases) that the tailored model OSU89B-MM, while showing a small mean value compared to the corresponding value of the pre-existing geopotential model OSU89B (-0.72 m cf. -2.59 m), also indicates slight improvement in the standard deviation of the differences (± 0.09 m cf. ± 0.11 m). Although the range of the absolute differences between OSU89B-MM and OSU89B (with respect to $N_{GPS/Levelling}$) is about 10 cm, these comparisons nevertheless have shown that quite large differences do exist between the absolute N values derived from these two models. After removing the systematic biases, it can be seen that there is a 1 cm improvement for the standard deviation of the differences. Thus, in general, these absolute differences numerically show how much better the tailored model fits the control data than does OSU89B.

The test was also carried out for relative geoid differences (ΔN) over the individual GPS baselines which range from 2 km to 30 km, in length. The N values at

stations derived from the best estimate of the GPS-derived ellipsoidal heights and orthometric heights were used to provide control for ΔN_{model} values for each individual baseline derived from both existing and tailored models. The mean value of these differences is expressed in terms of ppm of the length of the baselines as in equation (5.21). The comparisons of the ΔN values between these control points is shown in Figure: 5.13. Details of the results are summarised in Appendix L.

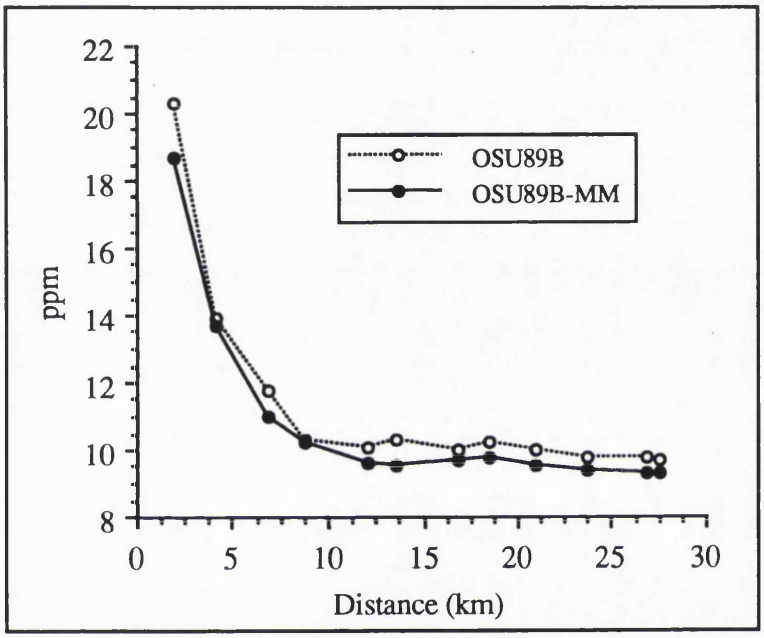

Figure: 5.13 - Relative differences between the N_{model} and the $N_{GPS/Levelling}$ for Federal Territory GPS Network

From the above figure, it is apparent that the relative agreement between the geoid height derived from these two models against $N_{GPS/levelling}$ shows that OSU89B-MM has a slight improvement over OSU89B of about 0.5 ppm for distances more than 10 km. The use of OSU89B-MM provides relative differences about 18.7 ppm to 10.2 ppm for distances less than 10 km when compared to the OSU89B (cf. 20.3 ppm to 10.3 ppm). By examining the above figure, it was found that the overall fitness of the relative differences between OSU89B-MM against the Federal Territory GPS network indicates this tailored model has a better medium to long wavelength signals compared to that provided from OSU89B. Again, it is clearly shown that an apparent local improvement in the tailored model is not so critical for point or mean gravity anomalies compare to ΔN, see Kearsley and Forsberg, (1990). Nevertheless, it is apparent that OSU89B-MM fits the gravity field across Peninsular Malaysia better than does OSU89B strongly suggesting that the former is the preferable reference model for geoid studies in this region.

5.8 Summary and Conclusion

The available geopotential model complete to harmonic degree and order 360, was tailored to the regional gravity data (including an updated set of point gravity anomalies) in Peninsular Malaysia. These updated gravity data are not released for the available geopotential model developments. The tailoring procedure was started with the computation of a set of gravity anomalies in this region from an a priori set of potential coefficients, i.e. OSU89B model. These anomalies were subtracted from the observed values to form a set of residual anomalies. The residual anomalies were then added to the original potential coefficients set. The process was iterated until an acceptable convergence was achieved. In this experiment, an improved reference model (tailored model) called OSU89B-MM was obtained where the critical long wavelength errors in the original model OSU89B, have been partly diminished. The results and tests show that the residual gravity anomalies and the geoid height differences (interms of both the absolute and the relative differences) are significantly improved in some test areas using OSU89B-MM when compared to OSU89B. Therefore, it could be concluded that the tailored model OSU89B-MM has a much better performance than the existing model OSU89B in Peninsular Malaysia.

As a result of this experiment, it can be suggested that the computation of a tailored model is an efficient and convenient way to take updated gravity field data into account if the existing geopotential models do not appear to fit these data well. The updated gravity data, however, must be accurate and evenly distributed over the region of the fit so that they represent high resolution gravity field information of the block means used to derive the corrections to the existing potential models. It is expected that the tailored model OSU89B-MM could be further improved by having adequate gravity points on the mountainous areas, i.e. Titiwangsa Range, Bintang Range and Timor Range, and incorporating the topographic effect (high frequency information) in the estimation of mean anomaly using a very dense DEM, e.g. 1km x 1km resolution or better. This approach has proven very successful in estimating mean anomalies used for the development of tailored model OSU91AT for Canada and the northern United States of America, especially in the region of the Rocky Mountains, see Li and Sideris, (1994). The standard deviation of the discrepancy between OSU91AT model and the GPS/levelling-derived geoid decreased by more than 50% compared to the original model OSU91A, (ibid).

CHAPTER 6

PRACTICAL GEOID COMPUTATION

6.1 Introduction

A wide range of gravimetric methods are used, or have been proposed for the solution of the BVP. These methods include Stokes' integral, LSC and the most recent one, FFT algorithms. Each method has its own theoretical and computational properties, as well as its flexibility and reliability. Practical considerations on the use of these methods are subjected to how they can handle the data set and the capability of computing resources. For example, Stokes' integral in principle requires a continuous gravity field (dense data), and it is also claimed that this method requires excessive computation time. The LSC may use randomly (or sparsely) distributed data and has the facility to predict errors in the estimated quantities. Unfortunately, this prediction method suffers from a practical disability in that it generates equations of the unknown equal to the number of observations. The FFT method is, as its name implies, computationally extremely fast; however it requires gridded data, and the transformation to the frequency domain may involve a modification of Stoke's kernel function. Recently, a more advanced spectral technique has been investigated to solve the BVP using different kinds of Stokes kernel functions, see Li and Sideris, (1994).

In this chapter, a discussion on the methods used in the estimation of geoid height for the three test areas (described in Section 4.3.2) is presented. These include the LSC and FFT methods. The basic formulae for the definition of LSC and FFT methods are described. The fundamental mathematical properties are outlined and serve as a reference for the development of covariance in the LSC method and for the development of frequency domain algorithms in the FFT method. Their practical evaluations and computer software used for geoid height estimations are also discussed. It should be mentioned here that most of the gravimetric geoid computations in this study were using slightly modified programs of the *GRAVSOFT* (GRAVimetric SOFTwares) computer software provided by The National Survey and Cadastre and Department of Geophysics, University of Copenhagen, Denmark - (Forsberg and Tscherning, 1994 - Private Communication). The presentation and analysis of the results will be given in the next chapter.

6.2 Least Squares Collocation

The least squares prediction techniques used for interpolation of gravity anomalies are generalised to estimate any element of anomalous gravity field from

geodetic data of different kinds. The fitting of analytical approximations to given functionals is called Collocation and the consideration of the minimum principle of mean square error in prediction leads to Least Squares Collocation (LSC). The LSC method provides a general theoretical basis for the optimal combination of a great amount of geodetic data presently available. On the basis of the given data (measurements), the most probable estimates are thus obtained for the unknown parameters and for the signals. The following sections will derive and describe the LSC formulae and also the covariance function, which is essential to the method. Details of the mathematical derivations of the LSC formulae can be found in several text book and publications, e.g. Moritz, (1976), Moritz, (1980) and Tscherning, (1985).

6.2.1 Collocation Model

The observational equations in the LSC are represented by the mathematical model, (Moritz, 1980):

$$l = AX + s + n \qquad .....(6.1)$$

where l is the vector of observations; A is a known fully populated matrix; X is the vector of parameters which represents the deterministic component; s is the vector of signals and n is the vector of observational errors.

In Physical Geodesy, equation (6.1) can be applied to any gravimetric quantities where the element s is the vector of anomalous field signals which are expressed by functionals of the disturbing potential. For example, in gravity measurements, l is the gravimeter reading, s represents the gravity anomaly Δg, n is the random measuring error, and X represents systematic parameters which may contain the parameters of the normal gravity formula and the instrumental constants as well as other systematic effects on the measurement such as drift.

The underlying principle of the collocation approach is the way in which the signal quantity in equation (6.1) is dealt with. If we consider the determination of parameter X as adjustment, the removal of the noise as filtering, and the computation of s at points other than the measuring points as prediction, we can see that the LSC model combines *adjustment, filtering* and *prediction.* Thus, the aim of LSC is to estimate signals and filter noise at points where observations are made, and predict signals at other points. Of importance is the fact that, statistically, both these values have an expectation of zero. It is also expected that a knowledge of the covariance structure of the discrepancy is given because the model will not be exact. The following text shows how these principles of observation equations are applied.

As previously described in Section 2.4, the disturbing potential T is a very small quantity and irregular, and it is very difficult to compute exactly. Therefore, in LSC, only an approximation to parameter T can be produced through the linear combination of a group of functions which operate on T. These functions should be chosen such that they satisfy Laplace's Equation (equation 2.25), i.e. harmonic outside the surface of the earth. We, therefore will have the following expressions:

$$T = L_i(T) \qquad .....(6.2)$$

and

$$L_i(T) = \sum_{k=1}^{q} L_i(\varphi_k) b_k = L_i(T') \qquad .....(6.3)$$

where φ_k is a linear combination of q functions φ; b_k are the coefficients which will satisfy certain conditions; and L_i (T') is the best linear approximation to the functional L_i (T).

The above equation produces a (qxq) system of equations which will provide the solution. Since the difference between L_i (T) and L_i (T') is very small then the error in interpolation should also be as small as possible. In this case, the function φ_k must be chosen such that the mean square error of the interpolation is a minimum. In general least squares, it can be written as:

$$\Sigma (L_i(T') - L_i(T))^2 \Rightarrow \text{minimum} \qquad .....(6.4)$$

whereby the functions are chosen as:

$$\varphi_K = K(P,Q) \qquad .....(6.5)$$

where K(P,Q) is known as a covariance function between values of T at point P and point Q. In general form, the covariance function is given by:

$$K(P,Q) = M(T(P), T(Q)) \qquad .....(6.6)$$

where M is an averaging operator.

The covariance function relies on the mean value of the signal whereby its statistical expectation should be as small as possible, preferably close to zero. If the case is otherwise, then the data can be centred by subtracting the mean value, or by altering the global reference system (e.g. using tailored method as discussed in Chapter 5), thus satisfying the condition. Details of the covariance function and its associated parameters are discussed in the next section.

Now,

$$\varphi_k(P) = L_k^Q K(P,Q) \qquad .....(6.7)$$

where L_k^Q is the functional relating data type Q to T.
In equation (6.7), P is the point where the prediction is being made and Q is a point where the value is known. From equation (6.3):

$$L_i(T_p) = \sum_{k=1}^{q} L_i^P L_k^Q K(P,Q) b_k \qquad .....(6.8)$$

or

$$L_i(T_p) = \sum_{k=1}^{q} C_{ik} b_k \qquad .....(6.9)$$

where C_{ik} is the covariance matrix, $L_i^P L_k^Q K(P,Q)$.

Referring to the beginning of this section, it can be seen that the stochastic component of the observations is expressed by equation (6.1) and consists of three basic covariance functions which are associate with the observations (C_{ll}), the signals (C_{ss}) and the noise (C_{nn}). The relation among them can be written as, (see Figure: 6.1):

$$C_{ll}(\psi) = C_{ss}(\psi) + C_{nn}(\psi) \qquad .....(6.10)$$

where ψ is the spherical distance.

At $\psi = 0$, we have:

$$C_{ll}(0) = C_{ss}(0) + C_{nn}(0) = C_o \qquad .....(6.11)$$

and it is called *variance.*

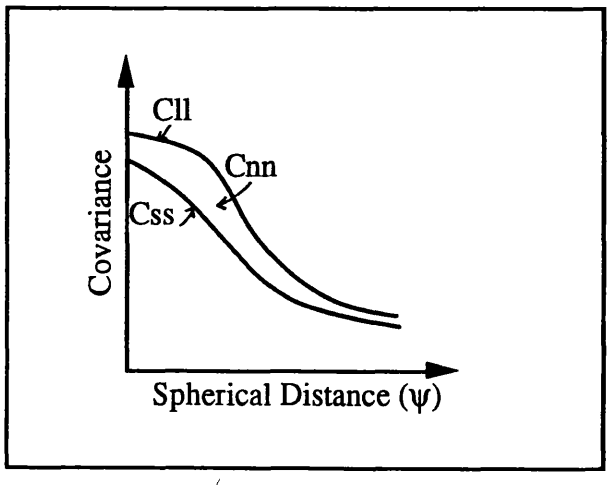

Figure: 6.1 - Covariance functions

From equation (6.10), a least squares solution is obtained by minimising the vector of residuals through:

$$l^T C_{ll}^{-1} l \Rightarrow \text{minimum} \qquad .....(6.12)$$

or may also be written as, (Moritz, 1980):

$$s^T C_{ss}^{-1} s + n^T C_{nn}^{-1} n \Rightarrow \text{minimum} \qquad .....(6.13)$$

This is the minimum *norm* condition of LSC which will derive optimal estimates of the signal. The vector of signals involved in the collocation formulae can include several different types of signal and the covariance matrices for these are the key to handling such heterogeneous data. A least squares best linear estimate for the gravimetric signals, $\hat{s}$, is given by the basic collocation formula:

$$\hat{s} = C_{sl} C_{ll}^{-1} l \qquad .....(6.14)$$

where C_{ll} is the observation variance-covariance matrix;

C_{sl} is the covariance matrix of observation of the predictions and the observations;

l is the vector of observations.

Again, referring to the beginning of this section, equation (6.9) gives

$$b_k = C_{ll}^{-1} l \qquad .....(6.15)$$

From the above equation, one may seen that the need to invert the matrix C_{ll} in order to solve the coefficients b_k, is the major disadvantage of the LSC method computationally.

As a statistical method, LSC is the only gravimetric solution to the BVP which provides error estimates for the predictions. Its ability to do this lies in the use of covariance matrices which imply the accuracy of the observations from which the predictions are made. The *error covariance matrix* of prediction is given by, (ibid):

$$C_{\varepsilon\varepsilon} = C_{ss} - C_{sl} C_{ll}^{-1} C_{ls} \qquad .....(6.16)$$

The matrices C_{sl} and C_{ls} are derived from the covariance function for T by the *law of covariance propagation*, (Moritz, 1980-p.86). The important of LSC solution is that the covariances involved should reflect the actual gravity field accurately in order to be as close to C_{ss} as possible.

From LSC solutions in equations (6.14) and (6.16), the contribution of gravity anomaly to geoid height computation, $N_{\Delta g}$ (see Section 3.5 - equation 3.17), can be computed as follows:

$$N_{\Delta g} = C_{N_{\Delta g},\Delta g_r}(C_{\Delta g_r,\Delta g_r} + C_{nn})^{-1}\Delta g_r \qquad .....(6.17)$$

and the error variance of $N_{\Delta g}$ is:

$$\sigma^2{}_{N_{Dg}} = C_{N_{\Delta g},N_{\Delta g}} - C_{N_{\Delta g},\Delta g_r}(C_{\Delta g_r,\Delta g_r} + C_{nn})^{-1}C^T{}_{N_{\Delta g},\Delta g_r} \qquad .....(6.18)$$

where $C_{N_{\Delta g},\Delta g_r}$ is the cross-covariance matrix of $N_{\Delta g}$, Δg_r;

$C_{N_{\Delta g},N_{\Delta g}}$ is the auto-covariance matrix of $N_{\Delta g}$;

$C_{\Delta g_r,\Delta g_r}$ is the auto-covariance matrix of Δg_r;

C_{nn} is the error covariance matrix of Δg_r, and defined by $C_{nn} = \sigma^2 \mathbf{I}$ where σ^2 the error variance of gravity anomaly and $\mathbf{I}$ is the unit matrix;

Δg_r is the residual gravity anomaly.

6.2.2 Covariance Function

It is obvious from the above equations that the covariance function plays a decisive role in the collocation solution. The reason for this is that, if data was available everywhere (evenly spread all over the earth), then the BVP discussed in Section 2.6, could be solved rigorously without having to use the covariance function to describe the gravity field as *stochastic process*. The covariance function can only be evaluated therefore based on suitable samples of data.

The covariance function is used to express the relationship between the observations and the estimated quantities. As all measurements represent quantities belonging to the earth's gravity field, they are inter-related by functional equations, and it is therefore possible to derive their respective auto and cross-covariances from one basic covariance function. In other words, the covariance function for any gravimetric value can be derived from the covariance function of the anomalous potential by the application of the linear functional through which the two values are related.

The covariance between two values, P and Q, is the expected product of:

$$C(P,Q) = E[(P\text{-}E(P))(Q\text{-}E(Q))] \qquad .....(6.19)$$

For the gravity anomaly , equation (6.19) would become:

$$C(\Delta g_P,\Delta g_Q) = E[\Delta g_P \Delta g_Q] \qquad .....(6.20)$$

and if these points were coincident:

$$C(\Delta g) = E\ [\Delta g^2] \qquad .....(6.21)$$

The above equation is a special case of covariance known as the variance (see also equation 6.11). The variance, as a square value, is chosen to characterise the signal behaviour. Equation (6.21) can be rewritten as:

$$C(\Delta g_P, \Delta g_Q) = M\{\Delta g_P \Delta g_Q\} \qquad .....(6.22)$$

Equation (6.22) forms the basic covariance function which implies the conditions of a *homogeneity* (no location dependence) and *isotropy* (no azimuth dependence). Thus, it makes the covariance function only a function of spherical distance ψ.

For the gravity anomaly, equation (6.22) is written as:

$$C(P,Q) = M[P,Q] = \int_0^{2\pi}\int_0^{\pi}\int_0^{2\pi} \{\Delta g_P \Delta g_Q\} \sin\varphi \partial\varphi d\lambda \partial\alpha \qquad .....(6.23)$$

From equation (6.23), it is seen that the covariance characterises the *statistical correlation* of the gravity anomalies Δg_P and Δg_Q. However, gravity anomalies at points that are far apart may be considered uncorrelated because the local disturbances that cause Δg_P have almost no influence on Δg_Q and vice versa.

By analogy to the above equation, the covariance function for the anomalous potential can also be written as:

$$K(P,Q) = \frac{1}{2\pi}\int_{\lambda_1}^{\lambda_2}\int_{\phi_1}^{\phi_2}\int_0^{2\pi} T(P)T(Q)\partial\alpha\partial\varphi\partial\lambda \qquad .....(6.24)$$

The triple integration in equations (6.23) and (6.24) express the homogeneity ($\partial\varphi\partial\lambda$) and isotropy ($\partial\alpha$) of the function. The computational requirements of a covariance function are that it is symmetric in P and Q, and harmonic, (Moritz, 1980). Unfortunately, minimum variance can only be achieved when the function is the complex *empirical covariance function* derived from the signals. A compromise between simplicity and optimality must be made by fitting a model to the empirical data, which naturally introduces a degree of smoothing and induces errors. The *covariance model fitting* or *synthetic model* will be discussed in Section 6.6.2.

6.2.3 Local Covariance Function

In the application to gravity field approximation, the empirical covariance function is of great value as it closely describes the nature of the anomalous gravity field, on whose values it is based. Since most gravity field studies are undertaken locally, the application of a global covariance function in equation (6.22) to a small area causes numerical instabilities. However, by removing the long wavelength of the geopotential model from the covariance function, the prediction of gravimetric quantities can be undertaken just within the selected area. This is called a *local covariance function,* which is described by Goad, et.al., (1984) as:

"*A special case of a global covariance function where the information content of wavelengths longer than the extent of the local area has been removed, and the information outside, but nearby, the area is assumed to vary in a manner similar to the information within the area* ".

The local behaviour of the covariance function can be characterised by means of three *essential parameters* namely; the *variance* (C_o), the *correlation length* (ξ) and the *curvature parameter* (χ), see Figure: 6.2. Due to isotropy, this function will appear the same in all directions, and it is *rotationally invariant.*

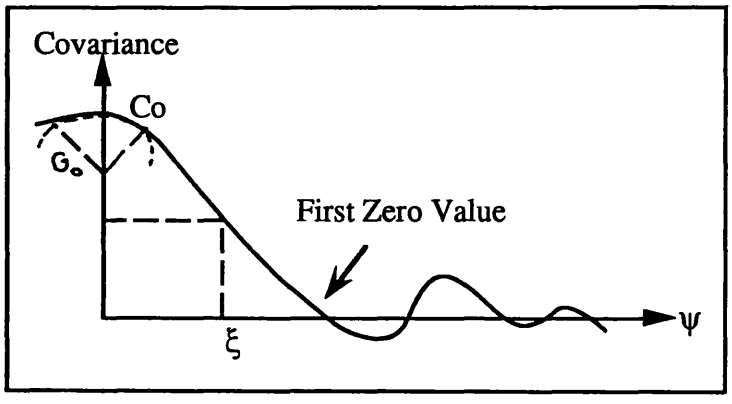

Figure: 6.2 - Essential parameters of covariance function

The variance C_o is the covariance for zero separation (equation 6.11) which is characterised as the mean square value of all observations. The variance acts as a scale factor for the interpolation errors. The correlation length ξ is the distance at which the covariance equals half of the variance. The curvature parameter χ is related to the curvature of the covariance function at the origin through the expression:

$$\chi = \frac{G_o \xi^2}{C_o} \qquad .....(6.25)$$

where G_0 is the horizontal gradient variance of the gravity anomalies.

The essential parameters C_o, G_o, ξ should be considered as quantities which characterise a certain local field. Typically, the covariance function will have a high variance and short correlation length in mountainous areas due to local mass disturbances, and the opposite in smoother terrain. It is shown in Figure: 6.1 that the function tends to undulate around zero at a distance. The shape of the covariance function at distances greater than about 1.5ξ has very little influence on the outcome of the collocation process, (Schwarz and Lachapelle, 1980).

6.2.4 Expansion and Propagation of the Covariance Function

The covariance function is the average of pairs of products over successive distances. For two points on the global sphere, we have:

$$K(P,Q) = \frac{1}{8\pi^2}\int_0^{2\pi}\int_{-\frac{\pi}{2}}^{\frac{\pi}{2}}\int_0^{2\pi} T(P)T(Q)\partial\alpha\partial\varphi\partial\lambda \qquad .....(6.26)$$

where α is the azimuth between the points and the spherical distance between them, ψ, is given by:

$$Cos\psi = Cos\phi_P Cos\phi_Q + Sin\phi_P Sin\phi_Q Cos\,(\lambda_P - \lambda_Q) \qquad .....(6.27)$$

Averaging pairs of product of T in spherical harmonics leads to:

$$K(\psi) = K(P,Q) = \sum_{n=2}^{\infty} k_n P_n(\cos\psi) \qquad .....(6.28)$$

where $$k_n = \sum_{m=0}^{n}(\bar{C}_{nm}^2 + \bar{S}_{nm}^2) \qquad .....(6.29)$$

due to the orthogonality of spherical harmonics which state that the average product of any two different harmonics is zero, see Heiskanen and Moritz, (1967, p. 29). The covariance function is extended into space by introducing a term in r as a scale factor:

$$K(\psi) = \sum_{n=2}^{\infty} k_n \left(\frac{R^2}{r_P r_Q}\right)^{n+1} P_n(\cos\psi) \qquad .....(6.30)$$

where r_P and r_Q are radius vectors for point P and Q, respectively; ψ is the angle between r_P and r_Q; $P_n(\cos\psi)$ are the Legendre polynomials; and R is the radius of some sphere completely inside the mean earth radius: namely the Bjerhammer sphere.

Equation (6.30) is the covariance function for the disturbing potential in spherical harmonics, and this equation can be transformed for other gravimetric quantities by the law of propagation of covariances. For example, from equation (2.41) in Section 2.6, the relation between Δg and T can be rewritten as:

$$\Delta g = -\frac{\partial T}{\partial r} - \frac{2T}{r} \qquad .....(6.31)$$

from which the covariance function for gravity anomalies can be obtained using covariance propagation as:

$$\begin{aligned} Cov(\Delta g_P, \Delta g_Q) &= \left(-\frac{\partial}{\partial r_P} - \frac{2}{r_P}\right)\left(-\frac{\partial K}{\partial r_Q} - \frac{2K}{r_Q}\right) \\ &= \frac{\partial^2 K}{\partial r_P r_Q} + \frac{2\partial K}{r_P \partial r_Q} + \frac{2\partial K}{r_Q \partial r_P} + \frac{4K}{r_P r_Q} \qquad .....(6.32) \end{aligned}$$

Applying this operator on equation (6.30) gives:

$$C(P,Q) = \sum_{n=N+1}^{\infty} c_n \left[\frac{R_B^2}{r_p r_q}\right]^{n+2} P_n(\cos\psi) \qquad .....(6.33)$$

where c_n , the gravity anomaly degree variances, are related to the disturbing potential degree variances by:

$$c_n = \frac{(n-1)^2}{R^2} k_n \qquad .....(6.34)$$

Different models of the covariance function can be obtained by defining c_n in different ways. For example, Tscherning and Rapp, (1974) defined c_n as:

$$c_n = \frac{A(n-1)}{(n-2)(n+B)} \qquad .....(6.35)$$

where A is the scale factor of the degree variance and B is a constant integer parameter describing the structure of the degree variances and cannot be obtained from local information. In practice, the summation is carried to a very high but finite degree.

6.2.5 Empirical Determination of the Covariance Function

In practice, observations are given for discrete points in the area and the calculation of the covariance function is done by numerical integration. In evaluation,

the integrals are replaced by summation since the data values will refer to equal size areas. As the function is assumed to be isotropic, then the covariance is approximated by the average sum of all pairs of products within a specified distance interval $\Delta\psi$:

$$C(P,Q) = \frac{1}{N}\sum_{1}^{N}(\Delta g_i \Delta g_j) \qquad .....(6.36)$$

where N is the number of pairs in the interval $\Delta\psi$.

The empirical evaluation of the variance is straightforward, as it is the mean square value of the signals. The parameter ξ can be interpolated from the curve produced by equation (6.36), but it must be the first point at which $C_\psi = C_o/2$. The horizontal gradient of gravity may be directly measured by torsion balance methods, but this is a cumbersome and, as yet, little used observation technique. Thus, the empirical determination of G_o will not be considered in this study.

It is important that the sample data set is sufficiently large and homogeneously distributed. The size of sample data is governed by two considerations: a good estimate of ξ is obtained when data from an area of at least 1.5ξ is used, and the area should be of an extent greater than, i.e, longer than the minimum wavelength that has been subtracted. If the sample distribution is adequate, then the variance may be accepted as the mean square value and the mean of zero more probably gives unbiased values of C_o and ξ. When using a covariance function derived from sparse gravity data with large gaps, solutions will be biased and thus a low accuracy is achieved. In the LSC method, the prediction errors and the estimation of heterogeneous quantities rely greatly on the optimal function being employed. The importance of reliable and consistent data is obvious.

6.3 Fast Fourier Transforms Method

A lot of research has been done in the application of Fast Fourier Tansforms (FFT) to Physical Geodesy in recent years. The following section will summarise some basic properties of the FFT and outlines its application for the evaluation of Stokes' Integral. Details of mathematical formulation, which follow directly from the definitions can be found in (Bracewell, 1978) and (Schwarz, et. al., 1990) and (Sideris, 1994).

6.3.1 Fourier-Stokes Formula

In a system of plane polar coordinates (α, s) the geoid height N of a point P can be computed by the following integrals, (Heiskanen and Moritz, 1967, p. 121):

$$N = \frac{1}{2\pi g_o} \int_{s=0}^{s_{max}} \int_{\alpha=0}^{2\pi} \frac{\Delta g}{s} s\,ds\,d\alpha \qquad .....(6.37)$$

where g_o is the mean gravity.

By expressing the differential surface $s\,ds\,d\alpha$ in a plane coordinates x, y:

$$s\,ds\,d\alpha = dx\,dy \qquad .....(6.38)$$

equation (6.37) can be transformed into a system of plane Cartesian coordinates:

$$N = \frac{1}{2\pi g_o} \int_{-x}^{x} \int_{-y}^{y} \frac{\Delta g}{r} dx\,dy \qquad .....(6.39)$$

where $r^2 = (x_P - x)^2 + (y_P - y)^2$

More specifically, equation (6.39) can be written in the form:

$$N(x_P, y_P) = \frac{1}{2\pi g_o} \int_{-x}^{x} \int_{-y}^{y} \Delta g(x,y) \frac{1}{[(x_P - x)^2 + (y_P - y)^2]^{\frac{1}{2}}} dx\,dy \qquad .....(6.40)$$

The above equation is a *2D-convolution integral,* see (Bracewell, 1978, p. 243). Using symbol (*) to denote convolution, and

$$l_N(x,y) = r^{-1}(x,y) = (x^2 + y^2)^{-1/2} \qquad .....(6.41)$$

equation (6.40) is abbreviated as:

$$N(x_P, y_P) = \frac{1}{2\pi g_o} \Delta g(x,y) * l_N(x,y) \qquad .....(6.42)$$

Now, this convolution can be evaluated using the two properties of the Fourier transforms, see (Bracewell, 1978, pp. 241, 244 - 245):

$$F\{h(x,y)*g(x,y)\} = F\{h(x,y)\}F\{g(x,y)\} = H(u,v)\,G(u,v) \qquad .....(6.43)$$

$$F^{-1}\{H(u,v)G(u,v)\} = F^{-1}\{H(u,v)\}*F^{-1}\{G(u,v)\} = h(x,y)*g(x,y) \qquad .....(6.44)$$

$$F\left\{\begin{matrix} \frac{\partial h(x,y)}{\partial y} \\ \frac{\partial h(x,y)}{\partial x} \end{matrix}\right\} = 2\pi j \begin{Bmatrix} u \\ v \end{Bmatrix} F\{h(x,y)\} = 2\pi j \begin{Bmatrix} u \\ v \end{Bmatrix} H(u,v) \qquad .....(6.45)$$

where j is the imaginary unit, $j = \sqrt{-1}$.

The symbols F and F^{-1} denote the direct and inverse Fourier transforms, respectively, and H, G denote the spectrums of the functions. u and v are the frequencies corresponding to x and y. Making use of equations (6.41), (6.43), (6.44) and (6.45) in equation (6.42) yields:

$$N(x,y) = \frac{1}{2\pi g_o} F^{-1}\{\Delta G(u,v) L_N(u,v)\} \qquad .....(6.46)$$

where

$$\Delta G(u,v) = F\{\Delta g(x,y)\} \qquad .....(6.47)$$

and from (Bracewell, 1978, p. 249);

$$L_N(u,v) = F\{l_N(x,y)\} = (u^2 + v^2)^{-1/2} \qquad .....(6.48)$$

The function L_N has an analytically defined spectrum. Hence, finally the geoid height can be computed using FFT technique in the form of:

$$N(x,y) = \frac{1}{2\pi g_o} F^{-1}\{\Delta G(u,v) \frac{1}{(u^2 + v^2)^{\frac{1}{2}}}\} \qquad .....(6.49)$$

It is seen that by the use of the Fourier transforms, the evaluation of Stokes' integral is greatly simplified. The numerical integration of Stokes' integral is replaced by one Fourier transform of the gravity anomaly and one product and finally one inverse Fourier transform.

6.3.2 Practical Considerations on the Use of FFT

In the practical implementation of the Fourier transform formulas, two approximations are employed: (i) the continuous integration are replaced by discrete summations and (ii) the infinite limits of summation are replaced by a finite domain. Using discrete Fourier transforms, this assumption replaces the convolution with cyclic convolution (Schwarz, et.al., 1990). Unavoidably this will result in an erroneous Fourier transforms. This effect is called *leakage* because some spectrum leaks from the main lobe to its side lobes, (ibid). It is only caused by the limited record length, which does not permit the long wavelengths to be accurately represented. To minimise this error, the technique known as *padding* is used. Padding consists of embedding the data margins with a border of zeros and the values of the kernel function are computed at both the data and the zero-padded points. The spectrum of the kernel function is

evaluated via discrete Fourier transforms. Not only does this remove the edge discontinuity but it also moves the margins further away from the real data, thus decreasing the likelihood of severe leakage contaminating the centre of the array. Details of the zero padding approach adopted in this FFT exercises are discussed in Section 6.7.2.

6.4 Criteria and Data Used for Test Areas

As previously mentioned in Section 4.3, the three test areas; Area A, Area B and Area C were chosen based on the information of available gravity points and detailed elevation data. These include a large variation in the sample size of gravity points between the test areas, the position and the irregular distribution of these points with respect to terrain types. These are therefore, both from a topographic and gravity coverage viewpoint, differences between the areas which are significant for the geoid determination. This experiment will also verify the importance of the relationship between the gravity coverage and the roughness of the terrain on deriving the expected prediction accuracy of the geoid heights over the test areas. To aid in the comparison of the three test areas, the classification in terms of the gravity field variations and terrain characteristics is summarised in Table: 6.1.

The 'R' value in Table: 6.1, represents a '*Goodness of Representation* ' which gives some objective measure or estimate of how well the gravity field variation is modelled by the gravity density and the roughness of the terrain in the test areas. This value can be calculated using 10^{-3} times the product of the average gravity coverage ($\bar{g}$) and the standard deviation of height data, σ_H, in the area of interest, see Kearsley, et.al., (1985).

Test Area	Gravity Coverage		Terrain Characteristics		'R'
	No. of Gravity Stations	Average Coverage $\bar{g}$ (km^2/pt)	Mean Height (metre)	σ_H (metre)	'Goodness of Representation'
Area A	190	40	525	485	19.4
Area B	420	25	300	246	6.2
Area C	224	25	20	32	0.8

Table: 6.1 - Details of gravity coverage and terrain characteristics for the Test Areas.

(Note: $R = \bar{g} \times \sigma_H \times 10^{-3}$).

In general, it can be shown that a low value of R indicates a well represented area, e.g. good spacing between stations with a smooth topography. Conversely, a high value indicates a poorly represented area, e.g. bad or large spacing in a rough topography, (ibid). Therefore, it will be of interest to see for example, how much better Area C and Area B are represented than Area A, having a good gravity coverage and, in parts, characterised by smooth and medium topography, respectively.

Probably the most striking feature of Table: 6.1 is the contrast in the gravity coverage between Area A and Area B. The gravity coverage in Area A is too low, i.e. about 1 point per 40 km^2 and irregularly located at lowland areas rather than on the mountain tops. The goodness of representation factor, R for Area A shows that the gravity field in this area is not modelled very well because its high value (R = 19.4) indicates a poorly represented area, i.e. no gravity value in a rough topography, see Figure: 4.5. Conversely, a low value of R = 6.2 in Area B (see Figure: 4.6) indicates a better represented area as the distributed gravity is considered to be at a reasonable spacing between stations with a smooth to moderate topography. However, in the central part of this area, there was no gravity data set available due to its rugged topography. It is interesting to see that the R value for Area C (see Figure: 4.7) is the lowest one (R = 0.8) despite having less sample gravity data with respect to Area B. This phenomenon has been characterised by the fact that this area is basically more smooth terrain, lying between 0 to 150 m, more or less split evenly in the east-west direction, and consequently the gravity density and its coverage are considered to be reasonably good.

6.5 Practical Determination of the Terrain Contribution

It has been mentioned in Section 3.6 that the rugged topography is a major cause of variations in the gravity field which will be local and of a high frequency signal. The irregularities of the local gravity field (especially in the mountainous areas), however, can be smoothed by a suitable gravity field terrain correction. In this way, it is possible to use even very sparse gravity data sets in areas with rugged topography and still obtain reasonably good approximation results, (Forsberg and Madsen, 1981). The computation of terrain effects in this study, serves for two purposes:

(i) To study the effect of the terrain-reduced anomalies in geoidal computation for the areas with smooth to medium topography and also with reasonably good gravity coverage (most part of Areas B and C); and

(ii) Naturally, it cannot do anything in a completely large unsurveyed area, i.e. the areas with rugged topography (most eastern parts of Area A and the central

part of Area B) except to use the topography to generate the RTM contribution to the gravity anomalies (Δg_{TC}) plus the gravity contribution from geopotential model (Δg_{GM}). This *'filled-in'* anomalies (Δg_{Fil}) will naturally give a biased geoid solutions but sometimes this is the only possible approach to estimate the gravity field information in the 'empty areas', and this is what is called working with a *geophysically predicted gravity field* (Tscherning, 1994 - Private Communication). Thus, in the absence of real observations, it should be accepted to use these data for the purpose of this study, see Section 1.3(v) and (vi). This choice is justified because due to the limitation of the gravity density and coverage, one must still endeavour to make a start at computing the geoid in this mountainous area, and at the same time assess the influence of the topography on the gravimetric solution.

The computation of terrain corrections was done for the three test areas using the program *TC1* (part of the GRAVSOFT software). This program has the option of evaluating the terrain contribution (short wavelength signals) by four different techniques, one of which is the RTM (see Section 3.6), for the effect on any combination of gravimetric quantities. The computation is based on two DEMs, a detailed and a coarse gridded height data which are used in the inner and outer zones, respectively. The two grids are assumed to have common boundaries, which is the case if the coarse grid have been constructed from the detailed grid by averaging. As previously mentioned in Section 3.6, the integration of the terrain effects is performed using the formulae for the gravitational effects of a homogeneous rectangular prism (see Figure: 3.8).

In the program TC1 , a consideration is taken of the very localised effect at, say, 1 km or less, from the computation point. The effect is found to be very significant for gravity anomalies, so around the computation point the finest DEM is densified using a bicubic spline interpolation procedure. Since gravity terrain effects are strongly dependent on the height of the computation point (i.e. through the term $2\pi G\rho h$), a special precaution is necessary when the height of the computation point does not agree with the interpolated height from the DEM. Either the computation points can be 'forced' to match the interpolated topography level, or the topography can be modified locally to give the 'right' value at the computation point. The first option was chosen in the RTM reduction for all test areas due to the gravity anomalies being closely correlated with height (see Figure: 4.3, Section 4.2.2). Less discrepancy is introduced this way. The discrepancy between the DEM and station heights will always be present, since the DEM will hardly ever have sufficient resolution to represent all features of rugged topography.

To further increase computation speed and allow the use of less detailed remote topography, it is practical to use a coarse and detailed grid system. The computation may be done out to a fixed distance from the computation point or for all masses in a given area. The detailed elevation grid is used out to a minimum distance, and the coarse elevation grid is used for the remainder of the topography. This is fully implemented in the program TC1 for all test areas. Figure: 6.3 shows that, in a small inner zone 3 x 3 grid points just around the computation point, the topographic data are densified using a bicubic spline interpolation, so that a 'finer' more smooth set of prisms is used to integrate the often large effects of the inner zone, see Forsberg, (1984).

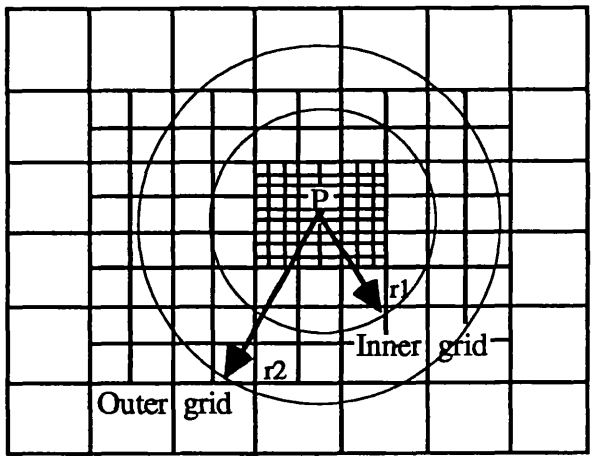

Figure: 6.3 - Use of innerzone, detailed and coarse height grids in TC1.

From the available detailed height data, the coarse heights were constructed for each of three areas. In RTM-reduction, a suitable mean height surface was interpolated using the program *TCGRID* from these coarse mean height grids. Basically, the degree of smoothing is determined through the resolution of the mean height surface. However, the outcome of the final prediction is almost insensitive to the choice of the resolution of the mean height surface, providing it is somewhat bigger than the resolution of the gravity data used in the collocation or FFT process, see Tscherning, (1981).

Due to the need for height data around every point to a specified distance, there will be a considerable overlapping of the grids within the computation areas defined by radius r_1 and radius r_2 (Figure: 6.3). The substantial value for r_2 is necessary to avoid aliasing effects of the high wavelength (Forsberg, 1984). In this experiment, the r_2 value was selected by computing for some points (evenly selected in the test areas) the contributions of the RTM to different distances from the computation points in such a way that beyond this distance, the results were quite similar showing not much

information gain in the terrain effect signal. Thus, the radii (r_1, r_2) chosen were (5km, 55 km) for Area A, (5km, 40km) for Area B, and (5km, 15km) for Area C. Table: 6.2 shows the resolution of height information that is used in the terrain effect evaluations for each of three areas. Appendix M shows the example of the input and output of program TC1.

Area	Detail Height	Coarse Heights	Gridded Mean Height Surface
Area A	30"x30" ~(1km x 1km)	2.5' x 2.5' ~(5km x 5km)	10' x 10' ~(18km x 18km)
Area B	1' x 1' ~(2km x 2km)	3.5' x 3.5' ~(6km x 6km)	10' x 10' ~(18km x 18km)
Area C	2' x 2' ~(4km x 4 km)	5' x 5' ~(10km x 10km)	15' x 15' ~(30 km x 30 km)

Table: 6.2 - Height resolution used for the RTM evaluation in the three test areas

6.6 The Computation Procedure Using the LSC

In this section, details of computational procedures using the LSC method is presented. These includes the pre-processing of the data, estimation of empirical and analytical covariance functions and geoid prediction in the test areas. The LSC program modules (except program GEOMOD) were used in this study. These LSC program modules consist of three main programs:

EMPCOV (EMPirical COVariance) - the program to produce (estimate) values of an empirical covariance function from a sample data set.

COVFIT (COVariance FITting) - the program to fit an analytical expression for the covariance function of the anomalous gravity field.

GEOCOL (GEOdetic COLlocation) - The program to estimate (predict) the gravity field model using LSC method (using parameters and functions) described in Section 6.2.

A general data flow and program module diagram used in the LSC method for geoid determination of each of the three test areas is shown in Figure: 6.4.

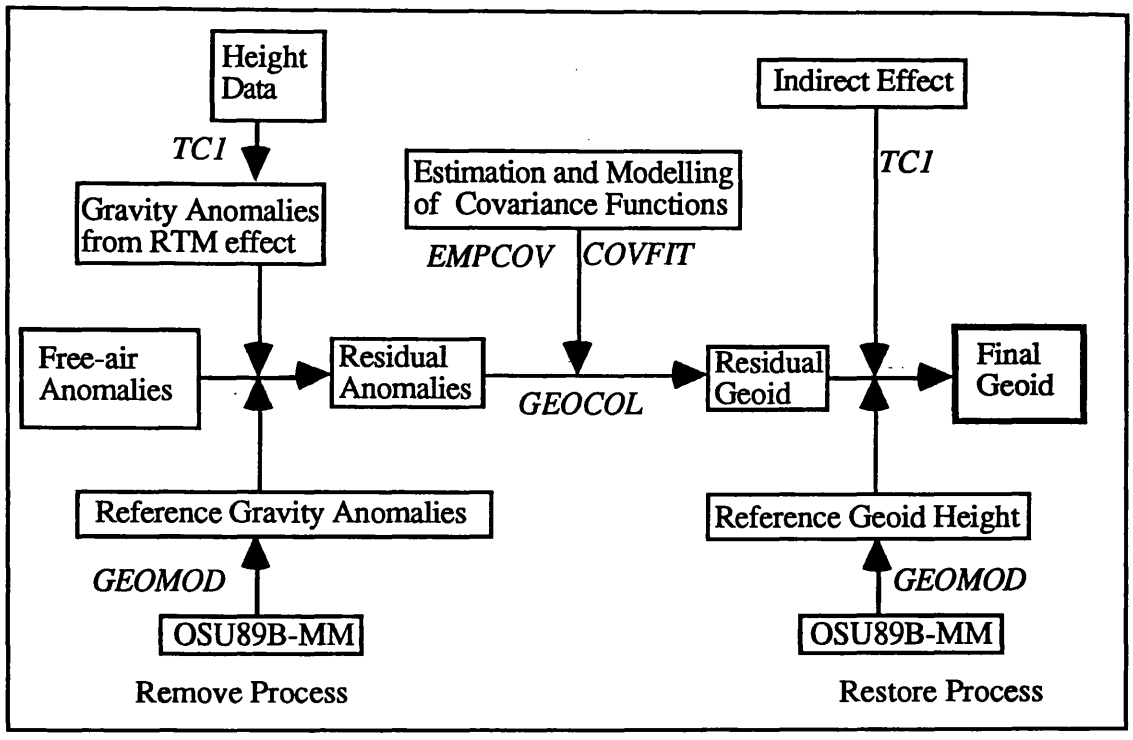

Figure: 6.4 - Data flow and program modules of LSC method used in geoid height computations

6.6.1 Pre-processing of the Data

A solution for equation (6.17) assumes that the expected value of the residual vectors over the test areas is as small as possible; preferably the mean value of the residuals should be zero. This condition can be satisfied by subtracting the regional trend from the measurements. The gravity data used for the prediction have been reduced for the effect of the tailored model OSU89B-MM. That is, the respective disturbing potential components at corresponding points, as derived from OSU89B-MM have been subtracted from observations forming a residual data set which will describe the local behaviour of the gravity field only. Thus,we have:

$$\Delta g' = \Delta g_{FA} - \Delta g_{GM} \qquad .....(6.50)$$

where Δg_{FA} is the point free-air anomaly, and Δg_{GM} is the gravity anomaly computed from OSU89B-MM using equation (3.19). The above equation is equivalent to equation (3.20) in Section 3.5. The effect Δg_{TC} of the topographic masses (RTM effects) is computed from gridded height data by integration (see Section 6.4), to get the terrain-reduced residuals:

$$\Delta g_r = \Delta g' - \Delta g_{TC} \qquad .....(6.51)$$

It should be emphasised here that, since the gravity coverage was not sufficient for Area A and Area B (see Figure: 4.5 and Figure: 4.6), the available reduced gravity anomalies (Δg_r) were merged with the 'filled-in' anomalies (Δg_{Fil}) which were obtained from the tailored model contribution (Δg_{GM}) and also from the RTM contribution (Δg_{TC}). A total of 450 (at 2'x2' spacings in area of $4.07° \leq \phi \leq 4.87°$, $101.20° \leq \lambda \leq 101.77°$) and 54 (at 3'x3' spacings in area of $3.00° \leq \phi \leq 3.35°$, $101.80° \leq \lambda \leq 102.2°$) Δg_{Fil} were used for Area A and Area B, respectively. The chosen grid spacings were based on the following reasons:

(i) To retain the amount of gravity field information (both Δg_{GM} and Δg_{TC}) in areas of greater geoid variations; and

(ii) To reduce the computational load in the LSC solutions, i.e. to avoid the extremely time-consuming matrix inversion and storage problems with the available computer resouces.

The 'merged' reduced gravity anomalies in Area A and Area B will be used throughout this study. Consequently, it is expected that the computed value of the residual geoid heights in these 'filled-in' areas will be systematically of low accuracy. This approach of 'filled-in' anomalies in large unsurveyed areas has been used by Despotakis, (1987) in his computation for gravimetric geoid heights at Laser Tracking Stations.

6.6.2 Estimation of Covariance Function

Two local empirical covariance functions have been estimated for each test area, i.e. using reduced anomalies from equation (6.50) and equation (6.51), respectively. Thus in total 6 covariance functions are estimated by the program EMPCOV using the technique of equation (6.36). This program requires only a set of reduced data observations, given either by equation (6.50) or equation (6.51). The distance interval and the number of steps must be specified along with the type of data. Appendix N shows a standard input file for the program, which provides the information required and guides the program through its several options by a series of 'logical' values (T = 'True' or F= 'False'). The output of EMPCOV is used for the fitting of a model, i.e. a synthetic function. Appendix N shows a sample of the corresponding output from the standard input file of the program EMPCOV.

The local empirical covariance function computed from program EMPCOV is replaced by a model in the form of equation (6.33) which will be specified by equation (6.35). The covariance function model used in this study was the Tscherning and

Rapp, (1974) model. The local model must be fitted to the empirical function by adjusting the free parameters of equations (6.34) and (6.35), so that the essential parameters of the empirical function are reproduced as closely as possible. These parameters are: a positive constant A, the radius of the Bjerhammer sphere R_B, and the order of the local covariance function N.

The parameter A is influenced by the variance and R_B is the correlation factor. This parameter is the radius of the Bjerhammer sphere and as such is a large value (~6371 kilometres). For ease of adjustment, the parameter R_B is replaced by (R_E-R_B) which is the depth of the Bjerhammer Sphere from the sphere of mean earth radius. This parameter will still be identified by R_B. The ease of fitting R_B depends on the data spacing relative to the correlation length. The order of N is selected by fitting the first zero value of the empirical covariance function, see Arabelos, et.al., (1987) and Gil, et.al., (1993). Thus, it has the effect of aiding the fit to the correlation length and maintaining as far as possible the first zero value of variance. However, in fitting the model to the empirical values of C_o and ξ (and also the first zero value of variance, ψ_o), it is not possible to get an exact agreement with each, and therefore, a compromise must be made.

The actual fitting procedure is undertaken by holding the variance so that the function is defined only by ξ, and then R_B and N are varied until the computed correlation length and zero variance more or less agree with the actual (the empirical function). The influence of R_B is the major cause of fitting ξ. A is determined directly from the current values of C_o. The analytical approximation of the empirical covariance functions are computed by the sequence of subroutine *COVAX*, *COVBX* and *COVCX* which form a part of the program COVFIT, (Knudsen, 1987). The standard input file and the corresponding output of the program COVFIT is given in Appendix O.

6.6.3 LSC Residual Geoid Prediction

The essential background work for the prediction of geoid height by LSC has been fully described in the preceding sections. This includes reducing data and fitting a model to the empirical covariance function. The way in which all these tasks were combined to produce a geoid database will be discussed here. The program GEOCOL was the main tool used in this prediction.

6.6.3.1 Program GEOCOL

The program GEOCOL computes an approximation to the anomalous potential, T, using LSC which can be transformed into any other related gravimetric disturbances,

(see Table: 2.3). GEOCOL is a vastly flexible program with a wide application to gravity field determination. It has a modular structure involving more than 50 subroutines and functions, although not all of these need be used for a particular run. GEOCOL has 18 possible input steps; the number used depends on the data being input and the required solution. Thus, the program allows several modes of input and output, the selection of which is specified to the program by user-defined logical variables.

In GEOCOL, the computation is performed in a number of steps equal to the number of observation sets. For each set, a harmonic function for T is produced, the combination of which will give the solution. Each function is produced by multiplying the constants b_k by the covariance between the observations and the prediction (C_{sl}) described in Section 6.2.1. Hence, for the geoid height:

$$N = \sum_{k=0}^{q} b_k C(N, \Delta g) \qquad .....(6.51)$$

GEOCOL accepts several kinds of data as input and will output similar quantities, as well as bias parameters. The program will also accept or output data on several reference systems and undertakes transformations between them; one system (e.g. GRS80) is nominated on which to approximate T, but the observations and predictions may be on any system, if the transformation parameters are specified. As previously mentioned in Section 2.3.2.2, the GRS80 (Code = 5 in GEOCOL program) is used in geoid height prediction for all test areas.

As a part of the standard input file, the program is required to output information according to the state of completion so far. The major tasks of the program are to reduce the observations and solve the normal equation for b_k which is very extremely time-consuming matrix inversion. The reduced anomalies, with associated information, and the solutions to the equations are written into a file called as *restart file*. The GEOCOL program also requires a temporary file for storing the normal equations as they are solved; this will be an extremely large file.

Appendix P shows a standard input file for GEOCOL which permits a full run for geoid height predictions either as a list of points (sequential latitude, longitude, geoid height) or in grid format which consists of the grid specification (ϕ_1, ϕ_2, λ_1, λ_2, $\Delta\phi$, $\Delta\lambda$) followed by bands of predictions. The latter option was selected since it involves considerably less computer space and can be easily manipulated for interpolation. The residual geoid heights were computed on 2', 3' and 5' spacing in each direction for Area A, Area B and Area C, respectively. These spacings were chosen so that detail was retained in areas of greater geoid variation (Area A and Area

B) and a decreased density would be reasonable for Area C where the geoid gradient is relatively low. In total two residual geoid height databases were computed for each test area, i.e. with and without terrain contributions, using the GEOCOL program. Appendix P shows a sample of the output of program GEOCOL.

6.6.3.2 Final LSC Geoid

The task of GEOCOL is to use gravity anomalies, already reduced for long wavelength and short wavelengths, to compute an approximation to the anomalous potential which can be converted to any other gravimetric quantity. These effects must be restored to the prediction (residual geoid heights) that have been produced by GEOCOL for a complete geoid height, either using equation (3.21) for long wavelength geoid height contribution, or using equation (3.17) for both the short and long wavelength geoid height contributions. The values of N_{TC} are computed at specified points using program TC1.

Given only a set of complete 'LSC geoid height' predictions, it is necessary to interpolate these to stations where geoid heights are required for comparison purposes, for example at GPS control points. Here, the program *GEOGRID* - GEOdetic GRIDding (also part of the GRAVSOFT program modules) was used to predict the geoid height (using weighted means method) for 51 GPS stations in Area B (the Federal Territory GPS Network) and for 5 GPS stations in Area C (part of the Southwest GPS Network - stations no. GP49, GP50, GP51, GP53 and GP61). No GPS control points were made available by the DSMM for Area A. The program GEOGRID is a fast program for gridding randomly distributed data into a rectangular grid, for interpolating data in profiles, or for interpolating individual points using enhanced fast weighted means interpolation or collocation-kriging method.

6.7 The Computation Procedure Using FFT

In the following section, details of practical geoid computation using the FFT method are presented. These include data requirement and pre-processing, and the computational procedure adopted for residual and final geoid computations. The main FFT program modules used in this study is the program *GEOFOUR* - GEOid FOURier (part of the GRAVSOFT program modules). Basically, the program GEOFOUR implements the Fourier method of modelling the gravity field (in a frequency domain) using gridded input data. The gridded data is produced by the program GEOGRID. As with the LSC, results of the FFT computations will also be presented and analysed in the next chapter. Figure: 6.5 shows the data flow and the FFT program modules used in this study.

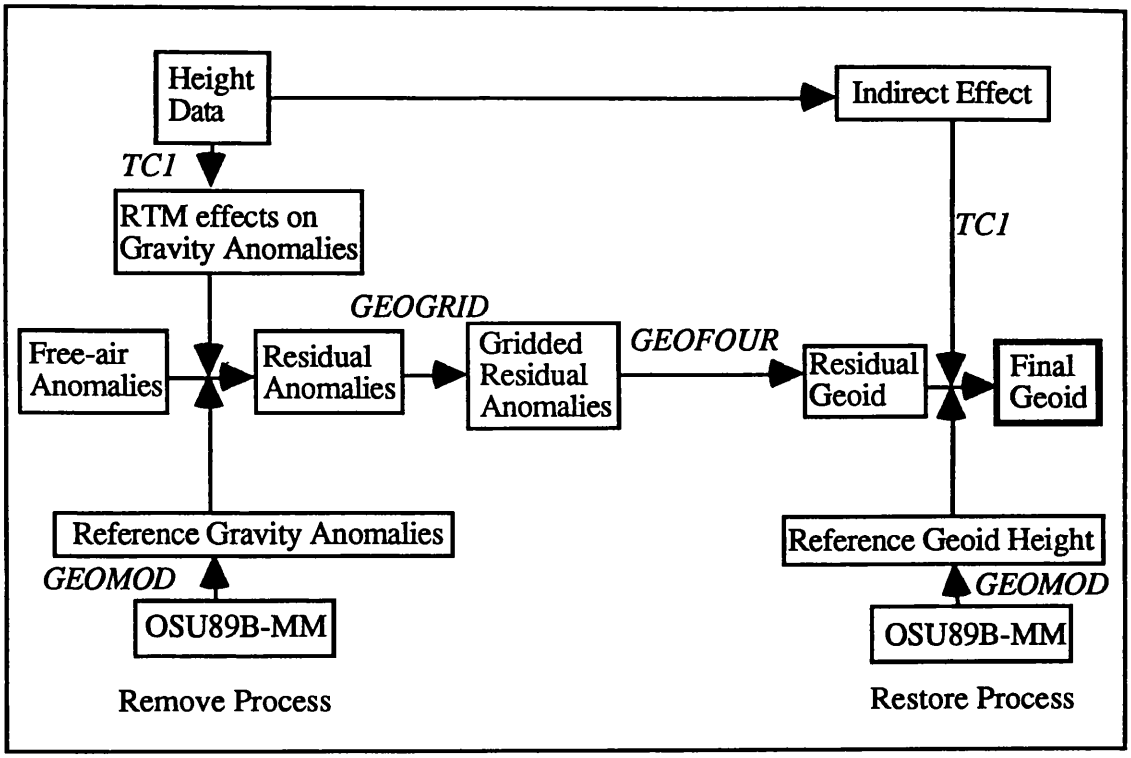

Figure: 6.5 - Data flow and program modules of FFT method used in geoid determination in three test areas

6.7.1 Data Requirements and Pre-processing

The FFT method of evaluating Stokes' Integral requires gravity anomalies (Δg) given on a grid. When the point anomalies are randomly distributed, an interpolation method has to be utilised in order to predict values at the nodes of the grid. To minimise aliasing effects (see Section 4.6.1), a small grid spacing must be selected, especially for the zone close to the computation point. The long wavelength variations of the gravity field have been taken care of by subtracting the effect of the tailored model OSU89B-MM, i.e. using equation (6.50). This also reduces the edge effects of the FFT. The short wavelength variations of the gravity field coming mainly from the topography were removed using gridded height data, and again this was done using program TC1.

The input data for the FFT computation of residual geoid heights were 2'x 2', 3'x3' and 5'x5' gridded reduced anomalies (with respect to both the tailored model OSU89B-MM and the RTM contributions) for Area A, Area B and Area C, respectively. These gridded residual anomalies were computed from randomly distributed point anomalies in those areas using the techniques of weighted means via the program GEOGRID. It has to be mentioned here again, that the 'filled-in' anomalies

were applied in the large unsurveyed areas of the eastern part of Area A and also in the central part of Area B. These 'filled-in' anomalies were then merged with the existing reduced anomalies before the gridding procedure took place.

In this present exercise, the above mentioned grid spacings were chosen in such a way that they can verify the correlation between the topographic variations (roughness) and the accuracy of the geoid over the test areas. Another reason is that by using a denser grid spacing of the data set in the rough variation of gravity field, e.g. Area A, some of this detail loss can be minimised.

6.7.2 FFT Residual Geoid Height Computation

The essential background work for the estimation of geoid height by FFT has been described in the preceding sections. This includes reducing and gridding data sets, which is part of the FFT requirement. The gridding of data was the most time consuming step in the FFT gravity field modelling process. The method in which all these tasks were combined to produce a geoid database will be discussed here.

The program GEOFOUR (GEOid FOURier) was the main tool used in this estimation. Taking gridded residual gravity anomalies as input, GEOFOUR uses Stokes' Integral by means of Fast Fourier transforms to compute the geoid heights on the same grid simultaneously. In principle, this program uses an approximated planar Stokes kernel function (in the frequency domain) given by equation (6.49). The values of the kernel function are evaluated via discrete Fourier transforms. For the sake of comparison with the LSC method, in total, only 3 residual geoid heights were computed using the GEOFOUR program whereby the input data were gridded from the reduced anomalies of equation (3.18). To be consistent with the LSC exercise, the geoid was computed at 2'x2', 3'x3' and 5'x5' grid spacings for Area A, Area B and Area C, respectively. Similar to the LSC exercises, these grid spacings were chosen in such a way that detail was retained in areas of greater geoid variation (Area A and Area B) and a decreased density would be reasonable for Area C where the geoid gradient is relatively low.

As previously mentioned in Section 6.3.2, the solution of the BVP using the FFT method suffers the effect of circular convolution. To prevent the effect of the circular convolution, a zero padding must be applied. In this exercise, the zero padding approach was done by embedding 100% zeros (50% to each side) around the data margins for all test areas. The geoid heights from discrete FFT with 100% zeros padding around gravity anomalies gives optimal results, i.e. the leakage effect (effect of circular convolution) is minimised, see Arabelos and Tziavos, (1994), Tsuie, et.al.,

(1994) and Sideris and She, (1995). A drawback with the border of zeros approach, in terms of this project which already involves computing exceeding large Fourier transforms, is that adding a border increases slightly the array size and hence the computation time. However, this is not a main drawback of the FFT when compared to the LSC exercise. For example, it has been encountered from these two exercises that, for local gravity field computations, the FFT method was about 10^4 to 10^5 times quicker than the LSC method, for no significant loss in accuracy. Appendix Q shows a standard input file and the output of the program GEOFOUR.

6.7.3 Final FFT Geoid

The task of GEOFOUR is to use gravity anomalies, already reduced for long wavelength and short wavelengths, to compute geoid height in a grid format. These effects must be restored to the prediction (residual geoid heights) that was output by GEOFOUR for a complete geoid height. Here, the same steps described in Section 6.6.3.2, were taken for obtaining the final FFT geoid height for each test area.

Similar to the LSC procedure, given only a set of complete 'FFT geoid height' estimations, it is necessary to interpolate these to stations where geoid heights are required for comparison purposes, i.e. at 51 GPS control points in Area B and also 5 GPS control points, i.e. GP49, GP50, GP51, GP53 and GP61 in Area C. As mentioned before, no GPS control points were available in Area A for comparison purposes. Again, the program GEOGRID was used to predict the geoid height for the available GPS points.

6.8 Summary of Practical Geoid Computation

In Sections 6.6 and 6.7, the geoid height computations were carried out for three test areas using the LSC and the FFT gravimetric methods. For the LSC method all residual gravimetric geoid heights were computed using anomalies that have been reduced to the following contributions:

(i) tailored model OSU89B-MM - (Case I),

(ii) tailored model OSU89B-MM and the RTM effects - (Case II).

For the sake of comparison with the LSC method, the residual gravimetric geoid heights in all test areas were also computed using the FFT method. In this FFT exercise, the input anomalies were 'gridded' from the residual anomalies which already have been reduced with respect to the tailored model and the RTM contribution only, i.e. Case II. Since the computation of residual geoid heights are based on the 'remove-

restore' procedure, these geoid height values have to be restored using either equation (3.21) for case I or equation (3.17) for case II.

In order to evaluate the accuracy of the computed gravimetric geoid, the external control data such as GPS/levelling points can be employed. In this study, the geoid height at 51 GPS stations in Area B (Federal Territory GPS Network) and 5 GPS stations in Area C (part of Southwest GPS Network) were interpolated from the gravimetric geoid height database. As mentioned previously, no GPS control points were made available by the DSMM for evaluation against the computed gravimetric geoid in Area A.

For the sake of the simplicity of representation and analysis of the results in the next chapter, all computational geoid height exercises are summarised in Table : 6.3.

Test Area	Area A		Area B		Area C	
LSC method (Main Programs): EMPCOV COVFIT GEOCOL	Case I	Case II	Case I	Case II	Case I	Case II
FFT method (Main Programs): GEOGRID GEOFOUR	-	Case II	-	Case II	-	Case II
Geoid Heights Interpolation at the available GPS control points (using GEOGRID)	-	-	-	Case II (LSC and FFT)	-	Case II (LSC and FFT)

Table: 6.3 - The Summary of Practical Geoid Computation for Three Test Areas

CHAPTER 7

PRESENTATION AND ANALYSIS OF RESULTS

7.1 Introduction

The mathematical formulation and the practical computation of geoid solutions using the LSC and the FFT methods have been described and discussed in the previous chapter. The geoid heights for the three test areas, i.e. Area A, Area B and Area C were computed using a number of different data combinations to enable an evaluation of the impact of the various types of data upon the results. The high frequency components are evaluated by the RTM effects; the medium frequency components of the gravity field are provided by point free-air anomalies, and the low frequencies are modelled by the OSU89B-MM tailored model coefficients complete to degree and order 360 which fit the gravity field of the Peninsular Malaysia region (see Chapter 5). All gravimetric geoid height computations were carried out on the GRS80 reference frame and using the 'remove-restore' procedure. The test results are summarised in Table: 6.3, Section 6.8. For the sake of consistency of representation and discussion of the results, similar notations, i.e. 'Case I' and 'Case II' described in Section 6.8 will be used again, in all relevant tables and figures throughout this chapter.

The results of the RTM computations in all test areas are first analysed in some detail in this chapter. The purpose of this section is to see the possible terrain effect on the anomalous gravity field (for gravity anomalies and geoid height) with respect to topographic viewpoints in the test areas. Then the discussion is focused on the results of practical estimation of covariance functions. As covariance reflects the statistical correlation between variables, the covariance function describes the correlation across the test areas by its variation with spherical distances. Thus, it has certain characteristics which are essential to the success of LSC. The solutions of LSC performed are then given for each test area for both cases, i.e. Case I and Case II. Comparisons between Case I and Case II are also discussed in order to see the effect of the terrain contribution in gravimetric solutions. The comparisons between the LSC and the FFT solutions are also presented, but this will be for Case II only. Finally, the gravimetric geoid heights obtained by the LSC and the FFT solutions (for Case II solution only), are compared with independent external results, that is the available GPS/levelling derived geoid heights. The discrepancies between the 'observed' and the 'computed' geoid heights are summarised and discussed in terms of both the absolute and the relative differences.

7.2 Results and Analysis of the Residual Terrain Model Contribution

As previously described in Section 6.5, the RTM contributions for gravity anomalies and geoid heights were computed using the program TC1 for all test areas. In brief, for these RTM computations, two height grids were used in addition to the reference grid; a fine grid for close information and a coarser grid for the more remote topography. The computations at points were carried out to a fixed radius based on these grids using the formulas for the gravitational effects of a homogeneous rectangular prism. The majority of the high frequency effects of the anomalous gravity field were due to very near topography.

Table: 7.1 contains the statistical results that are associated with the RTM contributions for these anomalous gravity field for each test area. Figures 7.1(i), (ii) and (iii) depict the contour plots for short wavelength contributions to gravity anomalies in Area A, Area B and Area C, respectively. Similar contour plots for the geoid heights for these test areas are also shown in figures 7.2(i), (ii) and (iii), respectively.

Test Area	Area A		Area B		Area C	
	Gravity Anomaly (mgal)	Geoid Height (m)	Gravity Anomaly (mgal)	Geoid Height (m)	Gravity Anomaly (mgal)	Geoid Height (m)
Mean	0.15	0.03	0.27	0.03	0.02	0.01
Std. Dev.	42.75	0.22	20.36	0.20	2.27	0.02
Min.	-51.50	-0.35	-42.45	-0.30	-2.10	-0.01
Max.	105.60	0.62	86.15	0.56	14.70	0.05

Table: 7.1 - The statistical results of the RTM contribution of gravity anomalies and geoid heights for each of test area

It is apparent from Table: 7.1 that the RTM contribution on the gravity anomalies and geoid heights is almost insignificant for smooth terrain such as Area C. In contrast, a lot of higher frequency gravity field information is gained by the RTM effect for the rough terrain of Area A and Area B. Of main interest are the magnitudes of the terrain effects on the gravity anomalies and the geoid heights in each of the areas. For example, the RTM contribution in Area A for gravity anomalies and geoid height amount to over 100 mgals and 0.5 m, compared to Area C which is about 15 mgals and 0.05 m, respectively,

From the same table and all figures, an analysis of the RTM contributions has shown that the total mass removed by using a reference surface was on average close to zero, but the major requisite is that the mass removed be a harmonic function. The average of zero masses corresponds to the fact that because the RTM is evaluated on a reference mean height surface (h_r), as 'finite elements' in effect, that may have a negative mass (below h_r) or positive mass (above h_r), only the masses extra to this reference surface are modelled as described in Section 3.6 (Figure: 3.7-C). As described in Section 2.6, the harmonic condition is very important for the solution of the BVP using any gravimetric method.

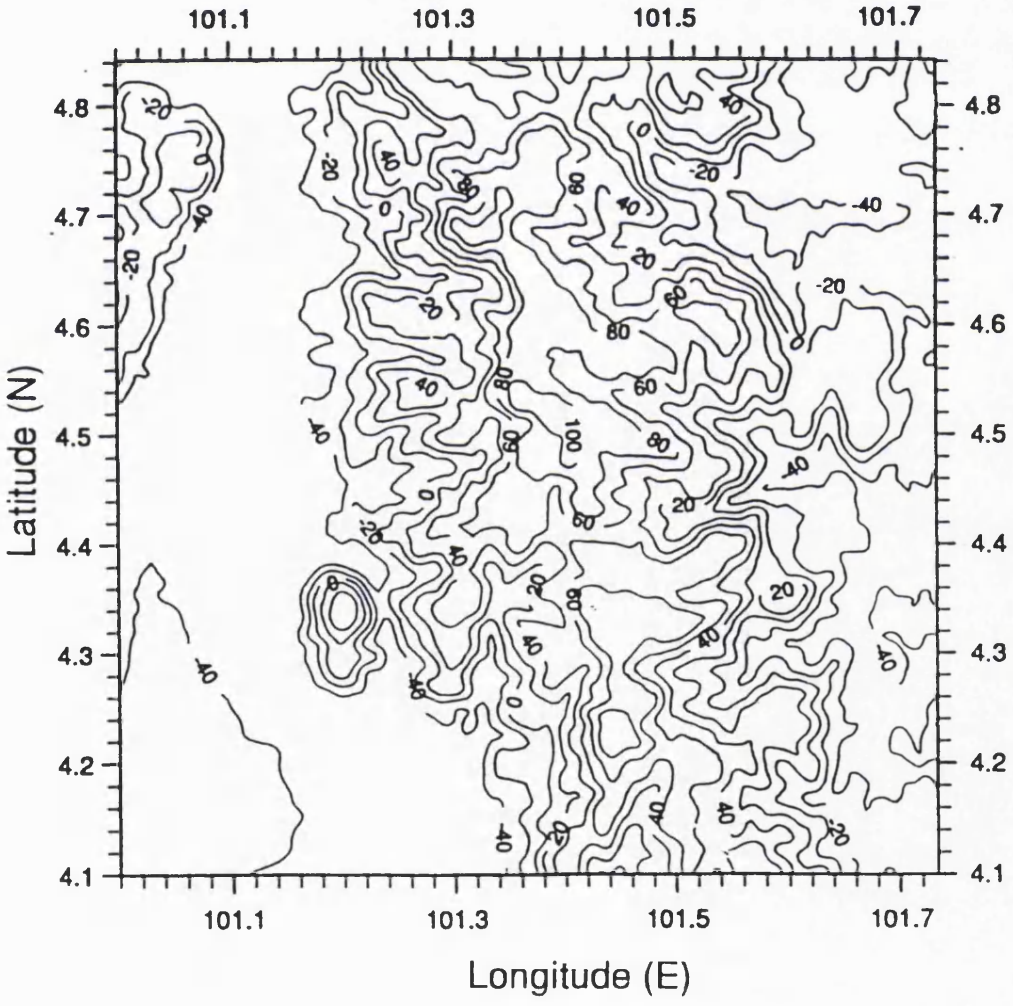

Figure: 7.1(i)-The RTM contribution of gravity anomalies for Area A - (C.I=20 mgals)

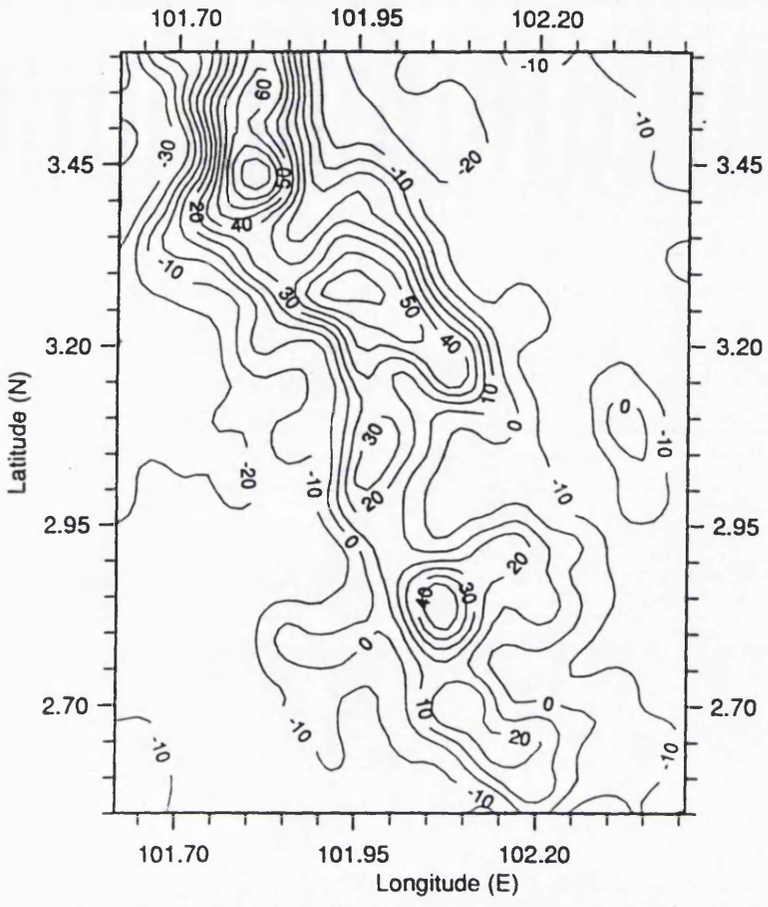

Figure: 7.1(ii)-The RTM contribution of gravity anomalies for Area B - (C.I=10 mgals)

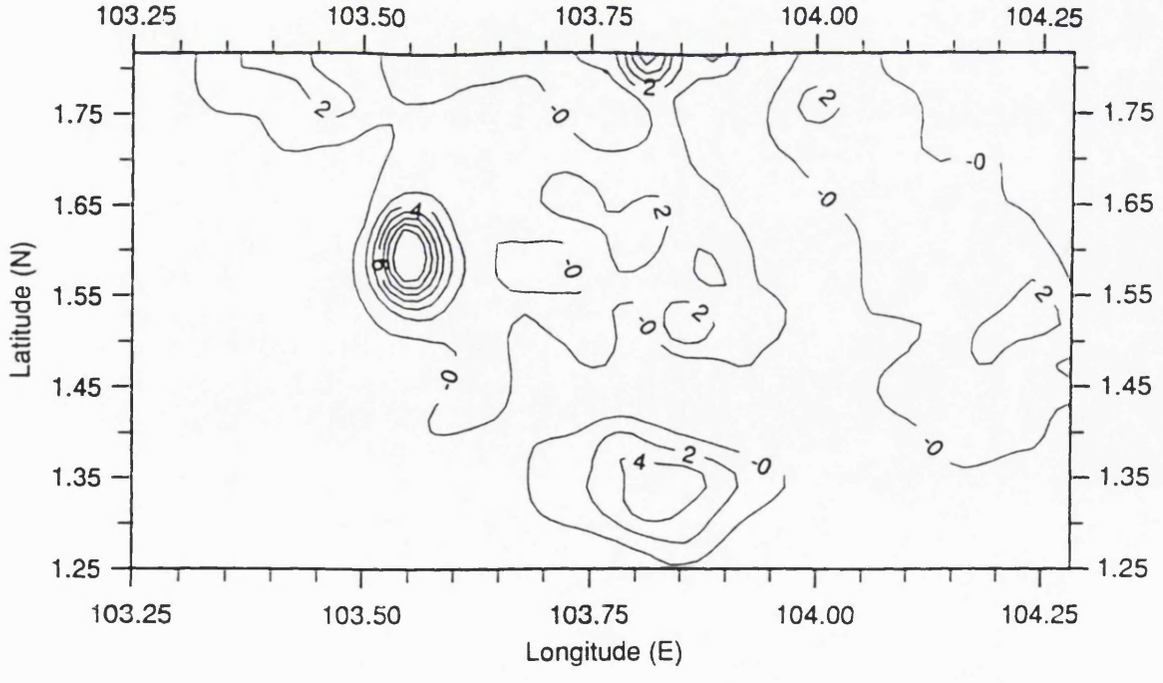

Figure: 7.1(iii)-The RTM contribution of gravity anomalies for Area C - (C.I=2 mgals)

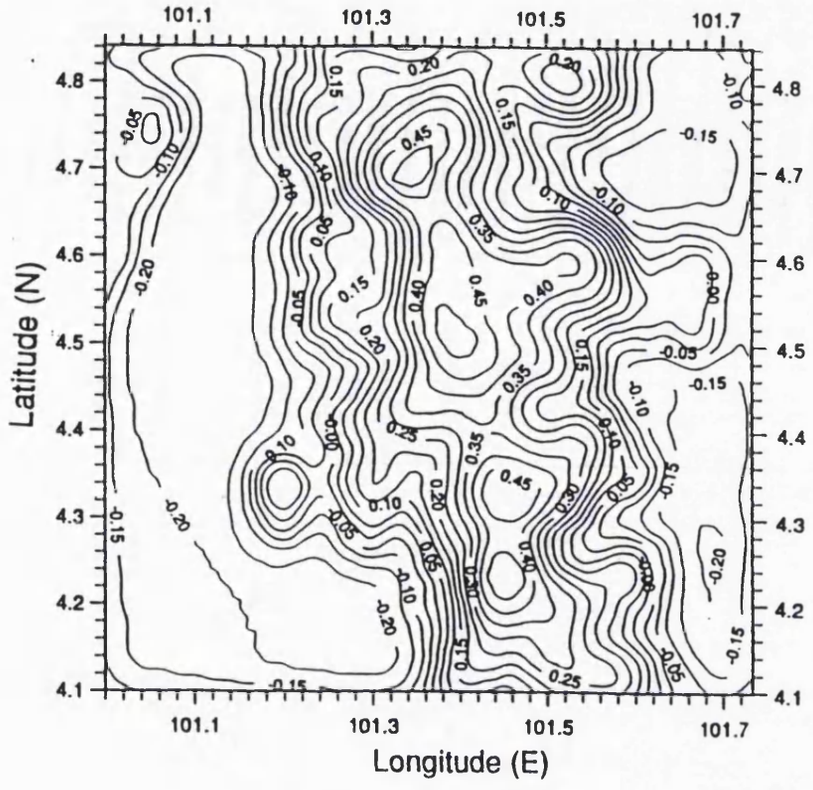

Figure: 7.2(i) - The RTM contribution of geoid heights for Area A - (C.I = 0.05 m)

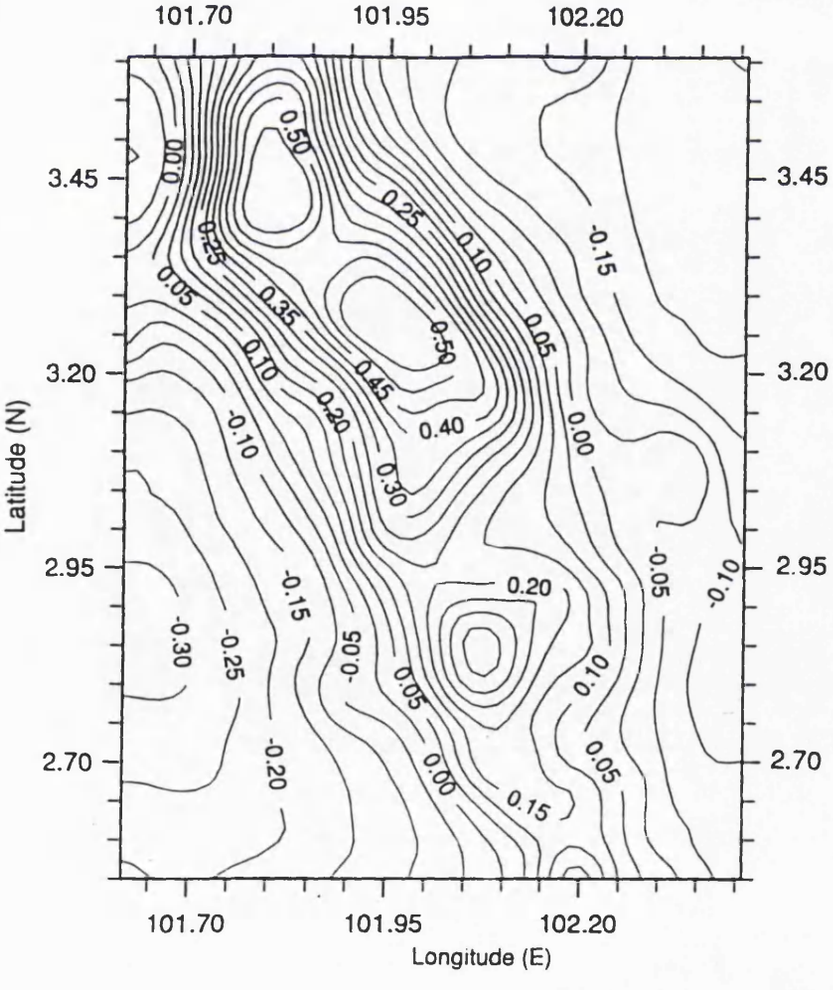

Figure: 7.2(ii) - The RTM contribution of geoid heights for Area B - (C.I = 0.05 m)

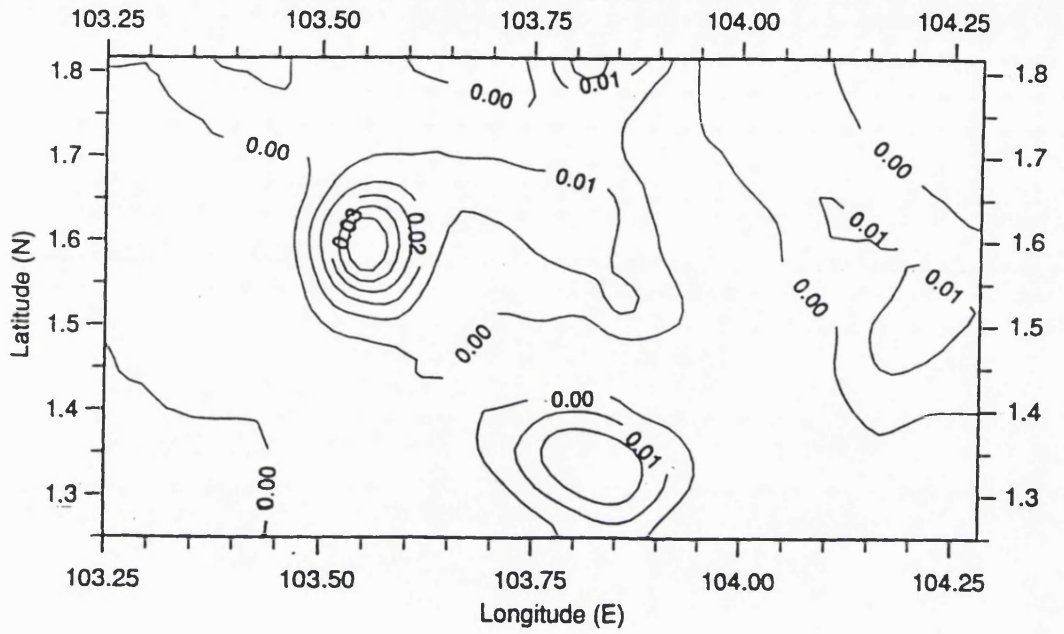

Figure: 7.2(iii) - The RTM contribution of geoid heights for Area C- (C.I = 0.01 m)

It is obvious that to see from figures 7.1(i) and 7.2(i) of Area A and figures 7.1(ii) and 7.2(ii) of Area B that the RTM contribution shows the usual strong correlation with the rough topography compared to the smoother area, Area C in figures 7.1 (iii) and 7.2(iii). In other words, the use of the RTM contribution has shown a lot of high frequency gravity field information in mountainous areas than those in lowland areas, implying that a strong gravity signal is due to the gravitational attraction of the topographic masses itself. The RTM contributions as shown in figures 7.1(i), (ii) and (iii) were used in the remove process for Case II, and subsequently the RTM contribution shown in figures 7.2(i), (ii) and (iii) will be used in the restore process, i.e. to be added to residual geoid heights, see equation (3.17).

From the above analysis, it is clearly seen that in the mountainous areas, the topographic effects completely dominate the shorter wavelength variations of the gravity field. In contrast, for smooth areas, the effect of topographic masse is insignificant, resulting in very small magnitudes, as would be expected. Therefore, it can be expected that by removing the terrain effects from observed anomalies (free-air anomalies) in the areas of interest, especially in mountainous areas (e.g. the eastern part of area A), the gravity field will become distinctly smoother with a much lower variation. This reason is due to the fact that the free-air anomalies tend to be linearly and strongly correlated with the topography of observed points, i.e. the free-air anomaly's high frequency variation comes primarily from the influence of the topography. Thus,

the terrain effect contribution in rough areas is very important as reduced data tends to be more isotropic and homogeneous for an optimum estimation of the LSC covariance function. A small prediction error can be achieved by a small variance C_o and a large ξ. It is recommended that the DEM resolution at 30" x 30" (equivalent to 1km x 1km) should be used to remove irregularities of the local gravity field (high frequency spectrum) in the mountainous areas of areas A and B. By utilising a good resolution of local DEM, it is possible to use even very sparse gravity data sets for geoid predictions in mountainous areas with reasonably good approximation results, see Sunkel, (1981) and Forsberg and Madsen, (1981).

7.3 Analysis of the Estimated Covariance Functions

A main requirement for the application of collocation to the geoid prediction from gravity anomalies is a good choice of the covariance function as it reflects the characteristics of the gravity field. For example, in mountainous areas where the gravity field is not smooth, the covariance will show greater variation and less correlation in the gravimetric signals. Since a major part of the short periodic variation of the gravity field in the rugged areas is due to the topographic masses, the irregularities of the local gravity field and hence the local covariance function is smoothed by the gravity field terrain-reduction before using any gravimetric method. In smooth areas, the effect of the topography has the least influence of the gravity anomalies. The optimal shape of a covariance function is defined by long correlation length and of course, a low variance (see Section 6.2.2). These characteristics, in turn will depend on the sample data set, e.g. sufficiently large and homogeneously distributed because the covariances involved should reflect the actual characteristics of the gravity field as adequately as possible. The characteristics of the gravity field in each of the test area will be analysed in this section.

As previously described in Section 6.4, three test areas were chosen, each with varying characteristics in terms of gravity coverage, density and topography. For modelling the gravity field of these test areas, the long wavelength and the short wavelength field were removed as the OSU89B-MM and the RTM contributions were subtracted from all observations, respectively. With the reduced anomalies, the empirical covariance function was estimated (using program EMPCOV) in order to obtain the best agreement between this empirical function and the model function. However, in fitting the model (using program COVFIT) to the empirical values of C_o and ξ, it is not possible to get exact agreement with each, and a compromise has been made in this exercise with respect to both parameters.

Tables 7.2(i)-(iii) shows some characteristics of the empirical and model covariance functions. Figures 7.3(i)-(vi) depict the empirical covariance functions of the local gravity field with their corresponding synthetic models for each test area of Case I and Case II, respectively. It can be seen clearly from tables 7.2 (i)-(ii) and figures 7.3 (i)-(iv) that in area A and area B where the gravity fields in these rugged areas are not smooth, the covariance functions have shown a greater variation and less correlation in the gravimetric signals. This is due to the fact that, for these areas, the reduced anomalies were merged with the 'filled in' anomalies from the tailored model contribution (Case I) and from both the tailored model and the RTM contributions (Case II). As pointed out in Section 6.5, these 'filled in' anomalies in the unsurveyed areas caused the variance to be too high and correlation length to be too short. Consequently, since the variance functions as a scale factor for the prediction process, it can be seen in the next section that the accuracy of geoid prediction for the rough areas such as Area A would be of low quality, but the solution is not necessarily wrong. The estimated covariance function for Area C as shown in Table: 7.2(iii) and figures: 7.3(v)-(iv), has described the gravity field behaviour adequately for local studies, i.e. low variance and long correlation distance. Despite data reduction, regional factors still influence individual gravity measurement within the area of study causing these slight variations. As previously mentioned in Section 6.2.2, the effect of these distant variations (>1.5ξ) does, however, have little effect in LSC application.

Respectively, it can be seen that in tables 7.2(i) and (ii) for test Area A and Area B, the degrees of expansion (or order of local function) was found to be too high compared to Area C. However, by reducing these optimal maximum degrees, a much better fit was obtained whereby the covariance was reproduced much more closely while the first zero is at about same spherical distance ψ. The adjusted parameter for R_B was also more sensible. It is apparent that from the empirical and model covariance functions that although they are quite close at first, at larger distances, the two functions begin to separate as the fit is no longer controlled by essential parameters. The model at these distances is not reproducing the gravity field behaviour to an adequate extent, but again the influence of this on the LSC solution is negligible.

From all figures 7.3, it is apparent that the estimated covariance functions varied greatly between each other, and not all behave in the theoretically expected manner. The better examples tend to be in the low or smoother areas of Area C compared to rugged areas, Area A and Area B. The geopotential model holds a lot of information in test Area C; medium wavelength information is most common and much of this is available from the gravity data. Area A and Area B are of particular interest as they both involve medium to rough terrain and show clearly the expected changes in the

essential parameters with each reduction, i.e. Case I and Case II. Thus, it is obvious that for these rugged areas, the terrain contributions have dominated the characteristics of the local covariance function in the expected manner. However, there will be major changes in the gravity field if one has some 'observed values' in these rough 'unsurveyed areas' as the terrain reduction can eliminate the strong correlation between the height and the free-air anomalies. In other words, the gravity field is expected to be smoother and more homogeneous as particular detail is removed to levels comparable with lowland areas, Area C. It is very interesting to see that although the RTM contribution is very small for area C, the consideration of this effect in the computation still seems to improve the gravity field variation slightly as shown in figures 7.3(v) and (vi). Therefore, any data reduction process, e.g. short and long wavelength effects which decrease the variance and increase the correlation length has to be considered in gravity field modelling.

By examining all figures, it can be said that the optimal synthetic models of covariance functions were carried out in a correct way although in reality the actual behaviour of the gravity field in the mountainuos areas were not available at the time of this study, i.e. no observed gravity values. Again, as previously pointed out in Section 6.5, this was the only possible means of testing the influence of both the tailored model and the terrain effects in these unsurveyed areas. The compromise between the empirical and the model covariance functions can also be considered successfully done.

	Empirical Function			Model Function				
Parameter	C_o (mgal2)	ξ (arc min)	ψ_o (arc min)	C_o (mgal2)	ξ (arc min)	ψ_o (arc min)	Order N	R_B-R_E (km)
Case I	313.12	12.6	22.2	313.10	12.0	22.5	313	-9.40
Case II	2678.01	10.5	17.4	2678.00	10.2	17.7	400	-8.05

Table: 7.2(i) - Characteristics of covariance functions for Area A

	Empirical Function			Model Function				
Parameter	C_o (mgal2)	ξ (arc min)	ψ_o (arc min)	C_o (mgal2)	ξ (arc min)	ψ_o (arc min)	Order N	R_B-R_E (km)
Case I	70.57	4.2	11.4	70.60	4.5	12.0	520	-1.15
Case II	327.42	10.8	18.6	327.40	11.4	18.0	362	-6.75

Table: 7.2(ii) - Characteristics of covariance functions for Area B

	Empirical Function			Model Function				
Parameter	C_o (mgal2)	ξ (arc min)	ψ_o (arc min)	C_o (mgal2)	ξ (arc min)	ψ_o (arc min)	Order N	R_B-R_E (km)
Case I	52.92	14.7	52.8	52.90	15.6	52.5	105	-3.55
Case II	50.08	14.7	49.2	50.10	15.6	48.6	110	-3.60

Table: 7.2(iii) - Characteristics of covariance functions for Area C

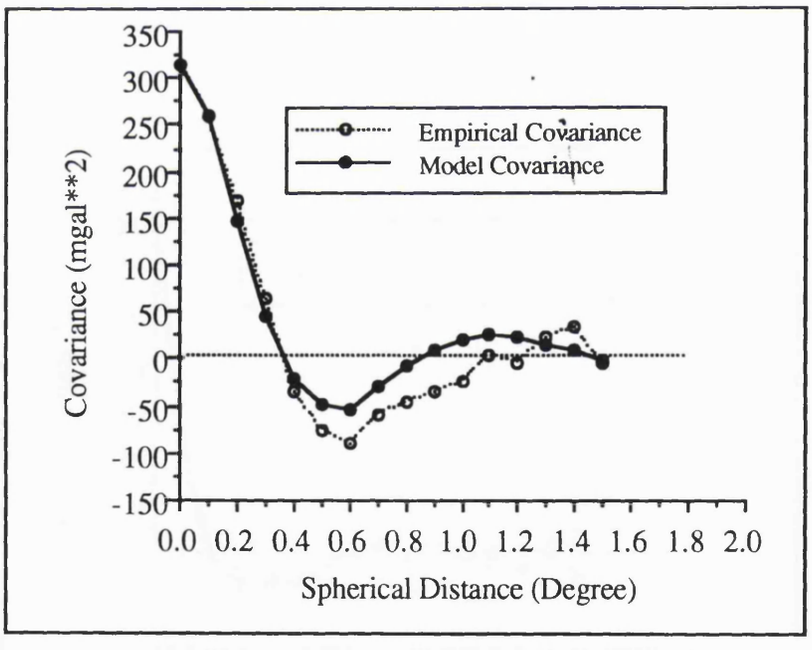

Figure: 7.3(i)-The empirical and model covariance functions for Area A-Case I

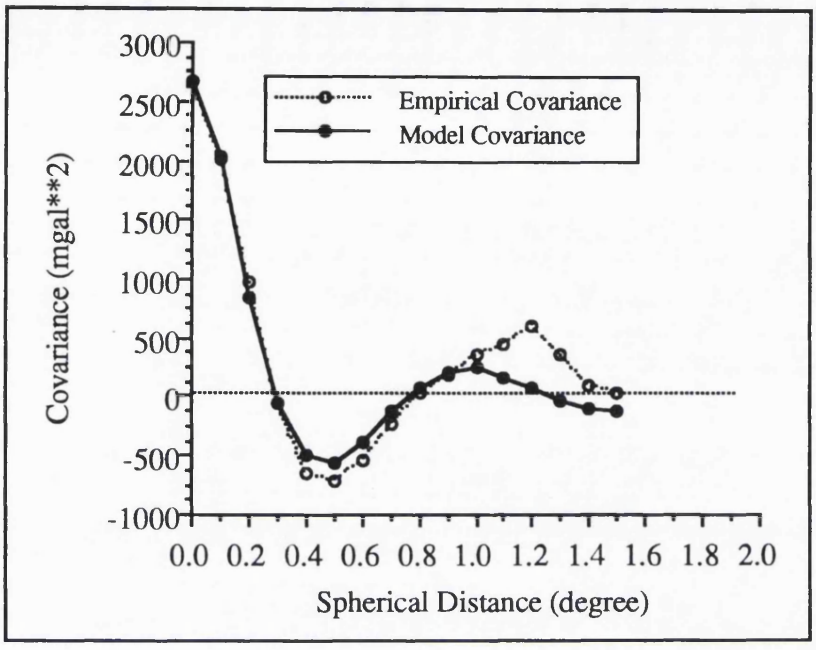

Figure: 7.3(ii) - The empirical and model covariance functions for Area A-Case II

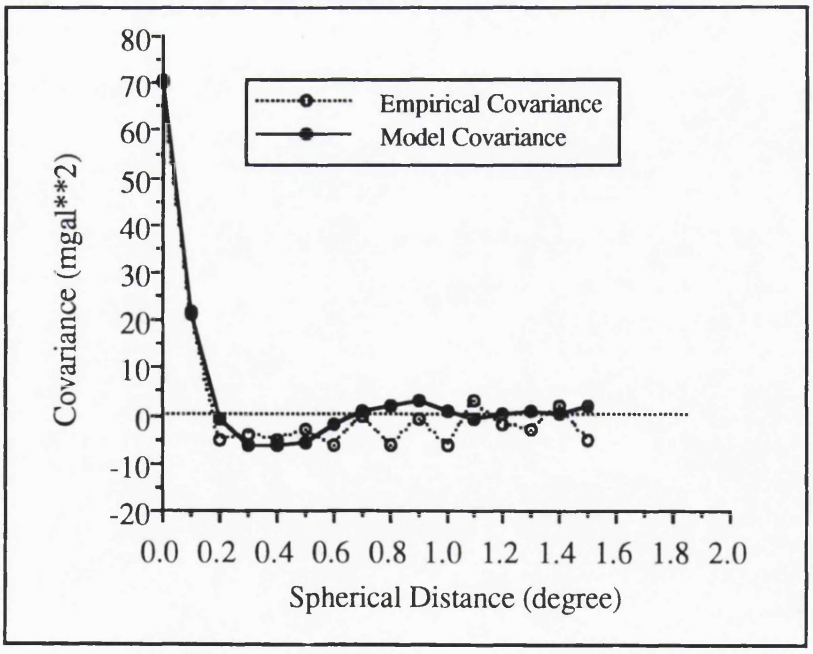

Figure: 7.3(iii)-The empirical and model covariance functions for Area B-Case I

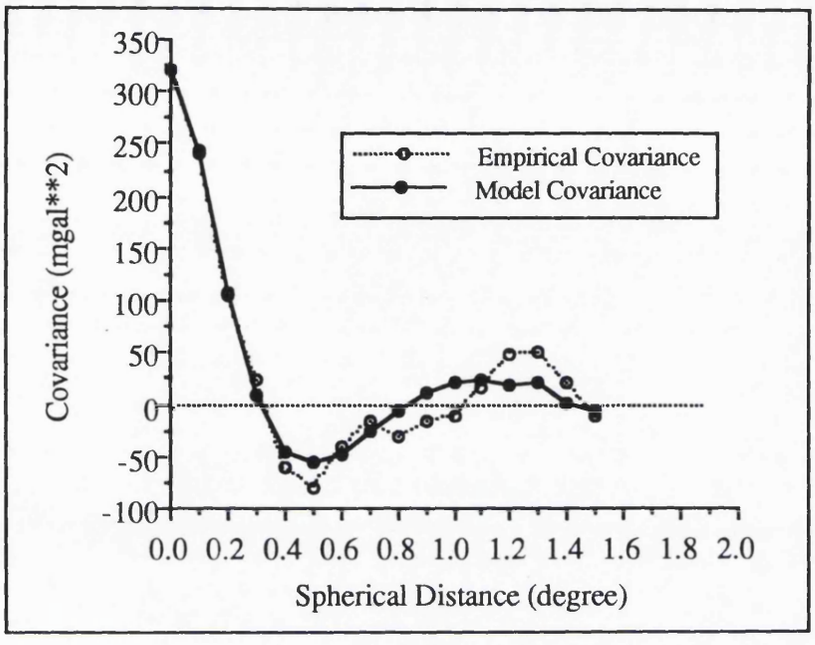

Figure: 7.3(iv)-The empirical and model covariance functions for Area B-Case II

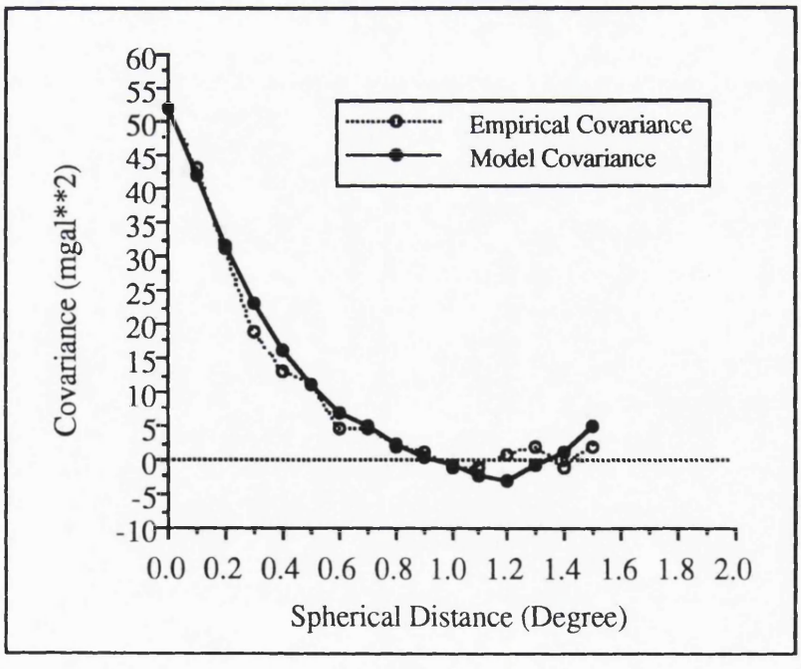

Figure: 7.3(v) -The empirical and model covariance functions for Area C - Case I

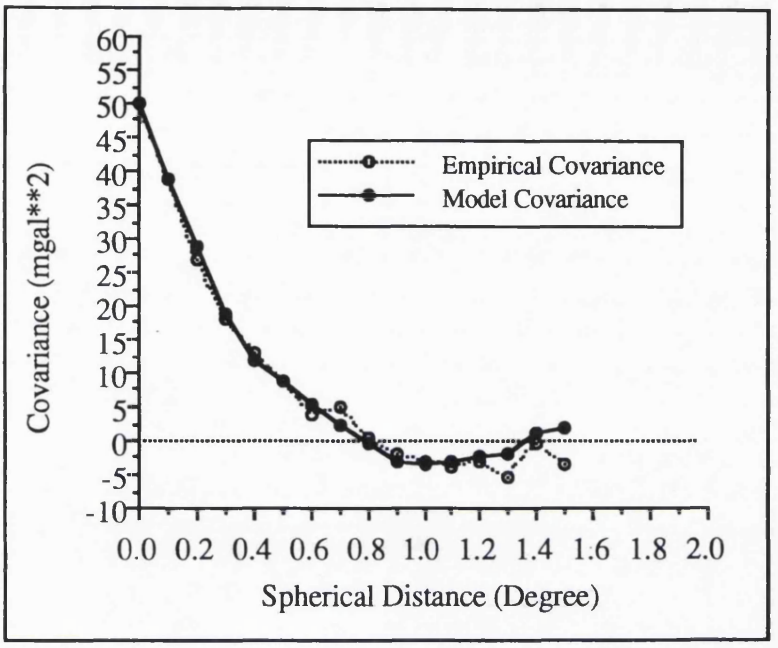

Figure: 7.3(vi)-The empirical and model covariance function for Area C-Case II

7.4 The LSC Test Results and Comparisons

Through the LSC geoid prediction method, two data sets of residual geoids (Case I and Case II) and hence two final gravimetric geoids for each of the three test areas were produced via remove-restore procedures. The residual geoids for each of test area were also produced using the FFT method, but as mentioned previously this was done for Case II only. This section compares results from the two cases, i.e. Case I and Case II and assesses the contribution of terrain effects in each test area. The test results and comparisons between the LSC and the FFT and the assessment of the merits of each method used in this study is discussed in the next section.

7.4.1 Test Area A

As previously mentioned in Section 6.4 and highlighted in Table: 6.1, Area A is basically characterised by a mixed terrain. One can see that the terrain changes from flat to rugged when proceeding from west to east. The trend varies from a 5 m low at the west coastline areas to approximately 2000m high at the eastern part of Titiwangsa Range.

As previously described in Section 6.6.3, the residual geoid heights for Area A were computed at 2' x 2' gridded format giving a total of 625 points for both cases, Case I and Case II, and these are given in Appendices R (i) and (ii), respectively.

Table: 7.3 summarised the statistical results of residual geoid heights for this test area. Figures 7.4 (i) and (ii) depict residual plots of geoid height computed using the LSC method for Case I and Case II, respectively.

Solution	Mean	Std. Dev.	Minimum	Maximum
Case I	0.15	0.21	-0.14	0.66
Case II	-0.16	0.55	-1.36	1.06
Case II-Case I	-0.31	0.39	-1.21	0.26

Table: 7.3 - The statistical results of the LSC residual geoid heights for Area A

It can be seen from Table: 7.3 that the standard error of the computed residual geoid heights found around 20 cm and 50 cm for Case I and Case II, respectively. The mean error of the predictions (see equation 6.16) was 22 cm and 56 cm for Case I and Case II, respectively. The values are obviously closely correlated with the quality of the respective covariance functions, i.e. the accuracy of the observations from which the predictions are made. By examining these values, as was to be expected this was due to the rough variation of the gravity field in the region for both cases. The quality of the covariance function used in LSC prediction for this area depends greatly on the amount of variation of the gravity field, and the extent to which the tailored model and the topographic model reduce this variation. Very unfortunately, most parts of the areas were void of the actual gravity values (observed anomalies), and so, these were replaced by the 'filled in' anomalies as described in Section 6.5. Consequently, the covariance function in Figure: 7.3(ii) was not of an optimum nature, i.e. poor gravity field information, resulting in a biased geoid. In other words, based on the functions that were determined, the residual geoid prediction is not to a high standard.

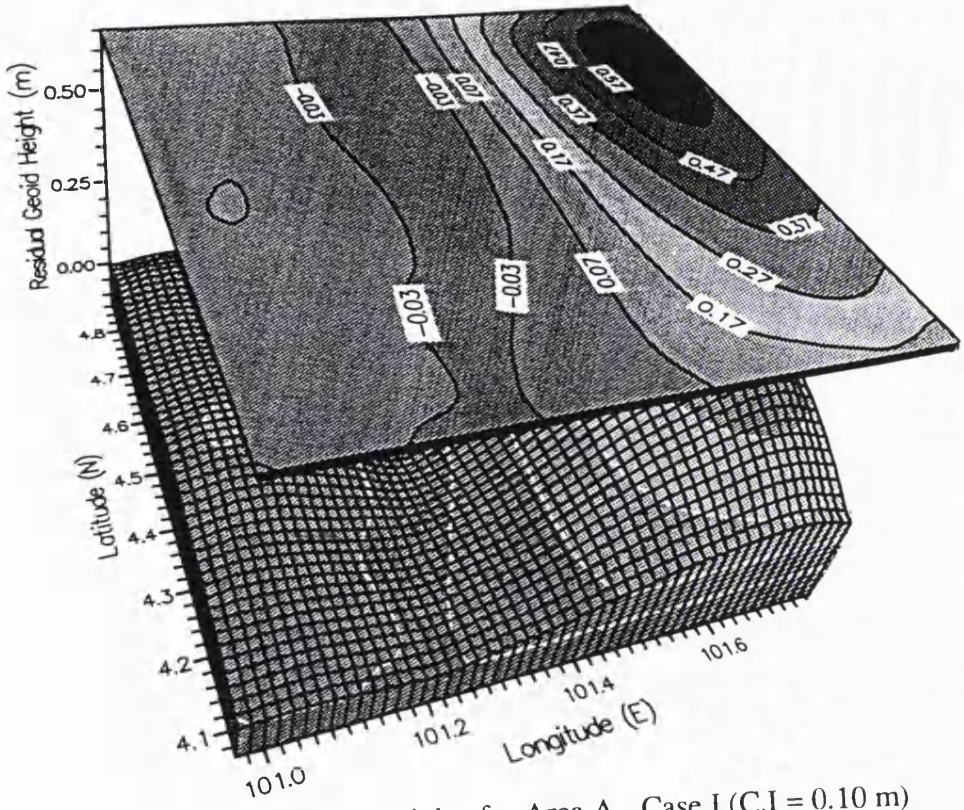

Figure: 7.4(i) - The LSC residual geoid heights for Area A - Case I (C.I = 0.10 m)

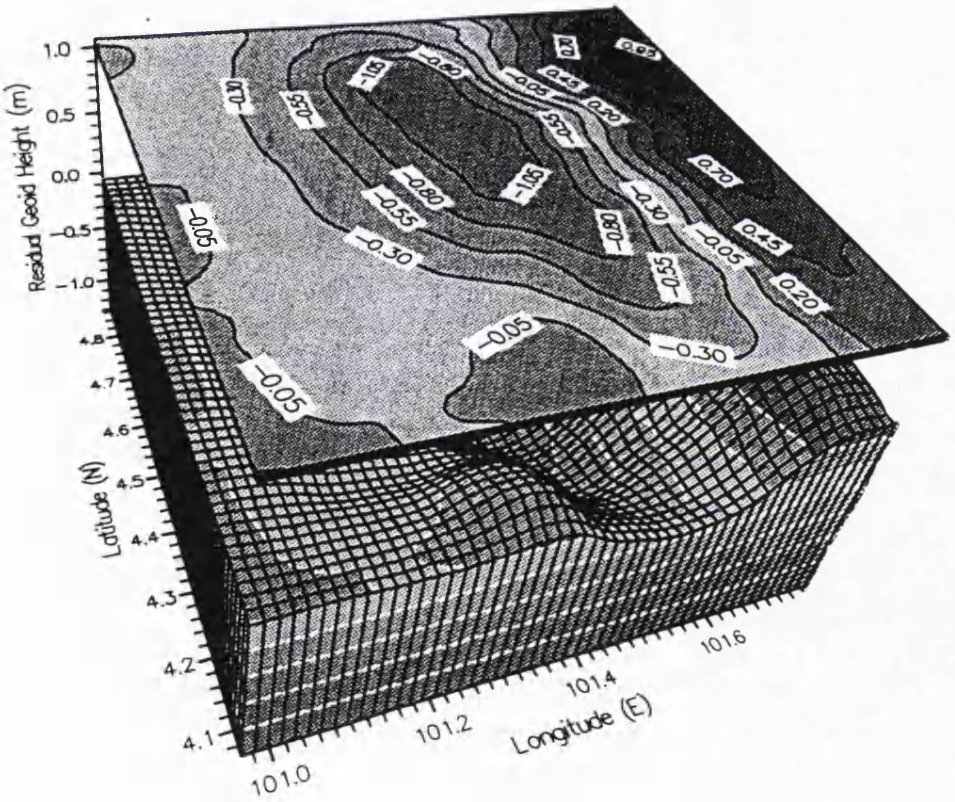

Figure: 7.4(ii) - The LSC residual geoid heights for Area A - Case II (C.I = 0.25 m)

After removing the long wavelength trend, i.e. Case II minus Case I, the effect of the RTM contribution can be clearly seen and this is shown in Figure: 7.5. In general, one can see that the pattern of this terrain effect on the geoid is quite similar to the topography of the areas as shown in Figure: 4.5. More fundamentally, much shorter wavelength components are apparent in the central and eastern part of the mountainous area. Thus, one should always use the terrain reduction concept, e.g. the RTM effect in the mountainous areas even the lack of data prohibits the estimation of the actual gravity field information. This is due to the fact that when appropriate methods are used for accounting the short wavelength signals in rough areas, the gravimetric methods such as the LSC or FFT can still estimate the geoid heights at similar accuracy with those obtained in lowland areas, see Forsberg and Madsen, (1981).

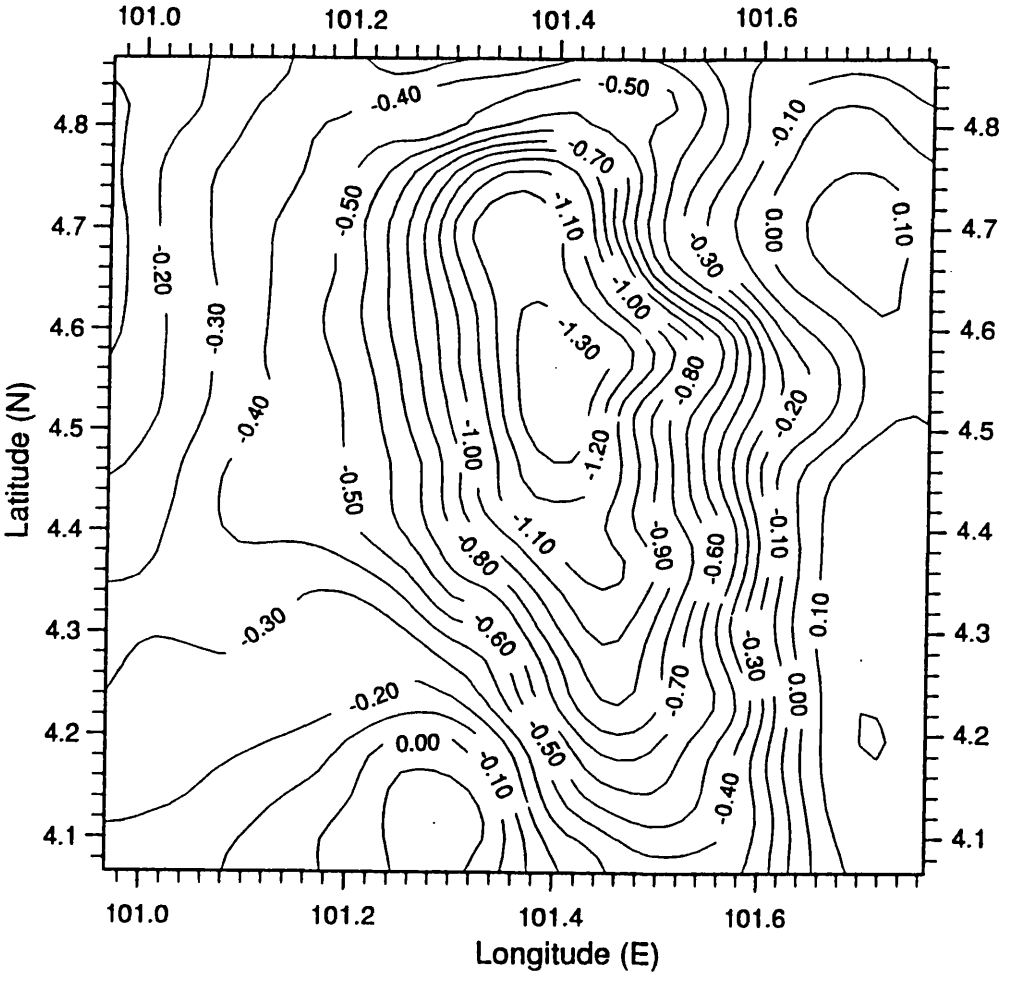

Figure: 7.5 - The residual geoid differences between Case I and Case II - Area A
(C.I = 0.10m)

The total contribution of geoid height (final geoid) for Case I and Case II is shown in figures: 7.6(i) and(ii), respectively. Appendices S(i) and (ii) show the output of the final geoid heights for these two cases, respectively. By examining these figures, it is obvious that the N_{GM} geoid, as the major source of geoid information (long wavelength features) dominated the geoid contour plots, but still, the effects of the high frequency of the gravity field information can be seen, especially in the mountainous areas. In the rest of the area, the overall geoid pattern is almost the same as the $N_{\Delta g}$ contributions is of considerably smaller magnitude, see Appendix R(ii). The final geoid contour shown in Figure: 7.6(ii) changes around 3 centimetres over 1 kilometre at its smoothest, and although it is in general smooth, there are slope variations. There are major changes, also, in the east-west trend and so the denser spacing in this direction is justified.

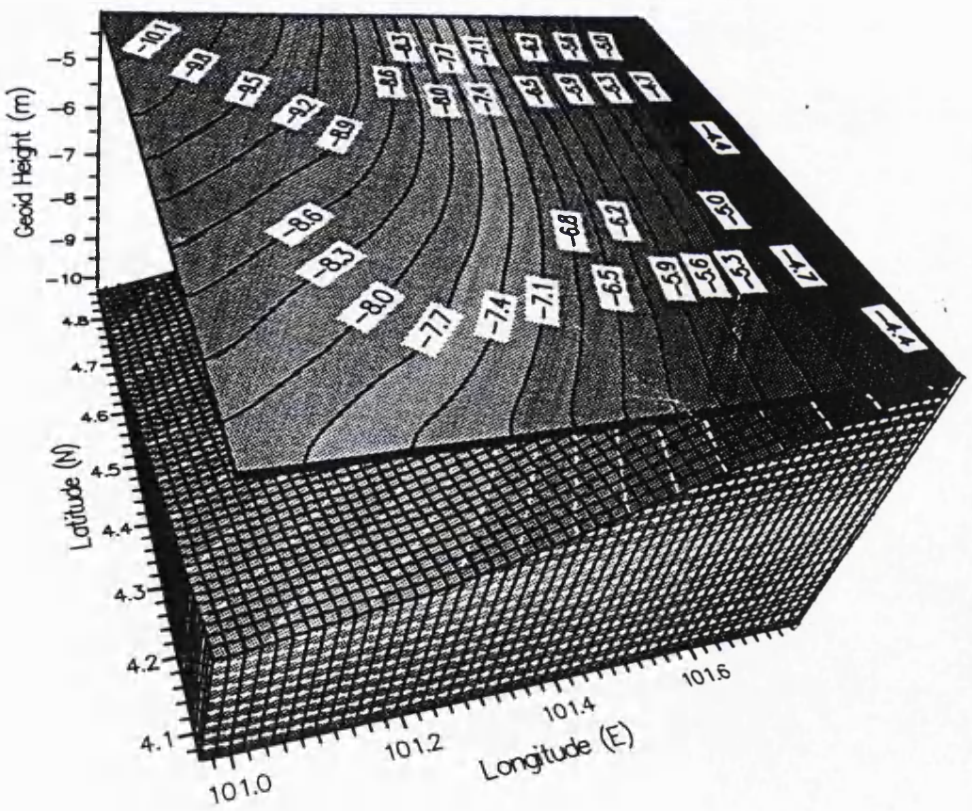

Figure: 7.6(i) - The final LSC geoid heights for Area A - Case I, (C.I.= 0.30m)

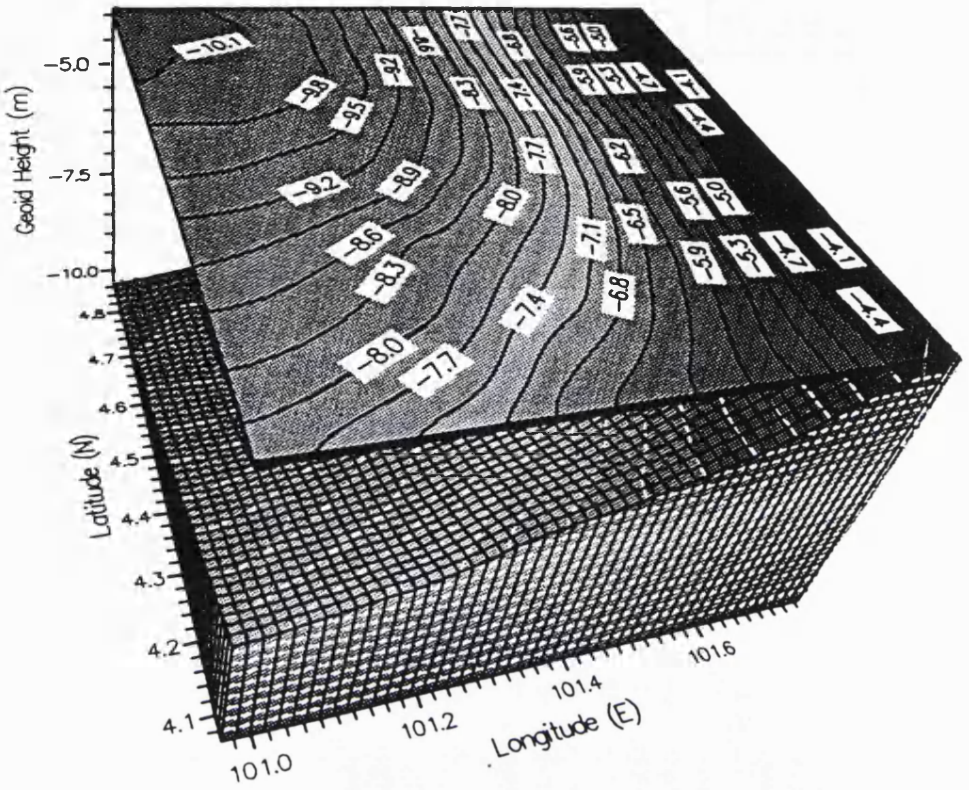

Figure: 7.6(ii) - The final LSC geoid heights for Area A - Case II, (C.I.= 0.30m)

7.4.2 Test Area B

Similar to Area A, the test Area B is also basically characterised by mixed terrain. The topography in this test area is however more moderate terrain where the trend varies from a 0 m low (near the coastline areas) at the southwest part to approximately 1600 m high at the northern and central parts of the Titiwangsa Range. However the gravity density and coverage in Area B is far better than Area A although more than 95% of the gravity points are predominantly from the valleys and lowland areas.

The residual geoid heights for Area B were computed at 3' x 3' gridded format giving a total of 391 points for both cases, Case I and Case II. Appendices T (i) and (ii) show the output of the residual geoid heights for Case I and Case II, respectively. The statistical result is summarised in Table: 7.4. Figures 7.7 (i) and (ii) are the residual geoid heights computed by equation (6.17) for Case I and Case II, respectively.

Solution	Mean	Std. Dev.	Minimum	Maximum
Case I	0.01	0.12	-0.17	0.15
Case II	0.15	0.20	-0.17	0.53
Case II-Case I	0.14	0.15	-0.18	0.48

Table: 7.4 - The Statistical results of residual geoid heights for Area B

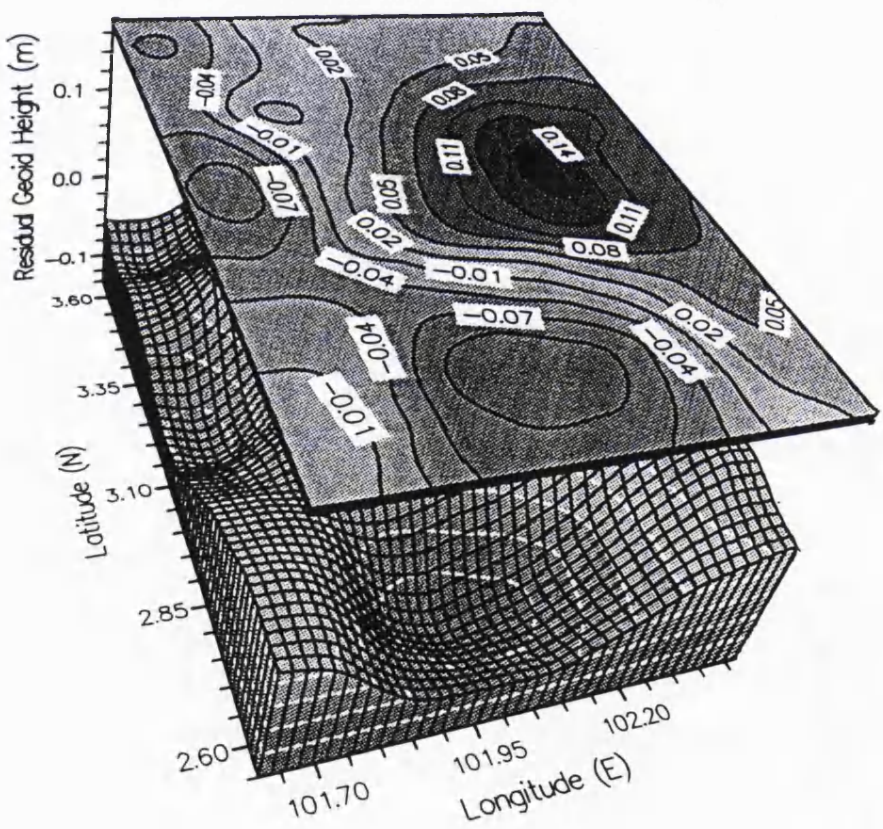

Figure: 7.7(i) - The LSC residual geoid heights for Area B - Case I, (C.I = 0.03 m)

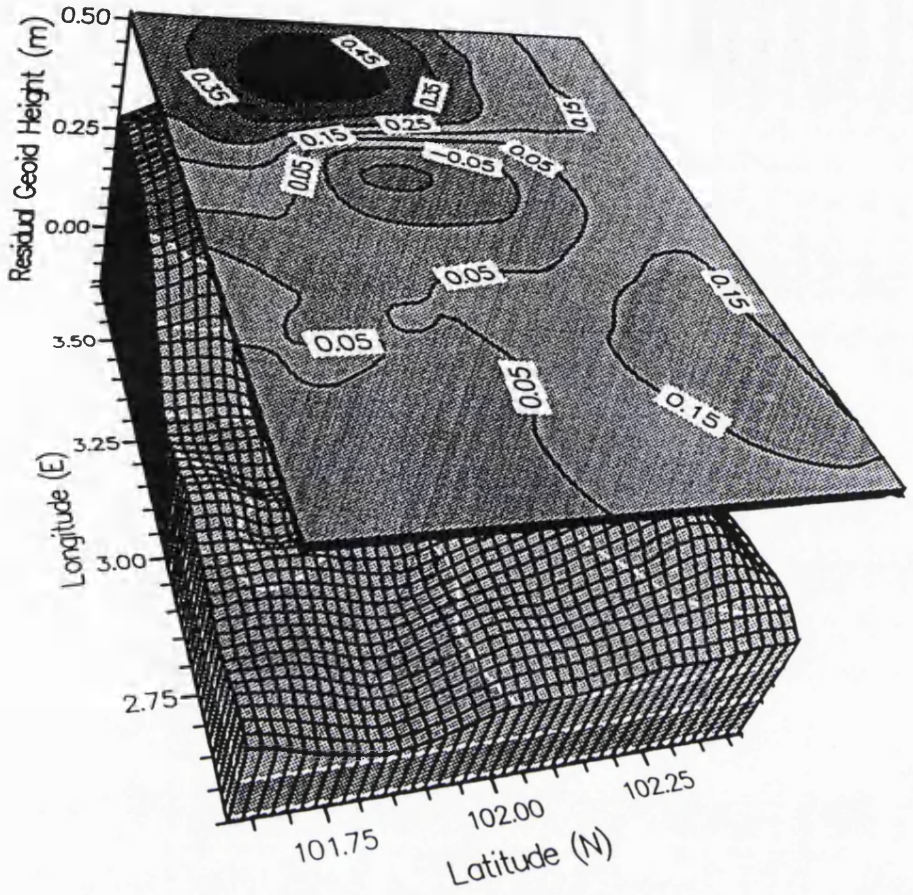

Figure: 7.7(ii) - The LSC residual geoid heights for Area B - Case II, (C.I = 0.10 m)

As shown in Table: 7.4, the accuracy of the computed residual geoid heights is about 10 cm and 15 cm for Case I and Case II, respectively. The mean error of the predictions was 13 cm and 20 cm for Case I and Case II, respectively. Again, this was expected due to possible degradation in rugged terrain which may occur because of a few 'filled in' anomalies (in central part of Area B- see Section 6.6.1). Consequently, the quality of the covariance function used in LSC prediction would not be able to describe the actual gravity field behaviour adequately for this area, i.e. did not aid the computation of optimal covariance functions. Another reason, perhaps, is due to the amount of high frequency detail that 0.5° mean anomalies used in the development of tailored model OSU89B-MM cannot portray. However, this phenomenon can still be considered as better than Area A because the functions (with small variations) can still reflect the characteristics of the gravity field in this area, see figures 7.3(i) - (iv). Presumely, when real gravity observations become available in this rough unsurveyed area, and the data is reduced properly and completely, then a situation may arise where the estimated covariance function would be more representative of the actual gravity

field. In other words, through gravimetric reduction as in equation (3.18), the covariance functions will behave in the theoretically expected manner whereby the variance will reduce significantly and the correlation length will also decrease.

Figure: 7.8 shows a map of the LSC residual geoid differences when the terrain effect is considered and when the terrain effect is not considered, i.e. Case II - Case I. Again one can see from this figure that the big differences occurred in the rough areas, and the pattern of the terrain effect on the geoid is quite similar to the topography of the area as shown in Figure: 4.6. The terrain contribution in this area amounts to about 50 cm which is considerable for the high wavelengths. In lowland areas (the north-eastern and south-western parts of Area B), there are no major differences in residual geoids between Case I and Case II.

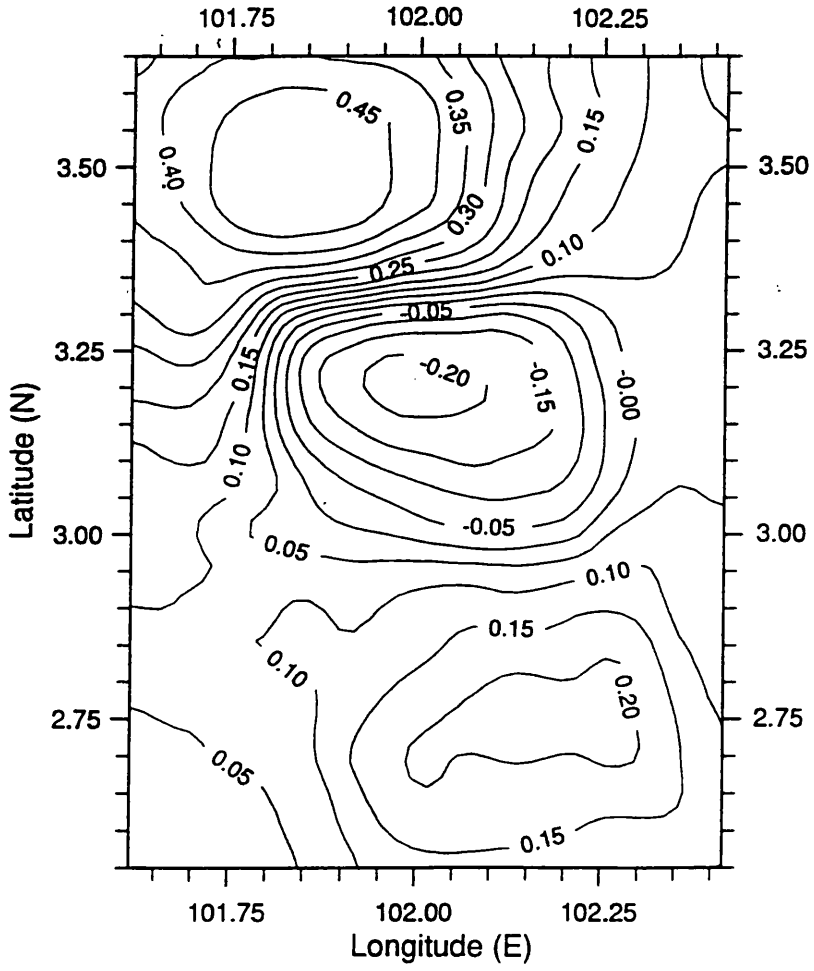

Figure: 7.8 - The residual geoid differences between Case I and Case II - Area B
(C.I.= 0.05m)

The final geoid heights for Case I and Case II is shown in figures 7.9(i) and (ii), respectively. The corresponding outputs of the final LSC geoid heights for Area B are shown in Appendices U(i) and (ii), respectively. Similar to figures 7.6 (i) and (ii), the N_{GM} geoid which is the source of long wavelength features dominated the geoid contour plots in this test area. However, by using the remove-restore procedure described in Section 3.5, the definite features are visible, i.e. effects of the local gravity field information, particularly in the north and central part of Titiwangsa Range. Thus, the terrain effect in rough areas of Area B is of importance to be considered in any gravimetric method because it is well known that the visual topography has greatest influence on the gravity anomalies. For the geoid, however, the local topographic effect is small, the variations being typically at the decimetre level, but on a larger scale the geoid height caused by the visual topography becomes very significant (Forsberg and Madsen, 1981).

From Figure: 7.9(ii), it is apparent that the effect of restoring the N_{TC} contribution on the lowland areas did not contribute any significant changes and thus the final geoids look similar to each other, although small detail differences exist. One can see from Figure: 7.9 (ii), the final geoid in this test area also changes around 3 centimetres over 1 kilometre for the smooth areas and there are slope variations in the north-south trend, especially in the area $3.3° < \phi < 3.5°$ N, $101.8° < \lambda < 101.9°$ E. One possible reason for this phenomenon might be that the addition of some local gravity data and height data in this particular area removes the smooth trend of the N_{GM}.

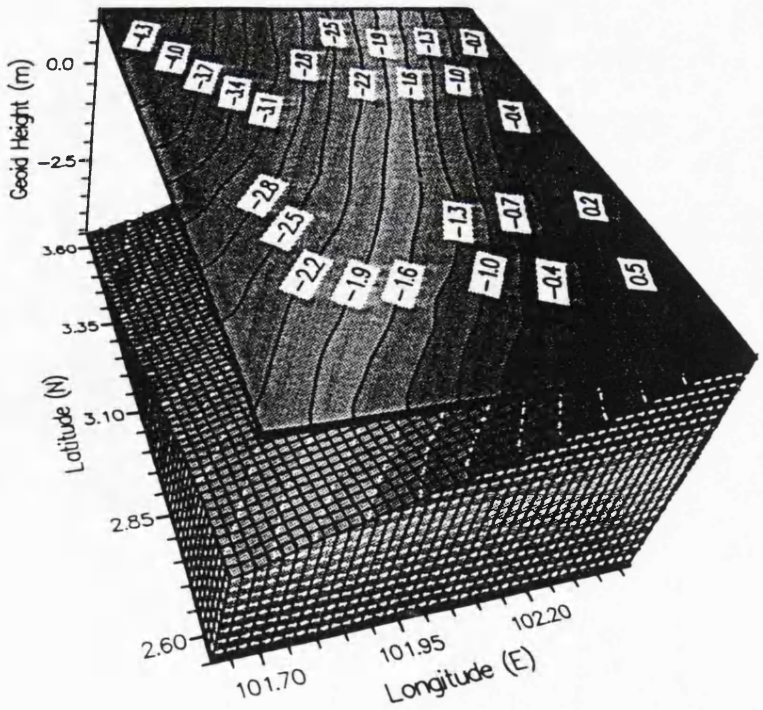

Figure: 7.9(i) - The final LSC geoid heights for Area B - Case I, (C.I. = 0.30m)

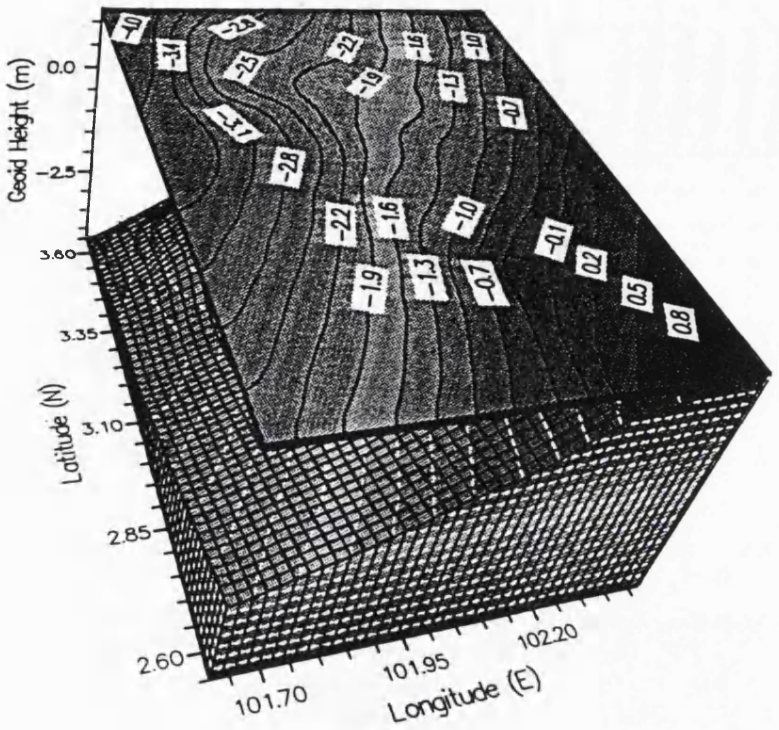

Figure: 7.9(ii) - The final LSC geoid heights for Area B - Case II, (C.I.= 0.30m)

7.4.3 Test Area C

As has already seen in Figure: 4.7, Section 4.3, the test Area C is relatively low and flat terrain with a maximum elevation of less than 150 m. The gravity density and coverage in this area are also good, and therefore are considered to represent the local gravity field variation in the expected manner, i.e. a smooth and homogeneous gravity field.

The residual geoid heights for Area C were computed at a 5' x 5' gridded format giving a total of 104 points for each case, and they are given in Appendix V (i) and (ii), respectively. Table: 7.5 summarised the statistical results of residual geoids for this test area while the plots showing the geoid contours are given as Figures: 7.10 (i), and (ii), respectively.

Solution	Mean	Std. Dev.	Minimum	Maximum
Case I	-0.08	0.09	-0.21	0.03
Case II	-0.08	0.08	-0.20	0.04
Case II-Case I	0.00	0.02	-0.04	0.02

Table: 7.5 - The statistical results of the LSC residual geoid height for Area C

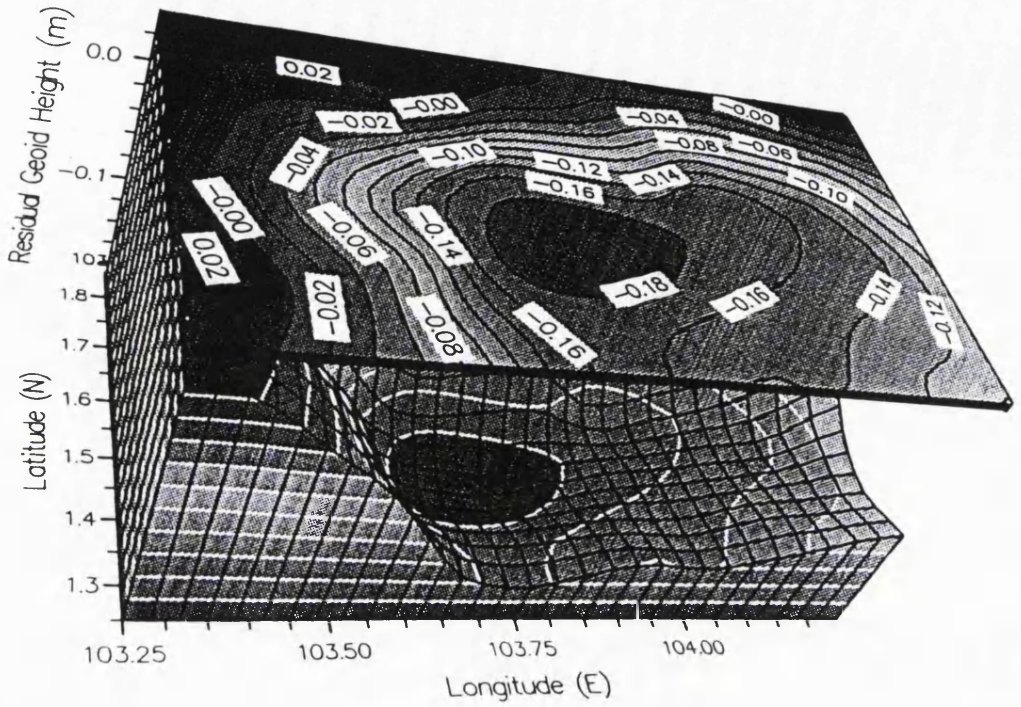

Figure: 7.10(i) - The residual geoid height for Area C - Case I, (C.I.= 0.02m)

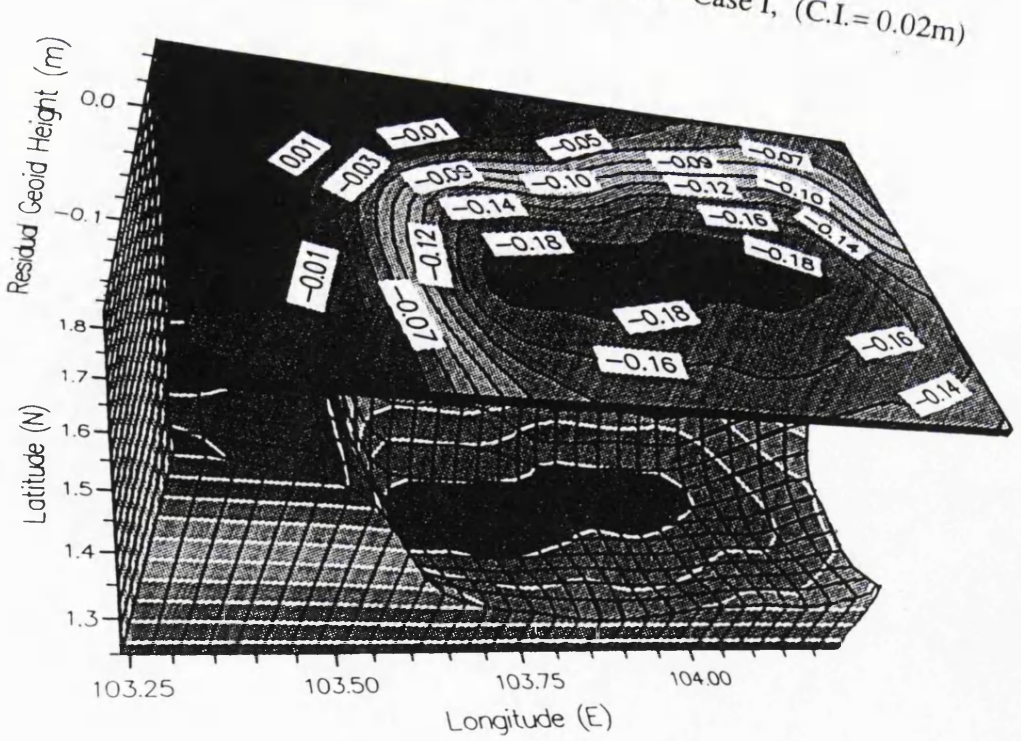

Figure: 7.10(ii) - The residual geoid heights for Area C - Case II, (C.I.=0.02m)

By examining Table: 7.5 and the corresponding figures 7.10(i) and (ii), one can see that the results obtained for the terrain corrected cases were almost identical to those which are not terrain corrected. The standard deviation of the computed residual geoid heights found around 10 cm for both Case I and Case II. The mean error of predictions was 12 cm for both cases. This is not a suprising result because in a smooth area such as Area C, the gravity anomalies of the RTM contribution for this test area (in Case II) is quite small. Similar results in the test area of Tennessee, USA has also been reported by Zhao, (1989). Nevertheless, the values are obviously closely correlated with the quality of the respective covariance functions which implies a good representation of the gravity field information in this test area compared to Area A and Area B. Again, the importance of fitting a synthetic covariance function as close as possible to the empirical functions lies in the need to obtain reliable prediction error estimates. The residual differences between Case I and Case II for Area C are shown in Figure: 7.11.

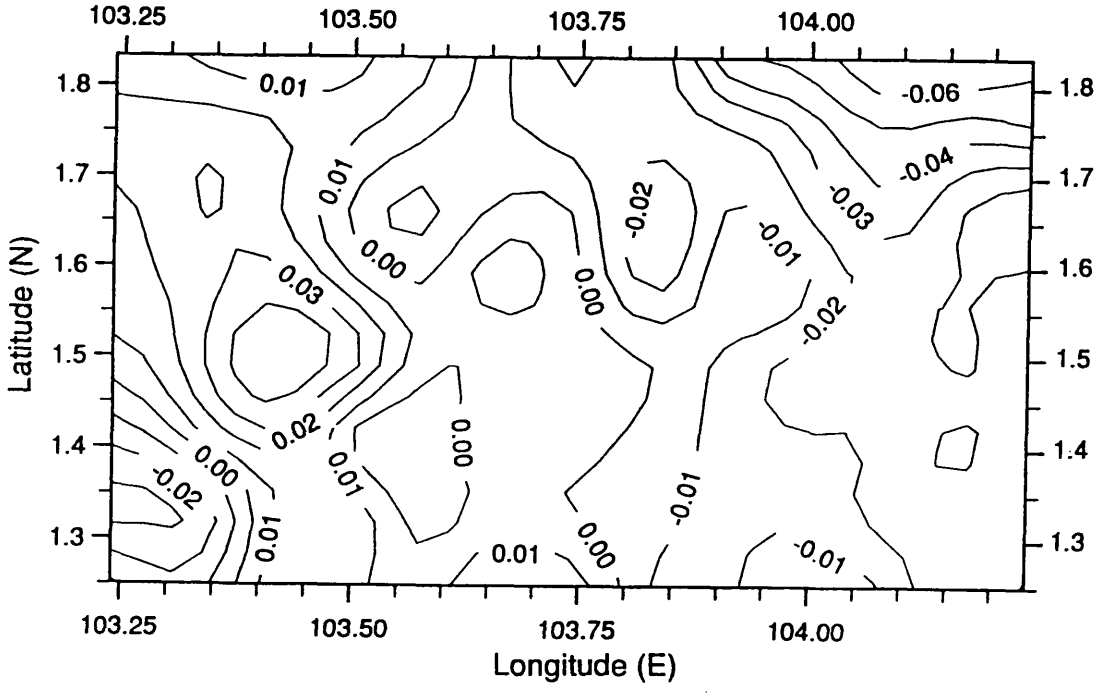

Figure: 7.11 - The residual geoid differences between Case I and Case II - Area C
(C.I.= 0.01m)

Since the residual geoid differences between Case I and Case II have a small magnitude, i.e. less than 6 cm, it was decided that only one final gravimetric geoid

(Case II) was computed for Area C, and this output is given in Appendix W. Figure: 7.12 depicts the contour map of the final geoid heights for this test area. It can be seen from this figure that the geoid contour pattern is mainly long wavelength in nature, i.e. corresponds to N_{GM}, but some small irregular variations did exist in this area due to the local data contribution. The final gravimetric geoid in Area C changes by approximately 2 centimetres over 1 kilometre for the whole area which is considered quite a smooth pattern compared to the final gravimetric geoids of both Area A and Area B (for Case II only).

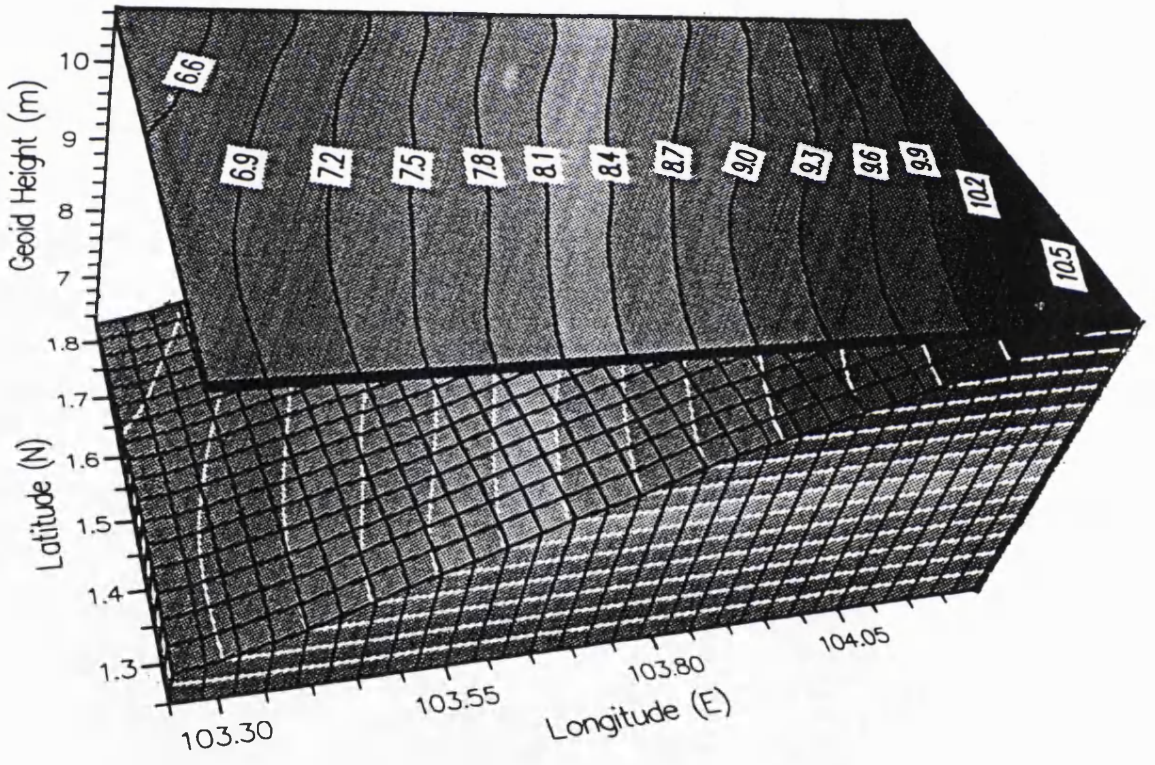

Figure: 7.12 - The final LSC geoid heights for Area C - Case II only (C.I.=0.30m)

7.5 The FFT Test Results and Comparison With the LSC Geoid

The LSC and the FFT methods have been applied to identical data sets of Case II. This section compares results from the two methods and assesses the merits of each with respect to Case II only. Appendices X(i), (ii) and (iii) list the results of residual geoid heights of FFT solutions for Test A, Test B and Test Area C, respectively.

The statistical results between the LSC and the FFT residual geoid and their corresponding differences for all test areas are summarised in Table: 7.6. Figures 7.13(i), (ii) and (iii) depict the FFT residual geoid heights for Area A, Area B and Area C, respectively. The plots showing the residual height differences between the LSC and the FFT solutions for Area A, Area B and Area C are given as Figures: 7.14(i), (ii) and (iii), respectively.

Test Area	Area A			Area B			Area C		
	LSC	FFT	Diff.	LSC	FFT	Diff.	LSC	FFT	Diff.
Mean	-0.16	-0.13	-0.03	0.15	0.13	0.02	-0.08	-0.07	-0.01
Std. Dev.	0.55	0.51	0.10	0.20	0.18	0.03	0.08	0.07	0.02
Min.	-1.36	-1.25	-0.17	-0.17	-0.16	-0.01	-0.20	-0.20	-0.06
Max.	1.06	0.98	0.13	0.53	0.51	0.07	0.04	0.03	0.03

Table: 7.6 - The statistical results of the LSC and the FFT residual geoids and their differences for all test areas - Case II only

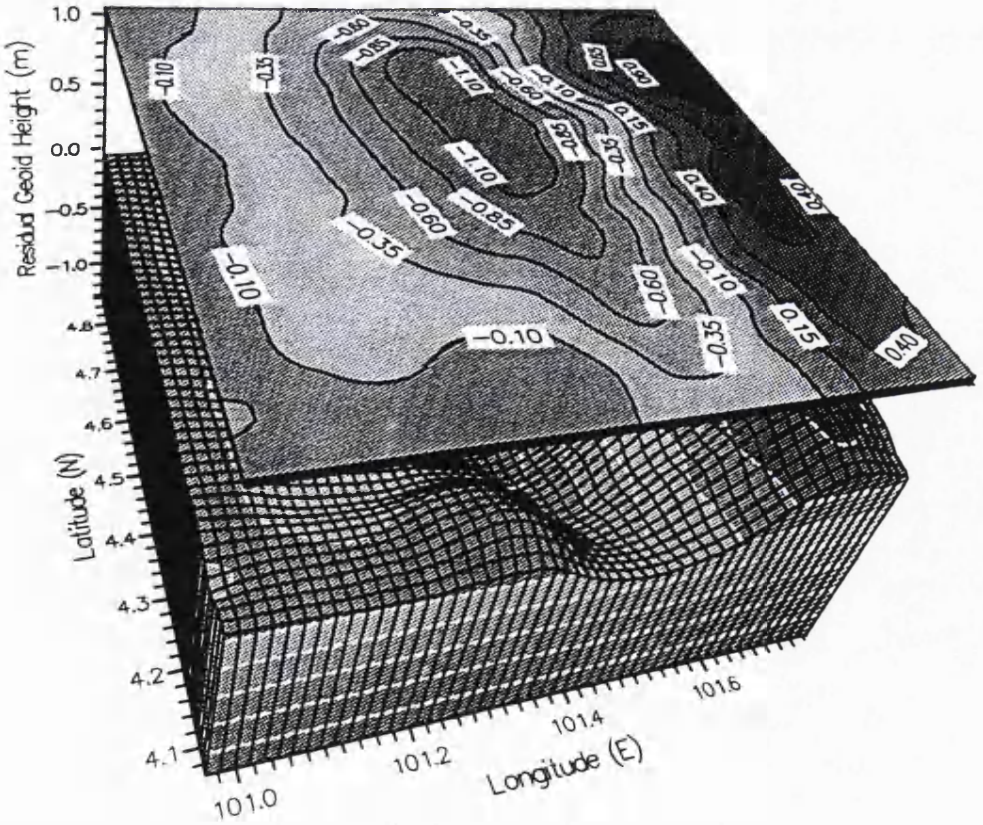

Figure: 7.13(i) - The FFT residual geoid heights for Area A - Case II only, (C.I.=0.25m)

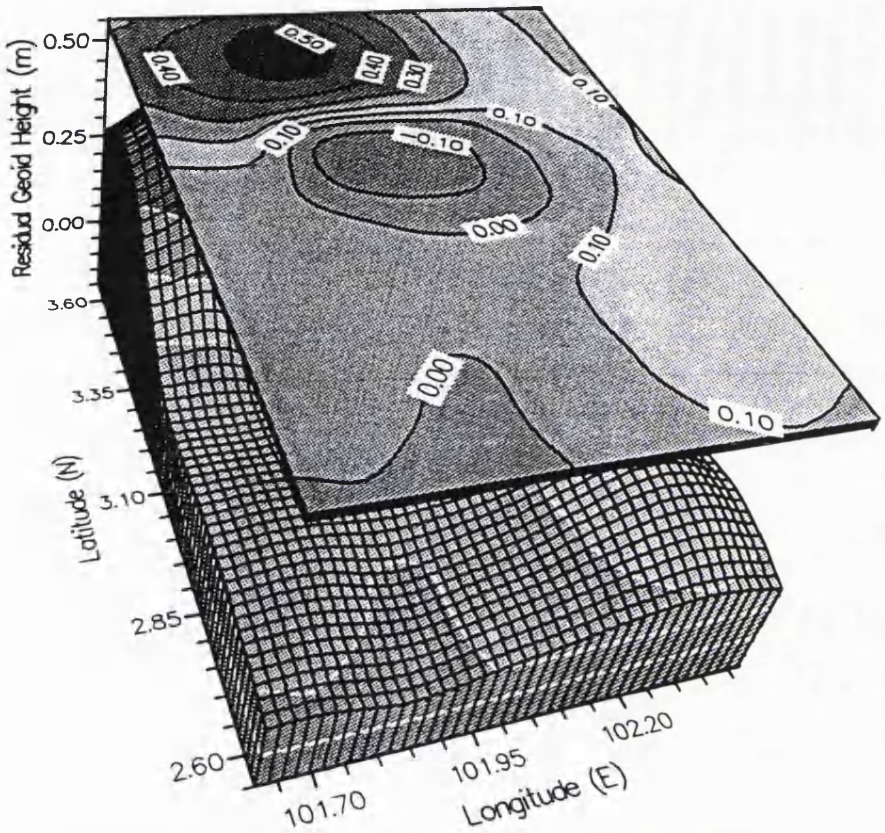

Figure: 7.13(ii) - The FFT residual geoid heights for Area B - Case II only,
(C.I.=0.10m)

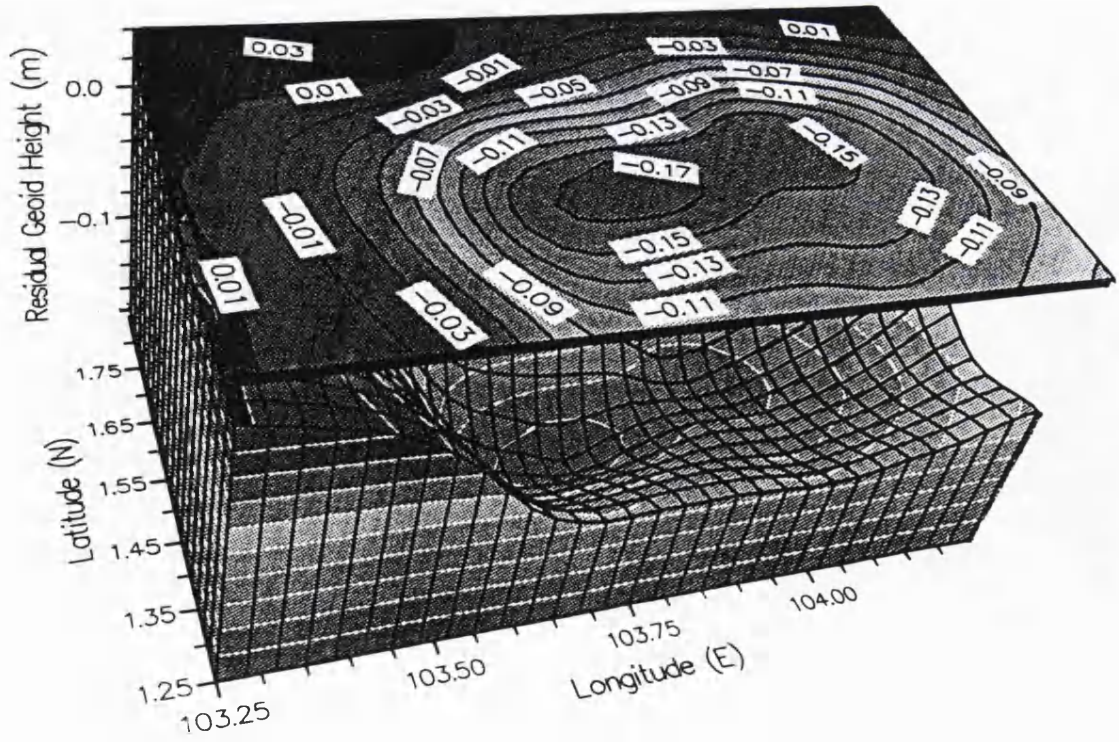

Figure: 7.13(iii) - The FFT residual geoid heights for Area C - Case II only,
(C.I.=0.02m)

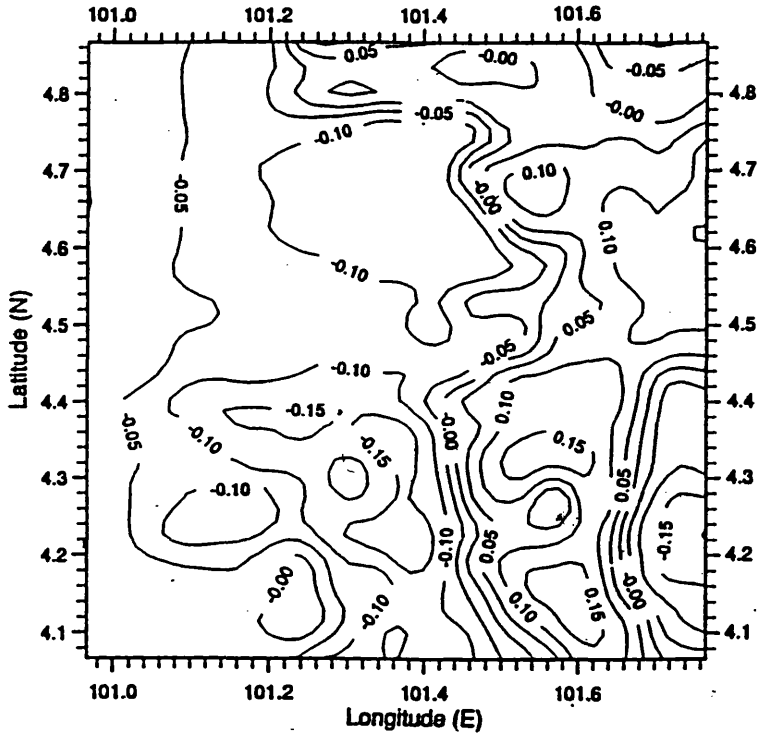

Figure: 7.14(i) - The residual geoid differences between LSC and FFT for Area A - Case II only, (C.I.= 0.05m)

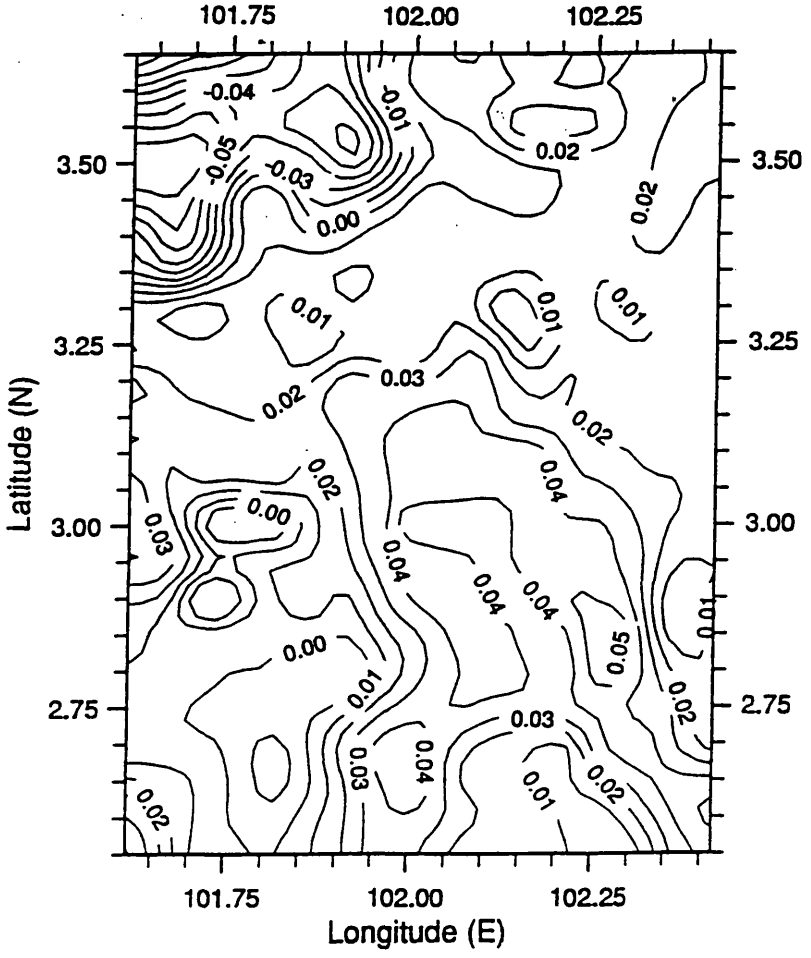

Figure: 7.14(ii) - The residual geoid differences between LSC and FFT for Area B - Case II only, (C.I.= 0.01m)

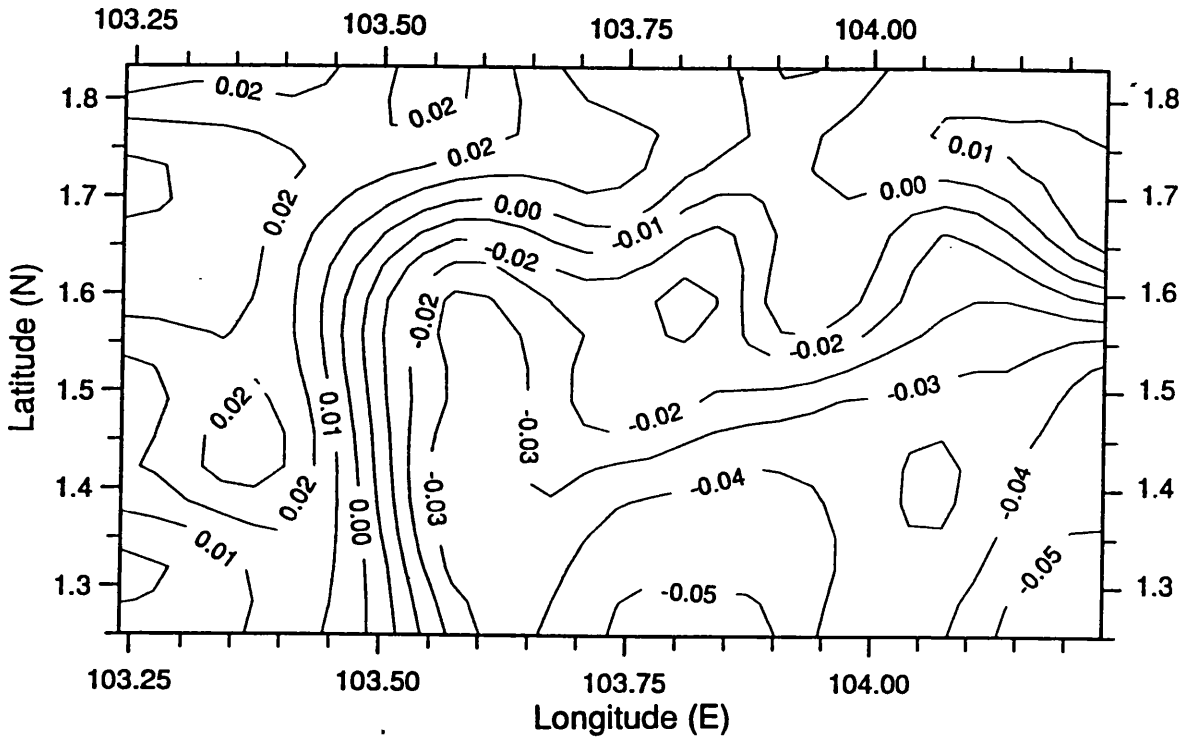

Figure: 7.14(iii) - The residual geoid differences between LSC and FFT for Area C - Case II only, (C.I.= 0.01m)

By examining Table: 7.6 and all figures, The FFT and LSC geoids appear to be compatible to a large extent but some departures of the two are apparent. Obviously, the differences in geoid height computations between the LSC and the FFT methods are due to the structures and mathematical properties of these two methods. As discussed in Sections 6.2 and 6.3, the LSC has a clear stochastic behaviour analysing each observation in two parts, i.e. the signal and the noise whereas the FFT procedures are based on Stokes' formula which is transformed in convolution form. Thus, the power of spectral density function in FFT methodology is equivalent to the covariance function in LSC but not absolutely the same thing.

A major discrepancy appears to be due to differences in the treatment of the input data. For example, the LSC prediction method using point values of reduced anomalies (see Figure: 6.3) whereas the FFT solution requires gridded data (see Figure: 6.4) which inevitably involves some smoothing. In general, the overall accuracy of the LSC solution is slightly less than the FFT solution. Again, one of the possible reasons for this might be that in this prediction method, the geoid was obtained through point anomalies which are closely correlated with the optimal estimation of the respective

covariance functions while the FFT-based method makes use of all the data on the grid. Another reason might be that in the discrete Fourier transform computation, the 100% zeros padding technique was applied in order to eliminate the unwanted errors causing by circular convolution, i.e. spectral leakage. As mentioned before, zero padding consists of embedding zeros around the values of the original field(input data) which practically doubles the dimensions of the arrays. The 100% zeros padding procedure will bring the data smoothly to zero at the edges of the record length, thus eliminating the discontinuities, and giving spectra as close as possible to the 'true' spectra, see Li and Sideris , (1994).

The geoid in all test areas is smoother when computed by FFT than by LSC. One can see that the largest differences occurred in the areas with rough topography of Area A and Area B, see Figure: 7.14(i) and (ii), respectively. These discrepancies may be due to the quality of the covariance function used in this area which did not characterise the gravity field behaviour correctly and consequently did not imply a good relative accuracy internally, i.e. a large mean error prediction.

As is expected, the major differences between these two gravimetric methods does not occur on the numerical results but rather on computing times. For example, to compute the residual geoid height for 104 points using about 250 reduced anomalies for the test Area C, the FFT was found to be about 10^5 quicker than the LSC method, for no appreciable loss in accuracy. As mentioned before, this was due to the main drawback of the LSC method where a system of linear equations with as many unknowns as the number of observations has to be solved, and this sometimes caused storage problems with the available computer resources.

7.6 Comparison of the LSC and the FFT Geoids With GPS/Levelling Derived Geoid Heights

Both results, computed by gravimetric methods described previously in Chapter 6, may contain some systematic errors such as those caused by the optimality of covariance functions (for LSC) and leakage effects (for FFT). It is important to compare solutions with independent external results. As mentioned in Section 1.1, it has become standard practice in recent years to compare computed gravimetric geoid heights with those derived (observed) independently from the combination of GPS observations and orthometric levelling, i.e. $N_{GPS/levelling}$. Therefore, for completeness, the LSC and the FFT solutions will be compared against the available $N_{GPS/levelling}$. Again, as previously mentioned in Section 4.5, only 51 GPS control points in Area B and 5 GPS control points (stations no. GP49, GP50, GP51, GP53 and GP61) in Area C were available for the comparison purposes but no of

GPS/levelling data in Area A were made available by the DSMM, simply because these control data have not yet been connected to the levelling network, i.e. there are no orthometric height values. Also, it has to be pointed out here that orthometric heights at the current GPS points have been determined with varying degrees of accuracy making comparisons between gravimetric and geometrical geoids inhomogeneous and unreliable. Therefore, at the time of this study, it cannot be used to ultimately test the quality of the gravimetric geoid but it does provide a valuable comparison. The geoid heights at the GPS control points were interpolated from the gravimetric geoid database (LSC and FFT final geoids - Case II only), and will used for comparison in terms of absolute and relative differences in the following sections.

7.6.1 Comparison of Absolute Differences

First, the comparisons are made on 51 GPS Federal Territory control points in test Area B. Table: 7.7 summarises the statistics of the differences before and after removing the systematic biases. Details of these differences are given Appendix Y (before removing the systematic biases).

	$N_{GPS/Lev}$ (N1)	N_{LSC} (N2)	N_{FFT} (N3)	∂N1=N1-N2	∂N2=N1-N3
Mean	-4.02	-3.32	-3.33	-0.70(0.00)	-0.69(0.00)
Std. Dev.	0.21	0.18	0.18	0.06 (0.05)	0.06(0.05)
Min.	-4.37	-3.69	-3.69	-0.86(-0.16)	-0.85(-0.16)
Max.	-3.61	-2.92	-2.93	-0.60(0.10)	-0.60(0.09)
Range	0.76	0.77	0.76	0.26(0.26)	0.25(0.25)

Table: 7.7 - Absolute differences between the N_{LSC}, N_{FFT} and the $N_{GPS/Lev}$ at 51 GPS control points - Area B; Number in parentheses represents values after removing the systematic biases. Unit in metres

As shown in the above table, the gravimetric geoid models computed from both the LSC and FFT methods have the absolute agreement with the GPS/levelling in terms of the standard error of about 6 cm. In general, it can be seen that the accuracy is improved by 5 cm compared to the absolute agreement between the GPS/levelling and the tailored model alone (see Section 5.7.3.2, Table: 5.8). The mean values of the absolute agreement with the control GPS points is about 70 cm for both the LSC and the FFT geoids. The overall result, however, indicates that there exists a significant

datum difference between the gravimetric geoid and the GPS/levelling. The differences can be due to a combination of unmodelled GPS errors, gaps in gravity coverage, the long wavelength geoid errors and again, most likely to be suspected, are the levelling errors.

The above accuracy of the gravimetric geoid with respect to the GPS/levelling can be further improved by using more precise GPS data which are accompanied by orthometric height data of similar precision. Moreover, the incorporation of more local gravity data with better quality and coverage, especially in the rough areas (Titiwangsa Range) as well as the high frequency from more accurate DEM can remove the long wavelength errors that are inherent in the tailored model OSU89B-MM.

The comparisons are also made on 5 GPS/Levelling points available in test Area C, see Appendix Z. Table: 7.8 summarises the statistics of the differences before and removing the systematic biases.

	$N_{GPS/Lev}$ (N1)	N_{LSC} (N2)	N_{FFT} (N3)	∂N1=N1-N2	∂N2=N1-N3
Mean	6.44	8.16	8.14	-1.71(0.00)	-1.70(0.00)
Std. Dev.	1.50	1.44	1.42	0.25(0.24)	0.25(0.24)
Min.	4.81	6.68	6.70	-1.92(-0.33)	-1.89(-0.33)
Max.	8.82	10.33	10.33	-1.38(0.21)	-1.37(0.19)
Range	4.01	3.65	3.63	0.54(0.54)	0.52(0.52)

Table: 7.8 - Absolute differences between the N_{LSC}, N_{FFT} and the $N_{GPS/Lev}$ at 5 GPS control points - Area C; Number in parentheses represents values after removing the systematic biases. Unit in metres.

Table: 7.8 indicates that the overall agreement between both gravimetric geoids and the GPS/levelling derived geoid heights is around 25 cm in terms of standard deviation, and there exist systematic biases between the two kinds of geoid representations with biases of about 1.7 m. These systematic biases might be due to the systematic differences between the gravimetric geoid and the orthometric height datum as well as the long wavelength errors in tailored model OSU89B-MM. After removing the systematic biases, it can be seen that there is a 1 cm improvement for the standard deviation of the differences. The remaining differences, mainly due to the effect of high frequency errors in residual anomalies

(from the RTM effect although it is small), the errors in GPS-derived ellipsoidal heights, the tailored model coefficients errors, and most likely the errors in levelling. Perhaps, these errors can only be further reduced by improving the data accuracy and density, and the most important thing is to tie up the GPS control points with the precise levelling network in future. It must be emphasised here that if GPS is to be used as a reliable control or test of the precision of gravimetrically determined geoids, it must be accompanied by orthometric height data of similar precision.

7.6.2 Comparison of the Relative Differences

To evaluate the relative agreement of the gravimetric geoid solutions with respect to the GPS/levelling data, relative differences were formed on all baselines of different lengths in the Federal Territory GPS Network. However, since the interpolated values of both the N_{LSC} and the N_{FFT} at these GPS control data are almost the same, it was decided that only N_{LSC} will be used to evaluate the relative agreement with respect to the $N_{GPS/levelling}$. Appendix AA summarised the result of these relative differences in ppm for the Federal Territory GPS Network and these are plotted against distance in Figure: 7.15.

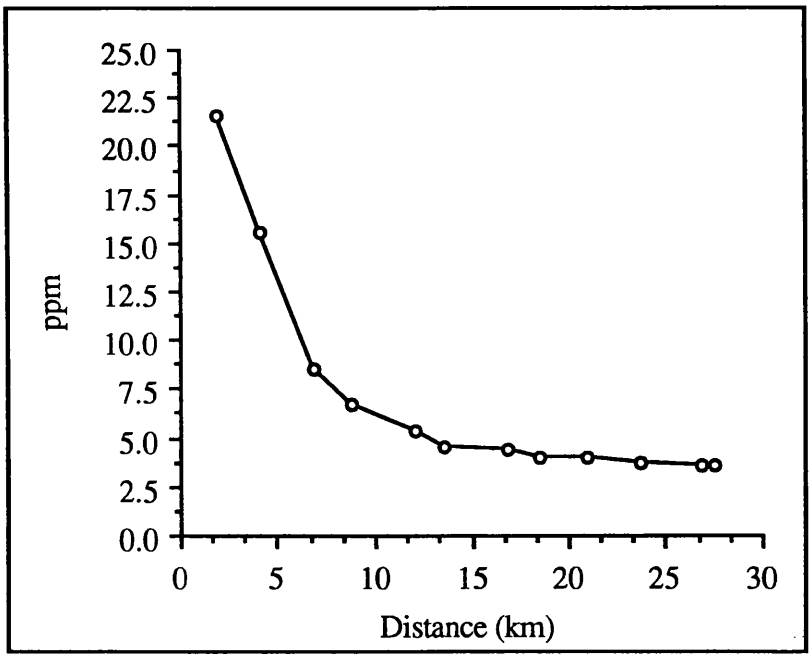

Figure: 7.15 - The relative differences between the N_{LSC} and $N_{GPS/levelling}$ for the Federal Territory GPS Network

Figure: 7.15 indicates that the overall relative agreement between the gravimetric solution and the GPS/levelling derived geoid in this small GPS network are subject to a distance dependent trend. For example, the relative agreement is between 21.3 to 6.7

ppm over short baselines of 1.5 to 10 km, 6.7 to 4.5 ppm for distances of 10 to 15 km and less than 4.5 ppm over a distances of 15 km to more than 25 km. By examining the above figure with the relative differences between the model-computed (OSU89B-MM) and the same GPS/levelling control data, see Figure 5.13, Section 5.7.3.2, one can see very clearly that the combination of tailored model with the local gravity data and height data has significantly improved the overall accuracy of the relative agreement. However over a very short distances, the accuracy of both the gravimetric geoid and the model geoid is almost the same. The possible reason might be due to the long wavelength errors of the tailored model, i.e. the model is unable to pick up more detail within a small area in the gravimetric solution. From this phenomenon, one may observe that for a very short distance, the accuracy of GPS-derived orthometric heights will never exceed spirit levelling.

The relative differences were also formed on all baselines of different lengths for 5 GPS control data in the test Area C, and are listed in Appendix AB. Figure: 7.16 plots the relative differences between the geoid representations in ppm for the GPS control data in area. The comparison of the OSU89B-MM tailored model and the GPS/levelling derived geoid heights is also illustrated in this figure.

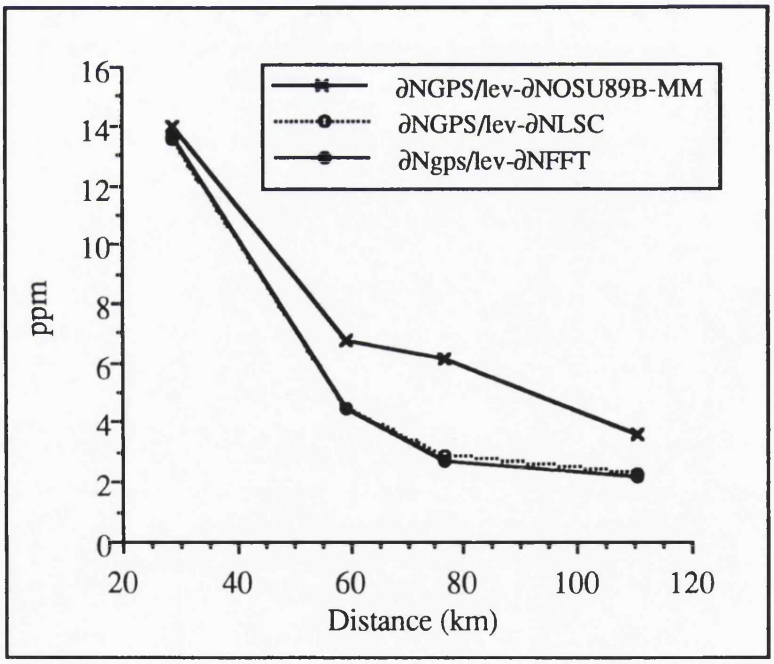

Figure: 7.16 - The relative differences between the N_{LSC}, N_{FFT} and $N_{GPS/levelling}$ for 5 GPS control points (part of the Southwest GPS network)

From the above figure, as to be expected there were no significant relative differences between the LSC and the FFT geoid solutions with respect to the GPS/levelling control data. Also, one can see that the relative differences at distances

up to 30 km are large, i.e. about 13 ppm. For the GPS baselines of 30 to 90 km in length, the relative agreement is between 4.5 to 2.8 ppm, and decreasing to about 2.5 ppm for distances between 90 to 120 km. By examining the same figure, one can notice that the relative agreement of the differences of the tailored model alone, are rather poor compared to the LSC and FFT geoids. This indicates that the incorporation of local data into the gravimetric solutions improves the reference geoid computed by the tailored model OSU89B-MM significantly, both absolutely and relatively over distances from 20 km to over 100 km. Again, by examining this figure, one may conclude that in any condition, the accuracy of GPS-derived orthometric heights will never exceed spirit levelling, where the dependency on distance is great. On the other hand, for long lines, height differences could be determined of in much shorter time and a more cost-effective manner. A redefinition of levelling tolerances may be necessary if GPS is to be used to determine orthometric heights, which accounts for the geoid evaluation methods as shown in Table : 3.5, Section 3.4.

CHAPTER 8

SUMMARY, CONCLUSION AND FUTURE WORK

8.1 Introduction

It has been mentioned in Chapter 1 that the main objective of this study is the development of a tailored model and the computation of preliminary geoid heights in Peninsular Malaysia, by utilising the advantage of all the available heterogeneous data sources, i.e. a global spherical harmonic gravity model (OSU89B), surface gravity data (including some updated gravity points) and the local height data. The development and usage of GPS allows the determination of orthometric height without the need for levelling by combining gravimetrically-determined geoid heights and GPS derived ellipsoidal heights. This chapter summarises the structure and computational procedures of the gravimetric methods used in this study. From the experiments, presentation and analysis outlined in the previous Chapters 5, 6 and 7, the major conclusions are presented. Finally, proposals for possible further work which can be considered for future studies to improve the present undertaking are proposed.

8.2 Summary

The geoid heights in three test areas (Area A, Area B and Area C) in Peninsular Malaysia have been predicted by the method of Least Squares Collocation using a combination of various gravity field information. In principle, the gravity field information can be categorised in three different wavelengths or spectrum resolution (see Table: 3.1, Section 3.3):

- The long wavelength part from the tailored model OSU89B-MM up to degree and order 360. This model was developed by fitting the updated regional gravity data to the pre-existing geopotential model OSU89B in the peninsular region - (Chapter 5).
- The medium wavelength part from point gravity anomalies - (Chapter 4)
- The short wavelength part from local height data - (Chapter 4)

The whole computation processes or the gravity field modelling was based on a 'remove-restore' procedure. In this method, the long wavelength reference field of the tailored model (using program GEOMOD) was removed mathematically from the observed gravity anomalies and these reduced anomalies were denoted as Case I solutions. The short wavelength topographic effects (RTM contribution using program TC1) were also removed mathematically from the reduced anomalies (Case I) to give

the Case II solution. The final geoid heights were obtained by restoring the geoid effects of the tailored model reference field (Case I) and also by the geoid effects of both the tailored model and the topography. For areas devoid of 'observed gravity field information', the anomalies were 'filled in' by the tailored model effect and the RTM effects.

The LSC prediction method (using program GEOCOL) depends essentially on the covariance function used because this function is responsible for the correct mathematical structure of the gravity field through covariance propagation and must be harmonic, (Section 6.2.2). The covariance functions were determined empirically by applying sample data in the test areas to equation (6.36). Here, the local covariance function was derived by only considering pairs of products within the smaller area based on the definition by Goad, et.al., (1984). These were done using the program EMPCOV. In the estimation of the empirical covariance function, the function is assumed to be isotropic and homogeneous. The computed covariance was assigned to the centre of the interval, i.e. the mean distance in that interval, and from this a curve of the empirical covariance function was plotted (Section 7.3). In practice, the local covariance function is replaced by a synthetic model in the form of equation (6.33) which is specified by the empirical degree variance, c_n. A popular degree variance model, and the one used in this study is based on the Tscherning-Rapp model-1974 (using program COVFIT). The model fitting of the covariance function was carried out with care, so that the essential parameters of the empirical function (variance C_o, correlation length ξ and zero variance ψ_o) are reproduced as closely as possible. Following this, the extent to which these covariance parameters were reproduced indicates the goodness of fit of the function in general.

The geoid database is compiled from point heights on 2'x 2', 3'x3' and 5'x5' grid spacings for Area A, Area B and Area C, respectively. These spacings were chosen in such a way that detail was retained in areas of greater geoid variation (Area A and Area B); a decreased density was reasonable for Area C where the geoid gradient is low.

The LSC method has a great potential in gravity field approximation; the degree of success with which it has determined residual geoids in the three test areas proves that the solutions are reliable. This method, however, is computationally inefficient and inconvenient due to the large number of observations, equal to the number of unknowns which was created several problems, e.g. very time-consuming and limited computer storage.

The convolution integrals of equation (6.39) allow the evaluation of Stokes' function by the Fast Fourier Transforms (FFT) method, provided that the data are given on regular grids. Thus, the geoid computations for the same test areas were also done in the frequency domain using this spectral method, mainly for comparison purposes, in Case II only. The FFT (using program GEOFOUR) gave results on the same grid as the grid the data were given on. One of the problems that one has to pay attention to in the FFT method is that of circular convolution. To prevent the effect of circular convolution, the recently well known procedure called zero-padding has been used. In all FFT solutions, 100% zero values were embedded (50% to each side) around the gravity anomalies. The values of the kernel functions were computed at both the data points and the zero-padded points to give optimal results in geoid height computations.

The performance of the geoid heights computed from the stochastic method (N_{LSC}) and the spectral method (N_{FFT}) were compared with those external results provided by the available $N_{GPS/levelling}$, i.e. 51 GPS stations in test Area B and 5 GPS stations in test Area C. Again, it has to be pointed out here that although the orthometric heights at these GPS points have been determined with varying degrees of accuracy, they do provide a valuable comparison with N_{LSC} and also N_{FFT}. The discrepancies are summarised in terms of both the absolute differences (in metres) and the relative differences (in ppm).

8.3 Conclusion

From the results and analysis presented in the last three chapters, the following conclusions can be drawn:

(I) It appears that the control of the long wavelength errors of high degree spherical harmonic reference fields play a major role in the quality of the geoid height determination. Thus, in areas of interest where the existing geopotential models show a relatively poor fit to the gravity field, a tailoring method as proposed by Weber and Zommorodian, (1988) is one of the solutions. The tailoring means fitting to the surface gravity data in a specific region.

(II) The result of the tests carried out in Sections 5.7, suggest that geopotential models fitted to the local gravity field may have important applications in local or regional geoid solutions. An improved reference model will result if the updated data (i.e. that not used in the evaluation of the potential model coefficients of the pre-existing geopotential model) becomes available.

(III) The data used in the tailoring procedure should be representative of block means used to derive the corrections to the potential coefficients. However, the

estimation of mean free-air anomalies can be difficult in mountainous areas with sparse data or having no local DEM.

(IV) The fit of the tailored models depends on the variation in the gravity field information in the area of interest. The reference models which were developed from insufficient data density and coverage will have poor long wavelength information. Such models will not produce suitable reference boundary values, i.e. reference anomalies for a BVP solution.

(V) The apparent local improvement in the tailored model is not so critical for point or mean anomalies compared to the relative geoid height differences.

(VI) The Least Squares Collocation method has been used successfully through the 'remove-restore' procedure for the determination of the geoid heights in all test areas. The LSC, therefore, has great potential in gravity field approximation in the Peninsular Malaysia region. This method, however, suffers from the practical problem that it generates a system of equations of unknowns equal to the number of observation points which can affect the memory requirements of the computer resources.

(VII) The errors in the LSC residual geoid heights are primarily due to non-optimality of the covariance function. The quality of covariance function depends on the amount of variation of the gravity field, and the extent to which the tailored model and topographic model reduce the variation. In this particular experiment, the covariance functions computed for the three test areas vary in complexity. In rugged terrain Area A, the functions are not of an optimum nature (due to 'filled-in' anomalies) and therefore more data reduction is necessary once the gravity data is available for this area. A denser DEM would contain a lot of information in this area, the extraction of which would leave the gravity field in the desired condition. Based on the functions that were determined, the geoid prediction is not of a high standard and observed gravimetric data are not well reproduced. In some parts of area B (where the gravity density and coverage are considered good) and most of Area C, the gravity field is more amenable to analysis and the geoid solutions were produced to an encouraging quality. For each stage of data reduction in Area C, theoretically correct behaviour of the gravity field was noted, which leads to an optimum covariance function and realistically low error predictions.

(VIII) The RTM contribution to the geoid height (indirect effect) can be in the order of decimetres in the rough topography in Area A and Area B where it will become the dominant source of systematic error. For the case in Area C, although the RTM

contribution is very small, i.e. a few mgals in Area C, consideration of it in the computation still seems to improve the results slightly.

(IX) The total masses removed by using the reference mean height surface in the RTM evaluation were on average very close to zero, and they were harmonic functions which is a vital requirement for the BVP solution, e.g. the LSC.

(X) By examining the absolute LSC geoids, it appears that very long wavelength errors in the spherical harmonic tailored model remained or dominated in the final geoid heights. However, with the inclusion of local gravity data and height data in the gravimetric solution, some extra detail in the residual geoid is apparent in most test areas, especially in the rough terrain.

(XI) Providing sufficient precautions have been taken to minimise the circular convolution errors, i.e. spectral leakage errors, the use of 100% zeros padding as suggested by Li and Sideris, (1994) around the marginal data gives optimal results which are comparable to those predicted by the LSC method.

(XII) In all test areas, the LSC residual geoid heights are apparently less accurate compared to the FFT 'method. One of the possible reasons for the lower accuracy of N_{LSC} might be due to the non-optimality of the covariance function (fitted covariance model). It is often difficult to know with confidence when the 'correct' or 'perfect' covariance function is being used, but as far as this experiment is concerned, the model has fitted the empirical function quite well to a certain spherical distance depending upon the gravity field information in the test areas, i.e. about 1.5 ξ, see figures 7.2(i) - (vi).

(XIII) From a practical computational viewpoint, the LSC method was extremely time consuming, due to large matrix inversion. Contrary to the LSC solution, the FFT method was found more efficient in terms of computational time.

(XIV) Comparison of gravimetric geoids with the GPS/levelling derived geoid heights of 51 GPS points in Area B and 5 GPS points in Area C shows the absolute agreement better than 30 cm and 10 cm in terms of standard deviation, respectively.

(XV) The relative agreement ranges for the GPS network in Area B is between 21.3 to 6.7 ppm over short baselines of 1.5 to 10 km, 6.7 to 4.6 ppm for distances of 10 to 15 km and less than 4.5 ppm over distances of 15 to more than 25 km. For the GPS network in Area C, the relative agreement is about 13 ppm for distances up to 30 km, 4.5 to 2.8 ppm over distances of about 30 to 90 km and about 2.5 ppm for baselines of 90 to over 120 km.

(XVI) The relative agreement of the differences of the tailored model alone, is rather poor compared to the LSC and FFT geoids. The incorporation of local data into the gravimetric solutions improve the reference geoid computed by the OSU89B-MM tailored model significantly, both absolutely and relatively over distances from 20 km to over 100 km. In other words, the improvement is attributed to the presence of some medium to short wavelength features of the local geoid.

(XVII) In any condition, the accuracy of GPS-derived orthometric heights will never exceed spirit levelling, where the dependency on distance is greater. On the other hand, for long lines, height differences could be determined within shorter periods and in a more cost-effective manner.

(XVIII) It must be mentioned that there may exist significant systematic datum difference between the GPS/levelling data and the gravimetric geoid computed from the LSC and FFT methods. This datum difference can be caused by a combination of errors coming from GPS heights, orthometric heights and the long wavelength errors in gravimetric geoid heights. It is very difficult to identify the exact contribution of each one of the error sources. It has been suggested by Sideris and She, (1995) that at least 4 levelling benchmarks should be occupied by GPS receivers to provide datum transformation parameters (see equation 3.32, Section 3.7) when the GPS heights are combined with gravimetric geoid heights to generate the orthometric height (equation 3.1).

(XIX) The absolute errors in the gravimetric geoid solution of the test areas are difficult to quantify, firstly because it is not known to what spectral and spatial extent the tailored model OSU89B-MM is in error. It was initially expected that in the future, the error in the gravimetric geoid in the test areas could be quantified by the precise GPS/levelling control data. At the present stage, the errors in the geoid can only be generated by potential coefficients of tailored model OSU89B-MM and terrestrial gravity uncertainties. Thus, without a more detailed GPS survey, it is difficult to identify true spurious long wavelength trends in all solutions. Moreover, if GPS is to be used as a reliable control or test of the precision of gravimetrically determined geoids, it must be accompanied by orthometric height data of similar precision. This was not the case for this particular study as the GPS data and especially the orthometric heights are of lower than expected quality and cannot provide the level of control on the gravimetric geoid expected when this study was proposed. Despite this, the tailoring approach of the existing geopotential model does show an improved agreement with GPS control data.

8.4 Suggestions for Future Work

From the work done in this study, the following proposals are considered to be worthy of future investigation:

(I) Since the precision of absolute gravimetric geoid heights is still limited by the fit of the tailored model OSU89B-MM (caused by the long wavelength coefficient errors) to the local field, this tailored model can be further improved by incorporating new gravity anomalies that have been observed by the DSMM and the GSM, see Section 4.2 (c) and (d). In addition to the existing local gravity data (old and new data), it is recommended that adequate gravity points in the large 'unsurveyed areas' of the mountainous areas, such as Titiwangsa Range, Bintang Range and Timor Range, also are very important for the development of a more superior reference field than the present one (OSU89B-MM). Furthermore, it is obvious that an improved higher degree and order geopotential model (which is expected to be available in the near future once a joint *DMA/GSFC Project* for improving the model of the earth's gravitational field is completed) should be used to provide reference field for precise gravimetric geoid determinations in Peninsular Malaysia - Rapp, (1995-Private Communication).

(II) Updating the available gravity and height data are of great influence in future computations. Bathymetric maps and marine gravity on the surrounding sea areas and over lakes are essential for updating. The compilation of satellite altimeter data and marine gravity data of the surrounding sea areas is highly recommended for improving the gravity field modelling in areas near coastlines or in small seas, i.e. the Malacca Straits and the South China Sea. The recovered gravity field information in these areas is very useful for both geodetic and geophysical purposes, e.g. oceanography studies related to the determination of the stationary sea surface topography from satellite altimeter data, mineral and oil explorations, etc.

(III) An accurate resolution of the local DEM with an optimal grid spacing, especially in the mountainous areas, e.g. Titiwangsa Range, Bintang Range and Timor Range is very important for reducing the irregularities of the local gravity field. It is recommended that the grid size of DEM should be at least 1 km x 1 km for rough topography (1000-2000 m), 2 km x 2 km for moderate topography (500-1000) and at 10 km x 10 km for smooth topography (0 - 500m). Here, the local gravity field in the mountainous areas can be smoothed by a suitable gravity field terrain modelling before using any gravimetric methods, e.g. Stokes' integral, LSC or FFT.

(VI) Since the distribution of point gravity anomalies in the peninsular region is mostly irregular and predominantly located in lowlands and the valleys rather than on the mountainous areas, height data can furnish the effect of visible topography (high spectral resolution) in combination with *airborne gradiometer data.* An economically feasible and efficient technique for observation of the high frequency field with high data density, regional coverage, regular data distribution and high data accuracy will be the *airborne gradiometry* ; the measurement of the earth's gravity field from aircraft. The choice of gravity sampling rate should reflects the irregularities of the topography so that the statistical properties of the gravity field (usually expressed in terms of a isotropic and homogeneous covariance function) could be adequately estimated. For a geoid height accuracy of about 5 cm/100 km resp. 20 cm/1000 km, it is recommended that the grid sizes for gravity data should be at least 5-10 km for smooth to moderate topography and between 3-5 km for rough topography, see Denker, et. al., (1988). These specifications therefore could be adopted for Peninsular Malaysia.

(V) No precise estimates of possible errors in the gravimetric geoid solution were attained in this study, due to deficiencies in the $N_{GPS/levelling}$ measurements. Therefore the entire GPS network must be connected by precise levelling to local tide gauges (which must be corrected to geophysical phenomena such as ocean currents, air pressure and water density variation) so that the true magnitude of such errors (systematic biases) can be revealed.

Finally,

"The task of the computation of a geoid in Peninsular Malaysia is an ongoing activity. With improvements of gravity data coverage, density and quality which might be realised by modern measurement techniques such as airborne gravimetry,the realisation of cm-accuracy geoids may be achievable and it is the author's hope that a complete and precise geoid will be available in the near future. This will in turn, make it possible to replace costly levelling procedures by GPS and gravimetric geoid data to generate the orthometric heights (or height differences) with sufficient accuracy for a wide range of scientific applications. It is very important for the author to stress here that there is a need for strong co-orperation between the DSMM, GSM and the higher institutions (e.g. UTM, USM) for the sake of producing a unified gravimetric geoid of high accuracy, which in turn, will lead to the redefinition of the Vertical Datum for Peninsular Malaysia ".

Appendix A

The Parameters of the Geodetic Reference System 1980 (GRS80)

(I) PRIMARY CONSTANTS

Semi-major axis	:	6378137.0 metres
J_2	:	1082.630×10^{-6}
Geocentric Gravitation	:	$398600.50 \times 10^{9} m^3 s^{-2}$
Rotation Speed	:	$7.292115000 \times 10^{-5}$ radian/sec

(II) DERIVED CONSTANTS

Square of First Eccentricity	:	0.00669438002290
Square of Second Eccentricity	:	0.00673949677547
Flattening	:	1/298.2572221012
Equatorial Normal Gravity	:	9.78032677 ms^{-2}
Polar Normal Gravity	:	9.83218637 ms^{-2}
Constant of Somigliana Formula	:	0.001931851353
Mean Earth Radius	:	6371007.2 metres
Mean Earth Normal Gravity	:	9.79764466 ms^{-2}
Normal Potential	:	62636860.850 m^2s^{-2}

(III) FULLY NORMALISED ZONAL SPHERICAL HARMONIC COEFFICIENTS OF THE ELLIPSOIDAL NORMAL GRAVITY POTENTIAL

Degree	C(n,0)
2	-0.484166854895874E-03
4	0.790304072882704E-06
6	-0.168725117564924E-08
8	0.346053239784696E-11
10	-0.265006217692820E-14

Appendix B

Format of Gravity Data Supplied by the University Technology Malaysia (UTM)

Stn.	Latitude (° ' ")	Longitude (° ' ")	Observed Gravity (mgals)	Free Air (mgals)	Bouguer Anomaly (mgals)	Height (m)
W1	2 44 29	101 51 46	978034.31	6.90	0.69	55.474
W2	2 43 33	101 53 13	978026.65	5.96	- 2.63	76.810
W3	2 43 23	101 54 29	978029.94	3.54	-2.98	58.217
W4	2 43 43	101 54 09	978030.25	2.97	-3.24	55.474
W5	2 43 52	101 52 54	978028.14	4.53	-3.02	67.483
W6	2 43 29	101 57 42	978028.43	-0.25	-5.94	50.902
W7	2 43 40	101 58 42	978026.00	-0.79	-7.18	57.089
W8	2 43 22	102 00 01	978022.41	0.42	-8.23	69.799
W9	2 43 15	102 01 39	978017.18	0.43	-9.58	89.428
W10	2 43 26	102 02 17	978006.06	3.21	-11.85	134.508
W11	2 43 40	102 03 18	977980.95	15.02	-13.42	254.203
W12	2 43 39	102 03 45	977988.47	12.29	-12.44	220.980
W13	2 43 53	102 04 00	978000.59	14.01	-13.34	155.021
W14	2 43 26	102 02 48	977992.12	7.40	-14.22	193.243
W15	2 44 17	102 06 36	978007.55	0.00	-13.39	119.695
W16	2 26 42	103 03 36	978038.37	20.63	11.80	78.943
W17	2 28 04	103 03 14	978044.15	16.54	11.22	47.594
W18	2 28 33	103 04 06	978043.18	16.45	10.79	50.957
K1	5 29 24	100 23 08	978096.28	17.30	16.89	3.658
K2	5 30 40	100 24 24	978098.36	19.05	18.63	3.780
K3	5 27 11	100 23 04	978093.38	15.03	14.63	3.658
K4	5 31 10	100 25 39	978099.48	20.37	19.82	4.877
K5	5 35 13	100 26 35	978103.17	24.29	23.24	9.449
K6	5 32 30	100 26 22	978100.55	20.62	20.23	3.475
K7	5 37 24	100 28 40	978100.69	20.23	19.52	6.401
K8	5 39 33	100 30 11	978091.83	13.00	11.46	13.716
K9	5 35 33	100 28 23	978103.03	25.19	23.72	13.106
K10	5 38 20	100 29 19	978092.84	17.98	17.57	3.658

Appendix C

Format of Gravity Data Supplied by the Department of Surveying and Mapping, Malaysia (DSMM)

Latitude (¤ ' ")	Longitude (¤ ' ")	Height. (m)	Observed Gravity (mgals)	Normal Gravity (mgals)	Free-Air (mgals)	Bouguer (mgals)
1 22 0	103 27 0	5.125	978065.30	978034.8	32.089	31.516
1 23 45	103 26 15	5.478	978065.43	978034.9	32.201	31.589
1 26 0	103 25 0	3.087	978066.72	978035.1	32.587	32.242
1 28 30	103 23 45	3.412	978065.15	978035.3	28.830	28.450
1 29 30	103 42 45	5.459	978052.00	978035.4	18.339	17.728
1 30 0	103 23 15	3.574	978064.76	978035.4	30.469	30.069
1 30 0	103 26 30	3.703	978063.44	978035.4	29.188	28.774
1 30 0	103 32 30	4.192	978055.19	978035.4	21.097	20.628
1 30 30	103 31 0	15.004	978057.67	978035.4	26.010	24.330
1 30 30	103 41 0	13.928	978056.85	978035.4	25.722	24.163
1 31 30	103 28 30	5.796	978062.65	978035.5	28.927	28.278
1 32 15	103 22 0	3.365	978065.07	978035.6	30.536	30.160
1 32 15	103 33 0	38.012	978043.49	978035.6	19.655	15.402
1 32 45	103 39 30	9.112	978062.84	978035.6	30.041	29.021
1 33 30	103 35 30	41.699	978042.13	978035.7	19.334	14.668
1 36 15	103 19 15	3.552	978064.81	978035.9	30.004	29.606
1 38 15	103 17 30	3.382	978066.14	978036.1	31.111	30.733
1 39 45	103 11 30	2.240	978069.44	978036.2	31.111	30.733
1 41 0	103 8 45	1.918	978069.22	978036.3	33.504	33.290
1 42 0	103 6 15	2.045	978069.54	978036.4	33.778	33.550
1 43 30	103 4 45	2.237	978067.21	978036.5	31.364	31.113
1 44 0	103 54 0	6.807	978060.04	978036.6	25.567	24.805
1 45 0	103 2 0	2.719	978057.67	978036.7	21.842	21.537
1 45 15	102 59 45	4.519	978054.08	978036.7	18.780	18.275
1 45 45	103 24 45	23.233	978062.08	978036.7	32.514	29.914
1 47 30	103 57 0	23.563	978057.38	978036.9	27.759	25.122
1 48 0	103 20 15	24.885	978058.19	978036.9	28.927	26.142
1 48 15	102 57 30	23.533	978049.94	978037.0	20.240	17.606
1 51 45	104 2 15	35.578	978060.72	978037.3	34.393	30.412
1 53 5	102 46 50	1.995	978071.26	978037.4	34.439	34.216
1 54 30	102 44 20	1.864	978065.20	978037.6	28.196	27.987

Appendix D

Format of Gravity Data Supplied by the Geological Survey Malaysia (GSM)

Station Number	Longitude (¤ ')	Latitude (¤ ')	Easting (m)	Northing (m)	Height (m)	Observed Gravity (mgal)	Free Air (mgal)	Density (g/cc)			Bouguer Anomaly (mgal)
1	101 7.08	4 36.13	347400	509320	51.90	3030.56	-18.50	2.67	.00H	.00Z	-24.31 B4/1
2	101 8.57	4 36.70	350160	510360	54.10	3023.46	-25.06	2.67	.04H	.00Z	-31.12 B4/1
3	101 9.85	4 39.27	352550	515080	75.40	3008.21	-34.35	2.67	.06H	.00Z	-42.80 B4/1
4	101 11.99	4 40.11	356500	516620	138.20	2989.56	-33.82	2.67	.48H	.00Z	-49.29 B4/1
5	101 9.71	4 41.07	352300	518400	81.00	3010.50	-30.77	2.67	.09H	.00Z	-39.84 B4/1
6	101 8.91	4 42.56	350830	521150	85.00	3013.21	-27.20	2.67	.03H	.00Z	-36.71 B4/1
7	101 7.78	4 38.32	348700	513350	63.90	3025.28	-20.60	2.67	.00H	.00Z	-27.76 B4/1
8	101 7.18	4 32.88	347560	503330	45.80	3034.08	-16.09	2.67	.00H	.00Z	-21.22 B4/1
9	101 7.89	4 31.75	348870	501240	44.40	3033.18	-17.15	2.67	.30H	.00Z	-22.13 B4/1
10	101 6.07	4 31.02	345500	499900	51.50	3041.75	-6.21	2.67	.02H	.00Z	-11.98 B4/1
11	101 4.18	4 32.12	342020	501940	31.10	3046.01	-8.51	2.67	.00H	.00Z	-11.99 B4/1
12	101 4.83	4 33.92	343220	505260	37.60	3041.99	-10.95	2.67	.00H	.00Z	-15.16 B4/1
13	101 5.53	4 38.18	344540	513100	42.10	3034.15	-18.43	2.67	.19H	.00Z	-23.14 B4/1
14	101 6.90	4 39.87	347100	516210	60.40	3025.47	-21.87	2.67	.00H	.00Z	-28.64 B4/1
15	101 7.43	4 41.49	348080	519200	72.80	3020.74	-23.17	2.67	.00H	.00Z	-31.32 B4/1
16	101 5.49	4 42.71	344500	521450	72.00	3023.50	-20.96	2.67	.31H	.00Z	-29.02 B4/1
17	101 5.24	4 40.97	344030	518240	60.80	3027.30	-20.18	2.67	.06H	.00Z	-26.99 B4/1
18	101 4.31	4 39.44	342300	515430	56.80	3028.60	-19.75	2.67	.19H	.00Z	-26.10 B4/1
19	101 3.16	4 37.63	340170	512100	53.40	3030.82	-18.13	2.67	.28H	.00Z	-24.11 B4/1
20	101 5.00	4 35.87	343550	508850	38.10	3038.44	-14.82	2.67	.00H	.00Z	-19.08 B4/1
21	101 8.15	4 35.11	349370	507430	50.70	3026.40	-22.79	2.67	.05H	.00Z	-28.47 B4/1
22	101 6.35	4 34.79	346050	506860	43.40	3035.91	-15.46	2.67	.00H	.00Z	-20.31 B4/1
23	101 2.92	4 33.89	339700	505220	42.10	3040.00	-11.55	2.67	.04H	.00Z	-16.26 B4/1
24	101 .72	4 29.69	335600	497500	46.60	3044.02	-5.15	2.67	.00H	.00Z	-10.37 B4
25	101 1.91	4 31.06	337800	500000	39.00	3041.48	-10.36	2.67	.03H	.00Z	-14.72 B4
26	101 0.00	4 28.29	334250	494920	47.50	3046.10	-2.46	2.67	.00H	.00Z	-7.78 B4
27	100 57.51	4 27.30	329650	493100	43.90	3054.06	4.62	2.67	.00H	.00Z	-.30 B4
28	101 0.03	4 26.19	334300	491050	28.50	3053.65	-0.30	2.67	.00H	.00Z	-3.49 B4
29	100 59.17	4 23.72	332700	486500	22.10	3059.95	4.60	2.67	.00H	.00Z	2.13 B4

Appendix E

Details of the Southwest GPS Network

GPS Code Station	GPS Location	Latitude (degree)	Longitude (degree)	Ellipsoidal Height (metre)	Ortho. Height (metre)	Geoid Height (metre)
GP10	Senawang	2.6824	101.9745	70.153	72.914	-2.761
GP11	Tanjung T.	2.4236	101.8634	15.309	17.807	-2.498
GP12	Lubuk Cina	2.4482	102.0717	15.879	17.332	-1.453
GP13	Tebong	2.4407	102.3393	46.701	47.066	-0.365
GP14	Gemas	2.5772	102.5950	46.133	45.391	0.742
GP15	Muar	2.0649	102.5564	2.932	2.086	0.846
GP16	Pagoh	2.1312	102.7338	35.158	33.500	1.658
GP34	Beserah	3.8593	103.3648	6.170	4.874	1.296
GP35	Airport K.	3.7893	103.2117	13.370	12.446	0.924
GP36	Paloh Inai	3.4831	103.1001	15.905	14.597	1.308
GP37	Tg. Aras	3.5106	103.4693	5.917	3.422	2.495
GP38	Tg. Batu	3.2058	103.4445	46.248	43.579	2.669
GP39	Kg. Bagon	2.9415	103.4197	6.901	3.914	2.987
GP40	Bkt. Payon	2.9754	103.1777	31.382	29.457	1.925
GP41	Felda S	2.6865	103.3616	62.251	58.826	3.425
GP42	Kg. Jawa	2.7057	103.5737	7.932	3.853	4.079
GP43	Kg. Mawar	2.6016	103.7788	10.095	5.034	5.061
GP47	Felda C.	2.3887	102.9332	50.106	47.849	2.257
GP48	Seri Medan	1.9761	102.9336	163.676	161.110	2.566
GP49	Benut	1.6261	103.1999	6.670	1.858	4.812
GP50	Pasong	1.5475	103.3954	8.971	3.211	5.760
GP51	Senai A.	1.6340	103.6668	41.614	35.525	6.089
GP53	Lukut	1.8043	103.8972	30.729	23.997	6.732
GP54	Sedeli B.	1.9255	104.0904	11.783	4.655	7.128

.....Continue

GPS Code Station	GPS Location	Latitude (degrees)	Longitude (degrees)	Ellipsoidal Height (h)	Ortho. Height	Geoid Height
GP55	Tenggaroh	2.0798	103.8889	35.653	29.415	6.238
GP56	Mersing	2.3916	103.8728	10.478	4.751	5.727
GP58	I. Haiwan	2.1217	103.4275	76.536	72.213	4.323
GP59	Air Hitam	1.9735	103.2277	44.102	40.194	3.908
GP60	Renggam	1.8845	103.3984	60.870	56.166	4.704
GP61	Paloh	1.3698	104.2674	58.720	49.900	8.820
GP84	Batu Pahat	1.8575	102.9417	6.050	3.211	2.839
GP85	Tanjong	1.9088	102.7358	3.858	2.003	1.855
GP91	Hulu Sed.	1.8793	103.6919	25.215	19.554	5.661
GP94	Pencor P.	3.6324	103.3051	6.378	4.591	1.787
GP98	Bkt. Seroh	2.9044	102.8123	23.334	22.247	1.087

Appendix F

Details of the Federal Territory GPS Network

Station Code	GPS Station Location	Latitude (¤ ' ")	Longitude (¤ ' ")	RSO Coord. (in metres)		Ellipsoid Height (metres)	Ortho. Height (metres)	Geoid Height (metres)
				Northing	Easting			
GU02	Bukit Idaman	3 14 30	101 38 55	358725	405878	85.338	89.705	-4.367
GU03	Sksb Selyang	3 14 30	101 40 35	358718	408965	64.669	68.895	-4.226
GU04	Tmn. Sri Go.	3 14 40	101 42 20	359016	412824	164.466	168.482	-4.016
GU05	Gombak	3 14 40	101 43 40	359012	414676	65.720	69.893	-4.173
GU06	Emp. Klang	3 14 20	101 45 10	358391	417453	110.899	114.784	-3.885
GU08	Sek.M. Jinj.	3 13 25	101 39 20	356727	406645	50.200	54.479	-4.279
GU09	Kem Kentom	3 13 20	101 40 40	356568	409114	44.294	48.364	-4.070
GU10	Tmn. Melew.	3 13 20	101 41 50	356562	411275	44.735	48.746	-4.011
GU11	Tmn. Melati	3 13 20	101 43 30	356555	414362	55.457	59.406	-3.949
GU12	Tmn. Melawa	3 13 20	101 45 00	356549	417140	55.004	58.817	-3.813
GU13	Manjalar	3 11 40	101 37 25	353511	403087	76.757	81.129	-4.372
GU14	Tmn. Petali.	3 11 55	101 39 05	353964	406175	40.998	45.245	-4.247
GU16	Tmn. Dato S	3 11 55	101 41 45	353952	411115	36.583	40.635	-4.052
GU17	Selangor Pew.	3 12 00	101 43 40	354098	414665	43.804	47.774	-3.970
GU18	Lembah Ker.	3 12 00	101 45 05	354706	417290	80.702	84.495	-3.793
GU19	Bukit Lanjan	3 10 15	101 37 00	350902	402309	41.305	45.660	-4.355
GU20	T. Sri Harta.	3 10 00	101 39 05	350432	406166	72.830	77.090	-4.260
GU21	Std. Tun Raz.	3 10 25	101 40 35	351193	408947	43.056	47.211	-4.155
GU22	Hos. Besar	3 10 15	101 42 15	350879	412033	33.066	37.124	-4.058
GU23	Esso Keram.	3 10 05	101 43 30	350566	414348	30.092	34.053	-3.961
GU24	Tmn. Sri Ke.	3 10 35	101 44 45	351482	416665	62.791	66.659	-3.868
GU26	Intan .D	3 08 30	101 38 55	347669	405669	60.137	64.357	-4.220
GU27	Sri Perdana	3 08 40	101 40 35	347969	408939	88.166	92.270	-4.104
GU29	Tmn. Maluri	3 08 20	101 44 05	347339	415421	39.280	43.129	-3.849
GU30	Tmn. Nirwan	3 08 45	101 45 20	348101	417738	47.101	50.902	-3.801
GU31	Srkt. Sea PJ	3 07 05	101 37 20	345065	402912	39.537	43.813	-4.276
GU32	Seksyen 13	3 07 05	101 38 40	345059	405382	45.106	49.301	-4.195
GU33	Kom. Sukan	3 07 20	101 40 25	345512	408624	32.938	37.013	-4.075
GU34	TUDM Sg.	3 07 10	101 42 35	345196	412637	29.436	33.389	-3.953

..... continued

Station Code	GPS Station Location	Latitude (¤ ' ")	Longitude (¤ ' ")	RSO Coord. (in metres)		Ellipsoid Height (metres)	Ortho. Height (metres)	Geoid Height (metres)
				Northing	Easting			
GU35	Bulatan TAR	3 06 50	101 43 40	344577	414643	49.215	53.026	-3.811
GU36	Kg. Cheras	3 06 30	101 44 55	343957	416957	101.443	105.198	-3.755
GU37	Kg. Tunku	3 05 40	101 37 25	342454	403060	35.848	40.043	-4.195
GU38	Seksyen 4. P	3 05 40	101 38 55	342448	405839	16.758	20.865	-4.107
GU39	Jln. Kucai	3 05 25	101 41 00	341978	409697	44.473	48.162	-3.989
GU40	Esso Salak	3 06 20	101 42 25	343661	412325	31.425	35.337	-3.912
GU41	Tmn. Midah	3 05 50	101 43 40	342734	414638	74.118	77.932	-3.814
GU42	Tmn. Cuepec	3 05 00	101 45 05	341192	417259	67.016	70.624	-3.608
GU43	Pucong Jaya	3 03 05	101 37 20	337694	402894	26.924	31.027	-4.103
GU44	Kinrara	3 03 40	101 38 55	338762	405830	14.463	18.535	-4.072
GU45	O.U.G.	3 04 05	101 40 45	339522	409228	39.168	43.120	-3.952
GU46	Sri Petaling	3 04 10	101 41 55	339670	411389	58.889	62.786	-3.897
GU47	Kem Sg. Besi	3 03 55	101 42 50	339205	413086	58.708	62.519	-3.811
GU48	Tmn. Suria	3 03 40	101 44 50	338736	416790	66.176	69.782	-3.606
GU49	Puchong	3 01 20	101 36 40	334472	401651	7.894	11.964	-4.070
GU52	Tmn. Pura J.	3 02 00	101 42 25	335675	412306	42.717	46.514	-3.797
GU53	Balakong	3 02 00	101 43 40	335670	414622	37.637	41.373	-3.736
GU54	Kg. Baru Bel.	3 02 15	101 44 55	336125	416939	56.762	60.405	-3.643
GK02	Seksyen 8	3 05 45	101 38 20	342604	404759	17.898	22.046	-4.148
GK03	Sungai Besi	3 07 50	101 42 25	346425	412332	51.434	55.412	-3.978
GK04	Kolam Air	3 10 25	101 41 35	351189	410799	62.723	66.877	-4.154
GK05	Damansara	3 08 25	101 37 20	347522	402918	38.562	42.879	-4.317

Appendix G

Mean Free-air Anomalies Used for a Tailored Model Development

No	Latitude (degrees)	Longitude (degrees)	Mean Height (metres)	Mean Anomaly (mgals)
1	6.75000	100.25000	33.45	11.90
2	6.25000	100.25000	5.56	15.59
3	6.25000	100.75000	44.93	6.54
4	5.75000	100.25000	9.75	12.88
5	5.75000	100.75000	44.80	3.41
6	5.75000	101.25000	290.15	9.02
7	5.75000	101.75000	338.56	16.21
8	5.75000	102.25000	43.29	12.60
9	5.25000	100.25000	19.87	4.29
10	5.25000	100.75000	31.36	-3.56
11	5.25000	101.25000	166.17	-4.13
12	4.75000	100.75000	22.39	-2.86
13	4.75000	101.25000	76.86	-16.13
14	4.25000	100.75000	9.55	11.51
15	4.25000	101.25000	32.88	-4.24
16	3.75000	100.75000	2.85	24.58
17	3.75000	101.25000	16.92	14.30
18	3.75000	101.75000	172.34	4.85
19	3.75000	102.25000	70.29	17.72
20	3.75000	102.75000	39.51	19.68
21	3.75000	103.25000	20.73	21.54
22	3.25000	101.25000	6.62	18.27
23	3.25000	101.75000	97.69	2.50
24	3.25000	101.25000	79.30	15.96
25	3.25000	103.25000	20.45	18.41
26	2.75000	101.75000	25.32	19.85
27	2.75000	102.25000	89.27	17.44
28	2.75000	102.75000	41.96	25.85

.....continued

No	Latitude (degrees)	Longitude (degrees)	Mean Height (metres)	Mean Anomaly (mgals)
29	2.75000	103.25000	25.21	15.99
30	2.75000	103.75000	18.93	27.76
31	2.25000	102.25000	15.09	20.64
32	2.25000	102.75000	21.35	25.05
33	2.25000	103.25000	33.79	21.45
34	2.25000	103.75000	39.33	19.82
35	1.75000	103.25000	15.01	29.03
36	1.75000	103.75000	28.97	25.88
37	1.75000	104.25000	19.12	25.15
38	1.25000	103.75000	13.26	32.70

Appendix H

Results of Mean Residual Anomalies for OSU89B and OSU89B-MM Analysed on 0.5° x 0.5° Block Basis

Latitude (degrees)	Longitude (degrees)	Mean Residual Anomalies (in mgals)	
		OSU89B	OSU89B-MM
1.25000	103.25000	6.92	0.02
1.25000	103.75000	1.15	-6.46
1.25000	104.25000	-1.25	-7.16
1.75000	102.75000	2.88	-3.71
1.75000	103.25000	0.21	-0.99
1.75000	103.75000	-2.11	-1.43
1.75000	104.25000	1.40	-1.22
2.25000	102.25000	-4.77	-3.52
2.25000	102.75000	-6.42	-0.21
2.25000	103.25000	-20.86	-1.57
2.25000	103.75000	-7.21	0.77
2.75000	101.75000	-15.92	-4.10
2.75000	102.25000	-4.04	-0.81
2.75000	102.75000	-9.90	-2.45
2.75000	103.25000	-3.17	0.09
2.75000	103.75000	2.21	1.91
3.25000	101.25000	-8.58	-1.42
3.25000	101.75000	-37.65	-3.73
3.25000	102.25000	-1.57	1.58
3.25000	102.75000	6.04	3.31
3.25000	103.25000	-1.49	0.66
3.75000	100.75000	9.32	5.80
3.75000	101.25000	-30.24	-5.54
3.75000	101.75000	-31.55	3.93
3.75000	102.25000	-5.79	-0.88
3.75000	102.75000	-13.89	-3.86
3.75000	103.25000	1.80	-0.31

.....continued

Latitude (degrees)	Longitude (degrees)	Mean Residual Anomalies (in mgals)	
		OSU89B	OSU89B-MM
4.25000	100.75000	1.71	0.78
4.25000	101.25000	-58.04	-3.50
4.25000	101.75000	-0.04	-11.74
4.25000	102.25000	-0.67	-9.80
4.25000	103.25000	1.60	-5.55
4.75000	100.75000	-31.77	1.32
4.75000	101.25000	-93.49	10.00
4.75000	101.75000	-52.96	-27.11
4.75000	102.25000	-35.30	-15.42
4.75000	103.25000	9.97	4.36
5.25000	100.25000	-16.15	3.80
5.25000	100.75000	-48.81	-0.60
5.25000	101.25000	-82.80	-1.47
5.25000	102.25000	-29.67	-4.45
5.25000	102.75000	-6.92	-18.43
5.25000	103.25000	9.51	4.79
5.75000	100.25000	-7.65	2.67
5.75000	100.75000	-42.54	-0.93
5.75000	101.25000	-49.65	8.53
5.75000	101.75000	-17.98	-0.38
5.75000	102.25000	-10.49	1.60
5.75000	102.75000	-1.57	-9.61
6.25000	100.25000	-8.02	2.42
6.25000	100.75000	-30.37	1.54
6.25000	101.25000	-47.88	-27.07
6.25000	101.75000	-2.97	-9.93
6.25000	102.25000	3.63	6.70
6.75000	99.75000	7.93	-5.00
6.75000	100.25000	-17.06	2.22
6.75000	100.75000	-6.80	-5.08
6.75000	101.25000	2.38	-8.99
6.75000	101.75000	5.21	-5.58

Appendix I

Comparison of Geoid Height Differences Between $N_{GPS/Levelling}$ and N_{OSU89B} and $N_{OSU89B-MM}$ for the Southwest Region (In Unit Metres)

GPS Code Station	Latitude °	Longitude °	$N_{GPS/Lev}$ N1	N_{OSU89B} N2	$N_{OSU89B-MM}$ N3	∂N1=N1-N2	∂N2=N1-N3
GP10	2.6824	101.9745	-2.761	0.040	-0.960	-2.801	-1.801
GP11	2.4236	101.8634	-2.498	-0.240	-0.820	-2.258	-1.678
GP12	2.4482	102.0717	-1.453	0.530	-0.020	-1.983	-1.433
GP13	2.4407	102.3393	-0.365	1.490	1.130	-1.855	-1.495
GP14	2.5772	102.5950	0.742	2.290	2.030	-1.548	-1.288
GP15	2.0649	102.5564	0.846	2.850	2.720	-2.004	-1.874
GP16	2.1312	102.7338	1.658	3.560	3.440	-1.902	-1.782
GP34	3.8593	103.3648	1.296	2.830	2.520	-1.534	-1.224
GP35	3.7893	103.2117	0.924	2.480	2.015	-1.556	-1.091
GP36	3.4831	103.1001	1.308	2.760	2.130	-1.452	-0.822
GP37	3.5106	103.4693	2.495	3.900	3.600	-1.405	-1.105
GP38	3.2058	103.4445	2.669	4.460	4.070	-1.791	-1.401
GP39	2.9415	103.4197	2.987	4.870	4.460	-1.883	-1.473
GP40	2.9754	103.1777	1.925	3.950	3.400	-2.025	-1.475
GP41	2.6865	103.3616	3.425	5.100	4.710	-1.675	-1.285
GP42	2.7057	103.5737	4.079	5.870	5.640	-1.791	-1.561
GP43	2.6016	103.7788	5.061	6.910	6.820	-1.849	-1.759
GP47	2.3887	102.9332	2.257	3.930	3.720	-1.673	-1.463
GP48	1.9761	102.9336	2.566	4.680	4.590	-2.114	-2.024
GP49	1.6261	103.1999	4.812	6.294	6.004	-1.482	-1.192
GP50	1.5475	103.3954	5.760	8.041	7.751	-2.281	-1.991
GP51	1.6340	103.6668	6.089	8.170	8.080	-2.081	-1.991
GP53	1.8043	103.8972	6.732	8.840	8.570	-2.108	-1.838
GP54	1.9255	104.0904	7.128	9.410	9.120	-2.282	-1.992

..... Continue

GPS Code Station	Latitude	Longitude	$N_{GPS/Lev}$ N1	N_{OSU89B} N2	$N_{OSU89B-MM}$ N3	∂N1=N1-N2	∂N2=N1-N3
GP55	2.0798	103.8889	6.238	8.300	7.980	-2.062	-1.742
GP56	2.3916	103.8728	5.727	7.710	7.550	-1.983	-1.823
GP58	2.1217	103.4275	4.323	6.300	6.050	-1.977	-1.727
GP59	1.9735	103.2277	3.908	5.790	5.670	-1.882	-1.762
GP60	1.8845	103.3984	4.704	6.610	6.460	-1.906	-1.756
GP61	1.3698	104.2674	8.820	10.692	10.502	-1.872	-1.682
GP84	1.8575	102.9417	2.839	4.930	4.850	-2.091	-2.011
GP85	1.9088	102.7358	1.855	4.120	3.860	-2.265	-2.005
GP91	1.8793	103.6919	5.661	7.840	7.580	-2.179	-1.919
GP94	3.6324	103.3051	1.787	3.110	2.700	-1.323	-0.913
GP98	2.9044	102.8123	1.087	2.640	2.250	-1.553	-1.163

Appendix J

A Summary of Relative Differences Between N_{OSU89B}, $N_{OSU89B\text{-}MM}$ With Respect to $N_{GPS/lev}$ for the Southwest GPS Network

Mean Distance (Km)	No. of Baselines	ΔN_{OSU89B} Mean (in ppm)	$\Delta N_{OSU89B\text{-}MM}$ Mean (in ppm)
18.5	19	5.8	5.5
48.6	58	6.1	6.0
72.0	80	5.0	4.8
95.1	90	3.6	3.3
122.2	108	3.3	3.4
157.9	79	3.0	2.8
181.5	63	2.9	2.6
204.6	49	2.8	2.7
228.0	45	2.9	2.7
255.7	17	2.7	2.6

Appendix K

Comparison of Geoid Height Differences Between $N_{GPS/Levelling}$ and N_{OSU89B} and $N_{OSU89B-MM}$ for the Federal Territory GPS Network

GPS Code Station	Latitude	Longitude	$N_{GPS/Lev}$ N1	N_{OSU89B} N2	$N_{OSU89B-MM}$ N3	∂N1=N1-N2	∂N2=N1-N3
GU02	3 14 30	101 38 55	-4.367	-1.69	-3.70	-2.677	-0.667
GU03	3 14 30	101 40 35	-4.226	-1.56	-3.61	-2.666	-0.616
GU04	3 14 40	101 42 20	-4.016	-1.44	-3.52	-2.576	-0.496
GU05	3 14 40	101 43 40	-4.173	-1.31	-3.45	-2.863	-0.723
GU06	3 14 20	101 45 10	-3.885	-1.25	-3.35	-2.635	-0.535
GU08	3 13 20	101 38 10	-4.279	-1.64	-3.63	-2.639	-0.649
GU09	3 13 25	101 39 20	-4.070	-1.54	-3.56	-2.530	-0.510
GU10	3 13 20	101 40 40	-4.011	-1.46	-3.49	-2.551	-0.521
GU11	3 13 20	101 41 50	-3.949	-1.34	-3.40	-2.609	-0.549
GU12	3 13 20	101 43 30	-3.813	-1.24	-3.32	-2.573	-0.493
GU13	3 13 20	101 45 00	-4.372	-1.76	-3.65	-2.612	-0.722
GU14	3 11 40	101 37 25	-4.247	-1.64	-3.58	-2.607	-0.667
GU16	3 11 55	101 39 05	-4.052	-1.45	-3.44	-2.602	-0.612
GU17	3 12 00	101 43 40	-3.970	-1.31	-3.33	-2.660	-0.640
GU18	3 12 00	101 45 05	-3.793	-1.22	-3.27	-2.573	-0.523
GU19	3 10 15	101 37 00	-4.355	-1.78	-3.61	-2.575	-0.745
GU20	3 10 00	101 39 05	-4.260	-1.62	-3.49	-2.640	-0.770
GU21	3 10 25	101 40 35	-4.155	-1.51	-3.43	-2.645	-0.725
GU22	3 10 15	101 42 15	-4.058	-1.39	-3.33	-2.668	-0.728
GU23	3 10 05	101 43 30	-3.961	-1.30	-3.26	-2.661	-0.701
GU24	3 10 35	101 44 45	-3.868	-1.22	-3.21	-2.648	-0.658
GU26	3 08 30	101 38 55	-4.220	-1.63	-3.43	-2.610	-0.790
GU27	3 08 40	101 40 35	-4.104	-1.49	-3.35	-2.614	-0.754
GU29	3 08 20	101 44 05	-3.849	-1.23	-3.15	-2.619	-0.699
GU30	3 08 45	101 45 20	-3.801	-1.15	-3.09	-2.651	-0.711
GU31	3 07 05	101 37 20	-4.276	-1.71	-3.45	-2.566	-0.826

..... continued

GPS Code Station	Latitude	Longitude	$N_{GPS/Lev}$ N1	N_{OSU89B} N2	$N_{OSU89B-MM}$ N3	∂N1=N1-N2	∂N2=N1-N3
GU32	3 07 05	101 38 40	-4.195	-1.61	-3.38	-2.585	-0.615
GU33	3 07 20	101 40 25	-4.075	-1.48	-3.30	-2.595	-0.775
GU34	3 07 10	101 42 35	-3.953	-1.32	-3.17	-2.633	-0.783
GU35	3 06 50	101 43 40	-3.811	-1.24	-3.10	-2.571	-0.711
GU36	3 06 30	101 44 55	-3.755	-1.15	-3.01	-2.605	-0.745
GU37	3 05 40	101 37 25	-4.195	-1.69	-3.38	-2.505	-0.815
GU38	3 05 40	101 38 55	-4.107	-1.57	-3.30	-2.537	-0.807
GU39	3 05 25	101 41 00	-3.989	-1.41	-3.18	-2.579	-0.809
GU40	3 06 20	101 42 25	-3.912	-1.32	-3.15	-2.592	-0.762
GU41	3 05 50	101 43 40	-3.814	-1.23	-3.05	-2.584	-0.764
GU42	3 05 00	101 45 05	-3.608	-1.12	-2.93	-2.488	-0.678
GU43	3 03 05	101 37 20	-4.103	-1.66	-3.27	-2.443	-0.833
GU44	3 03 40	101 38 55	-4.072	-1.45	-3.21	-2.522	-0.862
GU45	3 04 05	101 40 45	-3.952	-1.41	-3.13	-2.542	-0.822
GU46	3 04 10	101 41 55	-3.897	-1.33	-3.07	-2.567	-0.827
GU47	3 03 55	101 42 50	-3.811	-1.26	-3.01	-2.551	-0.801
GU48	3 03 40	101 44 50	-3.606	-1.11	-2.88	-2.496	-0.726
GU49	3 01 20	101 36 40	-4.070	-1.69	-3.22	-2.380	-0.850
GU52	3 02 00	101 42 25	-3.797	-1.26	-2.94	-2.537	-0.857
GU53	3 02 00	101 43 40	-3.736	-1.17	-2.88	-2.566	-0.856
GU54	3 02 15	101 44 55	-3.643	-1.09	-2.81	-2.553	-0.833
GK02	3 05 45	101 38 20	-4.148	-1.62	-3.34	-2.528	-0.808
GK03	3 07 50	101 42 25	-3.978	-1.34	-3.22	-2.638	-0.758
GK04	3 10 25	101 41 35	-4.154	-1.44	-3.38	-2.714	-0.774
GK05	3 08 25	101 37 20	-4.317	-1.73	-3.51	-2.587	-0.807

Appendix L

A Summary of relative differences between N_{OSU89B}, $N_{OSU89B-MM}$ with respect to $N_{GPS/lev}$ for the Federal Territory GPS Network

Mean Distance (Km)	No. of Baselines	ΔN_{OSU89B} Mean (in ppm)	$\Delta N_{OSU89B-MM}$ Mean (in ppm)
1.8	38	20.3	18.7
2.4	142	14.1	13.9
6.6	201	11.8	10.8
8.5	214	10.3	10.2
11.6	204	10.1	9.6
13.7	185	10.3	9.5
16.8	144	10.1	9.7
18.7	80	10.3	9.8
21.1	49	10.0	9.7
23.6	24	9.8	9.5
26.7	7	9.7	9.4
28.4	2	9.6	9.3

Appendix M

A Standard Input Format and Output of the Program TC1

```
INPUT FILE NAMES: (STATFILE/DTM1/DTM2/REFDTM/OUTFILE)
tc.north
dtmn.30s
dtm2.n
dtmn.ref
rtm.n
INPUT: ITYPE        (1 DG, 2 DEFL, 3 HA, 4 G+DEFL, 5 FA, 6 ALL
                     7 TZZ, 8 TXX TYY TZZ, 9 ALL GRAD)
       IKIND        (1 TOPP, 2 ISO, 3 T.C., 4 RTM)
       IZCODE       (0 CHG SH, 1 CHG TER, 2 FREE, 3 FREE+NOSP)
       IGTYP1        (1 STD, 2 RC8000, 3 NGS), DENSITY
       FI1, FI2, LA1, LA2   (MAX LIMITS, DEG)
       R1, R2 (KM=0, R2=0: NO GRID2)
5 4 1 1 2.67
4.06667 4.875 100.96667 101.76667
5 55
INPUT: N (>0: NO. OF PTS, 0: GRID, -1: ALL, -2: ALL (STAT  UTM)
-1
===== TC TERRAIN EFFECT COMPUTATION =====

- INPUT CODES: 5 4 1 1
 MAXAREA:  4.07   4.88   100.97    101.77
.COMPUTATION RADII:    5.0     55.0 KM
- STATIONS: 640, IN AREA:   4.0670  4.8750  100.9667 101.7667

DETAILED ELEVATION GRID:

--- GRIDLAB 4.0667  4.8750  100.9667  101.7667  0.0083  0.0083 98  97
--- SELECTED        4.0667  4.8750  100.9667  101.7667  0.0083  0.0083
POINTS: 98 x 97 = 9506, ZERO VALUES:  0, MISSING/9999:  0
HMIN  HMAX  MEAN STD.DEV:  3  2060  543.49  487.92
CORNER VALUES:  65  989  7  741

OUTER ZONE ELEVATION GRID:

--- GRIDLAB 4.0667  4.8750  100.9667  101.7667  0.0417  0.0417 19  19
--- SELECTED        4.0667  4.8750  100.9667  101.7667  0.0083  0.0083
POINTS: 19 x 19 = 361, ZERO VALUES:   0, MISSING/9999:  0
HMIN  HMAX  MEAN STD.DEV:  5  1664  508.89  461.08

REFERENCE ELEVATION GRID:

--- GRIDLAB         4.0667  4.8750  100.9667  101.7667  0.1667  0.1667 5  5
--- SELECTED        4.0667  4.8750  100.9667  101.7667  0.0083  0.0083
POINTS: 5 x 5 = 25, ZERO VALUES:       0, MISSING/9999:  0
HMIN  HMAX  MEAN STD.DEV:  96  656  558.68  241.73

======== RESULTS ========

STAT    FI       LA        H  DTMELV  DG/ANOM KSI     ETA     HA
972     4.0667  101.1468   6.9  11.0      -41.59648  0.0000 0.0000 -0.47339
974     4.0682  101.1948   16.1  16.0      -44.67244  0.0000 0.0000 -0.40922
....    .....   .....      ...   ...       .....      .....  .....  .....
```

A Sample of the Input and the Output of the Program EMPCOV

```
EMPIRICAL COVARIANCE FUNCTIONS, VERS.FEB 1991

INPUT TEXT DESCRIBING DATA (MAX 60 CHAR):
Area C - Case I
INPUT : SAMPLING INTERVAL (MINUTES(, NUMBER OF INTERVALS
TABLE OUTPUT TO SEPARATE FILE (T/F), MEAN VALUE SUBTRACTION (T/F)

6 25 1 f f f

INPUT: MAX NUMBER OF VALUES, INPUT MODE (WHERE 9 IS FREE FORMAT)
LATITUDE FIRST IN RECORD (T/F), ANGULAR TYPE: 1, DDMMSS.S
2: DDMM.M, 3: DD.D, OBSERVATION TYPE 1 (INTEGER) AND
TYPE 2 (INTEGER, 0 IF NOT PRESENT), SCALE OF HISTOGRAM
AND DATA TO BE SELECTED WITHIN GIVEN AREA (T/F)

300 9 t 3 3 0 10 f

INPUT NUMBER OF DATA AND DATA ELEMENT USED
1 1 0

INPUT NAME OF FILE HOLDING DATA
gresmm.south
LAST DATA FILE (T/F)?
t
244 VALUES INPUT FROM FILE
NUMBER OF OBS 3 =  244 MEAN = -2.44
HISTOGRAM, USING BIN SIZE=  10.0

      0 0  0 0 0 0 0 0 0 0 1  16 213 14 0 0 0  0 0 0 0 0 0 0 0
OUT -10 -9 -8 -7 -6 -5 -4 -3 -2 -1 0  1  2  3  4  5  6  7  8  9 10  OUT
```

PSI 0 M	COVA(3,3) (UNIT)**2	PROD. NUMB	STDV. OF COV. (UNIT)**2
0 0.00	52.90	587	3.9
0 6.00	42.97	2605	1.4
0 12.00	31.28	4196	1.0
0 18.00	19.47	5160	0.9
0 24.00	13.52	4954	0.8
0 30.00	11.06	4345	0.8
0 36.00	4.45	3270	0.9
0 42.00	4.70	2132	0.9
0 48.00	1.91	1317	0.9
0 54.00	1.05	733	0.9
1 00.00	-1.21	358	0.9
1 06.00	-1.14	165	1.0
1 12.00	0.70	69	1.8
1 18.00	2.00	31	2.5
1 24.00	-1.03	18	4.7
1 30.00	1.86	6	6.3

Appendix O

A Sample of the Input and the Output of the Program COVFIT

```
INTERACTIVE INPUT? (T/F)
t
INPUT MODE, TEST?, LEGENDRE SUM?, LAST?, OUTPUT TABLE? (T/F)
1 f f f f
COMPUTATION MODE= 1
INPUT TYPE OF COV.FCT.MODEL (1,2,3)
2
INPUT INTEGER(S) IN NUMERATOR
24
THE MODEL ANOMALY DEGREE-VARIANCES ARE EQUAL TO
      /((I-2)*(I+24))
INPUT -DEPTH TO BJ.SPH.(KM), GRAVITY VARIANCE, MAX DEG
ZERO DEGREE-VAR.?MODEL DEGVA?, TABLE ?(T/F)
-3.55 52.9 105 t f f
105 DEGREE-VARIANCES EQUAL TO ZERO
RATIO R/RE                                  =   0.999443
DEPTH TO BJERHAMMER SPHERE(R-RE)            =   -3.55 KM
THE FACTOR A, DIVIDED BY RE**2 IS           =   33.72 MGAL*2
INPUT NCOV, INTERVAL (MINU), AZIMUTH (DD MM SS.S) AND LAST?
20 6 0 0 0 t
3 TIMES (SOME MAY BE DUMMY): TYPE1,TYPE2
HEIGH1,HEIGHT2, LAST (T/F), WITH TYPE=1....25, HEIGHT IN KM
NEGATIVE TYPE, INDICATES USE OF ROTATED SYSTEM
1 1 0 0 f
3 1 0 0 f
3 3 0 0 t
TABLE OF COVARIANCES:
BETWEEN QUANTITIES OF KIND KP AND KQ, EVALUATED IN P,Q,
HAVING SPHERICAL DISTANCE PSI, HEIGHTS HP,HQ
AND AN AZIMUTH OF      0D  0M  0.00SEC FROM P TO Q
        KP=   1       1       3
        KQ=   1       3       3
        HP=     0.0     0.0     0.0
        HQ=     0.0     0.0     0.0
PSI
0   0.00        0.04451         1.28388         52.90000
0   6.00        0.04440         1.20995         41.94209
0  12.00        0.04152         1.06109         31.55517
0  18.00        0.03753         0.89657         23.01346
0  24.00        0.03289         0.73536         16.60759
0  30.00        0.02794         0.58451         11.38484
0  36.00        0.02292         0.44694          7.23686
0  42.00        0.01801         0.32383          4.80328
0  48.00        0.01335         0.21549          2.40919
0  54.00        0.00902         0.12173          0.53081
1  00.00        0.00509         0.04220         -0.92354
1  06.00        0.00162        -0.02421         -2.16458
1  12.00       -0.00138        -0.07789         -2.82881
1  18.00       -0.00390        -0.11988         -0.68272
1  24.00       -0.00593        -0.15116          1.72552
1  30.00       -0.00750        -0.17273          5.89098
```

Appendix P

A Sample of the Input and the Output of the Program GEOCOL

```
GEODETIC COLLOCATION, VERSION I FEB 1994, RELEASE 3 (UNIX)

NOTE THAT THE FUNCTIONALS ARE IN SPHERICAL APPROXIMATION
MEAN RADIUS=RE=6371 KM AND MEAN GRAVITY 981 KGAL USED.
MAX NUMBER OF OBS= 5600, MAX NUMBER OF PARAMETERS=239
MAX NUMBER OF OBS IN GIVEN REF.FRAME=3200
SIZE OF NORMAL EQ.BLOCKS=79600, SIZE OF POT.COFF.BLOCK= 130322
INTERACTIVE INPUT (T/F)
t
INPUT:LTRAN,TRUE IF NON-STANDARD REF.SYSTEM IS USED
      LPOT, TRUE IF SPHERICAL HARMONIC EXPANSION IS USED
      LTEST, TRUE IF TEST-OUTPUT IS NEEDED
      LLEG, TRUE IF LEGEND IS TO BE OUTPUT
      LPARAM, TRUE IS PARAMETERS ARE TO BE DETERMINED
      LNCOL, TRUE IF COLLOCATION IS NOT USED
      LIOSOL, TRUE IF SOLUTION IS STORED OR RECOVERED
f f t f f f t

INPUT:LWRSOL, TRUE IF SOLUTION IS OUTPUT ON UNIT 17 LPIPOT,LBICOV,
LB1SOL, TRUE IF POTENTIAL COEFF.
      COVARIANCE FCT.TABLE OR SOLUTION IS OUTPUT BINARY
      LIOSOL, TRUE IF BINARY SOLUTION IS USED
t f f f f

NAME OF RESTART FILE=restart.south

INPUT NAME OF FILE WITH NORMAL EQ.

noreq.south

NAME OF FILE HOLDING NORMAL EQUATIONS=nores.south

INPUT:LONEQ,TRUE IF COEFFICIENTS ARE OUTPUT
      LTIME: TRUE, IF TIMING IS MADE (ONLY UNIX)
      LTCOV:TRUE, IF OUTPUT FROM COV.CALCULATION
f t f

ARE ALL PARAMETERS OK?

t

INPUT CODE FOR BASIC REFERENCE SYSTEM:
0:USER DEFINED, 1:ED50 NORTH SEA, 2: ED50/EDDC,
3:NAD1927 /NEW MEXICO, 4: GS67, 5: GRS80, 6: NWL9D
7:BEST CURRENT, 8:BEST CURR. FAROE ISL, 9:ED50 FOR SF
10: IAG-75, 11=KRASSOWSKY, DDR, 12: GERMAN DHDN, BESS.
5
REFERENCE SYSTEM:
            GRS1980

A     = 6378137.00 M
```

..... continued

```
1/F     = 298.2572221
GM     =0.3986005000E+15
REF.GRAVITY AT EQUATOR = 978032.6772 MGAL
POTENTIAL AT REF.ELL = 62636860.8500 M**2/SEC**2
STARTT OF COLLOCATION I:
INPUT DEGREE-VARIANCE MODEL NO: (1,2,3)
2
INPUT NOMINATOR(S) MODEL
24
THE MODEL DEGREE-VARIANCES AREEE EQUAL TO
A*(I-1)
+       /((1-2)*(1+24)).

INPUT PARAMETER DESCRIBING COV.FCT.
 R - NEG. DEPTH TO BJ.SPHERE IN KM OR RATIO RB/RE
GRAVITY ANOMALY VARIANCE IN MGAL**2
MAX.DEGREE OF LEGENDRE FCT. EXPANSION
LZERO - TRUE IF FIRST COEFF. ALL ARE ZERO
LTABLE - TRUE IF COV. FCT. IS TABULATED IN 2D
LMODEL - TRUE IF DEGREE-VAR FROM PREDEFINED MODEL
LTABH - TRUE IF 1D TABULATION
-3.55 52.9 105 t f f f

105 DEGREE VARIANCES EQUAL TO ZERO
RATION R/RE                =        0.999443
DEPTH OF BJERHAMMER SPHERE (R-RE)     =  -3550.0 M
VARIANCE OF POINT GRAVITY ANOMALIES   =    52.90 MGAL**2
THE FACTOR A, DIVIDED BY RE**2 IS     =    31.94 MGALS**2
ARE ALL PARAMETERS OK?
t
OBSERVATIONS:

INPUT DATA LINE AND OUTPUT SPECIFICATIONS
POSITION OF STATION NUMBER (0:NO NUMBER, -1: NO OUTPUT U6)
POSITION LATITUDE AND LONGITUDE (E.G. 2, 3)
TYPE OF ANGULAR UNITS USED (1: DD MM SS.S, 2: DD MM.M, 3: DD.D)
POSITION OF HEIGHT (0: NO HEIGHT)
POSITION OF OBSERVATION 1 AND 2 (0 IF NO OBS. 1 OR 2)
DATA OR COMPUTATION QUANTITY TYPE CODE (11:GEOID,
  13 : GRAVITY, 15: TZZ, 26: (KSI,ETA), NEGATIVE: REF.SUBTR.)
COORD.SYST.CODE, - INDICATE GLOBAL SYSTEM, +100 REVERSE TR.
HEIGHT (IN M OR KM), ONLY USED IF NO INPUT HEIGHT
LPUNCH - TRUE IF OUTPUT OF RESULT TO FILE
LWLONG - TRUE IF LONGITUDE POSITIVE EAST
LMEAN - TRUE OBS. OR COMPUTED QUANTITY IS A MEAN VALUE
LSA - TRUE IF ALL ERROR ESTIMATES ARE IDENTICAL
LKM - TRUE IF HEIGHT IN KM
LADMU - TRUE IF UNREDUCED OR CONSTANTS * OR +
STAT - TRUE IF STATISTICS OF RESULT  WANTED
LAREA - TRUE IF DATA ONLY INSIDE SPECIFIC AREA, ARE USED
LFORM - TRUE IF FORMAT OF DATA IS INPUT
LIN4 - TRUE IF DATA NOT IN INPUT STREAM (FROM FILE)
```

..... continued

```
1 2 3 3 4 5 0 -1 0.00 f f f t f f t f f t
INPUT NAME OF FILE HOLDING DATA
gresmm.south
INPUT FORTRAN UNIT NUMBER
25
DATA INPUT FROM UNIT 25, FILE=gresmm.south
INPUT SAMPLING INTERVAL SIZE
0
INPUT COMMON STANDARD DEVIATION OF OBSERVATIONS
0.2
ALL SPECIFICATIONS OK?
t

SELECTED GEOCENTRIC SYSTEM USED.
0 NO  LATITUDE   LONGITUDE        H       DELTA G(MGAL)
      DEGREES    DEGREES          M
                                STD.DEV. = 7.27
                              OBS.     ERR
    1  1.23       103.00                      0.20
    ..  ..        ..          ..          ..     ..
    ..  ..        ..          ..          ..     ..
   ......(depending on the number of observations used)
-1
INPUT LSTOP, LRESOL_READ SOLUTION
t f
DATA TYPE= 13
NUMBER:    3
SOLUTIONS TO NORMAL EQUATIONS:
-0.109802431E+02  0.685208684E+01  0.184829939E+02  -0.459584049E+01
...               ...              ...              ...
...               ...              ...              ...
...               ...              ...              ...
...               ...              ...              ...
...               ...              ...              -0.111796505E+01

NUMBER OF EQUATIONS =  244
NORMALIZED SQUARE-SUM OF OBSEVATIONS       = 0.281467E+03
NORMALIZED DIFFERENCE BETWEEN SQUARE-SUM OF
OBSERVATIONS AND NORM OF APPROXIMATION    = -0.548033E+04

INPUT LCREF, TRUE IF ANOTHER COLLOCATION SOLUTION IS NEEDED
      LNEWDA, TRUE IF PARAMETERS ARE TO BE DETERMINED
PREDICTION:
f f f
```

..... continued

INPUT: LGRID - TRUE IF COMPUTATIONS IN A GRID
LERR - TRUE IF ERROR ESTIMATES ARE TO BE COMPUTED
OR REPRODUCED IN OUTPUT
LCOMP - TRUE IF COMPUTED VALUES ARE SUBTACTED FROM OBSERVED
INPUT GRID SPECIFICATION

MIN, MAX LATITUDE, MIN, MAX LONGITUDE, STEP IN LAT AND LONG
FUNCTIONAL TYPE (CODE), NEG. VALUE THEN SPH.EXP.SUBTRACTED
COORD.SYSTEM CODE (-1 THEN GLOBAL SYSTEM)
HEIGHT OF GRID POINTS (M)
LMAP - PRIMITIVE MAP OUTPUT
LPUNCH - OUTPUT TO UNIT 17
LMEAN - MEAN VALUES OUTPUT

t t f

1.25 1.81667 103.25 104.2830000 0.0833 0.0833

11 -1 0.0 f t f

INPUT NAME OF FILE TO HOLD RESULT

nreslscmm.sgrid

SIMULTANEOUS OUTPUT TO FILE: nreslscmm.sgrid

ALL SPECIFICATIONS OK?

t

						PRED
0	NO	LATITUDE	LONGITUDE	H	ERR	ZETA(M)
+	1	1.816670	103.250000	0.00	0.11	0.02
+	2	1.816670	103.333300	0.00	0.09	0.03
..	..	.....	.....	.....	.....	.....
..	..	.....	.....	.....	.....	.....
..	..	.....	.....	.....	.....	.....
+	104	1.25000	104.243300	0.00	0.10	-0.09

Stop ?

t

Appendix Q

A standard input and output file for the program GEOFOUR

```
*********************************************************
*       GEOFOUR - gravity field modelling by FFT - RF/KMS       *
*********************************************************
grdrtmm.n2     !       input gridded anomalies
dummy          !       dummy file (not used)
nresrtmm.fftn2!        output file for geoid height
1 0.0          !       Code for geoid height estimation
0 0 50 50 0    !       Zero padding
mode: 1
wanted sw corner:     0.0000          0.0000, points: 50      50, iwindow=0
Stokes formula - gravity (mgal) to geoid (metre)
data grid
gridlab:          4.0667  4.8750  100.9667  101.7667 0.0333 0.0333  25  25
selected: sw corner     4.0667          100.9667        50  50 . 2500
statistics of data selected from input grid:
pts  mean  std.dev.  min  max          625     -0.50   45.64  -125.90   107.50
zero padding done on grid, no of ows/cols/ S/N/E/W: 0  25  0  25
power space domain   519.90, mean -0.13
mean value subtracted from input data prior to fft
power freq. domain   519.88
min  and  max  computed values:  -1.25  0.98
```

Appendix R(i)

The LSC Residual Geoid Heights for Area A - Case I

ϕ_1	ϕ_2	λ_1	λ_1	$\Delta\phi$	$\Delta\lambda$
4.066670	4.875000	100.966670	101.766670	0.033330	0.033330

-0.01	0.00	0.01	0.01	0.02	0.01	-0.01	-0.04	-0.07
-0.11	-0.10	-0.06	-0.02	0.03	0.09	0.15	0.21	0.27
0.33	0.39	0.43	0.46	0.47	0.46	0.40		
0.00	0.02	0.03	0.03	0.03	0.02	0.00	-0.04	-0.07
-0.12	-0.11	-0.07	-0.02	0.03	0.10	0.18	0.26	0.33
0.40	0.47	0.52	0.55	0.57	0.55	0.48		
0.01	0.03	0.03	0.04	0.03	0.02	-0.01	-0.04	-0.08
-0.13	-0.12	-0.08	-0.02	0.04	0.11	0.19	0.28	0.36
0.44	0.51	0.56	0.60	0.62	0.60	0.52		
0.01	0.03	0.03	0.03	0.02	0.01	-0.01	-0.05	-0.08
-0.13	-0.12	-0.08	-0.02	0.04	0.12	0.20	0.29	0.38
0.46	0.53	0.59	0.63	0.64	0.63	0.54		
0.01	0.03	0.03	0.03	0.02	0.00	-0.02	-0.05	-0.09
-0.13	-0.12	-0.08	-0.02	0.04	0.12	0.21	0.30	0.38
0.47	0.54	0.60	0.64	0.66	0.64	0.56		
0.01	0.04	0.04	0.03	0.02	0.00	-0.02	-0.05	-0.09
-0.14	-0.13	-0.08	-0.03	0.04	0.12	0.21	0.29	0.38
0.47	0.54	0.60	0.64	0.66	0.64	0.56		
0.01	0.03	0.04	0.03	0.02	0.00	-0.03	-0.06	-0.09
-0.14	-0.13	-0.09	-0.03	0.03	0.12	0.20	0.29	0.38
0.46	0.54	0.59	0.64	0.65	0.63	0.55		
0.02	0.03	0.04	0.04	0.03	0.00	-0.02	-0.05	-0.09
-0.14	-0.13	-0.09	-0.03	0.03	0.11	0.20	0.28	0.37
0.45	0.52	0.58	0.62	0.64	0.62	0.54		
0.02	0.04	0.05	0.05	0.03	0.01	-0.02	-0.05	-0.08
-0.13	-0.12	-0.08	-0.03	0.03	0.11	0.19	0.28	0.36
0.44	0.51	0.57	0.61	0.62	0.61	0.53		
0.02	0.04	0.05	0.06	0.04	0.01	-0.01	-0.05	-0.08
-0.13	-0.12	-0.08	-0.03	0.03	0.11	0.19	0.27	0.35
0.43	0.49	0.55	0.59	0.60	0.59	0.52		
0.03	0.05	0.06	0.07	0.05	0.02	0.00	-0.04	-0.07
-0.12	-0.11	-0.08	-0.02	0.03	0.10	0.18	0.26	0.34
0.41	0.48	0.53	0.56	0.58	0.56	0.50		
0.03	0.06	0.07	0.07	0.06	0.03	0.00	-0.03	-0.06
-0.11	-0.10	-0.07	-0.02	0.03	0.10	0.17	0.25	0.32
0.39	0.46	0.51	0.54	0.55	0.54	0.47		
0.04	0.07	0.07	0.07	0.05	0.03	0.00	-0.02	-0.06
-0.10	-0.10	-0.06	-0.02	0.03	0.10	0.17	0.24	0.31
0.38	0.44	0.48	0.52	0.53	0.51	0.45		

..... continued

0.04	0.07	0.07	0.07	0.06	0.03	0.01	-0.02	-0.05
-0.09	-0.09	-0.05	-0.01	0.04	0.10	0.16	0.23	0.30
0.36	0.42	0.46	0.49	0.50	0.49	0.43		
0.04	0.06	0.07	0.06	0.05	0.03	0.01	-0.02	-0.05
-0.08	-0.08	-0.05	0.00	0.04	0.10	0.16	0.22	0.29
0.34	0.40	0.44	0.47	0.48	0.46	0.40		
0.04	0.05	0.06	0.06	0.04	0.03	0.00	-0.02	-0.05
-0.07	-0.06	-0.04	0.00	0.04	0.10	0.16	0.22	0.27
0.33	0.38	0.41	0.44	0.45	0.43	0.38		
0.02	0.04	0.05	0.05	0.05	0.01	-0.01	-0.03	-0.05
-0.07	-0.05	-0.03	0.00	0.05	0.10	0.15	0.21	0.26
0.31	0.35	0.39	0.41	0.42	0.41	0.35		
0.01	0.03	0.04	0.03	0.02	0.00	-0.02	-0.03	-0.05
-0.06	-0.04	-0.02	0.01	0.05	0.10	0.15	0.20	0.25
0.29	0.33	0.37	0.39	0.39	0.38	0.33		
0.01	0.03	0.03	0.02	0.01	-0.01	-0.03	-0.05	-0.05
-0.05	-0.03	-0.01	0.02	0.06	0.10	0.15	0.19	0.24
0.28	0.31	0.34	0.36	0.36	0.35	0.30		
0.00	0.02	0.02	0.01	0.00	-0.01	-0.04	-0.05	-0.06
-0.04	-0.02	0.00	0.02	0.06	0.10	0.14	0.18	0.22
0.26	0.29	0.31	0.33	0.33	0.32	0.27		
0.00	0.01	0.00	0.00	0.00	-0.02	-0.03	-0.05	-0.05
-0.03	-0.01	0.00	0.03	0.06	0.10	0.14	0.17	0.21
0.24	0.27	0.29	0.30	0.30	0.29	0.25		
0.00	0.00	0.00	0.00	-0.01	-0.02	-0.03	-0.04	-0.04
-0.02	-0.01	0.01	0.03	0.06	0.10	0.13	0.16	0.19
0.22	0.24	0.26	0.27	0.27	0.26	0.22		
-0.02	-0.01	-0.01	-0.01	-0.01	-0.02	-0.03	-0.04	-0.04
-0.02	0.00	0.01	0.04	0.06	0.09	0.12	0.14	0.17
0.19	0.21	0.23	0.24	0.23	0.22	0.19		
-0.03	-0.02	-0.02	-0.01	-0.02	-0.03	-0.03	-0.04	-0.03
-0.01	0.00	0.01	0.03	0.05	0.08	0.10	0.12	0.14
0.16	0.18	0.19	0.20	0.20	0.18	0.15		
-0.04	-0.03	-0.03	-0.03	-0.03	-0.04	-0.04	-0.05	-0.04
-0.02	0.00	0.00	0.02	0.04	0.06	0.07	0.09	0.11
0.12	0.13	0.14	0.15	0.14	0.14	0.11		

The LSC Residual Geoid Heights for Area A - Case II

ϕ_1	ϕ_2	λ_1	λ_1	$\Delta\phi$	$\Delta\lambda$			
4.06667	4.87500	100.96667	101.76667	0.03333	0.03333			
-0.06	-0.06	-0.05	-0.06	-0.11	-0.19	-0.30	-0.38	-0.23
-0.28	-0.34	-0.34	-0.33	-0.30	-0.23	-0.12	-0.06	0.11
0.22	0.32	0.42	0.50	0.51	0.52	0.50		
-0.04	-0.05	-0.06	-0.07	-0.16	-0.21	-0.30	-0.44	-0.58
-0.73	-0.74	-0.70	-0.66	-0.62	-0.59	-0.44	-0.34	-0.12
0.27	0.52	0.61	0.75	0.80	0.79	0.67		
-0.04	-0.03	-0.07	-0.07	-0.19	-0.28	-0.42	-0.44	-0.50
-0.55	-0.63	-0.64	-0.65	-0.51	-0.33	-0.20	-0.12	-0.02
0.26	0.52	0.71	0.81	0.85	0.84	0.76		
-0.04	-0.06	-0.11	-0.15	-0.22	-0.29	-0.41	-0.56	-0.70
-0.85	-1.01	-1.12	-1.09	-0.96	-0.70	-0.44	-0.09	0.07
0.32	0.57	0.76	0.87	0.92	0.92	0.83		
-0.06	-0.08	-0.12	-0.17	-0.24	-0.31	-0.45	-0.60	-0.77
-0.93	-1.10	-1.24	-1.21	-1.05	-0.82	-0.53	-0.13	0.18
0.44	0.65	0.88	0.99	1.01	1.06	0.94		
-0.04	-0.09	-0.11	-0.17	-0.27	-0.36	-0.50	-0.66	-0.84
-1.02	-1.22	-1.29	-1.21	-1.10	-0.82	-0.32	-0.04	0.30
0.59	0.69	0.90	1.01	1.01	0.98	0.91		
-0.06	-0.10	-0.14	-0.18	-0.25	-0.37	-0.47	-0.59	-0.82
-1.00	-1.17	-1.30	-1.26	-1.11	-0.87	-0.64	-0.10	0.12
0.41	0.65	0.88	0.97	1.01	0.99	0.87		
-0.07	-0.10	-0.12	-0.17	-0.26	-0.37	-0.50	-0.65	-0.82
-0.95	-1.10	-1.17	-1.32	-1.20	-0.97	-0.75	-0.55	-0.10
0.21	0.51	0.73	0.89	0.89	1.04	0.89		
-0.06	-0.09	-0.11	-0.16	-0.25	-0.36	-0.50	-0.62	-0.80
-0.95	-1.04	-1.21	-1.31	-1.29	-1.13	-0.95	-0.70	-0.51
-0.17	0.34	0.55	0.71	0.89	0.94	0.85		
-0.06	-0.07	-0.11	-0.17	-0.26	-0.36	-0.46	-0.60	-0.76
-0.89	-1.01	-1.16	-1.30	-1.30	-1.23	-1.07	-0.81	-0.53
-0.09	0.27	0.48	0.63	0.79	0.92	0.83		
-0.05	-0.06	-0.06	-0.14	-0.21	-0.30	-0.44	-0.56	-0.72
-0.90	-1.00	-1.13	-1.31	-1.30	-1.15	-0.78	-0.55	-0.30
-0.05	0.21	0.40	0.54	0.78	0.87	0.80		
-0.05	-0.04	-0.06	-0.15	-0.22	-0.30	-0.42	-0.54	-0.69
-0.82	-1.00	-1.09	-1.29	-1.36	-1.23	-0.97	-0.76	-0.40
0.16	0.32	0.56	0.65	0.78	0.86	0.77		
-0.03	-0.04	-0.06	-0.16	-0.23	-0.30	-0.38	-0.52	-0.63
-0.73	-0.88	-1.03	-1.15	-1.20	-1.11	-0.87	-0.64	-0.33
0.09	0.41	0.65	0.74	0.89	0.88	0.75		

..... continued

-0.03	-0.04	-0.06	-0.15	-0.22	-0.30	-0.34	-0.49	-0.63
-0.74	-0.93	-1.11	-1.19	-1.13	-1.07	-0.87	-0.34	-0.11
0.16	0.42	0.64	0.80	0.79	0.74	0.67		
-0.03	-0.08	-0.14	-0.21	-0.28	-0.36	-0.40	-0.51	-0.61
-0.76	-0.87	-0.94	-0.99	-0.93	-0.80	-0.58	-0.43	-0.24
0.02	0.36	0.68	0.79	0.76	0.70	0.62		
-0.04	-0.09	-0.11	-0.18	-0.18	-0.28	-0.40	-0.48	-0.60
-0.65	-0.83	-0.88	-0.93	-0.99	-0.93	-0.81	-0.57	-0.25
0.10	0.33	0.55	0.75	0.72	0.70	0.58		
-0.07	-0.07	-0.09	-0.12	-0.18	-0.23	-0.30	-0.40	-0.52
-0.57	-0.72	-0.68	-0.83	-0.92	-0.89	-0.72	-0.51	-0.21
0.15	0.43	0.64	0.70	0.67	0.65	0.58		
-0.06	-0.09	-0.11	-0.16	-0.21	-0.22	-0.26	-0.32	-0.37
-0.44	-0.48	-0.53	-0.75	-0.89	-0.85	-0.65	-0.41	-0.09
0.21	0.46	0.62	0.67	0.67	0.65	0.53		
-0.09	-0.07	-0.10	-0.13	-0.18	-0.21	-0.26	-0.28	-0.26
-0.34	-0.34	-0.39	-0.60	-0.68	-0.82	-0.60	-0.38	-0.13
-0.18	0.32	0.57	0.60	0.56	0.50	0.43		
-0.05	-0.07	-0.10	-0.20	-0.24	-0.25	-0.27	-0.24	-0.19
-0.19	-0.24	-0.31	-0.49	-0.68	-0.75	-0.69	-0.46	-0.26
-0.06	0.16	0.44	0.43	0.52	0.52	0.43		
-0.04	-0.07	-0.09	-0.10	-0.12	-0.12	-0.12	-0.04	0.03
0.04	-0.04	-0.19	-0.39	-0.56	-0.63	-0.47	-0.36	-0.20
-0.03	0.28	0.41	0.50	0.47	0.43	0.37		
-0.01	-0.04	-0.07	-0.07	-0.09	-0.11	-0.12	-0.10	0.07
0.06	0.01	0.10	-0.21	-0.38	-0.55	-0.45	-0.40	-0.15
0.09	0.30	0.40	0.41	0.40	0.45	0.32		
-0.04	-0.09	-0.07	-0.06	-0.07	-0.06	-0.05	0.02	0.10
0.17	0.13	0.01	-0.13	-0.36	-0.40	-0.38	-0.35	-0.20
-0.06	0.15	0.29	0.48	0.46	0.43	0.31		
-0.03	-0.03	-0.05	-0.04	-0.08	-0.02	-0.02	0.01	0.12
0.17	0.12	0.01	-0.18	-0.30	-0.29	-0.33	-0.30	-0.22
-0.06	0.12	0.25	0.45	0.36	0.34	0.23		
-0.04	-0.05	-0.04	-0.05	-0.05	-0.07	-0.07	-0.06	-0.05
-0.06	-0.01	-0.07	-0.15	-0.19	-0.24	-0.25	-0.22	-0.17
-0.11	0.12	0.23	0.31	0.33	0.31	0.30		

Appendix S(i)

The Final LSC Geoid Heights for Area A - Case I

ϕ_1	ϕ_2	λ_1	λ_1	$\Delta\phi$	$\Delta\lambda$
4.066670	4.875000	100.966670	101.766670	0.033330	0.033330

-10.40	-10.31	-10.19	-10.07	-9.93	-9.78	-9.63	-9.46	-9.27
-9.08	-8.82	-8.54	-8.21	-7.88	-7.53	-7.18	-6.82	-6.46
-6.11	-5.75	-5.41	-5.11	-4.82	-4.59	-4.41		
-10.31	-10.22	-10.11	-9.99	-9.85	-9.71	-9.57	-9.40	-9.23
-9.03	-8.78	-8.49	-8.16	-7.82	-7.46	-7.10	-6.73	-6.36
-5.99	-5.62	-5.28	-4.96	-4.69	-4.45	-4.28		
-10.24	-10.15	-10.03	-9.92	-9.78	-9.66	-9.51	-9.35	-9.18
-8.99	-8.73	-8.44	-8.12	-7.78	-7.41	-7.03	-6.66	-6.29
-5.91	-5.53	-5.19	-4.87	-4.60	-4.36	-4.20		
-10.15	-10.07	-9.96	-9.84	-9.73	-9.60	-9.46	-9.29	-9.11
-8.94	-8.69	-8.40	-8.07	-7.72	-7.36	-6.98	-6.59	-6.22
-5.84	-5.48	-5.12	-4.81	-4.52	-4.30	-4.13		
-10.07	-9.99	-9.88	-9.78	-9.66	-9.53	-9.39	-9.22	-9.05
-8.88	-8.63	-8.33	-8.02	-7.67	-7.31	-6.93	-6.55	-6.16
-5.79	-5.42	-5.08	-4.76	-4.48	-4.25	-4.09		
-9.99	-9.90	-9.79	-9.69	-9.59	-9.46	-9.33	-9.17	-8.99
-8.82	-8.56	-8.27	-7.96	-7.62	-7.26	-6.89	-6.50	-6.13
-5.74	-5.39	-5.03	-4.72	-4.45	-4.22	-4.07		
-9.89	-9.81	-9.71	-9.61	-9.51	-9.38	-9.25	-9.10	-8.93
-8.75	-8.50	-8.22	-7.90	-7.57	-7.21	-6.84	-6.47	-6.09
-5.71	-5.35	-5.02	-4.71	-4.43	-4.20	-4.05		
-9.80	-9.72	-9.62	-9.52	-9.40	-9.28	-9.16	-9.01	-8.83
-8.67	-8.44	-8.16	-7.84	-7.51	-7.16	-6.80	-6.43	-6.07
-5.70	-5.33	-5.00	-4.70	-4.43	-4.19	-4.05		
-9.70	-9.61	-9.51	-9.42	-9.30	-9.19	-9.06	-8.91	-8.75
-8.59	-8.36	-8.08	-7.77	-7.44	-7.11	-6.75	-6.40	-6.03
-5.69	-5.33	-5.00	-4.71	-4.42	-4.19	-4.03		
-9.58	-9.50	-9.40	-9.30	-9.19	-9.08	-8.96	-8.82	-8.65
-8.50	-8.27	-8.00	-7.70	-7.39	-7.05	-6.71	-6.36	-6.01
-5.66	-5.31	-4.99	-4.70	-4.42	-4.20	-4.04		
-9.47	-9.39	-9.29	-9.18	-9.08	-8.97	-8.86	-8.71	-8.56
-8.39	-8.19	-7.92	-7.63	-7.32	-6.99	-6.66	-6.31	-5.97
-5.63	-5.30	-4.98	-4.70	-4.43	-4.20	-4.06		
-9.35	-9.27	-9.17	-9.07	-8.96	-8.86	-8.73	-8.60	-8.46
-8.30	-8.08	-7.84	-7.55	-7.24	-6.93	-6.60	-6.28	-5.93
-5.59	-5.28	-4.97	-4.70	-4.43	-4.22	-4.06		
-9.23	-9.14	-9.06	-8.95	-8.84	-8.74	-8.62	-8.50	-8.35
-8.21	-7.99	-7.74	-7.46	-7.16	-6.87	-6.55	-6.22	-5.89
-5.57	-5.26	-4.96	-4.68	-4.44	-4.22	-4.08		

..... continued

-9.11	-9.02	-8.92	-8.83	-8.72	-8.61	-8.50	-8.37	-8.24
-8.09	-7.87	-7.64	-7.38	-7.09	-6.79	-6.49	-6.17	-5.86
-5.55	-5.24	-4.95	-4.68	-4.44	-4.24	-4.09		
-8.98	-8.89	-8.80	-8.71	-8.61	-8.49	-8.38	-8.26	-8.12
-7.97	-7.76	-7.53	-7.28	-7.01	-6.72	-6.43	-6.12	-5.83
-5.53	-5.23	-4.95	-4.69	-4.45	-4.24	-4.10		
-8.86	-8.78	-8.68	-8.57	-8.48	-8.38	-8.27	-8.14	-8.00
-7.86	-7.66	-7.43	-7.18	-6.92	-6.64	-6.36	-6.07	-5.79
-5.50	-5.22	-4.94	-4.69	-4.46	-4.26	-4.12		
-8.74	-8.65	-8.56	-8.45	-8.35	-8.26	-8.15	-8.02	-7.89
-7.73	-7.54	-7.32	-7.08	-6.83	-6.57	-6.29	-6.03	-5.74
-5.47	-5.19	-4.94	-4.69	-4.47	-4.28	-4.13		
-8.61	-8.53	-8.44	-8.34	-8.24	-8.15	-8.04	-7.91	-7.77
-7.61	-7.42	-7.21	-6.99	-6.74	-6.49	-6.22	-5.97	-5.70
-5.43	-5.17	-4.93	-4.69	-4.48	-4.30	-4.15		
-8.49	-8.40	-8.32	-8.23	-8.13	-8.03	-7.93	-7.80	-7.66
-7.49	-7.31	-7.10	-6.88	-6.65	-6.40	-6.16	-5.90	-5.65
-5.40	-5.15	-4.93	-4.69	-4.48	-4.31	-4.16		
-8.35	-8.28	-8.19	-8.11	-8.01	-7.91	-7.80	-7.69	-7.54
-7.38	-7.19	-6.99	-6.78	-6.55	-6.32	-6.09	-5.85	-5.61
-5.37	-5.14	-4.91	-4.68	-4.49	-4.32	-4.17		
-8.24	-8.16	-8.07	-7.98	-7.89	-7.78	-7.68	-7.56	-7.41
-7.25	-7.07	-6.87	-6.68	-6.46	-6.26	-6.03	-5.79	-5.57
-5.35	-5.12	-4.90	-4.68	-4.50	-4.33	-4.19		
-8.10	-8.03	-7.95	-7.86	-7.75	-7.66	-7.55	-7.43	-7.29
-7.13	-6.95	-6.77	-6.58	-6.38	-6.17	-5.96	-5.75	-5.53
-5.31	-5.09	-4.89	-4.70	-4.51	-4.34	-4.21		
-7.99	-7.92	-7.83	-7.73	-7.63	-7.54	-7.43	-7.30	-7.17
-7.01	-6.84	-6.67	-6.49	-6.29	-6.10	-5.90	-5.70	-5.50
-5.29	-5.09	-4.89	-4.70	-4.52	-4.35	-4.22		
-7.87	-7.80	-7.71	-7.61	-7.51	-7.41	-7.30	-7.18	-7.05
-6.90	-6.73	-6.57	-6.39	-6.22	-6.03	-5.84	-5.65	-5.46
-5.27	-5.08	-4.89	-4.71	-4.53	-4.37	-4.23		
-7.80	-7.72	-7.63	-7.52	-7.42	-7.33	-7.22	-7.10	-6.97
-6.82	-6.67	-6.50	-6.34	-6.17	-5.99	-5.81	-5.63	-5.46
-5.27	-5.09	-4.90	-4.73	-4.57	-4.41	-4.26		

The Final LSC Geoid Heights for Area A - Case II

ϕ_1	ϕ_2	λ_1	λ_1	$\Delta\phi$	$\Delta\lambda$
4.066670	4.875000	100.966670	101.766670	0.033330	0.033330

-10.42	-10.34	-10.23	-10.14	-10.02	-9.91	-9.82	-9.71	-9.59
-9.45	-9.23	-8.96	-8.65	-8.32	-7.95	-7.55	-7.15	-6.71
-6.26	-5.77	-5.33	-4.96	-4.64	-4.41	-4.25		
-10.37	-10.36	-10.28	-10.25	-10.17	-10.07	-9.97	-9.83	-9.63
-9.42	-9.20	-8.90	-8.56	-8.22	-7.83	-7.41	-6.99	-6.50
-6.08	-5.64	-5.23	-4.86	-4.53	-4.23	-4.08		
-10.36	-10.29	-10.20	-10.17	-10.15	-10.11	-10.00	-9.81	-9.63
-9.41	-9.20	-8.93	-8.58	-8.21	-7.79	-7.39	-6.95	-6.44
-5.96	-5.54	-5.14	-4.77	-4.45	-4.11	-3.98		
-10.31	-10.24	-10.13	-10.04	-10.09	-10.09	-9.98	-9.79	-9.55
-9.39	-9.20	-8.94	-8.60	-8.23	-7.80	-7.39	-6.97	-6.45
-5.92	-5.53	-5.06	-4.70	-4.34	-4.07	-3.89		
-10.30	-10.18	-10.05	-9.98	-10.04	-10.05	-9.95	-9.78	-9.56
-9.39	-9.19	-8.92	-8.58	-8.19	-7.77	-7.34	-6.88	-6.40
-5.96	-5.48	-5.03	-4.65	-4.34	-4.03	-3.85		
-10.16	-10.07	-9.98	-9.98	-10.03	-10.01	-9.93	-9.81	-9.62
-9.37	-9.18	-8.88	-8.54	-8.23	-7.80	-7.38	-6.89	-6.39
-5.91	-5.46	-5.01	-4.62	-4.30	-4.06	-3.84		
-10.09	-10.00	-9.95	-9.96	-9.98	-9.94	-9.87	-9.73	-9.59
-9.37	-9.15	-8.86	-8.55	-8.20	-7.80	-7.38	-6.88	-6.37
-5.91	-5.45	-5.02	-4.66	-4.32	-4.07	-3.85		
-9.93	-9.91	-9.89	-9.91	-9.88	-9.83	-9.76	-9.62	-9.42
-9.23	-9.09	-8.84	-8.56	-8.16	-7.78	-7.35	-6.88	-6.36
-5.87	-5.42	-5.03	-4.64	-4.31	-4.06	-3.86		
-9.79	-9.79	-9.80	-9.82	-9.79	-9.74	-9.65	-9.52	-9.33
-9.19	-9.02	-8.79	-8.52	-8.18	-7.79	-7.37	-6.89	-6.43
-5.89	-5.44	-5.07	-4.67	-4.31	-4.05	-3.86		
-9.71	-9.72	-9.73	-9.72	-9.67	-9.61	-9.54	-9.43	-9.25
-9.06	-8.89	-8.64	-8.42	-8.13	-7.82	-7.39	-6.93	-6.43
-5.91	-5.49	-5.07	-4.71	-4.36	-4.06	-3.87		
-9.68	-9.64	-9.65	-9.59	-9.55	-9.49	-9.44	-9.31	-9.12
-8.98	-8.81	-8.61	-8.38	-8.06	-7.72	-7.29	-6.87	-6.42
-5.96	-5.51	-5.08	-4.73	-4.37	-4.11	-3.89		
-9.55	-9.54	-9.52	-9.48	-9.42	-9.37	-9.30	-9.19	-9.05
-8.88	-8.75	-8.50	-8.27	-7.97	-7.64	-7.26	-6.81	-6.35
-5.89	-5.53	-5.06	-4.74	-4.37	-4.09	-3.87		

..... continued

-9.41	-9.40	-9.41	-9.35	-9.30	-9.26	-9.17	-9.09	-8.98
-8.77	-8.57	-8.41	-8.17	-7.89	-7.58	-7.17	-6.76	-6.30
-5.87	-5.47	-5.04	-4.68	-4.35	-4.06	-3.86		
-9.27	-9.27	-9.26	-9.23	-9.16	-9.10	-9.01	-8.93	-8.79
-8.57	-8.37	-8.26	-8.03	-7.78	-7.49	-7.13	-6.69	-6.23
-5.81	-5.44	-5.03	-4.64	-4.33	-4.06	-3.84		
-9.16	-9.15	-9.13	-9.09	-9.03	-8.95	-8.84	-8.75	-8.64
-8.43	-8.22	-8.06	-7.93	-7.67	-7.36	-7.04	-6.60	-6.22
-5.78	-5.39	-4.98	-4.64	-4.32	-4.05	-3.84		
-9.07	-9.03	-8.99	-8.93	-8.87	-8.78	-8.63	-8.43	-8.41
-8.24	-8.10	-7.90	-7.74	-7.53	-7.20	-6.87	-6.53	-6.12
-5.69	-5.32	-4.97	-4.61	-4.31	-4.04	-3.84		
-8.93	-8.89	-8.85	-8.78	-8.70	-8.63	-8.42	-8.19	-8.20
-8.11	-7.92	-7.73	-7.59	-7.34	-7.10	-6.79	-6.49	-6.12
-5.69	-5.33	-4.94	-4.63	-4.32	-4.06	-3.85		
-8.79	-8.76	-8.72	-8.65	-8.57	-8.49	-8.33	-8.12	-8.09
-7.93	-7.78	-7.58	-7.47	-7.25	-6.98	-6.67	-6.41	-6.09
-5.67	-5.28	-4.92	-4.61	-4.34	-4.07	-3.86		
-8.64	-8.61	-8.59	-8.52	-8.43	-8.35	-8.23	-8.08	-7.97
-7.78	-7.63	-7.45	-7.30	-7.06	-6.81	-6.58	-6.33	-6.05
-5.63	-5.24	-4.94	-4.61	-4.35	-4.10	-3.88		
-8.49	-8.47	-8.43	-8.38	-8.29	-8.20	-8.09	-7.97	-7.82
-7.57	-7.39	-7.27	-7.13	-6.93	-6.67	-6.39	-6.20	-5.93
-5.59	-5.24	-4.90	-4.63	-4.36	-4.09	-3.89		
-8.38	-8.34	-8.30	-8.22	-8.14	-8.03	-7.93	-7.80	-7.62
-7.36	-7.21	-7.09	-6.97	-6.77	-6.54	-6.33	-6.11	-5.85
-5.56	-5.18	-4.90	-4.63	-4.37	-4.12	-3.92		
-8.20	-8.19	-8.16	-8.08	-7.98	-7.88	-7.77	-7.64	-7.45
-7.20	-7.03	-6.90	-6.77	-6.60	-6.43	-6.21	-6.06	-5.76
-5.46	-5.14	-4.88	-4.64	-4.38	-4.15	-3.95		
-8.09	-8.06	-8.01	-7.91	-7.82	-7.74	-7.62	-7.48	-7.29
-7.04	-6.86	-6.74	-6.61	-6.43	-6.33	-6.14	-5.95	-5.71
-5.43	-5.18	-4.91	-4.65	-4.41	-4.16	-3.98		
-7.96	-7.90	-7.83	-7.73	-7.64	-7.54	-7.43	-7.28	-7.10
-6.85	-6.69	-6.57	-6.44	-6.35	-6.16	-6.05	-5.89	-5.64
-5.44	-5.18	-4.94	-4.64	-4.41	-4.21	-4.02		
-7.78	-7.71	-7.62	-7.52	-7.41	-7.32	-7.19	-7.06	-6.90
-6.70	-6.55	-6.44	-6.36	-6.29	-6.16	-6.03	-5.89	-5.71
-5.49	-5.24	-4.94	-4.66	-4.43	-4.24	-4.10		

Appendix T(i)

The LSC Residual Geoid Heights for Area B - Case I

ϕ_1	ϕ_2	λ_1	λ_1	$\Delta\phi$	$\Delta\lambda$
2.550000	3.633330	101.616670	102.433330	0.050000	0.050000

-0.05	-0.05	-0.05	-0.03	-0.01	0.01	0.01	0.01	0.01
0.02	0.02	0.02	0.02	0.02	0.03	0.04	0.03	
-0.05	-0.06	-0.05	-0.04	0.01	0.02	0.02	0.02	0.02
0.02	0.02	0.02	0.03	0.03	0.04	0.05	0.05	
-0.06	-0.06	-0.04	-0.02	-0.02	0.01	0.01	0.02	0.02
0.03	0.03	0.02	0.02	0.03	0.05	0.05	0.05	
-0.07	-0.07	-0.06	-0.03	0.02	0.01	0.00	0.02	0.03
0.03	0.04	0.04	0.04	0.05	0.05	0.06	0.05	
-0.06	-0.06	-0.04	-0.02	-0.01	0.01	0.00	0.02	0.03
0.04	0.05	0.05	0.06	0.06	0.07	0.07	0.06	
-0.07	-0.04	-0.03	0.00	0.01	0.01	0.02	0.02	0.04
0.06	0.07	0.08	0.08	0.08	0.08	0.08	0.07	
-0.07	-0.06	-0.03	0.02	0.06	0.01	0.00	0.03	0.05
0.08	0.09	0.10	0.11	0.10	0.10	0.10	0.08	
-0.07	-0.08	-0.06	-0.02	0.00	0.00	0.02	0.04	0.07
0.10	0.12	0.14	0.15	0.12	0.11	0.11	0.09	
-0.09	-0.10	-0.09	-0.05	-0.01	0.00	0.02	0.05	0.08
0.11	0.14	0.16	0.16	0.12	0.11	0.11	0.08	
-0.10	-0.12	-0.11	-0.07	-0.01	0.01	0.03	0.06	0.09
0.12	0.15	0.16	0.16	0.12	0.10	0.10	0.08	
-0.10	-0.12	-0.12	-0.08	-0.01	0.02	0.04	0.07	0.09
0.12	0.15	0.16	0.16	0.13	0.10	0.09	0.08	
-0.10	-0.12	-0.11	-0.07	0.00	0.03	0.05	0.07	0.10
0.13	0.15	0.16	0.16	0.13	0.10	0.09	0.08	
-0.09	-0.10	-0.09	-0.05	0.00	0.03	0.05	0.07	0.10
0.12	0.14	0.16	0.16	0.13	0.10	0.09	0.07	
-0.07	-0.08	-0.07	-0.05	0.00	0.02	0.04	0.06	0.08
0.10	0.12	0.14	0.14	0.11	0.09	0.08	0.07	
-0.06	-0.06	-0.06	-0.05	-0.04	-0.03	0.00	0.01	0.02
0.03	0.05	0.07	0.09	0.09	0.08	0.08	0.07	
-0.04	-0.04	-0.04	-0.05	-0.05	-0.05	-0.04	-0.03	-0.02
-0.01	0.01	0.03	0.05	0.06	0.07	0.07	0.06	
-0.03	-0.03	-0.03	-0.04	-0.06	-0.07	-0.07	-0.06	-0.04
-0.04	-0.02	0.00	0.02	0.04	0.06	0.06	0.05	

..... continued

-0.02	-0.02	-0.02	-0.03	-0.06	-0.09	-0.10	-0.11	-0.09
-0.08	-0.06	-0.04	0.00	0.03	0.05	0.06	0.04	
-0.01	-0.01	-0.02	-0.03	-0.08	-0.12	-0.12	-0.12	-0.12
-0.11	-0.10	-0.07	-0.02	0.02	0.04	0.05	0.04	
0.00	0.00	-0.01	-0.04	-0.08	-0.11	-0.12	-0.12	-0.13
-0.12	-0.10	-0.07	-0.03	0.00	0.03	0.05	0.04	
0.00	0.00	-0.01	-0.04	-0.08	-0.10	-0.11	-0.12	-0.11
-0.11	-0.09	-0.06	-0.03	0.00	0.03	0.03	0.03	
0.00	0.00	-0.01	-0.05	-0.08	-0.09	-0.10	-0.10	-0.10
-0.10	-0.08	-0.06	-0.03	0.00	0.01	0.02	0.02	
0.00	-0.01	-0.02	-0.04	-0.07	-0.08	-0.08	-0.08	-0.08
-0.08	-0.06	-0.05	-0.03	-0.01	0.00	0.01	0.02	

The LSC Residual Geoid Heights for Area B - Case II

ϕ_1	ϕ_2	λ_1	λ_1	$\Delta\phi$	$\Delta\lambda$
2.550000	3.633330	101.616670	102.433330	0.050000	0.050000

0.27	0.31	0.34	0.35	0.37	0.38	0.38	0.37	0.35
0.27	0.25	0.23	0.17	0.16	0.12	0.09	0.08	
0.29	0.33	0.35	0.40	0.46	0.47	0.47	0.48	0.42
0.36	0.27	0.21	0.17	0.16	0.13	0.11	0.08	
0.28	0.36	0.36	0.45	0.47	0.50	0.48	0.47	0.44
0.36	0.31	0.27	0.21	0.18	0.13	0.13	0.10	
0.27	0.34	0.38	0.48	0.52	0.52	0.48	0.47	0.44
0.36	0.28	0.22	0.18	0.15	0.14	0.13	0.10	
0.28	0.34	0.40	0.50	0.53	0.50	0.50	0.47	0.45
0.36	0.29	0.22	0.19	0.16	0.15	0.13	0.08	
0.28	0.30	0.35	0.44	0.46	0.44	0.44	0.41	0.38
0.34	0.28	0.22	0.18	0.17	0.16	0.13	0.10	
0.23	0.26	0.33	0.36	0.36	0.33	0.28	0.24	0.23
0.24	0.20	0.16	0.16	0.15	0.15	0.14	0.11	
0.22	0.27	0.29	0.24	0.05	-0.02	-0.03	-0.05	-0.03
-0.02	-0.03	0.06	0.11	0.13	0.14	0.14	0.11	
0.13	0.16	0.18	0.13	-0.03	-0.17	-0.17	-0.17	-0.14
-0.08	-0.04	-0.02	0.08	0.12	0.13	0.13	0.11	
0.12	0.11	0.10	0.08	-0.06	-0.17	-0.17	-0.17	-0.14
-0.09	-0.05	-0.01	0.07	0.10	0.13	0.13	0.10	
0.05	0.06	0.06	0.04	-0.02	-0.09	-0.11	-0.12	-0.10
-0.07	-0.04	-0.01	0.05	0.10	0.11	0.12	0.11	
0.03	0.03	0.05	0.05	0.03	-0.03	-0.04	-0.05	-0.04
-0.05	0.01	0.05	0.06	0.12	0.13	0.13	0.11	
0.06	0.03	0.04	0.05	0.06	0.01	0.01	0.01	0.01
0.02	0.03	0.05	0.08	0.13	0.14	0.15	0.11	
0.05	0.06	-0.01	-0.02	-0.01	0.04	0.04	0.06	0.04
0.03	0.05	0.10	0.11	0.18	0.17	0.15	0.13	
0.08	0.09	0.07	0.06	0.05	0.04	0.06	0.08	0.10
0.11	0.12	0.14	0.17	0.19	0.19	0.15	0.12	
0.05	0.06	-0.01	0.00	0.05	0.07	0.04	0.08	0.11
0.13	0.12	0.16	0.20	0.21	0.20	0.14	0.14	
0.05	0.05	0.07	0.08	0.04	0.04	0.03	0.06	0.09
0.13	0.16	0.15	0.20	0.24	0.22	0.15	0.14	

..... continued

0.04	0.05	0.06	0.04	0.03	0.01	0.00	0.03	0.08
0.11	0.15	0.18	0.19	0.26	0.24	0.18	0.12	
0.03	0.05	0.03	0.03	0.00	-0.02	0.00	0.04	0.08
0.11	0.13	0.17	0.22	0.24	0.22	0.20	0.13	
0.02	0.03	0.04	0.02	-0.02	-0.02	0.04	0.06	0.08
0.07	0.10	0.13	0.15	0.22	0.24	0.20	0.13	
0.04	0.04	0.03	0.00	-0.03	-0.02	0.02	0.06	0.10
0.07	0.10	0.12	0.14	0.17	0.20	0.19	0.15	
0.05	0.03	0.01	-0.01	-0.04	-0.02	0.01	0.05	0.07
0.08	0.09	0.11	0.12	0.13	0.15	0.16	0.15	
0.04	0.02	-0.01	-0.02	-0.04	-0.03	0.00	0.04	0.05
0.04	0.06	0.07	0.10	0.08	0.09	0.11	0.10	

Appendix U(i)

The Final LSC Geoid Heights for Area B - Case I

ϕ_1	ϕ_2		λ_1		λ_1	$\Delta\phi$		$\Delta\lambda$
2.550000	3.633330		101.616670		102.433330	0.050000		0.050000
-4.64	-4.48	-4.30	-4.07	-3.82	-3.57	-3.34	-3.12	-2.84
-2.56	-2.30	-2.04	-1.78	-1.48	-1.21	-0.96	-0.73	
-4.59	-4.43	-4.21	-4.02	-3.77	-3.52	-3.27	-3.05	-2.80
-2.51	-2.24	-1.96	-1.68	-1.41	-1.16	-0.89	-0.63	
-4.51	-4.36	-4.16	-3.94	-3.70	-3.48	-3.23	-2.97	-2.74
-2.47	-2.18	-1.89	-1.61	-1.34	-1.07	-0.81	-0.55	
-4.42	-4.26	-4.07	-3.87	-3.63	-3.42	-3.15	-2.93	-2.65
-2.39	-2.11	-1.82	-1.55	-1.26	-0.98	-0.72	-0.46	
-4.33	-4.17	-3.98	-3.77	-3.57	-3.33	-3.12	-2.86	-2.58
-2.30	-2.02	-1.72	-1.43	-1.15	-0.88	-0.61	-0.36	
-4.23	-4.07	-3.87	-3.65	-3.45	-3.26	-3.03	-2.75	-2.48
-2.21	-1.93	-1.64	-1.35	-1.07	-0.79	-0.51	-0.26	
-4.13	-3.97	-3.78	-3.52	-3.28	-3.12	-2.92	-2.65	-2.37
-2.12	-1.82	-1.54	-1.25	-0.97	-0.68	-0.42	-0.16	
-4.02	-3.87	-3.70	-3.48	-3.25	-3.05	-2.82	-2.57	-2.29
-2.01	-1.71	-1.41	-1.11	-0.84	-0.57	-0.31	-0.07	
-3.91	-3.77	-3.61	-3.39	-3.15	-2.91	-2.68	-2.44	-2.17
-1.90	-1.61	-1.31	-1.01	-0.75	-0.52	-0.25	0.00	
-3.78	-3.66	-3.50	-3.31	-3.01	-2.79	-2.56	-2.32	-2.05
-1.76	-1.49	-1.19	-0.92	-0.66	-0.39	-0.14	0.09	
-3.62	-3.49	-3.33	-3.13	-2.87	-2.66	-2.43	-2.20	-1.94
-1.66	-1.40	-1.11	-0.83	-0.57	-0.29	-0.05	0.19	
-3.47	-3.30	-3.14	-2.95	-2.78	-2.58	-2.34	-2.09	-1.85
-1.57	-1.30	-1.02	-0.76	-0.50	-0.25	0.01	0.26	
-3.33	-3.18	-3.00	-2.82	-2.64	-2.45	-2.26	-2.02	-1.79
-1.52	-1.22	-0.96	-0.69	-0.40	-0.13	0.14	0.40	
-3.19	-3.02	-2.85	-2.67	-2.52	-2.34	-2.13	-1.92	-1.67
-1.45	-1.19	-0.89	-0.63	-0.33	-0.05	0.20	0.47	
-3.05	-2.88	-2.71	-2.54	-2.40	-2.21	-2.01	-1.82	-1.59
-1.38	-1.12	-0.84	-0.53	-0.23	0.05	0.32	0.55	
-2.92	-2.74	-2.56	-2.39	-2.23	-2.06	-1.88	-1.67	-1.47
-1.26	-1.00	-0.72	-0.42	-0.12	0.17	0.43	0.66	
-2.76	-2.56	-2.42	-2.26	-2.09	-1.93	-1.78	-1.60	-1.39
-1.14	-0.90	-0.61	-0.30	-0.03	0.27	0.54	0.76	

..... continued

-2.63	-2.45	-2.27	-2.12	-1.95	-1.80	-1.65	-1.45	-1.24
-1.01	-0.77	-0.51	-0.20	0.09	0.40	0.65	0.87	
-2.51	-2.36	-2.18	-2.02	-1.86	-1.68	-1.47	-1.27	-1.06
-0.84	-0.61	-0.34	-0.10	0.19	0.44	0.71	0.95	
-2.42	-2.22	-2.06	-1.89	-1.73	-1.57	-1.40	-1.18	-0.96
-0.76	-0.52	-0.26	0.01	0.27	0.60	0.84	1.06	
-2.33	-2.14	-1.95	-1.74	-1.57	-1.37	-1.19	-0.99	-0.79
-0.58	-0.37	-0.06	0.22	0.37	0.62	0.89	1.14	
-2.26	-2.04	-1.84	-1.64	-1.45	-1.27	-1.07	-0.85	-0.64
-0.42	-0.20	0.00	0.23	0.48	0.76	0.98	1.24	
-2.17	-1.94	-1.72	-1.51	-1.33	-1.14	-0.94	-0.73	-0.51
-0.30	-0.08	0.10	0.34	0.57	0.82	1.09	1.32	

The Final LSC Geoid Heights for Area B - Case II

ϕ_1	ϕ_2	λ_1	λ_1	$\Delta\phi$	$\Delta\lambda$
2.550000	3.633330	101.616670	102.433330	0.050000	0.050000

-4.34	-4.10	-3.80	-3.45	-3.17	-3.01	-2.92	-2.78	-2.58
-2.42	-2.19	-1.89	-1.70	-1.49	-1.29	-1.07	-0.82	
-4.23	-3.94	-3.58	-3.24	-2.91	-2.82	-2.74	-2.63	-2.48
-2.28	-2.12	-1.85	-1.66	-1.49	-1.28	-1.02	-0.78	
-4.11	-3.87	-3.44	-3.00	-2.78	-2.75	-2.70	-2.53	-2.43
-2.25	-2.03	-1.79	-1.62	-1.41	-1.21	-0.96	-0.71	
-4.02	-3.76	-3.44	-2.85	-2.71	-2.65	-2.53	-2.41	-2.29
-2.18	-2.00	-1.79	-1.58	-1.37	-1.12	-0.87	-0.63	
-3.97	-3.68	-3.25	-2.84	-2.65	-2.48	-2.37	-2.25	-2.18
-2.08	-1.90	-1.70	-1.47	-1.27	-1.03	-0.78	-0.56	
-3.90	-3.59	-3.12	-2.61	-2.44	-2.31	-2.21	-2.06	-1.98
-1.90	-1.76	-1.59	-1.38	-1.16	-0.92	-0.68	-0.44	
-3.78	-3.46	-3.13	-2.77	-2.51	-2.34	-2.16	-2.01	-1.88
-1.81	-1.68	-1.51	-1.30	-1.08	-0.83	-0.58	-0.34	
-3.71	-3.52	-3.27	-3.03	-2.86	-2.63	-2.39	-2.14	-1.96
-1.83	-1.74	-1.47	-1.23	-0.99	-0.73	-0.47	-0.24	
-3.69	-3.61	-3.38	-3.16	-2.97	-2.69	-2.30	-1.99	-1.76
-1.62	-1.52	-1.39	-1.10	-0.89	-0.63	-0.39	-0.14	
-3.70	-3.59	-3.41	-3.16	-2.94	-2.71	-2.37	-1.98	-1.77
-1.48	-1.34	-1.24	-1.03	-0.79	-0.51	-0.26	-0.05	
-3.70	-3.55	-3.37	-3.13	-2.88	-2.66	-2.32	-1.94	-1.70
-1.40	-1.22	-1.10	-0.94	-0.65	-0.35	-0.15	0.07	
-3.62	-3.47	-3.25	-3.00	-2.74	-2.50	-2.17	-1.80	-1.56
-1.38	-1.16	-0.96	-0.78	-0.49	-0.20	0.03	0.18	
-3.48	-3.33	-3.13	-2.89	-2.62	-2.36	-2.02	-1.63	-1.43
-1.28	-1.10	-0.86	-0.65	-0.38	-0.10	0.16	0.30	
-3.37	-3.20	-3.06	-2.84	-2.59	-2.26	-1.88	-1.52	-1.35
-1.20	-0.96	-0.67	-0.49	-0.22	0.02	0.25	0.43	
-3.24	-3.06	-2.87	-2.65	-2.44	-2.18	-1.80	-1.48	-1.19
-0.99	-0.71	-0.46	-0.27	-0.06	0.14	0.34	0.50	
-3.16	-2.96	-2.83	-2.59	-2.30	-2.03	-1.77	-1.39	-1.03
-0.73	-0.51	-0.24	-0.07	0.10	0.25	0.41	0.63	
-3.03	-2.85	-2.63	-2.39	-2.19	-1.93	-1.66	-1.31	-0.92
-0.47	-0.27	-0.17	0.10	0.24	0.37	0.51	0.72	

..... continued

-2.91	-2.71	-2.50	-2.31	-2.05	-1.78	-1.52	-1.23	-0.87
-0.45	-0.22	-0.08	0.12	0.34	0.48	0.63	0.80	
-2.79	-2.58	-2.40	-2.18	-1.96	-1.73	-1.46	-1.17	-0.83
-0.47	-0.21	0.00	0.22	0.41	0.59	0.76	0.93	
-2.68	-2.46	-2.26	-2.05	-1.86	-1.62	-1.33	-1.06	-0.74
-0.41	-0.09	0.10	0.31	0.52	0.72	0.88	1.04	
-2.53	-2.33	-2.12	-1.94	-1.74	-1.50	-1.23	-0.97	-0.66
-0.39	-0.03	0.26	0.47	0.60	0.79	0.99	1.15	
-2.41	-2.23	-2.03	-1.83	-1.64	-1.39	-1.12	-0.86	-0.59
-0.32	-0.04	0.27	0.54	0.68	0.86	1.06	1.26	
-2.30	-2.09	-1.91	-1.70	-1.50	-1.26	-1.00	-0.74	-0.48
-0.26	0.01	0.36	0.78	0.76	0.96	1.15	1.32	

Appendix V(i)

The LSC Residual Geoid Heights for Area C - Case I

ϕ_1	ϕ_2	λ_1	λ_1	$\Delta\phi$	$\Delta\lambda$
1.250000	1.816670	103.250000	104.243333	0.083330	0.083330

0.02	0.03	0.03	0.03	0.01	0.02	0.01	0.01	0.01
0.02	0.01	0.02	0.03					
0.03	0.02	0.02	0.02	0.02	0.01	0.01	-0.03	-0.04
-0.04	-0.02	-0.02	-0.01					
0.01	0.00	-0.01	-0.01	-0.02	-0.07	-0.08	-0.08	-0.13
-0.11	-0.10	-0.09	-0.04					
0.02	0.00	-0.05	-0.08	-0.16	-0.18	-0.15	-0.14	-0.20
-0.18	-0.16	-0.11	-0.06					
0.01	-0.02	-0.08	-0.17	-0.18	-0.19	-0.21	-0.19	-0.17
-0.17	-0.15	-0.16	-0.10					
0.01	0.00	-0.04	-0.07	-0.19	-0.20	-0.20	-0.18	-0.16
-0.16	-0.15	-0.13	-0.11					
0.02	0.03	-0.02	-0.10	-0.14	-0.16	-0.16	-0.15	-0.15
-0.16	-0.12	-0.13	-0.11					
0.00	0.00	-0.04	-0.06	-0.10	-0.16	-0.17	-0.14	-0.13
-0.14	-0.13	-0.10	-0.09					

Appendix V(ii)

The LSC Residual Geoid Heights for Area C - Case II

ϕ_1	ϕ_2	λ_1	λ_1	$\Delta\phi$	$\Delta\lambda$
1.250000	1.816670	103.240000	104.243333	0.083330	0.083330

0.03	0.03	0.02	0.03	0.03	0.01	-0.03	-0.01	-0.03
-0.04	-0.04	-0.04	-0.03					
0.04	0.03	0.05	0.02	0.02	0.00	-0.01	-0.04	-0.05
-0.06	-0.07	-0.06	-0.06					
0.02	0.02	0.01	-0.02	-0.05	-0.07	-0.07	-0.13	-0.13
-0.13	-0.15	-0.10	-0.07					
0.02	0.02	-0.01	-0.08	-0.17	-0.15	-0.14	-0.19	-0.18
-0.17	-0.18	-0.13	-0.09					
0.01	0.01	-0.01	-0.11	-0.18	-0.20	-0.20	-0.18	-0.19
-0.20	-0.19	-0.16	-0.14					
0.02	0.02	-0.02	-0.10	-0.21	-0.18	-0.19	-0.19	-0.17
-0.18	-0.16	-0.18	-0.14					
0.02	-0.01	-0.03	-0.06	-0.16	-0.16	-0.17	-0.15	-0.17
-0.17	-0.15	-0.15	-0.14					
0.01	-0.01	-0.02	-0.05	-0.10	-0.13	-0.14	-0.16	-0.15
-0.13	-0.15	-0.14	-0.12					

Appendix W

The Final LSC Geoid Heights for Area C - Case II only

ϕ_1	ϕ_2	λ_1	λ_1	$\Delta\phi$	$\Delta\lambda$
1.250000	1.816670	103.250000	104.243333	0.083330	0.083330

6.18	6.41	6.72	7.03	7.33	7.64	7.96	8.27	8.52
8.93	9.22	9.59	10.02					
6.29	6.54	6.86	7.18	7.49	7.80	8.09	8.40	8.70
9.01	9.43	9.72	10.17					
6.42	6.67	6.99	7.32	7.64	7.95	8.27	8.53	8.80
9.10	9.44	9.85	10.26					
6.52	6.76	7.09	7.41	7.70	8.03	8.39	8.64	8.90
9.23	9.60	9.96	10.37					
6.65	6.86	7.18	7.47	7.75	8.11	8.46	8.84	9.14
9.44	9.73	10.07	10.45					
6.67	6.93	7.24	7.57	7.88	8.26	8.61	8.97	9.30
9.60	9.90	10.20	10.54					
6.68	6.94	7.27	7.64	8.00	8.36	8.73	9.08	9.40
9.67	9.98	10.32	10.63					
6.64	6.93	7.28	7.66	8.06	8.43	8.78	9.15	9.42
9.70	10.04	10.39	10.70					

The FFT Residual Geoid Heights for Area A - Case II Only

ϕ_1	ϕ_2	λ_1	λ_1	$\Delta\phi$	$\Delta\lambda$
4.066670	4.875000	100.966670	101.766670	0.033330	0.033330

-0.03	-0.02	-0.03	-0.05	-0.07	-0.12	-0.21	-0.29	-0.39
-0.48	-0.50	-0.48	-0.45	-0.41	-0.33	-0.22	-0.11	0.03
0.19	0.36	0.51	0.61	0.65	0.65	0.57		
-0.02	0.00	-0.01	-0.04	-0.09	-0.14	-0.24	-0.37	-0.50
-0.65	-0.68	-0.61	-0.57	-0.56	-0.46	-0.30	-0.21	-0.02
0.19	0.46	0.68	0.79	0.83	0.83	0.69		
-0.03	-0.03	-0.05	-0.08	-0.12	-0.19	-0.31	-0.44	-0.57
-0.69	-0.81	-0.80	-0.77	-0.68	-0.46	-0.30	-0.24	-0.03
0.24	0.52	0.73	0.84	0.88	0.90	0.75		
-0.02	-0.05	-0.09	-0.12	-0.16	-0.23	-0.34	-0.49	-0.63
-0.75	-0.89	-0.96	-0.96	-0.85	-0.58	-0.30	-0.16	0.03
0.34	0.54	0.76	0.88	0.95	0.95	0.78		
-0.05	-0.07	-0.10	-0.14	-0.19	-0.26	-0.38	-0.53	-0.68
-0.85	-1.02	-1.12	-1.05	-0.90	-0.64	-0.36	-0.04	0.20
0.41	0.62	0.81	0.91	0.97	0.98	0.80		
-0.05	-0.07	-0.10	-0.15	-0.20	-0.28	-0.39	-0.54	-0.69
-0.85	-1.11	-1.18	-1.08	-0.95	-0.69	-0.45	-0.14	0.17
0.43	0.64	0.82	0.93	0.98	0.91	0.78		
-0.07	-0.08	-0.11	-0.14	-0.21	-0.30	-0.40	-0.50	-0.69
-0.85	-1.04	-1.13	-1.11	-0.96	-0.74	-0.50	-0.23	0.01
0.30	0.58	0.76	0.84	0.92	0.88	0.76		
-0.07	-0.09	-0.11	-0.14	-0.20	-0.29	-0.40	-0.54	-0.69
-0.79	-0.92	-1.04	-1.17	-1.06	-0.83	-0.61	-0.43	-0.21
0.10	0.45	0.63	0.73	0.84	0.85	0.73		
-0.05	-0.08	-0.09	-0.12	-0.20	-0.29	-0.41	-0.54	-0.70
-0.86	-0.93	-1.07	-1.20	-1.17	-0.99	-0.81	-0.60	-0.42
-0.07	0.29	0.48	0.58	0.75	0.82	0.71		
-0.04	-0.06	-0.09	-0.12	-0.19	-0.28	-0.40	-0.52	-0.68
-0.81	-0.90	-1.03	-1.19	-1.18	-1.09	-0.91	-0.67	-0.41
-0.10	0.17	0.39	0.48	0.68	0.81	0.69		
-0.03	-0.05	-0.08	-0.11	-0.18	-0.26	-0.38	-0.52	-0.67
-0.87	-0.94	-1.09	-1.25	-1.21	-1.07	-0.83	-0.61	-0.32
-0.05	0.19	0.38	0.47	0.67	0.74	0.67		
-0.04	-0.04	-0.07	-0.11	-0.17	-0.25	-0.36	-0.49	-0.62
-0.75	-0.94	-1.01	-1.18	-1.19	-1.09	-0.88	-0.60	-0.28
0.05	0.26	0.49	0.52	0.68	0.76	0.67		
-0.03	-0.03	-0.07	-0.11	-0.17	-0.24	-0.32	-0.45	-0.57
-0.65	-0.79	-1.01	-1.11	-1.14	-1.04	-0.80	-0.56	-0.28
0.04	0.34	0.55	0.65	0.77	0.80	0.67		

..... continued

-0.03	-0.02	-0.06	-0.10	-0.15	-0.22	-0.28	-0.41	-0.53
-0.61	-0.79	-0.99	-1.04	-1.01	-0.96	-0.76	-0.47	-0.24
0.01	0.29	0.52	0.71	0.82	0.82	0.68		
-0.02	-0.03	-0.06	-0.10	-0.14	-0.19	-0.25	-0.36	-0.48
-0.60	-0.73	-0.83	-0.93	-0.92	-0.88	-0.76	-0.52	-0.39
-0.10	0.23	0.53	0.69	0.81	0.82	0.67		
-0.02	-0.04	-0.06	-0.07	-0.12	-0.14	-0.22	-0.32	-0.42
-0.49	-0.68	-0.68	-0.73	-0.83	-0.87	-0.77	-0.63	-0.37
-0.05	0.20	0.45	0.69	0.79	0.80	0.66		
-0.03	-0.05	-0.06	-0.06	-0.08	-0.14	-0.19	-0.28	-0.36
-0.46	-0.60	-0.55	-0.67	-0.76	-0.87	-0.82	-0.67	-0.40
-0.01	0.23	0.51	0.67	0.74	0.76	0.64		
-0.04	-0.04	-0.06	-0.07	-0.10	-0.13	-0.17	-0.23	-0.28
-0.32	-0.46	-0.41	-0.59	-0.72	-0.78	-0.73	-0.55	-0.29
0.04	0.29	0.51	0.66	0.73	0.76	0.61		
-0.03	-0.03	-0.05	-0.07	-0.08	-0.12	-0.14	-0.18	-0.19
-0.19	-0.28	-0.27	-0.44	-0.56	-0.69	-0.70	-0.49	-0.25
-0.01	0.14	0.38	0.61	0.70	0.70	0.59		
-0.03	-0.03	-0.05	-0.07	-0.08	-0.10	-0.12	-0.13	-0.11
-0.03	-0.04	-0.14	-0.31	-0.48	-0.64	-0.62	-0.50	-0.30
-0.14	0.04	0.34	0.57	0.67	0.68	0.56		
-0.02	-0.03	-0.05	-0.06	-0.07	-0.08	-0.09	-0.08	-0.04
0.06	0.06	-0.05	-0.21	-0.36	-0.53	-0.56	-0.49	-0.36
-0.16	0.11	0.33	0.54	0.63	0.64	0.52		
-0.01	-0.03	-0.05	-0.05	-0.06	-0.06	-0.06	-0.04	0.00
0.12	0.13	0.05	-0.08	-0.27	-0.43	-0.41	-0.46	-0.32
-0.11	0.11	0.30	0.49	0.57	0.59	0.48		
-0.02	-0.03	-0.04	-0.04	-0.03	-0.04	-0.03	-0.01	0.03
0.16	0.18	0.13	-0.01	-0.21	-0.34	-0.31	-0.37	-0.33
-0.20	-0.05	0.18	0.39	0.51	0.53	0.43		
-0.03	-0.03	-0.03	-0.02	-0.03	-0.03	-0.02	0.00	0.05
0.17	0.20	0.15	0.02	-0.18	-0.15	-0.21	-0.28	-0.24
-0.22	-0.08	0.09	0.33	0.43	0.44	0.36		
-0.03	-0.03	-0.03	-0.02	-0.02	-0.02	-0.02	-0.01	0.03
0.10	0.10	0.07	0.00	-0.08	-0.11	-0.14	-0.15	-0.13
-0.09	0.00	0.10	0.22	0.29	0.31	0.28		

Appendix X(ii)

The FFT Residual Geoid Heights for Area B - Case II Only

ϕ_1	ϕ_2	λ_1	λ_1	$\Delta\phi$	$\Delta\lambda$
2.550000	3.633330	101.616670	102.433330	0.050000	0.050000

0.25	0.30	0.33	0.36	0.40	0.43	0.41	0.38	0.33
0.28	0.22	0.18	0.15	0.13	0.10	0.08	0.05	
0.31	0.37	0.40	0.44	0.49	0.51	0.51	0.46	0.40
0.33	0.26	0.20	0.16	0.14	0.12	0.09	0.06	
0.34	0.41	0.44	0.49	0.50	0.51	0.50	0.50	0.43
0.35	0.27	0.21	0.16	0.14	0.12	0.10	0.07	
0.35	0.43	0.46	0.50	0.50	0.51	0.51	0.51	0.44
0.36	0.28	0.21	0.17	0.14	0.12	0.10	0.07	
0.34	0.41	0.44	0.48	0.51	0.51	0.50	0.47	0.42
0.35	0.28	0.22	0.17	0.15	0.13	0.10	0.07	
0.30	0.37	0.40	0.43	0.45	0.45	0.43	0.39	0.36
0.32	0.26	0.20	0.17	0.15	0.13	0.11	0.08	
0.25	0.31	0.34	0.35	0.34	0.30	0.25	0.22	0.21
0.22	0.18	0.15	0.14	0.14	0.13	0.12	0.09	
0.19	0.23	0.25	0.22	0.05	-0.03	-0.06	-0.06	-0.05
-0.04	0.00	0.05	0.09	0.13	0.13	0.12	0.09	
0.13	0.15	0.16	0.12	-0.05	-0.16	-0.16	-0.16	-0.15
-0.12	-0.07	0.00	0.06	0.10	0.12	0.12	0.09	
0.07	0.09	0.09	0.06	-0.07	-0.15	-0.16	-0.16	-0.17
-0.13	-0.08	-0.03	0.04	0.09	0.11	0.11	0.09	
0.03	0.03	0.03	0.02	-0.04	-0.12	-0.15	-0.16	-0.15
-0.12	-0.07	-0.03	0.03	0.09	0.10	0.11	0.09	
0.01	0.01	0.01	0.02	0.00	-0.04	-0.08	-0.09	-0.09
-0.08	-0.05	-0.01	0.03	0.09	0.11	0.12	0.10	
0.01	0.02	0.01	0.02	0.02	0.00	-0.02	-0.03	-0.04
-0.04	-0.02	0.01	0.05	0.10	0.12	0.12	0.10	
0.02	0.03	0.02	0.03	0.04	0.03	0.02	0.01	0.01
0.01	0.03	0.04	0.07	0.13	0.14	0.13	0.11	
0.03	0.04	0.04	0.03	0.03	0.03	0.04	0.04	0.05
0.06	0.08	0.09	0.12	0.15	0.15	0.14	0.11	
0.03	0.04	0.05	0.04	0.04	0.04	0.04	0.05	0.06
0.08	0.10	0.12	0.14	0.16	0.16	0.15	0.12	

..... continued

0.03	0.05	0.05	0.05	0.04	0.03	0.03	0.04	0.06
0.08	0.10	0.13	0.16	0.17	0.17	0.16	0.12	
0.03	0.04	0.04	0.05	0.03	0.02	0.02	0.03	0.05
0.07	0.10	0.13	0.17	0.19	0.19	0.16	0.11	
0.02	0.04	0.04	0.03	0.00	-0.02	0.00	0.01	0.04
0.06	0.09	0.13	0.17	0.20	0.19	0.16	0.12	
0.02	0.03	0.03	0.02	0.00	-0.02	0.00	0.01	0.03
0.05	0.09	0.12	0.16	0.17	0.18	0.17	0.12	
0.01	0.02	0.02	0.00	-0.01	-0.02	0.00	0.02	0.04
0.06	0.08	0.11	0.13	0.15	0.16	0.14	0.10	
0.00	0.01	0.00	-0.01	-0.03	-0.03	-0.01	0.01	0.03
0.05	0.07	0.09	0.11	0.13	0.13	0.12	0.09	
-0.02	-0.01	-0.01	-0.03	-0.04	-0.04	-0.02	0.00	0.02
0.03	0.05	0.06	0.08	0.08	0.09	0.08	0.06	

Appendix X(iii)

The FFT Residual Geoid Heights for Area C - Case II Only

ϕ_1	ϕ_2	λ_1	λ_1	$\Delta\phi$	$\Delta\lambda$
1.250000	1.833330	103.250000	104.243333	0.083330	0.083330

0.03	0.02	0.02	0.01	0.00	-0.01	-0.02	-0.02	-0.02
-0.03	-0.05	-0.05	-0.04					
0.02	0.02	0.02	0.01	0.00	-0.02	-0.03	-0.05	-0.05
-0.07	-0.09	-0.08	-0.06					
0.02	0.01	-0.01	-0.02	-0.03	-0.06	-0.08	-0.10	-0.12
-0.13	-0.12	-0.10	-0.07					
0.01	-0.01	-0.03	-0.06	-0.12	-0.12	-0.11	-0.15	-0.20
-0.17	-0.16	-0.10	-0.07					
0.01	-0.01	-0.04	-0.09	-0.15	-0.16	-0.20	-0.16	-0.16
-0.16	-0.15	-0.13	-0.08					
0.00	-0.02	-0.03	-0.09	-0.15	-0.16	-0.15	-0.14	-0.13
-0.14	-0.14	-0.13	-0.09					
-0.01	-0.02	-0.03	-0.06	-0.11	-0.13	-0.12	-0.12	-0.12
-0.13	-0.12	-0.10	-0.08					
0.00	-0.02	-0.03	-0.05	-0.08	-0.09	-0.09	-0.09	-0.10
-0.10	-0.09	-0.08	-0.06					

Appendix Y

The absolute differences between N_{LSC} and N_{FFT} with respect to $N_{GPS/lev}$ for the Federal Territory GPS Network

GPS Code Station	Latitude	Longitude	Orthometric Height (m)	$N_{GPS/lev} - N_{LSC}$ (m)	$N_{GPS/lev} - N_{FFT}$ (m)
GU02	3.24170	101.64860	89.71	-0.84	-0.83
GU03	3.24170	101.67640	68.89	-0.73	-0.72
GU04	3.24440	101.70560	168.48	-0.65	-0.65
GU05	3.24440	101.72780	69.89	-0.85	-0.86
GU06	3.23890	101.75280	114.78	-0.72	-0.73
GU08	3.22360	101.65560	54.48	-0.78	-0.76
GU09	3.22220	101.67780	48.36	-0.63	-0.62
GU10	3.22220	101.69720	48.75	-0.61	-0.63
GU11	3.22220	101.72500	59.41	-0.65	-0.67
GU12	3.22220	101.75000	58.82	-0.65	-0.64
GU13	3.19440	101.62360	81.13	-0.66	-0.68
GU14	3.19860	101.65140	45.75	-0.68	-0.70
GU16	3.19860	101.69580	40.63	-0.68	-0.66
GU17	3.20000	101.72780	47.77	-0.65	-0.64
GU18	3.20560	101.75140	84.49	-0.65	-0.62
GU19	3.17080	101.61670	45.66	-0.75	-0.77
GU20	3.16670	101.65140	77.09	-0.77	-0.75
GU21	3.17360	101.67640	47.21	-0.70	-0.72
GU22	3.17080	101.70420	37.12	-0.72	-0.72
GU23	3.16810	101.72500	34.05	-0.68	-0.69
GU24	3.17640	10.74580	66.66	-0.70	-0.70
GU26	3.14170	101.64860	64.36	-0.73	-0.72
GU27	3.14440	101.67640	92.27	-0.62	-0.62
GU29	3.13890	101.73470	43.13	-0.67	-0.65
GU30	3.14580	101.75560	50.90	-0.68	-0.68
GU31	3.11810	101.62220	43.81	-0.76	-0.75

..... continued

GPS Code Station	Latitude	Longitude	Orthometric Heights (m)	$N_{GPS/lev} - N_{LSC}$ (m)	$N_{GPS/lev} - N_{FFT}$ (m)
GU32	3.11810	101.64440	49.30	-0.76	-0.75
GU33	3.12280	101.67360	37.01	-0.70	-0.70
GU34	3.11940	101.70970	33.39	-0.67	-0.69
GU35	3.11390	101.72780	53.03	-0.62	-0.63
GU36	3.10830	101.74860	105.20	-0.70	-0.70
GU37	3.09440	101.62360	40.04	-0.61	-0.62
GU38	3.09440	101.64860	20.87	-0.69	-0.69
GU39	3.09030	101.68330	48.16	-0.69	-0.68
GU40	3.10560	101.70690	35.34	-0.66	-0.65
GU41	3.09720	101.72780	77.93	-0.61	-0.61
GU42	3.08330	101.75140	70.62	-0.62	-0.60
GU43	3.05140	101.62220	31.03	-0.61	-0.60
GU44	3.06110	101.64860	18.54	-0.74	-0.74
GU45	3.06810	101.67920	43.12	-0.67	-0.69
GU46	3.06940	101.69860	62.79	-0.74	-0.72
GU47	3.06530	101.71390	62.52	-0.66	-0.67
GU48	3.06110	101.74720	69.78	-0.65	-0.64
GU49	3 .02220	101.61110	11.96	-0.71	-0.72
GU52	3.03330	101.70690	45.61	-0.72	-0.71
GU53	3.03330	101.72780	41.37	-0.73	-0.73
GU54	3.03750	101.74860	60.41	-0.73	-0.72
GK02	3.09580	101.63890	22.05	-0.69	-0.70
GK03	3.13060	101.70690	55.41	-0.71	-0.69
GK04	3.17360	101.69310	66.88	-0.79	-0.78
GK05	3.14030	101.62220	42.88	-0.68	-0.69

Appendix Z

The absolute differences between N_{LSC} and N_{FFT} with respect to $N_{GPS/lev}$ and N_{FFT} at 5 GPS Control Points

GPS Code Station	Latitude	Longitude	Orthometric Height (m)	$N_{GPS/lev} - N_{LSC}$ (m)	$N_{GPS/lev} - N_{FFT}$ (m)
GP49	1.36980	104.26740	58.72	-1.54	-1.50
GP50	1.54750	103.39540	3.97	-1.37	-1.36
GP51	1.62610	103.19990	58.72	-1.87	-1.89
GP53	1.63400	103.66680	35.53	-1.92	-1.89
GP61	1.80430	103.89720	24.00	-1.85	-1.85

Appendix AA

A Summary of relative differences between N_{LSC} and $N_{GPS/lev}$ for the Federal Territory GPS Network

Mean Distance (Km)	No. of Baselines	ΔN Mean (in ppm)
1.8	38	21.3
2.4	142	15.5
6.6	201	8.5
8.5	214	6.7
11.6	204	5.3
13.7	185	4.6
16.8	144	4.4
18.7	80	3.9
21.1	49	3.9
23.6	24	3.2
26.9	7	3.0
28.4	2	2.8

Appendix AB

A Summary of the Relative Differences Between N_{LSC}, N_{FFT} With Respect to $N_{GPS/levelling}$ for 5 GPS Control Points

From	To	Distance (km)	ΔN_{LSC} (ppm)	ΔN_{FFT} (ppm)	$\Delta N_{OSU89B-MM}$ (ppm)
1	2	98.9	1.72	1.42	3.13
1	3	122.0	2.70	3.20	4.02
1	4	72.9	5.21	5.35	4.25
1	5	63.5	4.89	5.52	2.52
2	3	23.4	21.25	22.63	34.16
2	4	30.7	17.37	16.74	2.33
2	5	62.7	7.66	7.82	2.39
3	4	51.9	0.96	0.96	15.41
3	5	80.0	0.25	0.50	8.13
4	5	30.5	2.20	1.26	4.71

REFERENCES AND BIBLIOGRAPHY

Arabelos, D., (1989): Gravity Field Approximation in the Area of Greece with Emphasis on Local Characteristics. *Bulletin Geodesique, Vol. 63*, pp. 69 - 84.

Arabelos, D. and Tziavos, I., (1994): Marine Geoid Solutions by Spectral and Stochastic Methods. Examples for the Mediterranean Sea. *Papers Presented at the INSMAP Conference*, Hannover, Sept. 19-23.

Arabelos, D., Knudsen, P. and Tscherning, C., (1987): Covariance and Bias Treatment When Combining Gravimetry, Altimeter and Gradiometer Data by Collocation. *Proceedings Intersection Symposium Advances in Gravity Field Modelling, XIX General Assembly IAG*, Vancouver, Canada. pp. 443-454.

Ayhan, M., (1993): Geoid Determination in Turkey (TG-91). *Bulletin Geodesique, Vol. 67*, pp.10-21.

Basic, T., (1989): Untersuchungen Zur Regionalen Geoidbestmmung Mit 'dm' - *Genauigkeit, Wiss. Arb.der Fachr. Vermessungswesen der Universität Hannover, Nr. 157, Hannover.* pp. 132.

Basic,T., Denker, H., Knudsen, P. Solheim, D. and Torge, W., (1989): A New Geopotential Model Tailored to Gravity Data in Europe. *Papers Presented at the IAG General Assembly*, 3 - 12 August. Edinburgh, Scotland.

Barzaghi, R., Forsberg, R. and Tscherning, C., (1988): A Comparison Between SEASAT, GEOSAT and Gravimetric Geoids Computed by FFT and Collocation in the Central Mediterranean Sea. *Papers Presented at Chapman Conference on Progress in the Determination of the Earth's Gravity Field.* Ft. Lauderdale, Florida Sept. 13-16.

Bomford, G., (1980): Geodesy. *Fourth Edition, Clarendon Press*, Oxford

Bowring, R., (1976): Transformation from Spatial to Geographical Coordinates. *Survey Review, No. 181*, pp. 232-237.

Bracewell, R., (1978): The Fourier Transform and Its Applications, *2nd. Edition, McGraw-Hill Book Company*, New York.

Denker, H., (1993): Institute of Geodetic Sciences, University of Hannover, Germany - *Private Communication.*

Denker, H. and Wenzel, H., (1987): Local Geoid Determination And Comparison with GPS Results. *Bulletin Geodesique, No. 61*, pp. 349-366.

Denker, H., Torge, W, Wenzel, H., Lelgemann, D and Weber, G., (1988): Strategies and Requirements for a New European Geoid Determination. *Papers Presented at the International Symposium on the Definition of the Geoid*, Florence, Italy. May 26-30.

Despotakis, V., (1987): Geoid Undulation Computations at Laser Tracking Stations. *Report No. 383, Dept. Geod. Sci., Ohio State University*, Columbus.

DMA, (1987): World Geodetic System 1984 (WGS84). *Defence Mapping Agency Technical Report No. 8350.2*, 1987.

Dodson, A. and Gerrard, S., (1989): A Relative Geoid for the UK. *Paper Presented at the IAG General Meeting*, 3 - 12 August. Edinburgh, Scotland.

DSMM, (1994): Report on the Progress of Field Works for Geoid Undulation Project in Peninsular Malaysia, *Departmental Reports, Division of Geodesy & Topography, Department of Surveying & Mapping, Malaysia.*

Engelis, T., Rapp, R. and Tscherning, C., (1984): The Precise Computation Of Geoid and Undulation With Comparison to Results from GPS. *Geophysical Research Letters 11(9)* - pp. 821-824.

Engelis, T., Rapp, R. and Bock, Y., (1985): Measuring Orthometric Height Differences with GPS and Gravity Data. *Manuscripta Geodaetica*, pp. 187-194.

Featherstone, W., (1992): A GPS Controlled Gravimetric Determination of the Geoid of the British Isles. *Ph.D Thesis, Department of Earth Sciences, University of Oxford, England.*

Featherstone, W. and Olliver, J., (1994): A New Gravimetric Determination of the Geoid of the British Isles. *Survey Review, No. 32*, pp. 464-478.

Fosberg, R., (1984): A Study of Terrain Reductions, Density Anomalies and Geophysical Inversion Methods in Gravity Field Modelling. *Report No. 355, Dept. Geod. Sci., Ohio State University,* Colombus.

Forsberg, R., (1990): Preliminary Geoid Computations in the Philippines Area by FFT. *Austr. J. Geod. Photogramm. Surv., No. 52*, pp. 1-20.

Forsberg, R., (1994): National Survey and Cadastre, Charlottenlund, Denmark - *Private Communication.*

Forsberg, R. and Keasley, W., (1989): Precise Gravimetric Geoid Computations Over Large Regions. *Four-Dimensional Geodesy, Lecture Notes in Earth Sciences*, Springer-Verlag.

Forsberg, R. and Madsen, F., (1990): High precision Geoid for GPS/Levelling. *Paper presented at Proceeding of 2nd. International Symposium on Precise Positioning with GPS.* Ottawa, 3-7 September, pp. 1060-1074.

Forsberg, R. and Solheim, D., (1988): Performance of FFT methods in Local Gravity Field Modelling. *Paper Presented at Chapman Conference on Progress in the Determination of the Earth's Gravity Field,* Fort Lauderdale, Florida.

Forsberg, R. and Tscherning, C., (1981): The Use of Height Data in Gravity Field Approximation by Collocation. *Journal of Geophysical Research, Vol. 86, No. B9, pp.* 7843-7854.

Fosu, C., (1994): Combination of GPS and CCD to Determine Local Geoid for Levelling Purposes - A Preliminary Investigation. *Unpublished report for M.Phil. Department of Photogrammetry and Surveying, University College London,* pp. 70.

Gil, A., Sevilla, M. and Rodriquez, G., (1993): Geoid Determination in Central Spain From Gravity and Height Data. *Bulletin Geodesique, Vol. 67,* pp. 41-50.

Goad, C., Tscherning, C. and Chin, C., (1984): Gravity Empirical Covariance Values for the Continental United State. *Journal of Geophysical Research, Vol. 89, No. B,* pp. 7962-7968.

Heins, G., Leick, A. and Lambert, S., (1989): Integrated Processing of GPS and Gravity Data. *Journal of Surveying Engineering, Vol. 115, No. 1,* pp. 15-34.

Heiskanen, W. and Moritz, H., (1967): Physical Geodesy. *W.H. Freeman & Co.* San Francisco, USA.

Hipkin, R., (1988): Bouguer Anomalies and the Geoid. A Reassessement of Stoke's Method. *Journal of Geophysical Research, Vol. 92,* pp. 53-66.

Hipkin, R. and Steward, M., (1989): A High Resolution Precision Geoid Height for the British Isle. *Papers presented at IAG Symposium,* 3-12 August, Edinburgh. Scotland.

Jekeli, C., (1978): An Investigation of Two Models for the Degree Variances of Global Covariance Functions.*Report No. 275, Dept. Geod. Sci., Ohio State University,* Colombus.

Jeyapalan, K. and Erik, E., (1991): Elevation differences recovery from tests GPS observation and gravimetry. *Technical Paper Presented at ACSM-ASPRS Annual Convention, Vol. 1.* Baltimore, USA.

Kasenda, A. and Kearsley, W., (1992): A Preliminary Geoid for Irian Jaya, Indonesia. *Unisurv S-41,* NSW-Australia.

Kearsley, W., (1984): Precision Limitations and Data Requirements for the Determination of Relative Geoid heights From Gravimetry. *Report No. 26, University of Uppsala, Institute of Geophysics* , 110 pp.

Kearsley, W., (1988): Determination of the Geoid-Ellipsoid Separation for GPS Levelling. *The Australian Surveyor, Vol. 34, No. 1,* pp.11-18.

Kearsley, W. and Forsberg, R., (1990): Tailored Geopotential Models - Applications and Shortcomings. *Manuscripta geodaetica. Vol.15,* pp. 151 - 158.

Kearsley, W. and Holloway, R., (1989): Test on Geopotential Models in the Australian Region. *Aust. J. Geod. Photogr. Surv., No. 50.*

Kearsley, W., Sideris, M., Krynski, J., Forsberg, R. and Schwarz, P., (1985): White Sands Revisited- A Comparison of Techniques to Predict Deflections of the Vertical. *UCSE Reports No. 30007, University of Calgary,* Canada.

Khairul, A., (1993): Orthometric Heights Estimation from a Combination of GPS and Terrestrial Geodetic Data. *Ph. D Thesis. Department of Surveying, University of Newcastle-Upon-Tyne,* England.

Khairul, A., (1994): Faculty of Surveying, University Technology of Malaysia - *Private Communication.*

Knudsen, P., (1987): Estimation and Modelling of the Local Empirical Covariance Function Using Gravity and Satellite Altimeter Data. *Bulletin Geodesique,Vol. 61,* pp. 145-160.

Kostiainen, M. and Kakkuri, J., (1980): On the Accuracy of the Gravity Determined from the Bouguer Anomaly Register for Levelling Benchmarks. *Papers Presented at the NAD 1980 Symposium*, Ottawa.

Leick, A., (1990): GPS Satellite Surveying. *A Wiley-Interscience Publication*, John Wiley & Sons. pp. 352.

Lerch, J., Klosko, M., Laubscher, E. and Wagner, A., (1979): Gravity Model Improvement Using GEOS3 (GEM9 and 10). *Journal of Geophysical Research, Vol. 84, no. B8*, pp. 3897-3916.

Lerch, J. Klosko, M. and Patel, B, (1982): A Refined Gravity Model From Lageous (GEM-L2). *Geophysical Research Letters, 9-No.11*, pp. 1263-1266.

Li, Y. and Sideris, M., (1994): Minimization and Estimation of Geoid Undulation Errors. *Bulletin Geodesique, Vol. 68.* pp. 201-219.

Loke, M. and Lee, C., (1989): Gravity Survey in Peninsular Malaysia by USM, *Seminar Papers on Advanced Survey Technology*, August 10 - 12, Kuala Lumpur.

Lotti, J., (1992): GPS for Geodetic Control Surveying in Sweden. *Papers Presented at 6th. International Symposium on Satellite Positioning*, Colombus, USA.

Mainville, A., (1987): Intercomparison of Various Geoid Computation Methods at GPS Stations, *Paper presented at XIX General Assembly Int. Union of Geod. and Geophys.*, August 9-15.Vancouver, Canada.

Mainville, A., Forsberg, R. and Sideris, M., (1992): Global Positioning System Testing of Geoids Computed From Geopotential Models and Local Gravity Data: A Case Study. *Journal of Geophysical Research, Vol. 97, No. B7*, pp. 11137-11147.

Majid, K., (1992) and (1993): Faculty of Surveying, University of Technology Malaysia - *Private Communication.*

Majid, K., (1987): The Establishment of Gravity Base Network in Peninsular Malaysia. *Jurnal Teknologi, Bil. 9, Universiti Teknologi Malaysia.*

Majid, K., Ses, S., Khairul, A. and Kamaludin, O., (1989): Towards the Development of a National Gravity Database - *The Surveyor, Vol. 24.*

Milbert, D. and Schultz, D., (1993): GEOID93 - A New Geoid Model for the United States. *AGU Spring Meeting,* May 24- 28, Baltimore, Maryland.

Moritz, H., (1976): Covariance Functions in Least Squares Collocation. *Report No. 240, Dept. Geod. Sci., Ohio State University,* Colombus.

Moritz, H., (1980): Advanced Physical Geodesy. *Herbert Wichmann Verlag,* Karlsruhe.

Moritz, H., (1980a): Geodetic Reference System 1980 - The Geodesist Handbook 1980. *Bulletin Geodesique, Vol. 54, No. 3* , pp. 395-405.

Marsh, M. Lerch, J., Putney, H. Klosko, M., Pavlis, C., Patel, B., Chinn, S. and Wagner, A., (1988): An improved Model of the Earth's Gravitational Field ' GEM-T1'. *NASA Technical Memorandum 100713*, Greenbelt, Maryland. November, 1988.

Marsh, M., Lerch, J., Putney, H., Klosko, M., Pavlis, C., Patel, B., Robbin, W., Williamson, G., Engelis, T, Eddy, F., Chandler, L., Chinn, S., Kappor, S., Rachlin, E., Braatz, E. and Pavlis, C., (1989): The GEM-T2 Gravitational Model. *NASA Technical Memorandum 100746*, Greenbelt, Maryland. October, 1989.

Nagy, D., (1991): Gravimetric Geoid Computation for Canada, *Acta Geod. Geoph. Mont. Hung, Vol. 26(1-4)*, pp. 9-17.

Paul, M., (1978): Recurrence Relations for Integrals of Associated Legendre Function. *Bulletin Geodesique, No. 52,* pp. 177-190.

Radzi, I., (1986): Studies on the Measurements of the Earth's Gravity Field in Peninsular Malaysia. *B. Surv. Sc. Thesis, Universiti Teknologi Malaysia.*

Rapp, R., (1985): Detailed Gravity Anomalies and Sea Surface Height Derived from Geos3 and Seasat Altimeter Data. *Report No: 365, Dept. Geod. Sci., Ohio State University,* Columbus.

Rapp, R., (1994): The Use of Potential Coefficient Models in Computing Geoid Undulations. *Lecture Notes prepared for the International School for the Determination and Use of the Geoid.* Milano, Italy. October 10-15, pp. 24.

Rapp, R., (1995): Professor of Geodesy, Department of Geodetic Science, Ohio States University, Colombus, USA - *Private Communication.*

Rapp, R. and Cruz, J., (1986): The Presentation of the Earth's Gravitational Potential in a Spherical Harmonic Expansion to Degree 250. *Report No. 376, Dept. Geod. Sci., Ohio State University,* Columbus.

Rapp, R. and Pavlis, N., (1990): The Development and Analysis of Geopotential Coefficient Models to Spherical Harmonic Degree 360. *Journal of Geophysical Research,Vol. 95, No. B13,* pp. 885-911.

Rapp, R. and Wang, Y., (1993): Geoid Undulation Differences Between Geopotential Models. *Surveys in Geopyhsics, Vol. 14,* pp. 373-380.

Rapp, R., Wang, Y. and Pavlis, N., (1991): The Ohio State 1991 Geopotential and Sea Surface Topography Harmonic Coefficient Models. *Report No. 410, Dept. Geod. Sci., Ohio State University,* Columbus.

Samad, A., (1993): Geodesy in Malaysia. *Departmental Reports, Division of Geodesy & Topography. Department of Surveying & Mapping, Malaysia.*

Samad, A., (1993) and (1994): Division of Geodesy & Topography, Directorate Surveying & Mapping, Malaysia - *Private Communication.*

Sanso, F., (1993): International Geoid Service (Milano) - *Private Communication.*

Schwarz, K. and Lachapelle, G., (1980): Local Characteristic of the Gravity Anomaly Covariance Function. *Bulletin Geodesique, Vol. 54,* pp. 21-36.

Schwarz, K. and Sideris, M., (1985): Precise Geoid Heights and Their Use in GPS interferometry, *Contract Report 85-004, Geodetic Survey of Canada,* Ottawa.

Schwarz, K., Sideris, M. and Forsberg, R., (1987): Orthometric Height without Levelling. *Journal of Surveying Engineering.Vol. 113, No.1,* pp. 28-40.

Sevilla, M., (1993): Analysis and Validation of the DMA Gravimetric Data of the Mediterranean Sea - Mare Nostrum. *Geomed Report No. 3,* Milano, Italy.

Sideris, M. and She, B., (1995): A New, High Resolution Geoid for Canada and Part of the U.S. by the 1D-FFT Method. *Bulletin Geodesique, Vol. 69,* pp. 92-108.

Sideris, M. and Li, Y., (1993): Gravity Field Convolutions Without Windowing and Edge Effects. *Bulletin Geodesique, Vol. 67,* pp. 107-118.

Sideris, M. and Schwarz, K., (1986): Improvements of Medium and Short Wavelength Features of Geopotential Solutions by Local Data. *Proceeding of the Int. Symp. on the Definition of the Geoid*, 26-30 May, Florence, Italy.

Sideris, M. and Tziavos, I., (1988): FFT-Evaluation and Applications of Gravity Field Convolution Integrals with Mean and Point Data. *Bulletin Geodesique, Vol. 62*, pp. 521-540.

Sideris, M. and Li, Y., (1992): Improved Geoid Determination for Levelling by GPS. *Paper Presented at the Sixth Int. Geodetic Symposium on Satellite Positioning* March 17-20, Columbus, Ohio.

Sjoberg, L., (1980): A Recurrence Relation Relation for the β_n Function. *Bulletin Geodesique, No. 54*, pp. 67-72.

Smith, D., (1992): The Use of High Resolution Height Data in the Computation of High Precision Geoid Undulations on the Island of Maui. *Report No. 424, Dept. Geod. Sci., Ohio State University*, Columbus.

Strang Van Hees, G., (1990): Stokes' Formula Using Fast Fourier Techniques. *Manuscripta Geodaetica, Vol. 15*, pp. 235 - 239.

Sunkel, H., (1981): The Estimation of Free-Air Anomalies. *Report No. 315, Dept. Geod. Sci., Ohio State University*, Columbus.

Sunkel, H. and Kraiger, G., (1983): The Prediction of Free-Air Anomalies. *Manuscripta Geodaetica, Vol. 8*, pp. 229 - 248.

Szabo, B., (1986): The Estimation of the Earth's Gravity Field. *Report No. 369, Dept. Geod. Sci., Ohio State University*, Columbus.

Thomas, L. and Bo-Gunner, R., (1991): A consultancy Study of First Order Geodetic Network of Peninsular using GPS Surveys, *Swedsurvey Internal Report for the Directorate Surveying & Mapping*, Malaysia.

Tscherning, C., (1991a): The Use of Optimal Estimation for Gross-Error Detection in Databases of Spatial Correlated Data. *Bulletin d'Information, No. 68*, pp. 79 - 89. Bureau Gravimetrique International, France.

Tscherning, C., (1994): Department of Geophysics, University of Copenhagen, Denmark - *Private Communication.*

Tscherning, C. and Forsberg, R., (1986): Geoid Determination in the Nordic Countries from Gravity and Height Data. *Boll. di Geodasia Sci. Affini, Vol. XLVI,* pp. 21 - 43.

Tscherning, C. and Forsberg, R., (1992): Harmonic Continuation and Gridding Effects on Geoid Height Prediction. *Bulletin Geodesique, Vol. 66.* pp.41-53.

Tscherning, C., Forsberg, R. and Knudsen, P., (1992): The GRAVSOFT package for geoid determination. *Papers Presented at Continental Workshop on the Geoid in Europe*, Prague, May 11 -14.

Tscherning, C. and Rapp, R., (1974): Closed Covariance Expressions for Gravity Anomalies, Geoid Undulations and Deflections of the Vertical Implied by Anomaly Degree Variance Models. *Report No. 208, Dept. Geod. Sci., Ohio State University*, Columbus.

Tscherning, C., Rapp, R. and Goad, C., (1983): A Comparison of Methods for Computing and Evaluation Gravimetric Quantities from High Degree Spherical Harmonic Expansion. *Manuscripta Geodaetica ,Vol. 8,* pp. 249-272.

Tsuie, C., Arabelos, D., Forsberg, R., Sideris, M. and Tziavos, I., (1994): Geoid Computations Taiwan. *Papers Presented at the IGC/ICG Joint Symposium*, Graz, Austria, Sept. 11-17.

Tziavos, I., (1987): Comparison of the Gravity Spectrum as Derived From A 360x360 Geopotential Model and Regional Grvaity Data. *Proceedings of the IUGG XIX General Assembly.* Vancouver, Canada, August 10 - 22.

Tziavos, I., Arabelos, D. and Spatalas, S., (1993): Geoid Modelling and Comparisons with GPS and Satellite Altimetry in the Hellenic Area. *Papers Presented at XVIII General Assembly of the European Geophysical Society*, 3-7 May. Wiesbaden.

Tziavos, I., Sideris, M. and Schwarz, P., (1992): A Study of the contribution of Various Gravimetric Data Types on the Estimation of Gravity Field Parameters in the Mountains. *Journal of Geophysical Research, Vol. 97, No. B6,* pp. 8843-8852.

Vanicek, P. and Kleusberg, A., (1987): The Canadian Geoid-Stokesian Approach, *Manuscripta Geodaetica,Vol. 12,* pp. 86-98.

Vermeer, M., (1992): Terrain Reduction and Gridding Techniques For Geoid Determination. *Lecture Notes for NKG-Autumn School in Helsinki,* Finland. 7-13 September, pp.173-181.

Veronneau, M., (1992): Comparison of Geoid Models to GPS on Benchmarks. *Paper presented at AGU Spring Meeting*, Montreal. May 12 - 15.

Wang, Y., (1993): On the Optimal Combination of Potential Coefficient Model with Terrestrial Gravity Data for FFT Geoid Computations.*Manuscripta Geodaetica, No. 18*, pp. 406 - 416.

Wichiencharoen, C., (1984): A Comparison of Gravimetric Undulations Computed the Modified Molodensky Truncation Method and the Method of Least Square Spectral Combination by Optimal Integral Kernels. *Bulletin Geodesique, No. 58,* pp. 494-509.

Zawawi, W., (1994): Division of Geophysics, Geological Survey of Malaysia, *Private Communication.*

Zhao, S., (1989): The Computation of Detailed Geoids Using the Fast Fourier Transform Method. *Report No. 400, Dept. Geod. Sci., Ohio State University,* Columbus.

Zilkoski, D., (1992): Estimation of GPS-Derived Orthometric Heights Using High-Resolution Geoid Height Models. *Papers Presented at Spring AGU Meeting,* May 12-16, Montreal, Canada.

Addendum

SUPPLEMENTARY REFERENCES

Arabelos, D and Tziavos, I., (1992): Geoid Mapping in the Mediterranean Sea Using Heterogeneous Data. *More Nostrum I - Geomed Report.* pp. 78-98, Milano.

Chang, R., Chia-Chyang, C. and Jenn-Tout, L., (1989): A Gravimetric Geoid in Taiwan Area. *Papers Presented at IAG Symposium, August 10-11, Edinburgh,* Scotland.

Forsberg, R. and Madsen, F., (1981): Geoid Prediction in Northern Greenland Using Collocation and Digital Terrain Models, *Ann. Geophysics. Vol. 37, fascl.* pp. 31-36.

Kearsley, W., (1986): Data Requirements for Determining Precise Relative Geoid Heights from Gravimetry. *Journal of Geophysical Research, Vol. 91,* pp. 9193-9201.

Kearsley, W., (1987): Tests in the Recovery of Precise Geoid Height Differences from Gravimetry. *Papers Presented at the GPS Conference, Royal Melbourne Institute of Technology - August, Melbourne,* Australia.

Lerch, J., Putney, H., Wagner, A. and Klosko, M., (1981) : Goddard Earth Model for Oceanographic Application (GEM10B). *Marine Geodesy 5(2).* pp. 145-187.

Mainville, A., Forsberg, R. and Sideris M., (1990): GPS-levelling - Performance of Geopotential Models and Gravimetric Geoids Methods in the Great Slave lake Area. *Papers Presented at the International Symposium of Precise Positioning with the Global Positioning System,* Ottawa.

Rapp, H., (1978): A global 1 Degree by 1 Degree Anomaly Field Combining Satellite GEOS3 Altimeter and Terrestrial Anomaly Data. *Report No. 278, Dept. Geod.Sci, Ohio State University,* Colombus.

Rapp, H., (1981): The Earth's Gravity Field to Degree and Order 180 Using SEASAT, Altimeter Data, Terrestrial Anomaly Data . *Report No. 322 Dept. Geod.Sci, Ohio State University,* Colombus.

Schwarz, P., Sideris, M. and Forsberg, R., (1990): The Use of FFT Techniques in Physical Geodesy. *Geophysical Journal International. Vol. 100*, pp. 485-514.

Sevilla. M., Gil, A. and Rodrique, G., (1993): Preliminary Geoid Determination in Portugal. *Mare Nostrum. Geomed Report No. 3*, Milano, Italy.

Sideris, M., (1994): Geoid Determination by the FFT techniques. *Papers Presented at the International School for the Determination and Use of the Geoid, Oct. 10-15, Milano,* Italy.

Sideris, M. and Forsberg, R., (1990) : Review of Geoid Prediction Methods in Mountainous Region. Procedding of the 1st. International Geoid Commission. Milano, Italy.

Torge, W., (1989) : Gravimetry. *Walter de Gruyter*. Berlin, New York.

Tscherning, C., (1985): Local Approximation of the Gravity Potential by Least Squares Collocation. *Proceedings of the International Summer School on Local Gravity Field Approximation, Beijing,* China, Aug. 21-Sept. 4.

UTM, (1989): The Compilation and the Adjustment of Gravity Data for West Malaysia. *Unpublished Report, Faculty of Surveying, University of Technology Malaysia*, Skudai.

Weber, G and Zommorodian, H. , (1988) : Regional Geopotential Model Improvement for the Iranian Geoid Determination. *Bulletin Geodesique no. 62*, pp. 125-141.

Wenzel, G., (1985): Hochanflosende Kugelfunctionsmodelle fur das Gravitationspotential der Esde. *Wiss. Arb. Fachrichtung Vermessungwesen der Universitat Hannover, No. 137,* Hannover.

Wichiencharoen, (1982): The Indirect Effects on the Computation of Geoid Undulations. *Report No. 336, Dept. Geod. Sci., Ohio State University*, Colombus.